2019

From Sugar To Acetate - The Origins Of Acetyl-Coa Dictate Its Use In Cells And In Mice

Steven Zhao
University of Pennsylvania

From Sugar To Acetate - The Origins Of Acetyl-Coa Dictate Its Use In Cells And In Mice

Abstract

Changes in environmental factors, diet, and genetics all influence metabolism, which is frequently dysregulated at the cellular and organismal levels in diseases such as metabolic syndrome, cancer, and inborn errors of metabolism. These maladies are often intertwined; for example, metabolic diseases such as obesity and inborn errors of metabolism such as fumarate hydratase deficiency can both increase the risk for developing certain cancers. One metabolic pathway frequently altered in disease is de novo lipogenesis (DNL). Aberrant DNL is believed to play a critical role in pathogenesis of cancer and non-alcoholic fatty liver disease (NAFLD), a manifestation of metabolic syndrome in the liver. DNL requires the metabolite, acetyl-CoA, which is predominantly synthesized in the cytosol and nucleus from the cleavage of citrate through the action of ATP-citrate lyase (ACLY). Consistent with its role in DNL, elevated levels or activity of ACLY is frequently observed in cancer and NAFLD. Therefore, I utilized a genetic loss-of-function approach coupled with metabolomic methods to investigate how abrogating ACLY impacts metabolism in proliferating cells and the liver. Unexpectedly, impairment of ACLY leads to metabolic compensation through ACSS2-dependent acetate usage at the cellular and tissue levels. Moreover, by depleting ACLY, we identify a link between dietary carbohydrate and microbiome-derived acetate in supporting hepatic DNL. These findings have revised our understanding of acetyl-CoA metabolism in cells, and how nutritional sources feed into this pathway in disease contexts.

Degree Type

Dissertation

Degree Name

Doctor of Philosophy (PhD)

Graduate Group

Cell & Molecular Biology

First Advisor

Kathryn E. Wellen

Second Advisor

Luca . Busino

Subject Categories

Biochemistry | Biology | Molecular Biology

FROM SUGAR TO ACETATE – THE ORIGINS OF ACETYL-COA DICTATE ITS USE IN CELLS AND IN MICE.

Steven Zhao

A DISSERTATION

in

Cell and Molecular Biology

Presented to the Faculties of the University of Pennsylvania

in

Partial Fulfillment of the Requirements for the

Degree of Doctor of Philosophy

2019

Supervisor of Dissertation

_____

Kathryn E. Wellen, PhD

Associate Professor of Cancer Biology
Associate Investigator of the Abramson Family Cancer Research Institute

Graduate Group Chairperson

_____

Daniel S. Kessler, PhD

Associate Professor of Cell and Developmental Biology

Dissertation Committee

Luca Busino, PhD (Committee Chair) – Assistant Professor of Cancer Biology, Assistant Investigator of the Abramson Family Cancer Research Institute

Zoltan P. Arany, MD, PhD – Professor of Medicine

Aalim M. Weljie, PhD – Assistant Professor of Pharmacology

Terence P. Gade, MD, PhD – Assistant Professor of Radiology and Cancer Biology, Assistant Investigator of the Abramson Family Cancer Research Institute

FROM SUGAR TO ACETATE – THE ORIGINS OF ACETYL-COA DICTATE ITS USE IN CELLS

AND IN MICE.

ACKNOWLEDGMENT

First and foremost, I would like to express my deepest gratitude to my thesis advisor and mentor, Katy Wellen. Without her continual support, patience, and guidance, this work would not have been possible. The enthusiasm she brought to the lab everyday motivated me to always continue pushing, even when experiments were not working or ideas were hard to come by. I have learned a great deal from Katy towards becoming a better scientist, leader, and person in general. My time in her lab will always be one of my fondest memories, and it was, without a doubt, an absolute privilege to do my thesis in her lab.

I would also like to thank all of the past and present members of the Wellen Lab for their help and constructive feedback over the years, as well as for just being great people to work with every day. I have come to realize how hard it is to find such a dedicated, supportive, and positive group of people to interact with each day, and I am grateful for the opportunity to have done so for so many years. It has been a fun experience to see the lab grow from the early years, and I wish all the past, current and future Wellen Lab members the best of fortunes in their scientific endeavors.

Next, I would like to thank my committee members, Dr. Luca Busino, Dr. Zoltan Arany, Dr. Terence Gade, and Dr. Aalim Weljie, for the time and attention they have dedicated over the years both in and outside of my thesis committee meetings to offer their expertise, feedback, and support. I have learned a great deal through their insights, and have benefitted from their scientific and professional support.

I have been fortunate to have many excellent collaborators over the course of my PhD, and I thank all of them for their contributions and efforts. In particular, I would like to

acknowledge Dr. Cholsoon Jang, without whom much of the latter work in my dissertation may not have come to fruition as quickly as it did.

I also consider myself extremely fortunate to have experienced incredible scientific mentorship at the beginning of my career, which undoubtedly steered me towards the path of biomedical research. In particular, I would like to thank Dr. Sam Gunderson at Rutgers University for teaching me the joys and tribulations of doing academic research, recognizing my interest and potential in research, and creating the solid scientific foundation that has carried me to this day. In addition, I would like to thank Mr. Robert Pestka and PBL Assay Science for providing me with an opportunity to experience scientific research in a professional and highly productive setting. I learned a great deal from these experiences prior to embarking on my PhD journey, and am certain I would not have accomplished as much as I have without them.

To Kathy, Meagan, Anna, and Christina who do an amazing job with every CAMB student. I remember feeling incredibly welcomed during my interview at Penn, and after helping run recruitment for two years with them, I realized how much of that and all CAMB events happens due to their contributions. Thank you for being awesome!

I would like to thank my classmates and friends, who were always there to celebrate the good times and cheer me up during the difficult times. My time here would not have been nearly as enjoyable without them, and I wish them all the best in their future careers. A special thanks goes out to Stephen Bart, Devin McDougald, and David Walter for years of comradery at 522 S 22nd St.

Finally, I would like to thank my father, Shuyuan Zhao, and mother, Qi Xie, for all of their love and dedication to my success throughout my life. This accomplishment would not have been possible without their many sacrifices, and there are no words that can

express my appreciation for them. I think they're still probably holding out hope that I'll go to medical school one day, but nonetheless I know they're proud of what I've accomplished during my dissertation and I dedicate this work to them.

ABSTRACT

FROM SUGAR TO ACETATE – THE ORIGINS OF ACETYL-COA DICTATE ITS USE IN CELLS AND IN MICE.

Steven Zhao

Dr. Kathryn Wellen

Changes in environmental factors, diet, and genetics all influence metabolism, which is frequently dysregulated at the cellular and organismal levels in diseases such as metabolic syndrome, cancer, and inborn errors of metabolism. These maladies are often intertwined; for example, metabolic diseases such as obesity and inborn errors of metabolism such as fumarate hydratase deficiency can both increase the risk for developing certain cancers. One metabolic pathway frequently altered in disease is *de novo* lipogenesis (DNL). Aberrant DNL is believed to play a critical role in pathogenesis of cancer and non-alcoholic fatty liver disease (NAFLD), a manifestation of metabolic syndrome in the liver. DNL requires the metabolite, acetyl-CoA, which is predominantly synthesized in the cytosol and nucleus from the cleavage of citrate through the action of ATP-citrate lyase (ACLY). Consistent with its role in DNL, elevated levels or activity of ACLY is frequently observed in cancer and NAFLD. Therefore, I utilized a genetic loss-of-function approach coupled with metabolomic methods to investigate how abrogating ACLY impacts metabolism in proliferating cells and the liver. Unexpectedly, impairment of ACLY leads to metabolic compensation through ACSS2-dependent acetate usage at the cellular and tissue levels. Moreover, by depleting ACLY, we identify a link between dietary carbohydrate and microbiome-derived acetate in supporting hepatic DNL. These findings have revised our understanding of acetyl-CoA metabolism in cells, and how nutritional sources feed into this pathway in disease context

TABLE OF CONTENTS

LIST OF ILLUSTRATIONS

CHAPTER 1:

CHAPTER 2:

CHAPTER 1: ACETYL-CoA METABOLISM IN DISEASE

Acetyl-CoA production links catabolic and anabolic metabolism in cells.

Acetyl-coenzyme A (Acetyl-CoA) is a metabolite that links nutrient breakdown for energy and the synthesis of more complex metabolites. Due to this positioning within cellular metabolism, acetyl-CoA production and abundance is tightly regulated in response to nutritional availability and other signals such as oncogenic activation[1]. However, the mechanisms that govern this regulation are still not entirely understood. Adding to the complexity, acetyl-CoA can be synthesized in various cellular compartments and from different substrates. Discussed below are the sources and locations of acetyl-CoA production at the time of this work.

Pyruvate:

Glucose is taken into cells via the SLC2/GLUT family of transporters, which are expressed in a tissue-specific manner[2]. Following uptake, glucose is phosphorylated by hexokinase to glucose-6-phosphate and trapped within the cell. Glucose-6-phosphate is shunted into glycolysis, resulting in the production of pyruvate in the cytosol. Pyruvate is imported into the mitochondria by the mitochondrial pyruvate carrier (MPC), which is converted into acetyl-CoA within the mitochondria by the pyruvate dehydrogenase complex (PDC). Mitochondrial acetyl-CoA is condensed with oxaloacetate to form citrate, which can enter the citric acid cycle to fuel the generation of ATP, NADH, and $FADH_2$ or be exported from the mitochondria to the cytosol in exchange for malate via the transporter SLC25A1[3] (Figure 1.1). In addition to the mitochondria, the PDC has been reported to also function within the nucleus to generate nuclear acetyl-CoA[4].

Citrate:

In addition to glucose, catabolism of other nutrients such as fatty acids and amino acids within the mitochondria can also yield citrate (Figure 1.1). Once exported out of the mitochondria, nuclear-cytosolic citrate is cleaved into acetyl-CoA by the enzyme ATP-citrate lyase (ACLY) in an ATP-dependent manner, regenerating oxaloacetate as a by-product. Given the high concentrations of circulating glucose (~5 mM) and abundance of other nutritional sources, this is believed to be the major route of nuclear-cytosolic acetyl-CoA production *in vivo*. Consistent with this, congenital deletion of *Acly* in mice fails to produce viable offspring, displaying early embryonic lethality around E8.5[5]. Like the PDC, ACLY has also been found to localize to the nucleus[6], although its nuclear regulation and functions remains largely unknown.

Acetate:

In addition to citrate, another major route of acetyl-CoA synthesis is utilizing the short-chain fatty acid (SCFA) acetate. *In vivo*, levels of circulating acetate are relatively low (~100 μM), as compared to glucose (~5 mM), but can reach much higher levels in certain parts of circulation such as the portal vein that connects the intestine to the liver[7]. This is because the majority of acetate is produced in the large intestine by the gut microbiome, which ferment undigestible nutrients into SCFAs such as butyrate, propionate, and acetate. However, despite its lower circulating levels, turnover of acetate *in vivo* is very high[8], suggesting that it is avidly used by cells within the body. Acetate is taken up by mammalian cells through the proton-coupled monocarboxylate transporters such as MCT1 and MCT4[7], and directly ligated to free CoA in an ATP-dependent manner by the Acyl-CoA Synthetase Short Chain family of enzymes (ACSS1, ACSS2, ACSS3)[9]. Of these, ACSS1/3 are found in the mitochondria, whereas ACSS2 is found in the cytosol and nucleus like ACLY.

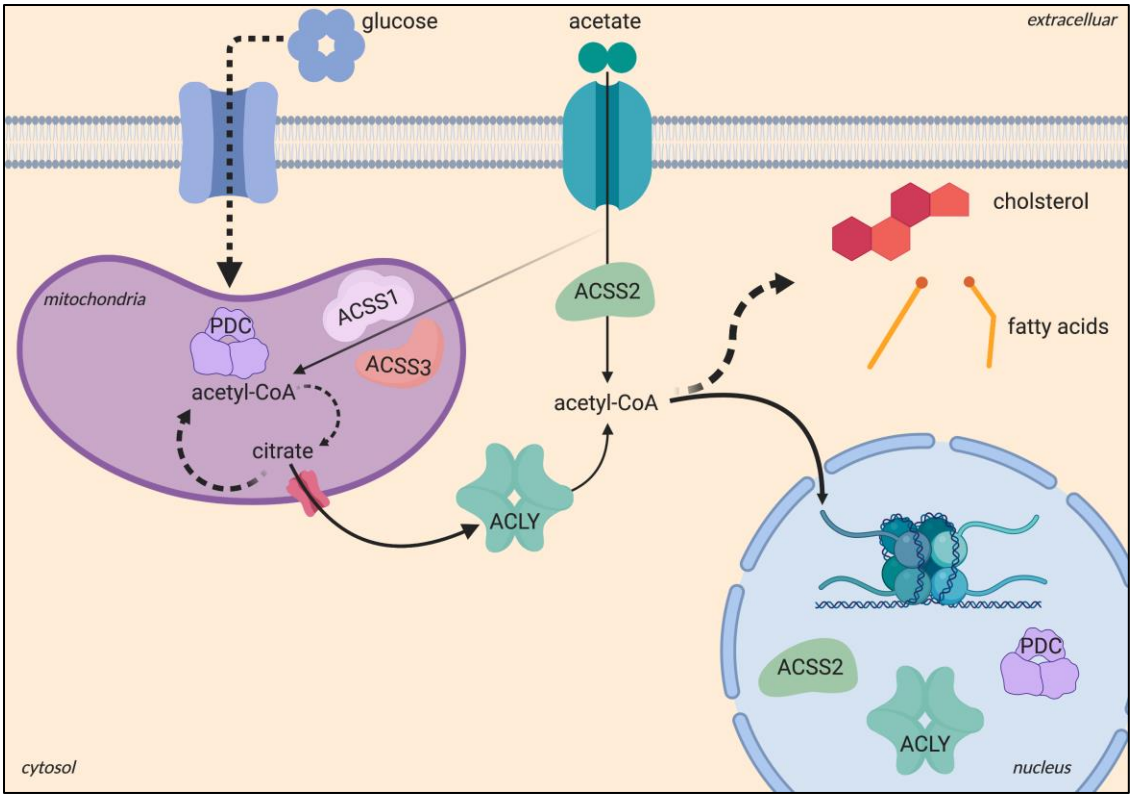

Figure 1.1 | Acetyl-CoA metabolism in mammalian cells.
Acetyl-CoA is synthesized using multiple substrates and in various cellular compartments. Mitochondrial acetyl-CoA is synthesized from pyruvate via glucose by the PDC, or acetate by ACSS1/3. Cytosolic acetyl-CoA is synthesized from citrate and acetate, by ACLY and ACSS2 respectively. Acetyl-CoA can diffuse from the cytosol to the nucleus, yet the PDC, ACLY and ACSS2 all localize to the nucleus. Acetyl-CoA is used for histone acetylation to regulate the epigenome, as well as for synthesis of lipids such as cholesterol and fatty acids.

Acetyl-CoA metabolism in cancer

In order for a cell to divide, it must effectively double its cellular contents, including nucleic acids, proteins, and lipids. As a disease of unrestrained proliferation, cancer cells must overcome this metabolic barrier and either acquire or generate enough molecular building blocks to divide frequently. To accomplish this, cancer cells rewire their metabolism to favor uptake of nutrients such as glucose and perform glycolysis even in the presence of oxygen, also known as the Warburg effect[10]. In addition, cancer cells will increase usage of anapleurotic metabolites such as glutamine[11], and even scavenge for macromolecules to break down into metabolic building blocks[12]. Discussed below are two prominent ways that acetyl-CoA metabolism promotes cancer growth: epigenetic regulation and lipid metabolism (Figure 1.1).

Metabolic Control of Epigenetics in Cancer[13]

Abstract

Alterations in the epigenome and metabolism both affect molecular rewiring in cancer cells and facilitate cancer development and progression. However, recent evidence suggests the existence of important bidirectional regulatory mechanisms between metabolic remodeling and the epigenome (specifically methylation and acetylation of histones) in cancer. Most chromatin-modifying enzymes require substrates or cofactors that are intermediates of cell metabolism. Such metabolites, and often the enzymes that produce them, can transfer into the nucleus, directly linking metabolism to nuclear transcription. We discuss how metabolic remodeling can contribute to tumour epigenetic alterations, thereby affecting cancer cell differentiation, proliferation and/or apoptosis, as well as therapeutic responses.

Introduction

Epigenetic plasticity in cancer facilitates the acquisition of its hallmark characteristics[14,15]. The metabolic traits of tumour cells are also crucial for adjusting to changes in the availability of oxygen and nutrients (carbohydrates, lipids and amino acids) in the tumour microenvironment, to sustain proliferation and resist mitochondria-dependent apoptosis[10,16,17]. Cellular metabolism and the epigenome interact with one another and with the genetic and molecular drivers of cancer, in a bidirectional manner. An integrative understanding of the interplay between the molecular, metabolic and epigenetic rewiring in cancer is far from complete, but conceptual themes are beginning to emerge. Further elucidation of these links is likely to lead to more effective cancer therapies.

Most post-translational modifications (PTMs), such as phosphorylation, acetylation and other acyl modifications, methylation and O-linked N-acetylglucosamine modification (O-GlcNAcylation), require metabolites as substrates (FIG. 1.2). In the nucleus, these metabolites are used for chromatin modifications, including acetyl-CoA for histone acetylation and S-adenosylmethionine (SAM) for histone and DNA methylation. The histone code hypothesis is based on writers, erasers and readers of chromatin marks6. This assumes that the 'ink' in this process is never limiting; however, based on a growing body of evidence that the availability of metabolites to the writers has an impact on chromatin modifications, we believe that it may be time to add a fourth parameter in this code: the metabolite-producing enzymes, which provide the ink for histone modification (FIG. 1.2). In this Review, we discuss how metabolic control of the epigenome is emerging as a crucial mechanism by which cancer cells can adapt to a changing environment.

Basic biochemistry of acetylation

More than 8,000 unique acetylation sites in proteins have been detected in mammalian cells[18–20]. Within the nucleus, histones comprise the bulk of acetylation loci. The chromatin of mammalian cells contains at least 10 billion potential acetylation sites, meaning that a global change in histone acetylation may lead to a substantial reduction in cellular or nuclear acetyl-CoA levels. Given the high amounts of energy stored in a molecule of acetyl-CoA, this may represent a potential energy sink[21].

Each histone octamer subunit (as well as the linker histone, H1) contains multiple lysine residues, which are positively charged in the nucleoplasmic environment, leading to attraction of the negatively charged DNA. More than 60 of these lysine residues are known to be acetylated in mammals (H1 has 16 sites, H2A has 10 sites, H2B has 16 sites, H3 has 13 sites and H4 has 9 sites)[22,23]. Acetylation neutralizes the positive charge of lysine, loosening the interaction between the histone and the negatively charged DNA and leading to a more open chromatin configuration (euchromatin) that is permissive for transcription. Histone deacetylation is usually associated with condensed, compacted chromatin (heterochromatin) and transcriptional repression.

Protein acetylation occurs both cotranslationally onto the N-terminal residue of a protein, catalysed by Nα acetyl- transferases, and post-translationally onto the Nε amino group of lysine residues. Lysine acetylation is catalysed by multiple families of lysine acetyltransferases (KATs) and reversed by lysine deacetylases (KDACs). Nα affects approximately 85% of human proteins and is important for their stability, localization and function[24,25]. Nε acetylation can alter protein function by altering its catalytic activity, interactions with other factors, subcellular localization and stability[26]. These effects can originate directly from changes in charge, from binding of proteins that contain acetyl-

lysine recognition bromodomains[27,28] or from prevention of other post-translational lysine modifications (including ubiquitylation, methylation and formylation)[26]. Nε acetylation can also occur through a non-enzymatic mechanism throughout the cell, and this is promoted in alkaline environments such as the mitochondrial matrix[29,30]. Thus, pH gradients, such as the one that occurs across the inner mitochondrial membrane (that is, mitochondrial membrane potential, which is increased in most tumours[31,32]), may directly influence acetylation reactions[33]. Conversely, acetylation of histones in the nucleus may influence intracellular pH (pHi) because acetate export from the cell is proton coupled[34]. Hence, in low-pHi conditions global deacetylation of histones generates acetate to be exported as a mechanism to extrude protons to neutralize pHi[34].

Owing to the very large amounts of acetate stored on his- tones, histone acetylation has been proposed to function as a pHi buffer[34]. Histone acetylation is variable within tumours, probably reflecting differences in the tumour microenvironment and cellular diversity. Attempts have been made to correlate clinical outcomes with histone acetylation levels in tumour specimens that, perhaps not surprisingly, have led to conflicting results[35–40]. As discussed, there are also many non-histone acetylation targets, a complexity that is very difficult to address in clinical specimens. Acetyl-CoA is the sole donor of acetyl groups for acetylation in eukaryotic cells[26]. This central metabolite comprises an acetyl moiety (CH_3CO) bound through a high-energy thioester bond to CoA, which is a derivative of vitamin B5, ATP and cysteine[21]. Hydrolysis of the energy-rich thioester bond results in the release of 31.4 kJ mol^{-1} of energy. To put this in perspective, the energy released by the hydrolysis of ATP to ADP + Pi is 30.5 kJ mol^{-1} [41,42]. This makes acetyl-CoA a very unstable molecule, suggesting that acetylation must occur very close to the site where acetyl-CoA is produced. Along with the fact that

acetyl-CoA cannot easily cross cellular membranes, this underlies the importance of acetyl-CoA compartmentalization in the regulation of acetylation reactions.

Basic biochemistry of methylation

Methylation is different from acetylation and other PTMs in that both proteins and DNA can be methylated. In human DNA, cytosines are typically methylated in the context of CpG dinucleotides. Overall, methylation of CpG islands in promoter regions typically inhibits transcription. Cancers frequently display global DNA hypomethylation compared with their healthy tissue counterparts, although at the same time, exhibiting hypermethylation of CpG islands in genomic regions responsible for the expression of tumour suppressor genes such as von Hippel–Lindau tumour suppressor (VHL), BRCA1 or retinoblastoma 1 (RB1)[43–46].

Histone methylation can occur on lysine or arginine

residues, ranging from mono- to trimethylation. These histone methyl marks can either activate or repress gene expression depending on which residue is modified and the number of methyl groups incorporated. DNA methylation tends to be a more stable modification than histone methylation, but much of tumour suppressor gene silencing is driven by histone modification, before DNA methylation occurs[47]. Nearly half of the known histone methyltransferases (HMTs) have been associated with cancer[48]. The first histone demethylase (HDM), that is, lysine-specific histone demethylase 1 (LSD1; also known as KDM1A), was discovered only in 2004[49], but since then several classes of demethylase, which we discuss below, have shown remarkable links to metabolism and cancer, including the Jumonji-C (JMJC) domain-containing HDMs (JHDMs), which can remove mono-, di- and trimethylation groups, and the TET enzymes, which are responsible for initiating the demethylation of DNA by hydroxylating 5-methylcytosine.

Similar to acetylation, methylation uses the energy stored in a sulfur bond to facilitate the reaction. SAM is the primary methyl group donor and is generated in the methionine cycle from methionine and ATP. The methionine cycle begins with the conversion of methionine into SAM, which is catalysed by a methionine adenosyltransferase. After donating its methyl group, SAM becomes S-adenosylhomocysteine (SAH). S-Adenosylhomocysteine hydrolase (SAHH) deadenylates SAH to make homocysteine. The cycle is completed when homocysteine accepts a methyl group from the folate cycle to regenerate methionine[50,51].

Metabolic control of epigenetics

The relationship between epigenetic regulation and metabolism is complex, with overarching themes but also context-specific mechanisms. We first discuss the role of metabolites as regulators of enzymatic activity, followed by the choreography of subcellular compart- mentalization of metabolic pathways as they relate to epigenetic modifications, focusing on acetyl-CoA producers as an example. We then describe the impact of oncogenic metabolic rewiring on acetyl-CoA production and histone acetylation in cancer cells.

Metabolites promote and inhibit enzyme activity.

In phosphorylation (which is the most thoroughly studied mechanism in signalling), kinases use an important intracellular metabolite, ATP, as a substrate. However, kinases typically have high affinity for ATP, and thus are regulated by other types of signalling cue but generally not by ATP availability. A notable exception is AMP-activated protein kinase (AMPK), which evolved to sense energy changes and becomes activated when the AMP/ATP ratio rises in the cell[52]. In contrast, many chromatin-modifying enzymes not only use metabolic intermediates as cofactors or substrates but are also regulated by

their availability. Thus the levels of these metabolites can influence the capacity of the cell to write or erase chromatin marks, pointing to an intimate relationship between metabolic and epigenetic regulation.

As described above, DNA and HMTs use SAM as a methyl donor, while the product SAH inhibits methyl- transferase activity[50] (FIG. 1.2). Similarly, the Krebs cycle (also known as the tricarboxylic acid (TCA) cycle) inter- mediate α-ketoglutarate (α-KG) is a required co-substrate for JHDMs and TET methylcytosine dioxygenases, which participate in a multi-step DNA demethylation process; whereas structurally related metabolites such as succinate, fumarate and 2-hydroxyglutarate (2-HG) are competitive inhibitors of these α-KG-dependent dioxygenase enzymes[53–56].

Acetylation is similarly promoted by the acetyl group donor acetyl-CoA and inhibited by its product, CoA[1,57,58] (FIG. 1.2). Adding complexity, recent evidence suggests that other acyl-CoAs, notably palmitoyl-CoA[59], can also act as inhibitors of KAT reactions. Crotonyl-CoA, conversely, is used as an alternative substrate by the acetyltransferase p300 (crotonylation)[60]. Deacetylation reactions are also metabolically responsive. Sirtuin deacetylases, in both mitochondria and nuclei, use NAD+ as a cofactor, and energy-depleted conditions that promote AMPK activation increase NAD+ levels and promote sirtuin-mediated deacetylation[61] (FIG. 1.2). Whereas deacetylation reactions are energetically favourable, sirtuins are intriguing as they catalyse the reaction in a seemingly wasteful way: one NAD+ molecule is hydrolysed to produce NADH and O-acetyl-ADP-ribose. In order to understand the importance of these reactions, factors beyond deacetylation need to be considered; for example, the anabolic fate of O-acetyl-ADP-ribose in cancer cells or interactions with ‘nearby’ acetyl-CoA producers that also

regulate and are regulated by the NAD+/NADH ratio, like the pyruvate dehydrogenase complex (PDC; which we discuss below). In addition to metabolic regulation of sirtuin deacetylases, metabolic products, including the glycolytic product lactate and the ketone body β-hydroxybutyrate, have been identified as endogenous inhibitors of KDACs[62,63]. With numerous metabolites potentially affecting each histone modification, understanding the true influences of metabolism on chromatin might seem hopelessly com- plex. Towards reducing this complexity, a recent metabolomics study in cancer cells analysed the relationship of global histone acetylation with levels of various metabolites, including acetyl-CoA, CoA, NAD+ and β-hydroxy- butyrate, upon dose-dependent glycolytic inhibition, and found that the level of acetyl-CoA was the best predictor of histone acetylation levels in this context[64].

The spatial choreography of metabolism in subcellular compartments.

Acetyl-CoA is present in the mammalian cell in multiple, distinct pools: mitochondrial, cytosolic, nuclear, peroxisomal and in the endoplasmic reticulum (ER). Acetyl-CoA cannot readily cross organelle membranes and thus these pools are physically separated. In addition, owing to its inherent instability, it is likely that acetyl-CoA is synthesized locally according to its intended use in the cell. Thus, localized sub-pools of acetyl-CoA may be locally produced and used in specific functions.

The largest and best understood pools of acetyl-CoA in the cell are the mitochondrial, cytosolic and nuclear pools. Mitochondrial acetyl-CoA has key roles in the Krebs cycle and mitochondrial ATP production, whereas the cytosolic pool supplies fatty acid, cholesterol and hexosamine biosynthesis pathways. Mitochondria are the major site of acetyl-CoA production from nutrient catabolism. Acetyl-CoA is produced in mitochondria from glycolysis-derived pyruvate through the glucose oxidation gate-keeping enzyme

PDC; catabolism of branched chain amino acids and β-oxidation of fatty acids also contribute to the mitochondrial acetyl-CoA pool depending on cell type and conditions[21,65]. Acetyl- CoA condenses with oxaloacetate inside mitochondria to generate citrate, which is oxidized within the Krebs cycle to produce the electron donors NADH and $FADH_2$ or citrate is exported to the cytoplasm. After export from the mitochondria, citrate is cleaved into oxaloacetate and acetyl-CoA by the enzyme ATP-citrate lyase (ACLY) in an ATP-dependent manner. This pathway is a major route for extramitochondrial acetyl-CoA production in mammalian systems under nutrient-replete conditions[66]. However, under stressed conditions, such as low nutrient availability or hypoxia, citrate can be generated through reductive carboxylation of glutamine in the cytoplasm through isocitrate dehydrogenase 1 (IDH1), in addition to the mitochondrial pathway, which involves IDH2[67–69]. Acetate can also be activated upon ligation to CoA to produce acetyl-CoA in an ATP-dependent reaction by acyl-CoA synthetase short-chain family member 2 (ACSS2). Although not normally a fuel in most mammalian cells, acetate uptake and use increases in tumours[70,71], particularly under hypoxic conditions in which acetate has been shown to contribute a significant fraction of the lipogenic acetyl-CoA pool[72,73]. Under hypoxic conditions, acetate also promotes histone acetylation globally and at the promoters of lipogenic genes, promoting their expression[74] (FIG. 1).

Global levels of nuclear histone acetylation are sensitive to overall acetyl-CoA levels; however, it is attractive to speculate that localized production of acetyl-CoA by spatial regulation of acetyl-CoA producers could confer specificity to metabolic regulation of acetylation. Presently, it is known that several acetyl-CoA-producing enzymes are localized to the nucleus, in addition to other cellular compartments. ACLY and ACSS2 have been known for several years to be present in the nucleus in addition to the

cytoplasm, and to participate in the regulation of overall histone acetylation levels[66,75]. ACSS2 has recently been described as predominantly nuclear in some tumours[76], and exposure to exogenous acetate promotes its nuclear localization[76]. Additionally, the PDC was recently shown to dynamically translocate from mitochondria to nuclei following serum stimulation, epidermal growth factor (EGF) signalling or mitochondrial stress, where it produces acetyl-CoA to promote histone acetylation[4]. These data, as well as other evidence of acetyl-CoA producers localizing to the nucleus in disease states such as cancer[73,76,77], suggest that acetyl-CoA production may be spatially controlled, potentially conferring specificity to the effects of metabolism on acetylation (FIG. 1.3).

It is unclear whether nuclear ACLY, ACSS2 and PDC are redundant or fulfil distinct roles in the nucleus. Studies have pinpointed a metabolic role for nuclear ACSS2 in stress responses, whereby acetylation of hypoxia-inducible factor 2α (HIF2α) by the acetyltransferase CREB-binding protein (CBP; also known as CREBBP) is dependent on nuclear translocation of ACSS2 to supply acetyl-CoA[76,77]. Similarly, as discussed, mitochondrial stress was shown to promote PDC translocation to the nucleus to increase histone acetylation involved in cell cycle progression[4]. Additionally, the presence of a functional Krebs cycle was shown to be important for maintaining overall levels of histone acetylation, regardless of the availability of exogenous acetate68. Parsing out the relative contributions and mechanisms of compensation between each of these enzymes in different contexts will be important for both understanding the physiological control mechanisms for acetylation and identifying opportunities for targeting these pathways. Moreover, the mechanisms governing their nuclear localization remain elusive, as none has a reported nuclear localization sequence. It is likely that the

mechanism by which each of the acetyl-CoA-producing enzymes are brought into the nucleus has a substantial impact on their function within the organelle.

Oncogene rewiring of acetyl-CoA metabolism.

The importance of acetyl-CoA in several pathways and multiple cellular compartments implicates it as a chief target of the metabolic remodelling and molecular rewiring in cancer. Indeed, evidence that frequent primary molecular changes or driver mutations in cancer can directly affect acetyl-CoA homeostasis suggests an intimate link between molecular and metabolic signalling. MYC and AKT both fulfil prominent roles in stimulating nutrient uptake and rewiring cellular metabolism in cancer cells[78–80]. Among their metabolic roles, both have been shown to promote acetyl-CoA production through ACLY. MYC regulates acetyl-CoA production for use in lipid synthesis and histone acetylation[81], and MYC- deficient cells maintain lower acetyl-CoA levels, despite evidence of compensatory mechanisms[82,83]. AKT directly phosphorylates and activates ACLY[84,85], thus enabling cells to maintain histone acetylation even when glucose availability is limited[1]. Conversely, AKT inhibition decreases cellular acetyl-CoA and histone acetylation levels. Notably, overall histone acetylation levels in human prostate tumours and gliomas correlate significantly with phosphorylated Ser473 on AKT[1]. Thus, AKT activation in cancer cells may enable them to sustain a high nuclear level of acetyl-CoA, preventing histone acetylation from fluctuating with microenvironmental nutrient availability. Such a mechanism could conceivably enable cells to maintain pro-proliferative gene expression programmes in a harsh microenvironment, enabling them to respond more rapidly when adequate nutrients for growth become available.

Tyrosine kinases can phosphorylate pyruvate dehydrogenase kinase (PDK) and activate it, thus indirectly inhibiting PDC[86]; they can also directly phosphorylate and inhibit

PDC[87,88]. The net result is a decrease in PDC activity and thus a net decrease in mitochondrial acetyl-CoA pro- duction and Krebs cycle activity, with all its downstream effects, including reduced α-KG, citrate and NADH levels. EGF can promote PDC translocation in the nucleus, where it can remain constitutively active, producing acetyl-CoA, because PDK, which tonically inhibits PDC in mitochondria, is absent from the nucleus, at least in some cancers[4]. Although it is becoming increasingly clear that oncogenic alterations in acetyl-CoA homeostasis facilitate tumorigenesis and progression, delineating the effects on metabolism and molecular signalling has remained elusive. Below, we propose three models of how metabolic rewiring can lead to remodelling of the epigenome landscape in tumours as part of a greater bidirectional feedback mechanism between molecular signalling and metabolism in cancer.

Potential models of coordination

As the body of literature on metabolic control of the epigenome has grown, it has become clear that a single mode of regulation does not apply universally to all scenarios in which metabolism influences chromatin marks. Therefore, in delineating the relationship between cellular metabolism and epigenetic modification, we propose three models that we believe encapsulate the types of regulation that have been observed thus far (FIG. 1.4). These models provide a framework within which to understand the diverse roles for metabolism in epigenetic control in cancer biology and how the molecular and metabolic rewiring may influence these processes, although raising questions that remain to be addressed.

Model 1: inhibitor metabolite production and chromatin regulation. Some chromatin-modifying enzymes use metabolites as substrates, but these metabolites are not normally regulatory for the function of the enzyme, except in the presence of inhibitor

metabolites. For example, α-KG is a co-substrate required for the activity of some histone and DNA demethylases, as discussed above (FIG. 1.2). Metabolites that interfere with the use of α-KG by these enzymes, including 2-HG, succinate and fumarate, which are structurally similar to α-KG, can inhibit some demethylases when their levels are elevated. The discovery of mutations in IDH1 and IDH2, through genomic studies of gliomas and other cancers, led to the identification of the first oncometabolite, (R)-2-hydroxyglutarate (R-2HG), produced by the mutant IDH enzymes[89–93]. Tumours harbouring IDH1 or IDH2 mutations exhibit increased histone and DNA methylation and more poorly differentiated gene expression profiles[93–96] (FIG. 1.4). For in-depth discussion on the biology of IDH mutations and R-2HG, see recent review articles[56,97]. Interestingly, the other enantiomer, S-2HG, is produced by lactate dehydrogenase (LDH) under hypoxic conditions, in which it also affects histone methylation and hypoxic transcriptional responses[98,99]. Accumulation of succinate or fumarate, which occurs in tumours deficient for succinate dehydrogenase (SDH) or fumarate hydratase (FH), similarly inhibit α-KG- dependent enzymes, resulting in hypermethylation[54,55,100]. Conversely, embryonic stem cells (ESCs) maintain an elevated α-KG/succinate ratio that is crucial for maintaining histone and DNA demethylation and pluripotency[101]. Thus, production of inhibitor metabolites in both physiological and pathological conditions can alter the activity of chromatin-modifying enzymes.

Model 2: nutrient sensing and regulation of chromatin. Chromatin modifications can also occur in direct response to physiological changes in nutrient availability. Such mechanisms may enable cells to optimize crucial short- and long-term adaptation mechanisms in conditions of limited fuel supply, such as those commonly found in many tumours. A canonical example of metabolite sensing is that of AMPK, which responds to

AMP and/or ADP availability[52]. As cells conduct work, ATP is consumed and ADP produced. The adenylate kinase reaction buffers cellular ATP concentrations, converting two ADP molecules into ATP and AMP. Hence, rising AMP levels convey energetic stress to the cell, doing so by binding to the γ-subunit of the AMPK heterotrimer, facilitating a conformational change that promotes phosphorylation of AMPKα-Thr172 by liver kinase B1 (LKB1; also known as STK11). AMPK has been described as regulating numerous activities in the cell[52,102], generally serving to restore energy balance by inhibiting energy consuming pathways and activating mechanisms that promote ATP production. Recent evidence implicates AMPK in stress-induced histone phosphorylation[103], suggesting that insults to the energy status of the cell can be translated into functional outputs in part through histone modification and gene regulation (FIG. 1.4).

Another example of how the overall supply of nutrients can be sensed and can affect epigenetic mechanisms comes from the dependence of methylation reactions on diet-derived essential amino acids (BOX 1). Owing to dependence on the essential amino acid methionine (up to 50% of the daily intake of methionine is converted into SAM[104]) and folate to propagate the methionine cycle, the serum levels of SAM and SAH in patients, as well as the degree of methylation in tumours, change with diet[105,106]. For example, dietary folate supplementation increases global DNA methylation of rectal mucosa[107] and colonic polyps[108]. Furthermore, tumour samples from patients with colon cancer who consumed more than 400 μg folate per day seem to have more global DNA methylation than tumour samples from patients consuming less than 200μg folate per day[109]. This may have direct effects on tumorigenesis, as consuming a methyl donor-deficient diet has been shown to reduce spontaneous tumour formation in animals

predisposed to intestinal tumours[110]. Moreover, methylation of specific histone residues (H4K3-trimethyl (me3)) is directly related to the availability of dietary methionine and intracellular production of SAM, further linking metabolism to epigenetic regulation[111].

Finally, nuclear and cytosolic acetyl-CoA levels may be sensed by the cell, enabling it to gauge its metabolic health. Acetyl-CoA levels are dynamic and parallel growth and proliferation, as well as histone acetylation, in both yeast and mammalian cells. This suggests that cells may sense acetyl-CoA to optimize the metabolic needs of proliferation with nutrient supply[1,112–114]. The evidence for acetyl-CoA availability affecting acetylation levels first emerged from an elegant study conducted in yeast[75]. Unlike mammalian cells, Saccharomyces cerevisiae relies on a single enzyme outside mitochondria to produce acetyl-CoA, Acs2p, the orthologue of mammalian ACSS2. Deletion of ACS2 resulted in a rapid drop in overall histone acetylation levels, and reconstitution with either a nucleus- or cytosol-confined enzyme, but not with a mitochondria-confined enzyme, restored histone acetylation. This study demonstrated the need for continuous production of acetyl-CoA in the nucleus or cytoplasm to sustain histone acetylation levels, and additionally provided experimental evidence for the separation of the mitochondrial and nuclear–cytosolic acetyl-CoA pools. Importantly, acetyl-CoA availability is also crucial for sustaining histone acetylation levels in mammalian cells, mediated largely through ACLY[1,66].

If acetyl-CoA levels are indeed ‘sensed’, this implies that one or more acetyltransferases are potential sensors, mediating acetylation reactions in a nutrient-responsive manner. According to a nutrient-sensing model, bulk cellular acetyl-CoA levels fluctuate with nutrient availability or metabolic state to influence histone acetylation. Acetyl-CoA

concentrations in yeast oscillate during metabolic cycles, over a range of approximately 3–30 μM, corresponding to periods of growth[112]; increased acetyl- CoA coincides with rising levels of histone acetylation both globally and locally at the promoters of growth-associated genes[112]. This regulation occurs in a manner dependent on the SAGA acetyltransferase complex[112], as yeast Gcn5 has a high KD for acetyl-CoA (approximately 8.5 μM) and can therefore be affected by acetyl-CoA oscillations. In addition to requiring acetyl-CoA for their activity, KATs are also subject to inhibition by their product, that is, CoA. Thus, it has been hypothesized that it may be the acetyl-CoA/CoA ratio that regulates KAT activity and histone acetylation in mammalian cells[57,58]. Moreover, the acetyl-CoA/CoA ratio not only influences the enzymatic activity of KATs, but also alters their specificity[115,116]. Glucose restriction or inhibition of signal transduction through the PI3K–AKT pathway results in a decline in both total acetyl-CoA levels and the acetyl-CoA/CoA ratio, corresponding to reduction in histone acetylation[1]. Experiments in isolated nuclei further showed that bulk histone acetylation can indeed be regulated by the acetyl-CoA/CoA ratio[1]. The acetyl-CoA/CoA ratio is also affected in liver by fasting and refeeding, suggesting its relevance to nutritional responses in whole organisms[117]. Conversely, glycolysis inhibition with 2-deoxy-D-glucose (2-DG) caused acetyl-CoA levels to fall, but acetyl-CoA/CoA ratio to rise, suggesting that these effects may be driven by alternative mechanisms in addition to feedback inhibition[64]. Such apparent differences may also be reflective of measuring whole-cell instead of nuclear levels of these metabolites, as necessitated by current mass spectrometry methods. Collectively, these findings suggest that acetyl-CoA levels and/or the acetyl-CoA/CoA ratio is a major indicator of the metabolic status of a cell, and that this should perhaps

now be added to the AMP/ATP and NAD+/NADH ratios, which have already been established as crucial rheostats in metabolic sensing (FIG. 1.5).

Model 3: localized metabolite production and chromatin regulation. We discussed how nuclear acetyl-CoA- producing enzymes (ACLY, ACSS2 and PDC) provide the ink in an expanded definition of the histone code and can regulate global histone acetylation and global acetyl-CoA homeostasis. There is now emerging evidence that direct recruitment of metabolic enzymes to specific sites on chromatin can facilitate site-specific cofactor or substrate production and histone modification (FIGS 1.3,1.4). Such regulation could participate in altered gene regulation in cancer and contribute to diverse cancer phenotypes.

One of the first examples of local production of a metabolite through recruitment of a metabolic enzyme into a transcription factor complex was described for S-adenosylmethionine synthase isoform type 2 (MAT2A), which is recruited through a direct protein–protein interaction to the DNA binding sites of the transcription factor MAFK[118]. There, MAT2A locally synthesizes SAM[118], which can then be used for localized histone methylation through interactions with HMTs such as SETDB1[119] (FIG. 1.4).

Very recently, two additional complexes containing acetyl-CoA-producing enzymes were described. The aryl hydrocarbon receptor (AHR), a transcription factor associated with xenobiotic metabolism, forms a complex on chromatin with pyruvate kinase M2 (PKM2), PDC and the acetyltransferase p300[120]. This complex results in acetylation of H3K9 at the enhancer of CYP1A1, an AHR target gene, enhancing its transcription[120]. In this complex, PKM2 uses phosphoenolpyruvate to produce pyruvate and ATP, as it does in

the cytoplasm. The pyruvate is then used by PDC to produce acetyl-CoA, which is provided to p300 for histone acetylation. The PDC, which despite its very large size is translocated as an intact complex and remains functional in the nucleus[4], can efficiently use this locally produced metabolite to produce acetyl-CoA and acetylate the target histone lysine through p300, as all the enzymes and the transcription factor form a complex (FIG. 1.3). This beautiful example of a targeted local acetylation system in the nucleus raises the intriguing possibility that such mechanisms may be commonly used to regulate transcription.

Additionally, recent evidence in yeast has shown that the yeast PKM2 orthologue, Pyk1, forms a large complex with serine biosynthesis and methionine cycle enzymes, as well as Acs2p. The existence of this complex, coined serine-responsive SAM-containing metabolic enzyme (SESAME), is another example of metabolic enzymes acting in concert to regulate epigenetic marks. The SESAME complex interacts with the Set1 methyltransferase complex, providing the necessary SAM for H3K4 methylation at target genes[121]. Moreover, serine produced by members of the SESAME complex is proposed to activate Pyk1 kinase activity, increasing H3T11 phosphorylation at sites where the SESAME complex is recruited by Set1[121]. It remains to be determined whether an analogous SESAME complex exists in mammalian cells.

Local metabolite production may also influence chromatin-dependent processes beyond transcription, such as the repair of DNA damage. Consistent with this possibility, a recent study implicated nuclear FH in non-homologous end-joining DNA double-strand break repair[122]. Recruitment of FH facilitates localized production of fumarate, which inhibits the activity of the α-KG-dependent lysine-specific demethylase 2B (KDM2B),

resulting in elevated histone H3K36 methylation and DNA repair protein recruitment to double-strand DNA break sites.

By considering these three models, it is clear that metabolic influences on the cancer epigenome can occur through multiple mechanisms. These mechanisms are not mutually exclusive and tumours probably engage all three modes of regulation. The first model (inhibitor metabolite production), is probably the best understood mechanism of regulation in the context of cancer biology at present, owing to intense investigation of the mechanisms through which IDH1 and IDH2 mutations contribute to tumorigenesis. The second model (nutrient sensing-mediated regulation of chromatin) clearly occurs and is altered in tumours, although a mechanistic understanding of how it regulates specific biological processes is lacking. Much more work is needed in this area to elucidate both the sensing mechanisms and how they mediate specific responses. The third model (localized metabolite production) is just beginning to gain attention, as demonstrated by several very recent studies and it seems likely that additional examples of this type of regulation will emerge. As new examples of metabolic regulation of chromatin are studied, considering them in the framework of these three models may help in elucidating the logic and biological functions of such regulation.

Impact on major cell decisions

Despite the evidence that the overall availability of acetyl-CoA levels (or the acetyl-CoA/CoA ratio) can regulate histone acetylation, at this point it may be premature to conclude that this can also directly regulate major cell decisions in a coordinated manner, affecting all cellular compartments. For example, does an increase in this rheostat of metabolism promote cell proliferation, cell death or differentiation? If so, this would imply that drugs that would ultimately increase or decrease acetyl-CoA levels may

regulate such cell decisions that form the foundation of many diseases such as cancer or degenerative diseases. Evidence has emerged that an increase in nuclear acetylation is associated with cell cycle progression and proliferation (FIG. 1.6). As discussed, increased acetyl-CoA levels are associated with increased histone acetylation, proliferation and growth, and a large proportion of acetyl-CoA-responsive genes are involved in cell growth and cell cycle progression[1,112]. Indeed, nuclear acetylation may promote the expression of proliferation genes at the expense of differentiation, at least in certain contexts[4,123]. For example, mouse ESCs have very high levels of acetyl-CoA, which, upon induction of the differentiation process, decrease significantly[124]. A similar fluctuation of acetyl-CoA during differentiation has also been observed recently in human ESCs, which produce acetyl-CoA through glucose metabolism but rapidly suppress this function during differentiation. Loss of pluripotency is associated with decreased glycolytic activity, lowered acetyl-CoA levels and histone deacetylation[123]. In contrast, when acetyl-CoA levels are preserved through exogenous supply of acetate, preserved histone acetylation delays stem cell differentiation[123].

Cell survival and death decisions are also affected by acetyl-CoA availability. Autophagy, a catabolic process that is crucial for organelle quality control and cell survival during metabolic stress, is suppressed by high acetyl-CoA availability. In the nucleus, acetyl-CoA induces histone acetylation and repression of pro- autophagic genes[125]. Additionally, high cytoplasmic levels of acetyl-CoA suppress autophagy in a p300-dependent manner[126] (FIG. 1.6). Furthermore, organelle-specific depletion of acetyl-CoA owing to loss of function of the transporter responsible for the import of acetyl-CoA into the ER, which is crucial for lysine acetylation of proteins in the ER, induces autophagy[127]. Interestingly, low levels of acetyl-CoA are also associated with protection

against pro-apoptotic stimuli. The anti-apoptotic protein BCL-XL (also known as BCL2L1) suppresses acetyl-CoA levels and N-terminal acetylation of caspase 2, promoting cell survival[21,128]. Alterations in metabolite availability for chromatin modification during ageing may also have a role in modulating the survival of whole organisms. At mid-life, flies (Drosophila melanogaster) were found to exhibit increased ATP-citrate lyase (termed ATPCL in flies) activity, acetyl-CoA levels and levels of acetylation on several histone lysines compared with young flies. Interfering with ATPCL or the acetyltransferase Chameau extended lifespan[129]. The evidence is mounting that acetyl-CoA levels are important regulators of major cellular decisions, spanning the fate of individual stem cells to the life expectancy of an entire organism.

The global effects of methylation are more difficult to interpret given the interplay between histone and DNA methylation, that is, overall hypomethylation in cancer, but increased methylation of CpG islands. In ESCs, maintaining an elevated α-KG/succinate ratio decreases suppressive methylation marks on DNA and histones, which promotes pluripotency[101]. Methionine metabolism and the availability of SAM also regulate stem cell differentiation and the transition from naive to primed ESCs[130–132]. Tumours exhibiting hypermethylation, including those with IDH and SDH mutations, are associated with poorly differentiated gene expression profiles[93,94,96,100,133,134] (FIG. 1.6). Moreover, interfering with either 2-HG production or DNA methylation promotes differentiation in the context of IDH mutation[134–138]. It has recently emerged that disruption of demethylation also promotes carcinogenesis at least in part through regulation of chromatin structure. In IDH-mutant glioma, hypermethylation of CCCTC binding factor (CTCF) binding sites was shown to result in the loss of CTCF binding and interaction between previously insulated topologically associating domains (TADs). This

enabled a constitutive enhancer to aberrantly interact with and upregulate the oncogene platelet-derived growth factor receptor-α (PDGFRA)[139]. Consistent with recent evidence that conserved CTCF binding sites are frequently mutated in cancer and can affect differentiation and tumorigenesis[140–142], mutations of IDH genes may promote tumour growth by disrupting chromatin structure in addition to methylation patterns in genes and regulatory elements. Thus, metabolic control of demethylation through α-KG participates in maintaining chromatin organization and regulating differentiation processes, both of which are disrupted by the production of inhibitory metabolites such as 2-HG.

Acetylation promotes metabolic rewiring

In addition to histones, acetylation can directly regulate the function or intracellular localization of many proteins that are crucial to carcinogenesis (FIG. 1.7). For example, acetylation seems to directly promote mitochondrial suppression and glycolysis upregulation. Hyperacetylation of mitochondrial enzymes owing to loss of sirtuin 3 (SIRT3) has been shown to predispose rodents to cancer as well as other proliferative diseases in animals and humans, such as pulmonary arterial hypertension[143–145]. Acetylation can suppress mitochondrial function by several mechanisms: inhibition of the production of acetyl-CoA-producing pathways such as PDC[87] and β-oxidation[146,147]; inhibition of the activity of Krebs cycle enzymes like IDH2[148] and SDH[149,150]; suppression of complex I of the electron transport chain[151] and dismutation of superoxide by mitochondrial super-oxide dismutase (MnSOD; also known as SOD2)[152]; and increase in the nuclear transcriptional activity of the HIF1α–aryl hydrocarbon receptor nuclear translocator (ARNT) complex[153], which subsequently suppresses mitochondria by several mechanisms including upregulation of PDK[154]. As acetylation inhibits PDC by promoting the recruitment of PDK, and PDK is not found in the nuclear fraction of PDC,

this may be an escape mechanism by which PDC is able to produce acetyl-CoA in the nucleus without inhibiting itself. However, mitochondrial suppression may be offset by competing mitogenic transcription factors, as acetylation inhibits peroxisome proliferator-activated receptor-γ co-activator 1α (PGC1α) but activates nuclear respiratory factor 1 (NRF1) and NRF2 (also known as NFE2L2)[155,156]. Similarly, acetylation has opposing effects on HIF1 and HIF2 (activating HIF1 and inhibiting HIF2). These transcription factors are known to have different roles in the cell, with HIF1 pre- dominantly mediating the effect of hypoxic signalling on tumour metabolism[157]. Thus, the overall effect of acetylation is likely to be cell type specific or context specific.

Acetylation in the cytoplasm also promotes the trans- location of several glycolytic enzymes to the nucleus where they are proposed to 'moonlight' as transcriptional regulators in proliferative states, for example, glyceraldehyde 3-phosphate dehydrogenase (GAPDH)[158,159] and PKM2[160], as well as the nuclear accumulation or increased activity of pro-proliferative transcription factors such as MYC[161–163] and signal transducer and activator of transcription 3 (STAT3)[164]. The mTOR complex 2 (mTORC2) member, rapamycin-insensitive companion of mTOR (RICTOR) can also be acetylated in a metabolically responsive manner, promoting resistance to cancer therapies[165]. Acetylation in the cytoplasm may also redirect carbon sources towards biomass generation by increasing the production of nucleosides by the pentose phosphate pathway (PPP) through stimulation of the activity of 6-phosphogluconate dehydrogenase (PGD)[166,167].

Importantly, ACLY itself can be acetylated in a glucose-sensitive manner, promoting its stability[168]. This increase in ACLY activity increases generation of lipogenic acetyl-CoA

in tumour cells from citrate derived from either the Krebs cycle or the reductive glutamine pathway, which is upregulated in cancer[68,69]. Conversely, ACSS2 is deacetylated and activated by SIRT1, potentially providing a compensatory source of cytosolic acetyl-CoA under low-nutrient conditions[169].

Conversely, acetylation of p53 in response to DNA damage and tubulin acetylation are insensitive to silencing of ACLY or PDC, suggesting that modulating nuclear–cytosolic acetyl-CoA availability alone does not have a global impact on all cytoplasmic protein acetylation[4,66]. Identifying nuclear and cytoplasmic proteins that are acetylated in an acetyl-CoA-dependent manner will be a considerable step towards understanding how many cellular and molecular events respond to changes in nutrient availability.

Translational implications

Although cancer metabolism and epigenetic mechanisms, particularly histone acetylation, have independently been the focus of intensive efforts for drug development, many of which are in clinical trials, the presence of a metabolism–epigenome axis may have several important translational implications. For example, the effects of inhibitors that target metabolic pathways may reach epigenetic mechanisms and alter the levels of many gene products, beyond what their direct metabolic effects would have predicted. Thus the interpretation of their effects now needs to consider epigenetic mechanisms.

Drug specificity may be increased by considering the targeting of histone modifications in a condition-specific manner. For example, loss of the 9p21 tumour suppressor locus, one of the most common deletion events in cancer, has recently been shown to cause deregulated methionine metabolism owing to deletion of the gene encoding the enzyme methylthioadenosine phosphorylase (MTAP)[170–172]. Importantly, these MTAP-deficient cancer cells are now sensitized to inhibition of the protein arginine N-methyltransferase 5

(PRMT5), opening a new therapeutic opportunity based on this interaction of methionine metabolism and the epigenome[170–172].

Given the direct effects of the nuclear acetyl-CoA producers on histone acetylation, inhibitors of ACLY, ACSS2 and PDC may now be seen as perhaps a new class of drugs that target the metabolism–epigenome axis, compared with their current approach as metabolic modulators. Several of these drugs under development (previously or currently) include the ACLY inhibitors SB-204990 (pre- clinical)[173,174], BMS-303141 (preclinical)[175], ETC-1002 (phase II clinical trial)[176–178], and hydroxycitrate (phase IV clinical trial)[179,180] and the ACSS2 inhibitor, N-(2,3-di-2-thienyl-6-quinoxalinyl)-N´-(2-methoxyethyl)urea (pre-clinical)[70]. Following preclinical studies, the PDC activator dichloroacetate (DCA) which activates PDC by inhibiting PDK20, has entered clinical development in phase I clinical trials in cancer[181–183]. By increasing the activity of the Krebs cycle, DCA can increase acetyl-CoA production in the mitochondria and cytoplasm. However, at least in some cancers, PDK, despite forming a complex with PDC in mitochondria, does not follow the translocation of PDC to the nucleus[4], suggesting that nuclear PDC may be constitutively active or ‘immune’ to DCA. In contrast, as PDC is directly inhibited by tyrosine kinases (TKs), TK inhibitors may activate both mitochondrial and nuclear PDC[86,88,184].

The conflicting results in the efficacy of KDAC inhibitors in cancer treatment may be because many of these inhibitors target multiple KDACs instead of a single target and histone remodelling is heterogeneous depending on context, tissue and cancer type[185–187]. Moreover, the large number of acetylated proteins in addition to histones adds to the complexity of responses to KDAC inhibition. Further investigation is needed to clarify

contexts for effective use of existing KDAC inhibitors, as well as for development of more effective and specific drugs.

The consideration of a metabolism–epigenome axis may alter the way we approach biomarker studies in cancer (BOX 1). For example, metabolomic studies should be considered in parallel with transcriptomic studies under the same experimental conditions. Several parameters that take into account dietary intake are controlled in metabolomic studies, but currently this is not typically done in transcriptomic studies from human specimens, potentially influencing the accuracy and variability in these studies. Notably, it has been shown that serum methionine levels in humans are variable between individuals over a range that could affect histone methylation; moreover, approximately 30% of the variation in methionine concentration is explained by dietary factors[111].

Box 1 | The metabolism–epigenetics axis and its systemic effects on multi-organ organisms in vivo

Most of the discussion in this Review is focused on the regulation of the metabolism–epigenome axis in a single cell. In complex organisms, additional levels of complexity are likely to be activated to optimize and synchronize energy use with growth, perhaps via the circadian rhythm machinery and peripheral clocks, which are closely linked to metabolism and acetylation[353,354]. Starvation reduces acetyl-CoA and protein acetylation levels in several organs, including the heart and muscle. This is prevented by strategies that promote acetyl-CoA production: for example, the pyruvate dehydrogenase complex (PDC) activator dichloroacetate (DCA)[126]. However, starvation does not affect acetyl-CoA levels in the brain[126] although it increases acetyl-CoA and protein acetylation levels in the liver[355]. Circulating ketone bodies produced by one organ, for example, the liver under starvation, may regulate acetylation mechanisms in other organs and may be involved in the explanation of these organ-specific effects. For example, β-hydroxybutyrate can inhibit several lysine deacetylases (KDACs)[63]. In addition, alternative sources of acetyl-CoA exist in specific cell types such as neurons, which can generate acetyl-CoA through β-hydroxybutyrate[356], or hepatocytes, which can generate acetyl-CoA from ethanol[357]. These data underlie the importance of recognizing that often acetyl-CoA homeostasis mechanisms can be context, cell type or organ specific. This needs to be considered in the studies of cancers arising from different organs or in the interpretation of the global effects of cancer therapies or metabolic modulators on the metabolism–epigenetic axis in the whole organism. Similarly, dysregulation of metabolic homeostasis is likely to prove important in our understanding of cancer cachexia.

Conclusions and perspectives

Although considerable progress has been made in understanding the link between metabolism and epigenetics, several outstanding questions remain. The list of metabolic

enzymes present in the nucleus has grown extensively in recent years. As more metabolic enzymes are identified in the nucleus, understanding their role in this compartment will be crucial in elucidating the links between metabolism and epigenetic regulation. Of particular importance, many of these nuclear metabolic enzymes function in complex with one or multiple other proteins. Thus, uncovering interacting partners of metabolic enzymes in the nucleus will be telling with regard to their function. Additionally, although we have focused here on metabolic enzymes that use their metabolic activity to produce substrates for chromatin modification, several metabolic enzymes have been reported to use alternative, non-metabolic functions in the nucleus; distinguishing metabolic and other moonlighting functions of these enzymes is crucial to understanding their biological roles in the nucleus. Lastly, although many metabolic enzymes have now been found in the nucleus, how they arrive there remains unclear, as many lack a canonical nuclear localization sequence.

Metabolic rewiring in cancer affects the epigenome in a manner that facilitates tumour development and/or progression. Furthering our understanding of the roles of metabolic enzymes in affecting epigenetics and cell fate decisions has great potential to lead to novel strategies to battle cancer.

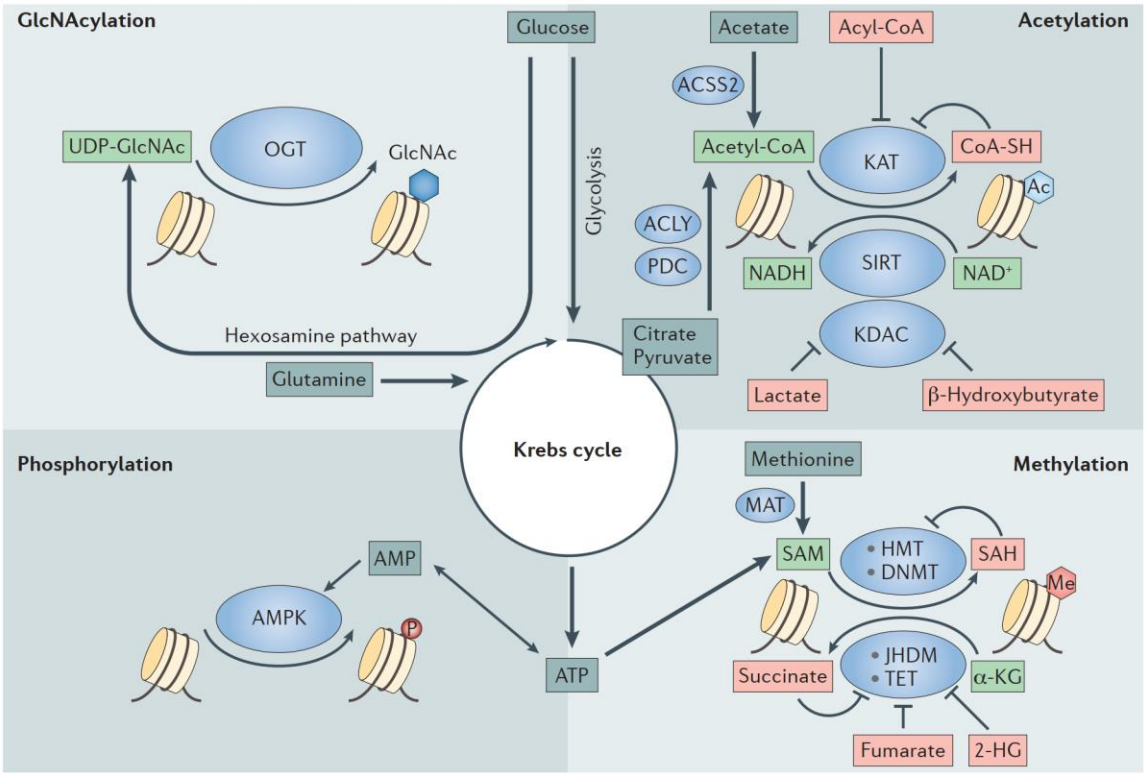

Figure 1.2 | Histone code writers require metabolites as ink to write epigenetic marks.

N-Acetylglucosamination (GlcNAcylation) by O-GlcNAc transferase (OGT) uses the metabolite UDP-glucosamine (UDP-GlcNAc) synthesized by the hexosamine biosynthetic pathway from inputs such as glucose and glutamine (top left). Acetylation uses the metabolite acetyl-CoA, which is synthesized in the cytoplasm and nucleus from acetate, citrate or pyruvate by acyl-CoA synthetase short-chain family member 2 (ACSS2), ATP-citrate lyase (ACLY) and pyruvate dehydrogenase complex (PDC), respectively. The lysine acetyltransferase (KAT) reaction releases CoA-SH, a product that can inhibit these enzymes. Certain fatty acyl-CoAs have also been shown to inhibit KAT enzymes (top right). Lactate, a glycolytic product, and β-hydroxybutyrate, a ketone body, have been identified as endogenous lysine deacetylase (KDAC) inhibitors. S-Adenosylmethionine (SAM), synthesized from the essential amino acid methionine and ATP by methionine adenosyltransferase (MAT) enzymes, is the substrate for histone methyltransferases (HMTs) and DNA methyltransferases (DNMTs), resulting in the production of S-adenosylhomocysteine (SAH), which in turn can inhibit HMTs and DNMTs. Other metabolites, such as fumarate, succinate and 2-hydroxyglutarate (2-HG), have been identified as inhibitors of Jumonji-C (JMJC) domain-containing histone demethylases (JHDMs) and TET demethylases, which rely on the structurally similar metabolite α-ketoglutarate (α-KG) as a co-substrate (bottom right). Energetic stress can also affect epigenetic regulation by activating AMP-activated protein kinase (AMPK), leading to stress-induced histone phosphorylation (bottom left). SIRT, sirtuin.

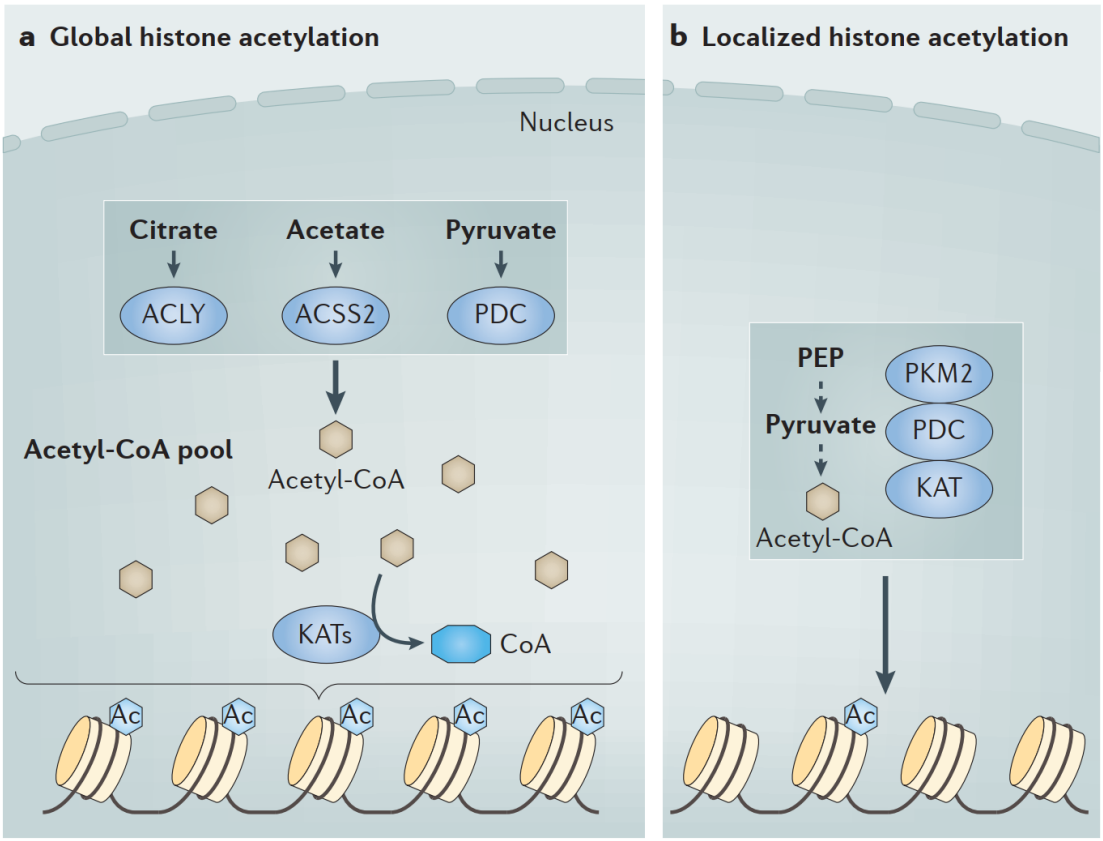

Figure 1.3 | Histone acetylation may be mediated by global or local production of acetyl-CoA.

a, Nuclear acetyl-CoA producers ATP-citrate lyase (ACLY), acyl-CoA synthetase short-chain family member 2 (ACSS2) and pyruvate dehydrogenase complex (PDC) create pools of acetyl-CoA that can be accessed non-specifically by lysine acetyltransferases (KATs) in the nuclear domain.

b, Acetyl-CoA is generated locally in a subnuclear domain by a complex of proteins that directly link production of acetyl-CoA (that is, pyruvate kinase M2 (PKM2)) with acetyl-CoA production (that is, PDC) with a KAT to locally acetylate specific histone targets. Ac, acetylation; PEP, phosphoenolpyruvate.

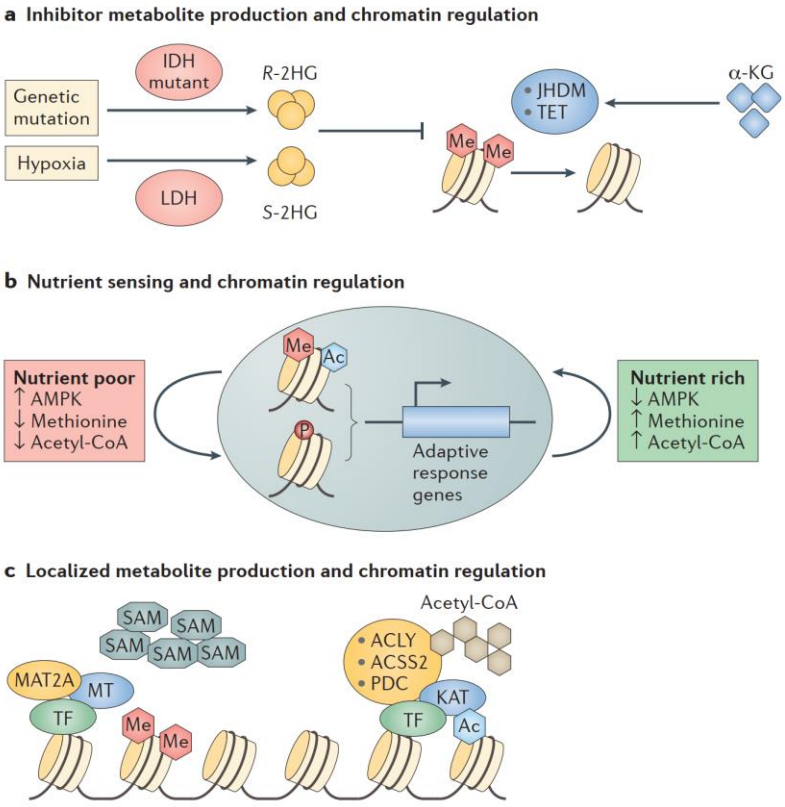

Figure 1.4 | Models of coordination between metabolism and the epigenome.

a, Model 1: inhibitor metabolite production and chromatin regulation. The production of inhibitor metabolites such as R-2-hydroxyglutarate (R-2HG) and S-2HG by mutant isocitrate dehydrogenase (IDH) and promiscuous lactate dehydrogenase (LDH) activity, respectively, increases histone and DNA methylation by competitively inhibiting the α‑ketoglutarate (α-KG)-dependent Jumonji-C (JMJC) domain-containing histone demethylases (JHDMs) and TET demethylases.
b, Model 2: nutrient sensing and chromatin regulation. The availability of metabolites used as the ink for histone writers fluctuates based on the energy status of the cell. For example, a nutrient-poor cell may have activation of AMP-activated protein kinase (AMPK) and a reduction in methionine and acetyl-CoA levels, leading to altered expression of adaptive response genes owing to changes in the phosphorylation (P), methylation (Me) and acetylation (Ac) of chromatin.
c, Model 3: localized metabolite production and chromatin regulation. Direct recruitment of metabolic enzymes to specific sites on chromatin facilitates site-specific substrate production and histone modification. For example, S-adenosylmethionine (SAM) synthase isoform type 2 (MAT2A) locally produces SAM for histone methylation (Me) at specific sites. Similarly, nuclear ATP-citrate lyase (ACLY), acyl-CoA synthetase short-chain family member 2 (ACSS2) and pyruvate dehydrogenase complex (PDC) locally generate acetyl-CoA to be used by lysine acetyltransferases (KATs) to acetylate (Ac) histones, resulting in regulation of specific genes. MT, methyltransferase; TF, transcription factor.

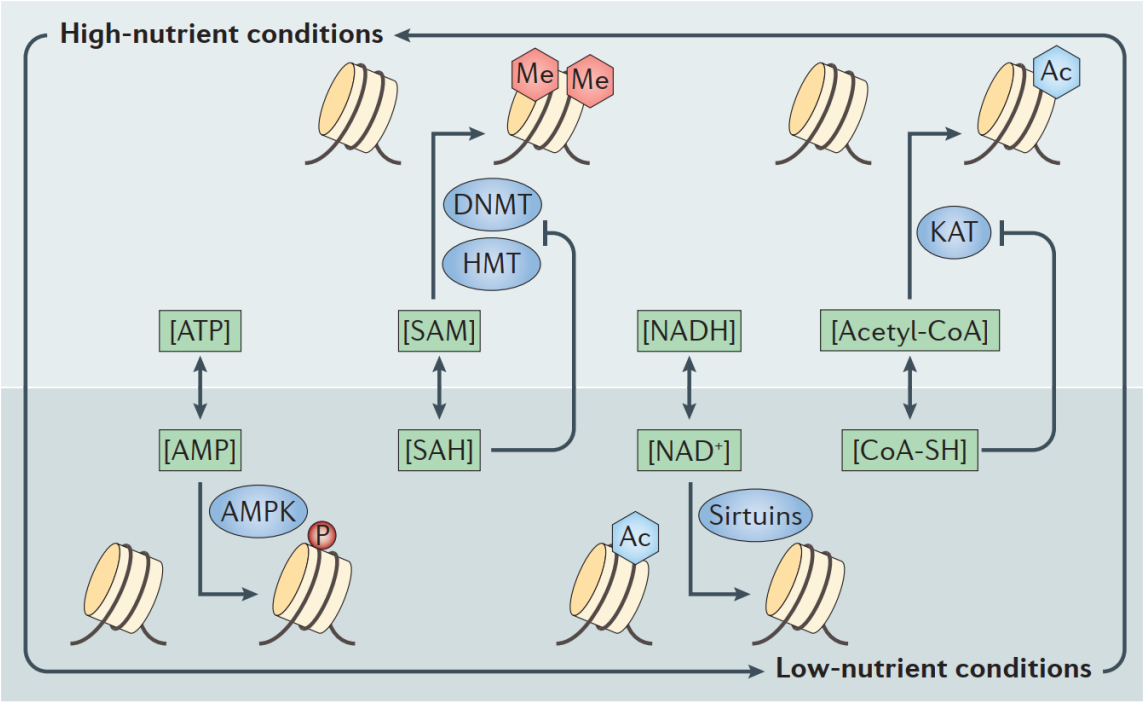

Figure 1.5 | Metabolites as rheostats of cellular nutritional state.
Metabolic state can be conveyed to chromatin through fluctuations in concentrations of several metabolites that are substrates or regulators of chromatin modifiers. Levels of S-adenosylmethionine (SAM) and acetyl-CoA increase in high-nutrient conditions (abundant methionine or glucose, respectively), favouring increased histone methylation and acetylation (top). Under low-nutrient conditions (bottom), AMP levels rise, activating AMP-activated protein kinase (AMPK) and inducing targeted histone phosphorylation. NAD+ levels also rise under low-nutrient conditions, leading to the activation of sirtuin deacetylases. Furthermore, levels of product metabolites S-adenosylhomocysteine (SAH) and CoA may increase with nutrient limitation in a context-dependent manner, feeding back to inhibit methyltransferases and acetyltransferases, respectively. These feedback mechanisms enable cells to dynamically modulate their chromatin modification landscape in response to metabolic conditions. Ac, acetylation; DNMT, DNA methyltransferase; HMT, histone methyltransferase; KAT, lysine acetyltransferase; Me, methylation; P, phosphorylation.

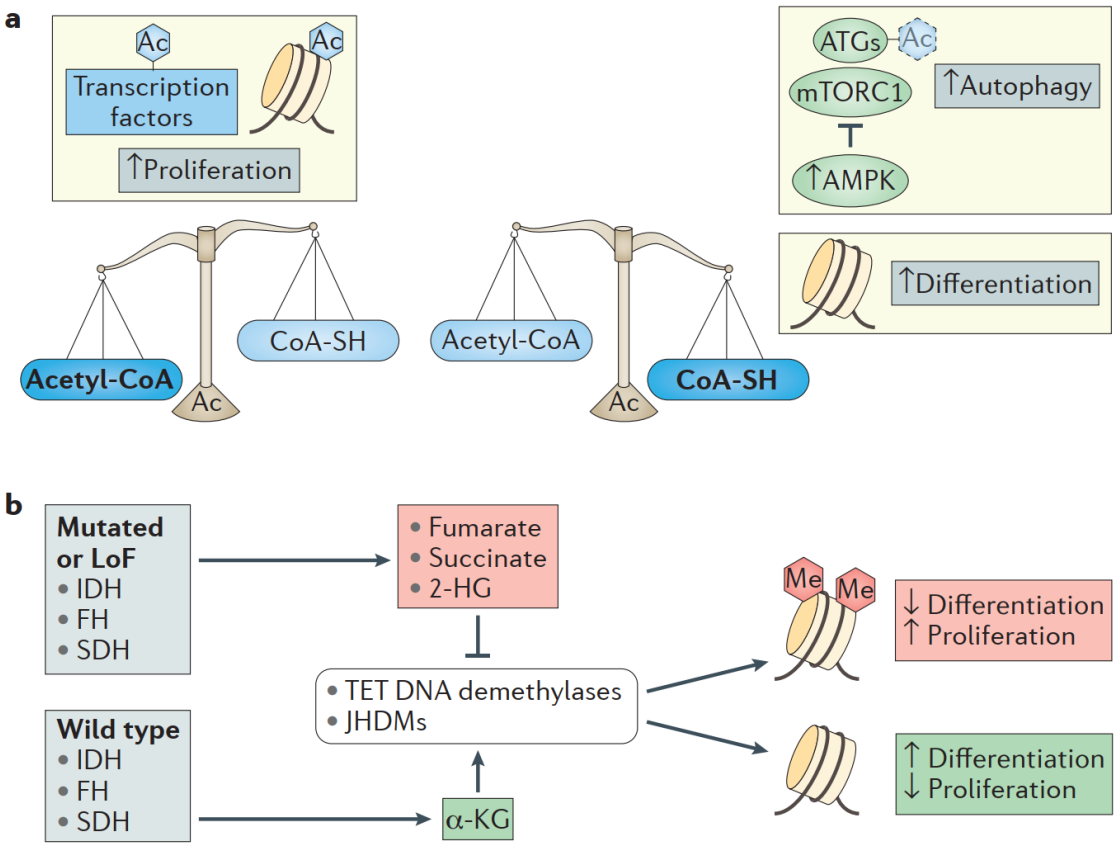

Figure 1.6 | The metabolic–epigenome axis regulates major cell decisions.
a, A high acetyl-CoA/CoA-SH ratio promotes the acetylation (Ac) of histones and transcription factors involved in proliferation. Conversely, reduction in the acetyl-CoA/CoA-SH ratio and thus histone deacetylation signals a change from proliferation to differentiation. Depletion of acetyl-CoA favours the deacetylated, active versions of proteins involved in autophagy (autophagy-related genes (ATGs)), and an AMP-activated protein kinase (AMPK)-dependent inhibition of mTOR complex 1 (mTORC1), causing activation of several enzymes crucial for the biogenesis of autophagosomes.
b, Increased histone and DNA methylation (Me) due to inhibition of histone and DNA demethylases by fumarate, succinate and 2-hydroxyglutarate (2-HG) (from loss-of-function (LoF) or mutant isocitrate dehydrogenase (IDH), fumarate hydratase (FH) and succinate dehydrogenase (SDH)) promotes proliferation over differentiation. Conversely, histone and DNA demethylation stimulated by production of the demethylase reaction cofactor α-ketoglutarate (α-KG) promotes pluripotency. JHDM, Jumonji-C domain-containing histone demethylases.

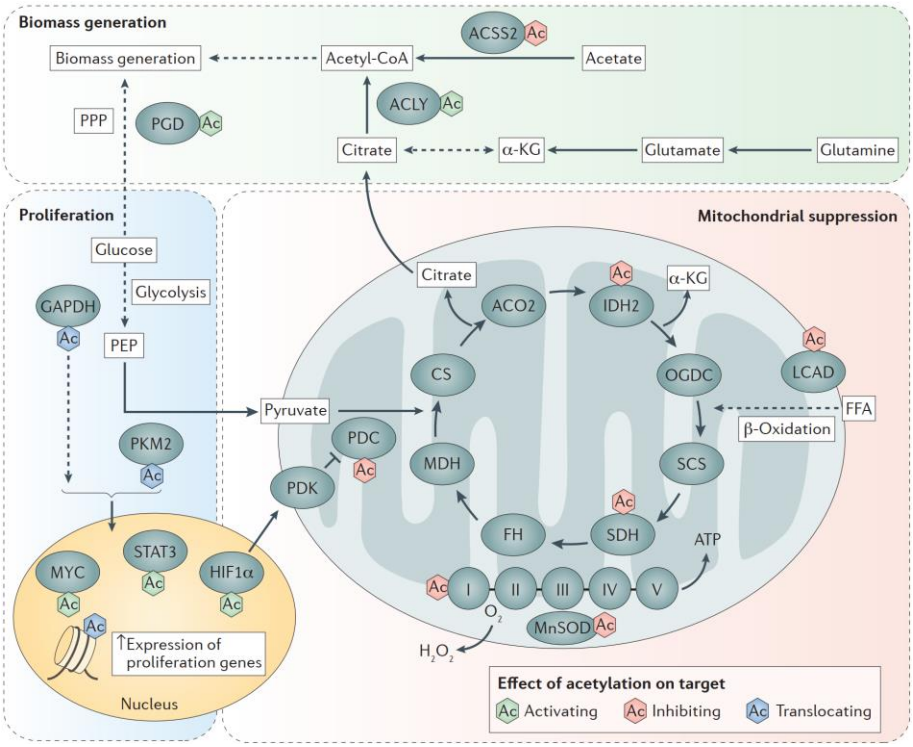

Figure 1.7 | Acetylation promotes molecular and metabolic rewiring in cancer.

Acetylation (Ac) of proteins may activate, inhibit or promote their translocation to a different subcellular compartment. Mitochondrial suppression: acetylation globally suppresses mitochondria by inhibiting the Krebs cycle enzymes isocitrate dehydrogenase 2 (IDH2) and succinate dehydrogenase (SDH) as well as complex I (I) in the electron transport chain and mitochondrial superoxide dismutase (MnSOD). Furthermore, acetylation prevents the entry of acetyl-CoA into the Krebs cycle by inhibiting β‑oxidation (inhibition of long-chain acyl-CoA dehydrogenase (LCAD)) and glucose oxidation (inhibition of pyruvate dehydrogenase complex (PDC)), which is potentiated by the upregulation of PDC inhibitor pyruvate dehydrogenase kinase (PDK) secondary to activating acetylation of hypoxia-inducible factor 1α (HIF1α) in the nucleus. Proliferation: acetylation of glyceraldehyde 3-phosphate dehydrogenase (GAPDH) and pyruvate kinase M2 (PKM2) promotes the nuclear translocation and moonlighting of these glycolytic enzymes, whereby they join MYC and signal transducer and activator of transcription 3 (STAT3) (each activated by acetylation in the nucleus) to promote proliferation. Biomass generation: in the cytoplasm, acetylation activates ATP-citrate lyase (ACLY) to generate lipogenic acetyl-CoA from citrate derived from both the Krebs cycle and the reductive glutamine pathway, while reducing acetyl-CoA derived from acetate by inhibiting acyl-CoA synthetase short-chain family member 2 (ACSS2). Also in the cytoplasm, acetylation activates 6-phosphogluconate dehydrogenase (PGD) in the anabolic pentose phosphate pathway (PPP) to produce NADPH and nucleoside precursors. Thus, a global increase in acetylation is associated with suppression of mitochondria and a proliferative phenotype, a fact that may be applicable to other proliferative diseases, beyond cancer. ACO2, aconitase 2; α-KG, α‑ketoglutarate; CS, citrate synthase; FFA, free fatty acid; FH, fumarate hydratase; MDH, malate dehydrogenase; OGDC, oxoglutarate dehydrogenase complex; SCS, succinyl-CoA synthetase.

Acetyl-CoA production provides the substrate for *de novo* lipogenesis.

In addition to its role as a substrate for histone and non-histone protein acetylation, acetyl-CoA is also the substrate for *de novo* lipogenesis (DNL), which is the intracellular synthesis of lipids such as fatty acids and sterols (Figure 1.1, Figure 1.8).

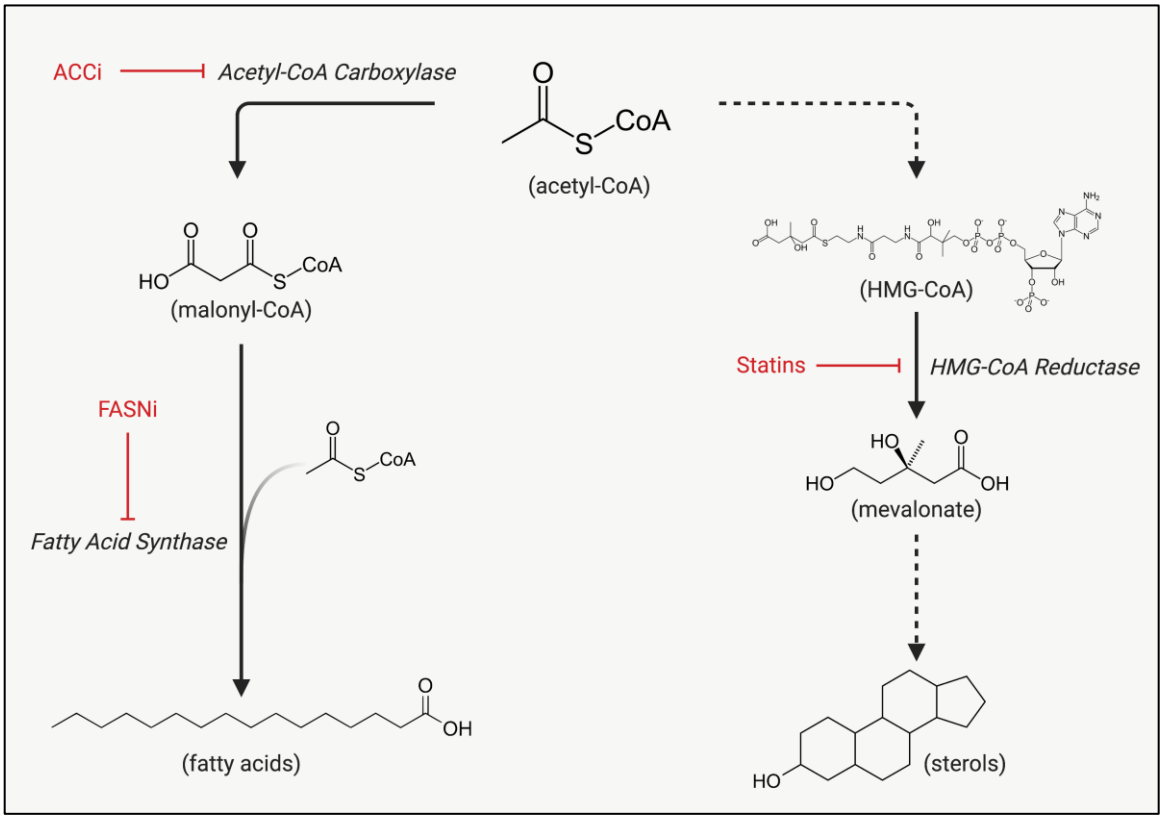

Figure 1.8 | Nuclear-cytosolic acetyl-CoA is required for de novo lipogenesis.
ACLY and ACSS2 synthesize nuclear-cytosolic acetyl-CoA, which is further metabolized into malonyl-CoA by acetyl-CoA carboxylase (ACC). Fatty acid synthase (FASN) utilizes acetyl-CoA and multiple malonyl-CoA molecules to synthesize nascent fatty acids, such as palmitic acid. Acetyl-CoA can also be metabolized into HMG-CoA, which is converted into mevalonate for sterol synthesis. Inhibitors of these reactions that have been used in human patients are indicated.

During fatty acid synthesis, nutrients such as carbohydrates or amino acids are broken down into acetyl-CoA, and following export from the mitochondria, acetyl-CoA is metabolized into malonyl-CoA by Acetyl-CoA Carboxylase (ACC) at the rate-limiting step of fatty acid synthesis[188]. Subsequently, Fatty Acid Synthase (FASN) utilizes acetyl-CoA and multiple molecules of malonyl-CoA to produce nascent fatty acids. These fatty acids can be further modified into more complex lipids, which often play structural roles within cellular membranes[189]. At the organismal level, fatty acid synthesis is thought to be an energy storage process, whereby excess nutrients are broken down and converted into fatty acids for storage as triglycerides in lipid droplets[190]. As such, many nutrients activate molecular signals that promote production of lipogenic acetyl-CoA and downstream lipid products. These signals can be at the transcriptional or post-translational levels. For instance, the transcription factor Sterol Regulatory Element Binding Protein 1 (SREBP-1) is activated downstream of insulin signaling following carbohydrate consumption[191]. SREBP-1 promotes the transcription of lipogenic enzymes such as ACLY, ACC, and FASN, among others[192]. At the post-translational level, production of lipogenic acetyl-CoA and malonyl-CoA are tightly regulated. For instance, ACLY is phosphorylated downstream of insulin action by the kinase AKT, resulting in a several-fold induction of activity[84,85,193]. Additionally, ACLY has been reported to be phosphorylated by the Branch Chain Ketoacid Dehydrogenase Kinase (BCKDK)[194], which also regulates amino acid catabolism, thereby linking the two processes. Conversely, ACC is negatively regulated by phosphorylation downstream of the energy stress sensor, AMPK[195,196]. Importantly, malonyl-CoA is itself a negative regulator of fatty acid catabolism through its interaction with Carnitine Palmitoyltransferase 1 (CPT1)[197]. Thus, the balance between nutrient catabolism for energy production and anabolism for

energy storage can be tightly regulated. When this balance is disrupted, lipid accumulation in adipose tissue, as well as ectopic lipid deposition, can occur, resulting in obesity, insulin resistance, and other metabolic diseases[198]. In many cancers, DNL is markedly elevated, a phenomenon believed to support biogenesis of cellular membrane for rapid cell division[199,200]. As such, inhibitors of ACC and FASN are being investigated as therapeutic target for treatment of cancer and metabolic diseases, and have reached various stages of clinical trials[201–204].

In addition to fatty acids, sterols comprise another major lipid fate of acetyl-CoA. Sterols are a product of the mevalonate pathway, a multistep process in which acetyl-CoA is converted into 3-hydroxy-3-methylglutaryl-CoA (HMG-CoA). HMG-CoA is then metabolized into mevalonate by the enzyme HMG-CoA Reductase (HMGCR) in what is considered the rate-limiting step of the mevalonate pathway, and is also the mechanistic target of the statin class of drugs (Figure 1.8). Like fatty acids and their derivatives, sterols are also an important component of intracellular lipid pools due to their role in maintaining fluidity of cellular membranes[189]. As such, cholesterol synthesis is also frequently deregulated in diseases such as cancer[205]. This can be achieved through activation of the transcription factor SREBP-2, which controls the expression of cholesterol biosynthetic and uptake genes[192]. Unlike SREBP-1 which is stimulated by nutrient availability, SREBP-2 is regulated by a sterol feedback mechanism in which high levels of cholesterol prevent its activation, thereby ensuring its activation when cholesterol is in demand[206].

Among tissues in mammals, the liver and adipose tissues display the highest levels of DNL[207]. At normal levels in these tissues, DNL helps to maintain lipid homeostasis in

tissues and circulation. However, improperly regulated DNL serves an important role in promoting both cancer and metabolic diseases, particularly in the liver, as discussed below.

Role of *de novo lipogenesis* and ACLY in hepatic maladies.

Liver cancer is now the fifth most common cancer worldwide with over half a million new cases diagnosed each year[208]. Hepatocellular carcinoma (HCC) is the most common cancerous malignancy of the liver, accounting for up to 90% of all primary liver cancers[209]. HCC incidence in the United States has increased over 3-fold since the 1970s[208,210], and is one of the fastest rising causes of cancer deaths in the United States, owing to a poor 5-year survival rate of 17%[211]. This is largely due to the fact that most HCC patients are diagnosed at advanced stages of disease when treatment options are limited. Moreover, HCC does not present with a predominant oncogenic driver in patients, which is an obstacle towards developing targeted therapies[212,213]. This lack of a defined oncogenic driver reflects the multitude of causes linked to HCC. In many countries, fibrosis resulting from hepatitis B and C virus infection remains the most significant identifiable cause of HCC[209]. However, epidemiological evidence from the United States and many other Western countries estimates that up to 40% of HCC cases present without viral origins[214,215], highlighting the need to identify and understand non-viral causes of HCC. One such cause linked to HCC is the growing epidemic of metabolic syndrome.

Metabolic syndrome is an umbrella term for a collection of metabolic diseases including obesity, diabetes, and dyslipidemia. Over one third of the United States population fits the criteria for metabolic syndrome, and over two thirds are considered overweight or

obese[216,217], underscoring the significant public health challenge presented by these diseases. Obesity has been implicated in increasing the risk of death from multiple cancer types, including liver cancer[218,219]. In addition to obesity, type-2 diabetes mellitus (DM) has also been implicated in increasing cancer risk. Two recent meta-analyses examining the association between DM and HCC from multiple case-control and cohort studies concluded that DM increases the risk of developing HCC and HCC-associated mortality rate by 2 to 2.5-fold[220,221]. In the liver, metabolic syndrome manifests as non-alcoholic fatty liver disease (NAFLD). NAFLD is characterized by excess lipid accumulation in the liver, termed steatosis, and when combined with inflammation eventually progresses to non-alcoholic steatohepatitis (NASH). NASH can progress to fibrosis and cirrhosis, which ultimately gives rise to HCC (Figure 1.9). Patient studies in the United States and other Western countries have linked NAFLD with causing HCC[222,223], and it is projected that NAFLD will soon become the predominant cause of HCC as a result of the obesity epidemic[224]. In light of this, multiple recent studies have shown that high-fat diet-induced obesity can promote HCC development in mice[225–228].

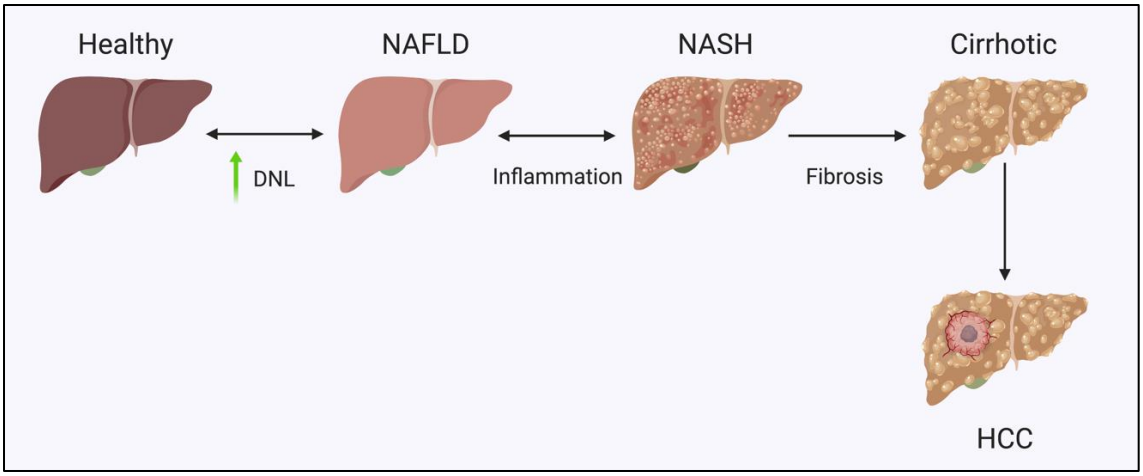

Figure 1.9 | Stage-wise progression of hepatic disease.
Progression from healthy liver to NAFLD is associated with an increase in DNL, followed by inflammatory responses that promotes progression to NASH, fibrosis and ultimately cirrhosis. Hepatocellular carcinomas frequently develop in cirrhotic livers, and there is growing evidence for increased HCC incidence in patients who have not progressed beyond NAFLD or NASH.

De novo lipogenesis links non-alcoholic fatty liver disease and hepatocellular carcinoma

A common molecular feature to NAFLD and HCC is *de novo* lipogenesis of both fatty acids[229,230] and cholesterol[231]. Notably, DNL accounts for roughly a quarter of liver lipid content, and that DNL contributes over two-fold more to liver lipid content in obese patients with severe steatosis than in those with mild steatosis, implicating hepatic DNL as a key contributor to NAFLD development[229,230]. DNL also plays a prominent role in HCC, where it has been shown that expression of lipogenic genes is high compared to healthy liver tissue[232]. High-carbohydrate diets promote DNL by inducing expression of lipogenic genes, and fructose is an even stronger inducer of DNL compared to other carbohydrate sources such as glucose[233,234]. In contrast, high-fat diets actually suppress expression of lipogenic genes[235,236]. Thus, while high-fat diets and high-fructose diets both promote development of NAFLD, the mechanisms by which they do so likely differ. This is supported by studies demonstrating that a high-fructose and fat diet promotes

more liver lipid accumulation than a high-fructose or high-fat diet alone[237]. Epidemiological data shows that between the 1970s and 1990s, consumption of fructose increased by 1000% due to the increased usage of high fructose corn syrup as a food sweetener[238,239]. Fructose has been shown to be a potent promoter of hepatic lipid accumulation and inflammation in rodent and human studies[233,240–246]. While limited in number, studies on dietary fructose and HCC in rodents have shown a pro-tumorigenic role[247,248], though the exact mechanisms behind this require further investigation. Given the growing disease burden spurred by dietary obesity, uncovering the mechanisms by which modern dietary factors promote HCC development will be crucial for effective diagnosis and treatment of this disease.

ACLY levels are dysregulated in metabolic disease of the liver and HCC.

ACLY is highly expressed in metabolic organs such as adipose, pancreas, and liver[249]. ACLY levels in the liver are sensitive to diet and the whole-body metabolic state; high-fat feeding suppresses ACLY levels in the liver and fat tissues[235,236]. In contrast, a high-carbohydrate diet elevates ACLY expression in the liver, but this effect is blunted in diabetic animals[250]. Furthermore, leptin receptor-deficient (*db/db*) mice, an established model for studying obesity and diabetes, display elevated ACLY expression specifically in the liver and not adipose tissues[251]. RNA interference-mediated silencing of *Acly* in livers of (*db/db*) mice suppressed DNL and protected against hepatic lipid accumulation. These data suggest that hepatic ACLY is an important regulator of metabolic function in the liver. Moreover, studies have identified that ACLY is upregulated or activated in HCC[252,253]. Thus, ACLY may be a promising therapeutic target for the treatment and prevention of NAFLD and HCC.

ACLY has been envisioned as a therapeutic target for decades, beginning with the competitive citrate analogue hydroxycitrate[254–258]. ACLY inhibitors decrease serum fatty acid and cholesterol levels in humans, dogs, and rodents[174,176,178,259]. These studies have contributed to the development of a hepatotropic ACLY inhibitor, ETC-1002, that is currently in clinical trials for treatment of dyslipidemia as a statin alternative, and appears to be safe and well-tolerated[176–178,259–261]. However, the use of ETC-1002 as an anti-cancer therapeutic has not been clinically tested to date. A significant hurdle in combating HCC has been identifying effective targeted therapies, with Sorafenib remaining the stand-alone targeted therapy used as a standard of care[212,262]. A key point to note is that the average age of diagnosis for HCC is 65[263], whereas obesity, diabetes and NAFLD are diagnosed throughout adulthood. This suggests that progression to HCC is a prolonged process, which presents a window for therapeutic intervention. Unfortunately, efforts to further understand how ACLY loss affects development of NAFLD, HCC and other hepatic maladies have been hampered because the *Acly* knockout mouse is early embryonic lethal[5]. Thus, whether targeting ACLY is beneficial in treatment of hepatic diseases has remained largely unexplored, and is the question that the following work in this dissertation addresses.

CHAPTER 2: ATP-Citrate Lyase Controls a Glucose-to-Acetate Metabolic Switch[264].

SUMMARY

Mechanisms of metabolic flexibility enable cells to survive under stressful conditions and can thwart therapeutic responses. Acetyl-coenzyme A (CoA) plays central roles in energy production, lipid metabolism, and epigenomic modifications. Here, we show that, upon genetic deletion of Acly, the gene coding for ATP-citrate lyase (ACLY), cells remain viable and proliferate, although at an impaired rate. In the absence of ACLY, cells upregulate ACSS2 and utilize exogenous acetate to provide acetyl-CoA for de novo lipogenesis (DNL) and histone acetylation. A physiological level of acetate is sufficient for cell viability and abundant acetyl-CoA production, although histone acetylation levels remain low in ACLY-deficient cells unless supplemented with high levels of acetate. ACLY-deficient adipocytes accumulate lipid in vivo, exhibit increased acetyl-CoA and malonyl-CoA production from acetate, and display some differences in fatty acid content and synthesis. Together, these data indicate that engagement of acetate metabolism is a crucial, although partial, mechanism of compensation for ACLY deficiency.

INTRODUCTION

Acetyl-coenzyme A (CoA) is a central molecule in cell metabolism, signaling, and epigenetics. It serves crucial roles in energy production, macromolecular biosynthesis, and protein modification[21,265]. Within mitochondria, acetyl-CoA is generated from pyruvate by the pyruvate dehydrogenase complex (PDC), as well as from catabolism of fatty acids and amino acids. To enter the tricarboxylic acid (TCA) cycle, acetyl-CoA condenses with oxaloacetate, producing citrate, a reaction catalyzed by citrate synthase.

Transfer of acetyl-CoA from mitochondria to the cytosol and nucleus involves the export of citrate and its subsequent cleavage by ATP-citrate lyase (ACLY), generating acetyl-CoA and oxaloacetate. This acetyl-CoA is used for a number of important metabolic functions, including synthesis of fatty acids, cholesterol, and nucleotide sugars such as UDP-N-acetylglucosamine. Acetyl-CoA also serves as the acetyl-group donor for both lysine and N-terminal acetylation[21,265]. ACLY plays an important role in regulating histone acetylation levels in diverse mammalian cell types[1,6,113,266].

In addition to ACLY, nuclear-cytosolic acetyl-CoA is produced from acetate by acyl-CoA synthetase short chain family member 2 (ACSS2)[9]. Recent studies have revealed an important role for this enzyme in hypoxia and in some cancers[7,70–74,267]. Acetate can be produced intracellularly by histone deacetylase reactions or can be imported from the environment[265]. Levels of acetate in circulating blood are rather low, ranging from 50 to 200 μM in humans, although acetate concentrations can increase substantially in certain conditions, such as following alcohol consumption, high-fat feeding, or infection, or in specific locations such as the portal vein[268–274]. Acetate is also exported by cells under certain conditions, such as low intracellular pH[34], and thus could potentially be made available for uptake by other cells in the immediate microenvironment. Two additional acetyl-CoA-producing enzymes, the PDC and carnitine acetyltransferase (CrAT), have been reported to be present in the nucleus and to contribute acetyl-CoA for histone acetylation[4,275]. The PDC was shown to translocate from mitochondria to the nucleus under certain conditions, such as growth factor stimulation; within the nucleus, the complex is intact and retains the ability to convert pyruvate to acetyl-CoA[4]. The relative contributions of each of these enzymes to the regulation of histone acetylation

and lipid synthesis, as well as the mechanisms of metabolic flexibility between these enzymes, are poorly understood.

Whole-body loss of ACLY is early embryonic lethal, indicating that it serves non-redundant roles during development[5]. Silencing or inhibition of ACLY suppresses the proliferation of many cancer cell lines and impairs tumor growth[173,276–280]. Depending on the context, ACLY silencing or inhibition can also promote senescence[281], induce differentiation[173], or suppress cancer stemness[282], further pointing to its potential as a target for cancer therapy. Inhibition of ACLY in adult animals and humans is reasonably well tolerated and produces blood lipid-lowering effects[174,176,178]. Thus, there may be a therapeutic window for ACLY inhibition in treatment of cancer and/or metabolic diseases; although the extent to which cells could leverage other compensatory mechanisms upon reduced ACLY function is not clear.

In this study, we aimed to elucidate two questions: first, does use of glucose-derived carbon for fatty acid synthesis and histone acetylation require ACLY; and second, can cells compensate for ACLY deficiency and, if so, by which mechanisms or pathways? To address these questions, we generated a conditional mouse model of *Acly* deficiency (*Acly*$^{f/f}$ mice), as well as immortalized mouse embryonic fibroblast (MEF) cell lines (*Acly*$^{f/f}$ MEFs). As a complement to these models, we used CRISPR-Cas9 genome editing to delete ACLY from human glioblastoma cells. ACLY deficiency in both MEFs and glioblastoma cells potently impaired proliferation and suppressed histone acetylation levels. Both lipid synthesis and histone acetylation from glucose-derived carbon were severely impaired in ACLY-deficient MEFs. Cells partially compensated for the absence of ACLY by upregulating ACSS2, and ACLY-deficient MEFs became dependent on

exogenous acetate for viability. Acetate was used to supply acetyl-CoA for both lipid synthesis and histone acetylation, although global histone acetylation levels remained low unless cells were supplemented with high levels of acetate. ACSS2 upregulation in the absence of ACLY was also observed in vivo upon deletion of *Acly* from adipocytes in mice. *Acly*$^{FAT-/-}$ mice exhibited normal body weight and adipose tissue architecture, and production of acetyl-CoA and malonyl-CoA from acetate was enhanced in ACLY-deficient adipocytes. Upon deuterated-water (D_2O) labeling of wild-type (WT) and *Acly*$^{FAT-/-}$ mice, we observed that de novo synthesized fatty acids were present in white adipose tissue (WAT) in both genotypes, although some differences between depots were apparent. Visceral (epididymal) WAT (VWAT) exhibited no significant differences between WT and *Acly*$^{FAT-/-}$ mice in quantities of de novo synthesized fatty acids, while synthesized saturated fatty acids were reduced in subcutaneous (inguinal) WAT (SWAT) of *Acly*$^{FAT-/-}$ mice. Histone acetylation levels were also significantly altered in *Acly*$^{FAT-/-}$ SWAT. Taken together, this study demonstrates that ACLY is required for glucose-dependent fatty acid synthesis and histone acetylation and that a major, albeit partial, compensatory mechanism for ACLY deficiency involves engagement of acetate metabolism.

RESULTS

Genetic Deletion of *Acly* in Cells Is Consistent with Viability but Impairs Proliferation

To facilitate investigation of the role of ACLY in vitro and in vivo, we generated a conditional mouse model of *Acly* deficiency, using a conventional Cre-lox strategy (*Acly*$^{f/f}$ mice) (Figure S2.1A). MEFs from *Acly*$^{f/f}$ mice were immortalized (*Acly*$^{f/f}$ MEFs). *Acly* was efficiently deleted from *Acly*$^{f/f}$ MEFs upon administration of Cre recombinase (Figure S2.1B). *Acly*$^{\Delta/\Delta}$ MEFs continued to proliferate, although more slowly than parental cells

(Figure S2.1C). However, over time, these cells regained ACLY expression, indicating that deletion occurred in less than 100% of cells and that those that retained ACLY had a growth advantage over *Acly*$^{\Delta/\Delta}$ cells (Figure S2.1B). To address this, we generated three clonal *Acly* knockout (KO) cell lines, designated PC7, PC8, and PC9 (Figure 2.1A). ACSS2 was strikingly upregulated in these cell lines (Figure 2.1A). Proliferation in the absence of ACLY was significantly slower in each of the KO cell lines than in the parental *Acly*$^{f/f}$ cells (Figure 2.1B). We also used CRISPR-Cas9 to delete ACLY from LN229 glioblastoma cells (Figure 2.1C). ACSS2 levels were high at baseline in LN229 cells and only modestly increased with ACLY deletion (Figure 2.1C). However, similar to the ACLY-deficient MEFs, ACLY-deficient LN229 clones exhibited a marked proliferative impairment (Figure 2.1D). Two of the ACLY-KO clones, PC7 and PC9, were reconstituted with wild-type ACLY (ACLY-WT) or a catalytically inactive ACLY mutant (ACLY-H760A) (Figures 2.1E and S2.1D). ACLY-WT, but not ACLY-H760A, significantly restored proliferation in the KO clones (Figures 2.1F and S2.1E). Of note, despite comparable expression upon initial reconstitution (data not shown), ACLY-H760A failed to stably express as highly as ACLY-WT (Figure S2.1D), further pointing to a strong selective advantage for cells expressing catalytically active ACLY. ACSS2 levels were elevated in both the nucleus and cytoplasm of ACLY-deficient cells, and this was reversed upon reconstitution of ACLY-WT (Figure 2.1E). Next, we inquired whether ACSS2 upregulation was induced by ACLY deletion or whether growing up ACLY-deficient clones selected for those that already had high ACSS2 expression. To test this, we examined the timing of ACSS2 upregulation upon loss of ACLY function. In *Acly*$^{f/f}$ MEFs, ACSS2 was rapidly upregulated in parallel to loss of ACLY protein following Cre administration (Figure 2.1G). Moreover, treatment of MEFs with an ACLY inhibitor (BMS-

303141) led to increased ACSS2 within 96 hr (Figure 2.1H). Thus, we conclude that the loss of ACLY activity induces ACSS2 upregulation.

ACLY-Deficient MEFs Require Use of Exogenous Acetate for Viability

The amount of acetate in the serum used in these experiments was quantified by nuclear magnetic resonance (NMR). Undiluted calf serum (CS) contained ~800–900 μM acetate, while acetate was undetectable in dialyzed fetal bovine serum (dFBS) (Figures 2A and S2A). Given that acetate was also undetectable in DMEM, our standard culture conditions (DMEM + 10% CS) exposed cells to slightly less than 100 μM acetate. ACLY-deficient cells began to die when cultured in the absence of exogenous acetate (DMEM + 10% dFBS) (Figures 2.2B–2D), and adding 100 μM acetate was sufficient to restore viability (Figures 2.2C and 2.2E). No added proliferative benefit was gained by further increasing the amount of acetate supplemented (Figure 2.2F). Additionally, reconstitution of ACLY-WT, but not ACLY-H760A, restored the ability of KO cells to grow in acetate-depleted conditions (Figures 2.2B and 2.2E). To test whether acetyl-CoA production by ACSS2 was required for viability, we used CRISPR-Cas9 to delete Acss2 in *Acly*$^{f/f}$ MEFs (Figure S2.2B). Little to no difference in the proliferation rate was observed upon *Acss2* deletion when *Acly* was intact (Figure S2.2C). However, subsequent deletion of *Acly* resulted in extensive toxicity (Figures 2.2G and S2.2D), which was not observed in cells expressing *Acss2*, confirming that cells rely on ACSS2 for survival in the absence of ACLY.

Physiological Levels of Acetate Support Lipid Synthesis in the Absence of ACLY

ACLY deficiency did not alter rates of glucose or glutamine consumption, although lactate and glutamate production were elevated (Figure 2.3A). To confirm the requirement for ACLY for glucose-dependent fatty acid synthesis and test the use of

acetate, we set up parallel stable isotope tracer experiments in which *Acly*$^{f/f}$, PC9, PC9-ACLY-WT, and PC9-ACLY-H760A cells were incubated for 48 hr either with [U-^{13}C]glucose (10 mM) and unlabeled acetate (100 μM) or with [1,2-^{13}C]acetate (100 μM) and unlabeled glucose (10 mM) (Figure 2.3B). In ACLY-proficient cells, palmitate was strongly labeled from glucose-derived carbon, as expected. In PC9 ACLY-KO cells, labeling of palmitate from ^{13}C-glucose was nearly abolished; this could be restored by reconstitution of ACLY-WT but not ACLY-H760A (Figure 2.3C). Conversely, a marked increase in use of acetate for fatty acid synthesis was observed in PC9 and PC9-ACLY-H760A cells (Figure 2.3D). We also examined the use of glucose and acetate carbon for synthesis of HMG (hydroxymethylglutaryl)-CoA, an intermediate in the mevalonate pathway and ketone body synthesis. Again, parental and PC9-ACLY-WT cells used glucose-derived carbon for HMG-CoA synthesis (Figure 2.3E). In the absence of ACLY, glucose carbon use for HMG-CoA synthesis was extremely limited (Figure 2.3E); instead, acetate was used (Figure 2.3F). Total levels of HMG-CoA trended slightly lower in the PC9 cells, though this difference was not statistically significant (Figure 2.3G). The data thus show that, in MEFs, glucose-dependent synthesis of fatty acids and HMG-CoA is nearly completely dependent on ACLY, and a physiological level of acetate can at least partially support lipid synthesis in its absence.

ACLY Is the Primary Supplier of Acetyl-CoA for Maintaining Global Histone Acetylation

Histone acetylation is another major fate of nuclear-cytosolic acetyl-CoA. Consistent with previous data using RNAi-mediated ACLY silencing[1,66], global levels of histone acetylation were strikingly reduced upon genetic deletion of *Acly*, despite increased ACSS2. Moreover, although 100 μM acetate was sufficient to restore survival in dFBS-cultured KO cells, it failed to rescue histone acetylation levels. However, incubating cells

with a high level of acetate (1 mM) markedly increased histone acetylation levels in KO cells (Figure 2.4A). Reciprocally, histone acetylation levels were low in WT MEFs when cultured in 1 mM glucose and increased with greater glucose concentrations. In KO cells, histone acetylation levels were low at all concentrations of glucose tested, up to 25 mM (Figure S2.3A). Reconstitution of PC9 cells with ACLY-WT but not, ACLY-H760A, restored histone acetylation levels to those in the parental cells (Figure 2.4A).

To determine the respective use of glucose- and acetate- derived carbon for histone acetylation in each of the MEF cell lines, we conducted stable isotope tracer experiments under three conditions: (1) [U-^{13}C]glucose (10 mM) and unlabeled acetate (100 μM), (2) physiological [1,2-^{13}C]acetate (100 μM) and unlabeled glucose (10 mM), or (3) high [1,2-^{13}C]acetate (1 mM) and unlabeled glucose (10 mM) (Figure S2.3B). In condition 1, histone acetyl groups were strongly labeled from ^{13}C-glucose in *Acly*$^{f/f}$ and PC9-ACLY-WT cells (Figures 2.4B, 2.4E, and S2.3C). In PC9 and PC9-ACLY-H760A cells, labeling of histone acetyl groups from glucose carbon was severely compromised (Figures 2.4B, 2.4E, and S2.3C). Moreover, aligning with western blot data, total levels of histone acetylation were lower in cells lacking functional ACLY (Figure 2.4E). Thus, the data indicate that ACLY is required for the majority of glucose-dependent histone acetylation. In cells lacking functional ACLY (PC9 and PC9-ACLY-H760A), 100 μM acetate contributed carbon to histone acetylation with ~40%–60% of the acetyl groups derived from acetate after 24-hr labeling (Figure 2.4C), but total acetylation remained low (Figures 2.4F and S2.3D). In 1 mM ^{13}C-acetate, total histone acetylation levels rose (Figures 2.4G and S2.3E), consistent with western blot data, and acetate carbon constituted the majority of histone acetyl groups (Figure 2.4D). These data indicate that ACLY is the dominant supplier of acetyl-CoA for histone acetylation in standard, nutrient-

rich conditions and that, in its absence, cells can use acetate to supply acetyl-CoA for histone acetylation, although high exogenous acetate availability is needed to bring histone acetylation up to levels matching those of ACLY-proficient cells. Of note, high acetate did not produce a corresponding rescue of proliferation (Figure 2.2F). Thus, while ACLY-deficient cells exhibit both slower proliferation and lower histone acetylation levels, histone acetylation can be raised with high acetate without restoration of normal rates of proliferation, supporting the notion that metabolism regulates histone acetylation at least partially independently of proliferation.

We previously defined acetyl-CoA-responsive gene sets in LN229 glioblastoma cells[1]. Cell-cycle- and DNA-replication-related genes were enriched among those genes that were suppressed in low glucose and increased by both glucose and acetate, although only glucose impacted doubling time[1]. As observed in MEFs, ACLY deletion in LN229 cells abolished glucose-dependent regulation of global histone acetylation (Figure S2.4A). Acetate supplementation increased histone acetylation in ACLY null LN229 cells in a dose-dependent manner (Figure S2.4A). Consistently, the ability of glucose to promote expression of proliferation-related genes (*E2F2*, *MCM10*, and *SKP2*) was potently inhibited in ACLY-deficient cells. Expression of these genes exhibited dose-dependent rescue by acetate (Figure S2.4B), correlating with global histone acetylation levels, despite the lack of a proliferation rescue (Figure S2.4C). In addition, we were surprised to find that whole-cell acetyl-CoA levels were minimally impacted in ACLY-KO as compared to WT LN299 cells in high-glucose conditions (Figure S2.4D).

Acetyl-CoA Levels Are Maintained by Acetate in ACLY-Deficient Cells

In prior studies, global histone acetylation levels have tracked closely with cellular acetyl-CoA levels[1,64,112]. It was, therefore, unexpected to find these uncoupled in ACLY-KO

LN229 cells (Figure S2.4D). We further explored this in ACLY-KO MEFs and found that acetyl-CoA levels were significantly higher in the KO cells than in the WT *Acly*$^{f/f}$ cells when cultured in 10 mM glucose and 100 μM acetate (Figure 2.5A). These data suggested either that mitochondrial acetyl-CoA, which is inaccessible for histone acetylation[75], is elevated in ACLY-KO cells or that ACSS2 compensation allows plentiful nuclear-cytosolic acetyl-CoA production from acetate but that this acetate-derived acetyl-CoA is used less effectively than glucose-derived acetyl-CoA for histone acetylation. We reasoned that mitochondrial and extra-mitochondrial acetyl-CoA pools in ACLY KO cells could be distinguished based on whether whole-cell acetyl-CoA is derived from glucose or from acetate (Figure 2.5B). This is because, in the absence of ACLY, glucose carbon does not meaningfully contribute to nuclear-cytosolic acetyl-CoA, as determined by its minimal use for either lipid synthesis or histone acetylation (Figures 2.3 and 2.4). Within mitochondria, both glucose (via PDC) and acetate (via mitochondrial acetyl-CoA synthetases) can be used to generate acetyl-CoA for citrate synthesis. However, as assessed by enrichment of citrate and malate, acetate contributes minimally to mitochondrial metabolism in both WT and KO cells, while glucose is oxidized in both cell lines under these conditions (albeit to a somewhat lesser extent in KO cells) (Figures 2.5C, 2.5D, S2.5A, and S2.5B). These data suggest that, in ACLY-KO cells, any glucose-derived acetyl-CoA is mitochondrial, whereas acetate-derived acetyl-CoA is predominantly nuclear cytosolic (Figure 2.5B). Thus measuring the contribution of glucose and acetate to whole-cell acetyl-CoA should allow us to distinguish whether the increase in acetyl-CoA in ACLY-KO MEFs reflects elevated mitochondrial or extra-mitochondrial acetyl-CoA. Therefore, we incubated cells with [U-^{13}C]glucose (10 mM) and 100 μM unlabeled acetate or, reciprocally, [1,2-^{13}C]acetate (100 μM) and 10 mM

unlabeled glucose. In WT (*Acly*$^{f/f}$) cells, as expected, acetyl-CoA, malonyl-CoA, and succinyl-CoA were more strongly enriched from glucose than acetate (Figures 2.5E–2.5G). Interestingly, despite minimal labeling of malonyl-CoA from acetate in WT cells (consistent with palmitate enrichment in Figure 2.3D), 20% of the acetyl-CoA pool was enriched from ^{13}C-acetate (Figures 2.5E and 2.5F), further hinting at differential partitioning of acetate- and glucose-derived acetyl-CoA. In contrast, in the PC9 ACLY-KO cells, acetyl-CoA was minimally labeled from glucose, and ~80% of the acetyl-CoA pool was labeled from acetate after 6 hr (Figure 2.5E). Malonyl-CoA, but not succinyl-CoA, was also strongly enriched from ^{13}C-acetate in PC9 cells (Figures 2.5F and 2.5G). In sum, these data indicate that acetate is the major source of acetyl-CoA in the absence of ACLY, and it appears to predominantly supply the extra-mitochondrial pool.

A second implication of these data is that, at least in KO cells, the mitochondrial acetyl-CoA pool is likely quite low in comparison to the extra-mitochondrial pool, since acetyl-CoA is minimally labeled from glucose-derived carbon. A large difference in relative acetyl-CoA pool size can explain the apparently paradoxical finding that, in KO cells, citrate is labeled from glucose, despite minimal acetyl-CoA enrichment (Figures 2.5C and 2.5E). This interpretation is consistent with findings from a recent study of the mitochondrial metabolome, which found that matrix acetyl-CoA levels are very low unless complex I is inhibited, which increases the NADH/NAD ratio, reducing the activity of citrate synthase[283]. Notably, another implication of this result is that a much larger nuclear-cytosolic acetyl-CoA pool in cultured cells would explain why whole-cell acetyl-CoA measurements in ACLY-proficient cells correlate closely with histone acetylation levels[1,64]. Together, these data indicate that acetate carbon is used to supply acetyl-CoA for nuclear and cytosolic processes in the absence of ACLY. Nevertheless, histone

acetylation levels remain low in the absence of ACLY unless a high level of acetate is supplied, and proliferation remains constrained even in the presence of high acetate. Thus ACSS2 is a key, but partial, mechanism of compensation for ACLY deficiency.

ACSS2 Is Upregulated In Vivo upon Deletion of Acly from Adipocytes

Finally, we sought to determine whether ACSS2 is upregulated upon loss of ACLY in vivo. Glucose uptake and glucose-dependent lipid synthesis in adipocytes are closely associated with insulin sensitivity and systemic metabolic homeostasis[284,285]. Moreover, our prior work implicated ACLY in regulating histone acetylation levels and expression of key genes in glucose metabolism, such as *Glut4*, in 3T3-L1 adipocytes[66]. To interrogate the role of adipocyte ACLY in vivo, we bred $Acly^{f/f}$ mice to Adiponectin-Cre transgenic mice, which express Cre specifically in adipocytes[286]. ACSS2 was upregulated in SWAT and VWAT upon deletion of *Acly* (Figures 2.6A and 2.6B). In VWAT, ACSS2 upregulation was more apparent at the protein level than the mRNA level (Figures 2.6A and 2.6B). Fatty acid synthase (FASN) protein levels were also elevated in the absence of ACLY, particularly in SWAT (Figure 2.6A). Lipid droplets formed normally in $Acly^{FAT-/-}$ adipocytes; in VWAT, adipocytes were larger than in WT mice, while in SWAT, adipocyte lipid droplet size was comparable between genotypes (Figure 2.6C). Body weight was indistinguishable between WT and $Acly^{FAT-/-}$ mice fed a regular chow diet (Figure 2.6D). However, overall gene expression patterns were altered, with lower expression of adipocyte genes such as *Glut4* in the $Acly^{FAT-/-}$ mice (Figure 2.6E).

Adipocyte Acetyl-CoA and Lipid Metabolism Is Altered in the Absence of ACLY

These data suggested that acetate metabolism might, at least partially, compensate for ACLY deficiency in adipocytes in vivo. Similar to that observed in MEFs, acetyl-CoA levels were higher in both VWAT and SWAT from $Acly^{FAT-/-}$ as compared to WT mice,

while liver acetyl-CoA levels were slightly reduced (Figure 2.7A). To test whether *Acly*$^{FAT-/-}$ adipocytes supply acetyl-CoA and dependent biosynthetic processes using acetate, we isolated primary visceral adipocytes and tested acetate uptake. Indeed, acetyl-CoA, as well as malonyl-CoA and HMG-CoA, were more enriched from [1,2-^{13}C]acetate in primary adipocytes from *Acly*$^{FAT-/-}$ mice as compared to those from WT mice (Figures 2.7B–2.7D).

Next, we investigated the extent to which de novo synthesized fatty acids were present in adipose tissue in the absence of ACLY. To capture rates of de novo lipogenesis (DNL) in vivo, D_2O was administered to mice via a bolus injection and subsequent addition to drinking water for 3 weeks. At the conclusion of labeling VWAT, SWAT, and liver were collected, and total (saponified) fatty acids from each were analyzed by gas chromatography-mass spectrometry (GC-MS). Plasma D_2O enrichment was confirmed to be equivalent between genotypes (Figure S2.6A). In both VWAT and SWAT, abundance of the saturated fatty acids palmitic acid (C16:0) and stearic acid (C18:0) was significantly reduced (Figures S2.6B and S2.6C). Conversely, monounsaturated fatty acids, oleic acid (C18:1n9), and palmitoleic acid (C16:1n7), as well as the essential fatty acid linoleic acid (C18:2n6), were elevated in SWAT from *Acly*$^{FAT-/-}$ mice (Figure S2.6B). A slight reduction in palmitic acid was also observed in liver (Figure S2.6D). Fractional enrichment of fatty acids was not significantly different in VWAT between genotypes, although SWAT exhibited a moderate reduction in palmitic acid fractional synthesis (Figures S2.6E and S2.6F). Fractional synthesis was not different between genotypes in the liver, except for a small reduction for palmitoleic acid (Figure S2.6G).

The relative quantities of de novo synthesized fatty acids present in each tissue were calculated using plasma D_2O enrichment, fatty acid labeling, and abundance. Notably, DNL-derived fatty acids present in WAT may be synthesized in adipocytes or produced in the liver and transported to fat. In the SWAT of *Acly*$^{FAT-/-}$ mice, total de novo synthesized palmitic acid and stearic acid were significantly reduced (Figure 2.7E). In contrast, no significant differences in the quantities of DNL-generated fatty acids were detected between *Acly*$^{FAT-/-}$ and *Acly*$^{f/f}$ mice in VWAT (Figure 2.7F). Liver DNL was largely unchanged by adipocyte ACLY deficiency, although a slight reduction in palmitic acid synthesis was observed (Figure 2.7G). Since DNL-derived fatty acids were reduced in SWAT of *Acly*$^{FAT-/-}$ mice, this depot may maintain lipid droplet size through greater storage of diet-derived fatty acids, as suggested by elevated levels of linoleic acid (Figure S2.6B).

Histone acetylation levels were also analyzed. Despite ACSS2 upregulation and elevated acetyl-CoA levels, H3K9ac and H3K23ac were significantly lower, and H3K18ac trended lower, in the SWAT of *Acly*$^{FAT-/-}$ mice (Figure 2.7H). Interestingly, this difference was not observed in VWAT, suggesting that acetate compensation for ACLY deficiency may be more complete in this depot or that other factors are dominant in determining histone acetylation levels (Figure 2.7I). No differences in histone H3 acetylation were detected in the liver (Figure 2.7J). Altogether, the data suggest that, in vivo, adipocytes lacking ACLY partially compensate by engaging acetate metabolism.

DISCUSSION

The findings of this study demonstrate that ACLY is required for the vast majority of glucose-dependent fatty acid syntheses and histone acetylations under standard culture conditions and that ACSS2 upregulation and use of acetate carbon is a major

mechanism of compensation for ACLY deficiency. Additionally, despite ACSS2 upregulation and higher acetyl-CoA levels, ACLY deficiency results in lower overall histone acetylation levels, slower proliferation, and altered gene expression patterns. The data suggest that ACLY and ACSS2 likely play distinct roles in the regulation of histone acetylation and gene expression but also indicate that the potential for metabolic compensation from acetate should be considered if ACLY is pursued as a therapeutic target. From a clinical perspective, prior study of PET (positron emission tomography) imaging in human hepatocellular carcinoma patients using ^{11}C-acetate and ^{18}F-fluorodeoxyglucose (FDG) revealed a dichotomy between acetate and glucose uptake. Patient tumors, or regions within tumors, with high ^{11}C-acetate uptake demonstrated low ^{18}F-FDG uptake and vice versa. More- over, tumors with high ^{18}F-FDG uptake were more proliferative[287]. These data support the concept that mammalian cells – cancer cells, in particular – possess an intrinsic flexibility in their ability to acquire acetyl-CoA from different sources to adjust to changing metabolic environments in vivo. Further elucidation of the mechanisms connecting ACLY and ACSS2, as well as the differential phenotypes observed downstream of their activity, could point toward synthetic lethal strategies for cancer therapy or improved tumor imaging protocols.

In considering the roles of these enzymes in normal physiology, given the importance of GLUT4-dependent glucose uptake and glucose-dependent fatty acid synthesis for systemic metabolic homeostasis[284,285], deletion of *Acly* in adipocytes results in a surprisingly mild phenotype, with no overt metabolic dysfunction observed for mixed-background mice on a regular chow diet. Nevertheless, larger adipocytes and reduced expression of genes, such as *Glut4*, observed in this model are also characteristic of obesity and are associated with poorer metabolic function. This suggests that *Acly*$^{FAT-/-}$

mice may be more susceptible to metabolic dysfunction when nutritionally stressed, for example, with high fructose feeding. Another interesting question is whether these mice will exhibit exacerbated metabolic phenotypes under conditions that alter acetate availability in the blood- stream, such as ethanol consumption or antibiotic treatment.

The differential impact of ACLY on SWAT and VWAT also warrants further investigation. It is not clear why SWAT, but not VWAT, exhibits reduced histone acetylation and de novo fatty acid synthesis, despite evidence for compensatory mechanisms such as FASN upregulation. One possible explanation relates to an overall greater fraction of fatty acids that are de novo synthesized in SWAT, as compared to VWAT (Figures S2.6E and S2.6F), placing a greater demand for acetyl-CoA. Potentially, in a tissue with a lower DNL rate, acetate may be more readily able to compensate in both DNL and histone acetylation. Distribution of fatty acids in *Acly*$^{FAT-/-}$ WAT depots is also altered; SWAT, in particular, exhibits increased levels of monounsaturated and essential fatty acids (Figure S2.6B). Palmitoleate, which has been implicated as an insulin-sensitizing lipokine[288], is elevated in ACLY-deficient SWAT, raising questions about how altered levels of bioactive lipid species in the absence of ACLY may influence metabolic phenotypes. More mechanistic work is also clearly needed to elucidate the relationship between ACLY and gene regulation. The relationship between global histone acetylation and gene expression is not entirely consistent between VWAT and SWAT, possibly reflecting gene regulatory mechanisms that are specific to ACLY.

A noteworthy observation in this study is that acetyl-CoA and histone acetylation levels appear to become uncoupled in the absence of ACLY, suggesting that acetate-derived acetyl-CoA may not be efficiently used for histone acetylation. Several possible

mechanisms could account for this. First, it may be that, in MEFs, an insufficient amount of ACSS2 is present in the nucleus to efficiently drive histone acetylation. ACSS2 has been found to localize prominently to the nucleus in some conditions[70,76,77]; thus, investigation of whether acetate more readily contributes to overall histone acetylation levels in these contexts will be informative. However, potentially arguing against this possibility, hypoxia promotes ACSS2 nuclear localization[77]; yet, although acetate does regulate histone acetylation in hypoxic cells, a high level of acetate (~2.5 mM) is required[74]. A second possibility is that, within the nucleus, acetyl-CoA producing enzymes are channeled, compartmentalized into niches, or sequestered with particular binding partners. Through such a mechanism, acetylation of specific proteins may be regulated not only by the relevant acetyltransferase but also by a specific acetyl-CoA-producing enzyme. Consistent with this possibility, acetylation of HIF2a was shown to be exclusively dependent on ACSS2 as a source of acetyl-CoA[76,77]. A third possibility is that ACLY-deficient conditions may result in altered lysine acetyltransferase (KAT) or HDAC (histone deacetylase) activity. Finally, a fourth possibility is that lower use of acetyl-CoA for histone acetylation could be a feature of slow proliferation in the absence of ACLY (i.e., secondary to the proliferation defect). However, prior findings that histone acetylation is sensitive to glucose availability over a range that did not impact proliferation[1] and that the TCA cycle (which supplies ACLY substrate citrate) and mitochondrial membrane potential have distinct and separate roles in regulating histone acetylation and proliferation, respectively[289], as well as data in the present article showing that histone acetylation can be boosted by high acetate without a corresponding rescue of proliferation, argue against this as a sole explanation. Nevertheless,

elucidation of the mechanisms that constrain proliferation in the absence of ACLY could help to definitively address this.

Investigating these possibilities will illuminate whether cells possess mechanisms to differentially detect ACLY-generated versus ACSS2-generated acetyl-CoA as well as define the functional relationship between histone acetylation levels and cellular functions and phenotypes. Given that ACLY dominates in nutrient- and oxygen-replete conditions, whereas ACSS2 becomes important in nutrient- and oxygen-poor conditions[73,74], having mechanisms such as different acetylation substrates to distinguish between acetyl-CoA produced by each enzyme could be advantageous to cells. For example, such mechanisms could potentially cue cells to grow when ACLY serves as the acetyl-CoA source and to mediate adaptive responses when ACSS2 is the primary acetyl-CoA source. The roles of these enzymes in gene regulation appear to be complex, and in-depth analysis of the respective roles of ACLY and ACSS2 in genome-wide histone acetylation and acetylation of other protein substrates is needed to begin addressing these questions.

Recent work has shown that the PDC is present in the nucleus and is able to convert pyruvate to acetyl-CoA for use in histone acetylation[4], raising the question of how the findings of the present study can be aligned with the described role of nuclear PDC. We suggest two potential models that are consistent both with our data and with a role for nuclear PDC in histone acetylation. In the first model, ACLY is the primary acetyl-CoA producer for regulation of global levels of histone acetylation, while PDC (and, potentially, other nuclear acetyl-CoA sources such as CrAT) could participate in mediating histone acetylation at specific target genes but not globally. A recent report

that PDC forms a complex with PKM2, p300, and the arylhydrocarbon receptor (AhR) to facilitate histone acetylation at AhR target genes is consistent with such a possibility[120]. In the second model, the role of ACLY in glucose-dependent histone acetylation regulation could be context dependent, with a larger role for PDC emerging in certain conditions or cell types. This possibility is supported by observations that PDC nuclear translocation is stimulated by conditions such as growth factor stimulation and mitochondrial stress[4]. Further investigation will be needed to evaluate these models.

In sum, this study points to a crucial interplay between glucose and acetate metabolism to supply the nuclear-cytosolic acetyl- CoA pool for fatty acid synthesis and histone acetylation. At the same time, it shows that, despite compensatory mechanisms, ACLY is required for optimal proliferation, and simply increasing nuclear-cytosolic acetyl-CoA production is insufficient to fully replace ACLY. This could point to the importance of ACLY's other product, oxaloacetate; a build-up of ACLY's substrate citrate; deficiencies in anapleurosis and/or mitochondrial function upon loss of a major catapleurotic pathway; or a signaling mechanism that is specific to ACLY. Clearly, more work is needed both to understand the mechanisms through which ACLY facilitates cell proliferation and to further define the ways that cells partition and use acetyl-CoA produced by different enzymes. The findings of this study raise a number of important questions for future investigation, as discussed earlier. They also clarify the importance of ACLY in glucose-dependent acetyl-CoA production outside of mitochondria and provide key insights into the mechanisms of metabolic flexibility used for production of nuclear-cytosolic acetyl-CoA. Understanding these compensatory mechanisms will be important to consider for therapeutic targeting of acetyl-CoA metabolic pathways.

EXPERIMENTAL PROCEDURES

Generation of *Acly*$^{f/f}$ and *Acly*$^{FAT-/-}$ Mice

A Knockout First targeting vector was obtained from the Knockout Mouse Project (KOMP) that targets exon 9 of Acly (KOMP: 80097), predicted to result in a truncated protein subject to nonsense-mediated decay. The Knockout First allele is initially null but can be converted to a conditional floxed allele upon Flp recombination[290]. Recombinant 129/B6 hybrid embryonic stem cells (ESCs) were generated in Penn's Gene Targeting Core, and blastocysts were injected at Penn's Transgenic and Chimeric Mouse Core. Upon acquisition of the chimeric mice, animals were bred to obtain germline transmission. *Acly*$^{f/+}$ progenies were selected through sequential breeding with wild-type C57Bl/6J mice (purchased from Jackson Laboratory) and mice expressing Flp recombinase (B6.Cg-Tg(ACTFLPe) 9205Dym/J, Jackson Laboratory). Finally, *Acly*$^{f/f}$ mice were generated by inter- breeding and selected by genotyping (see the Supplemental Information). Immortalized *Acly*$^{f/f}$ MEFs were generated from these mice (see the Supple- mental Information). To produce *Acly*$^{FAT-/-}$ mice, *Acly*$^{f/f}$ mice were bred to adiponectin-Cre transgenic mice (stock no: 010803; B6;FVB-Tg(Adipoq-cre) 1Evdr/J, Jackson Laboratory). The University of Pennsylvania's Institutional Animal Care and Use Committee (IACUC) approved all animal experiments.

In Vivo De Novo Lipogenesis

13-week-old male *Acly*$^{f/f}$ (n = 6) and *Acly*$^{FAT-/-}$ (n = 7) mice (C57Bl/6 back-crossed) were injected intraperitoneally (i.p.) with 0.035 mL/g of body weight of 0.9% NaCl D_2O (Sigma-Aldrich). For 3 subsequent weeks, mice were provided water bottles containing 8% D2O. At the end of 3 weeks, mice were fasted for 6 hr and sacrificed, and plasma, liver,

VWAT, and SWAT were collected and snap frozen. Plasma from four additional mice (two *Acly*$^{f/f}$ and two *Acly*$^{FAT-/-}$ that were not given D_2O was used as controls.

Cell Culture and Proliferation Assays

MEFs (generation described in the Supplemental Information) were cultured in DMEM (GIBCO) supplemented with 10% Cosmic Calf Serum (CS) (HyClone, SH30087.03, lot number AXA30096). LN229 cells were cultured in RPMI 1640 medium (GIBCO) supplemented with 10% CS (HyClone SH30087.03, lot number AXA30096) and 2 mM L-glutamine. For experiments using dFBS, cells were cultured in glucose-free DMEM + 10% dFBS (GIBCO 26400044), with indicated concentrations of glucose and sodium acetate added. For proliferation assays, cells were plated in triplicate at the indicated density and allowed to adhere overnight. Culture medium was changed the following day, and cells were allowed to proliferate until the indicated days following plating. Cells were collected and counted on a hemocytometer. Cell lines used for viral production included Phoenix E and HEK293T cells, which were purchased from ATCC. Cells were cultured in DMEM + 10% CS and used at low passage. All cell lines were routinely monitored and confirmed to be free of mycoplasma.

Acyl-CoA Quantification and Isotopologue Analysis

Acyl-CoA species were extracted in 1 mL 10% (w/v) trichloroacetic acid (Sigma-Aldrich, catalog #T6399). Isotopologue enrichment analysis to quantify the incorporation of 10 mM [U-^{13}C]glucose and 100 mM [1,2-^{13}C]acetate into acyl-CoA thioesters was performed by liquid chromatograpy-mass spectrometry/high-resolution mass spectrometry (LC-MS/HRMS). For quan- titation, internal standards containing [$^{13}C_3{}^{15}N_1$]-labeled acyl-CoAs generated in *pan*6-deficient yeast culture[291] were added to each sample in equal

amounts. Samples were analyzed by an Ultimate 3000 autosampler coupled to a Thermo Q Exactive Plus instrument in positive electrospray ionization (ESI) mode using the settings described previously[292].

Statistics

Student's two-tailed t tests (two-sample equal variance, two-tailed distribution) were used for analyses directly comparing two datasets except tissue gene expression and acyl-CoA datasets (Figures 6 and 7), for which Welch's t test was used. Significance was defined as follows: *$p < 0.05$; **$p < 0.01$; ***$p < 0.001$; and ****$p < 0.0001$.

Genotyping

Tail-snips from mice were placed in digestion buffer (10% SDS, 5M NaCl, EDTA, Tris, H_2O, proteinase K) for two hours while shaking at 56°C. Genomic DNA was isolated and then used for genotyping using the following primer sets: Cre-Fw: TGCCACGACCAAGTGACAGC; Cre-Rv: CCAGGTTACGGATATAGTTCATG; tm1c (floxed allele)-Fw: AAGGCGCATAACGATACCAC; tm1c-Rv: CCGCCTACTGCGACTATAGAGA; Acly wild-type allele: WT-Fw: TGCAATGCTGCCTCCAATGAT; WT-Rv: GGAGCCAGAGGAGAAAAAGGC

Generation of *Acly*$^{f/f}$ MEFs

For mouse embryonic fibroblast (MEF) generation, two homozygous fertile females were placed on a dedicated mating cage with a homozygous fertile male. On day 15.5, pregnant females were sacrificed and the fetuses were surgically removed and placed in a 10-cm dish, washed two timed with PBS. Head and liver were removed from each fetus, the remaining part was trimmed, pooled in a 50- mL tube and washed again with PBS. Tissue remnants were digested with 5mL of Trypsin 0.25% at room temperature for 30 minutes. The digestion was stopped with DMEM+10%

CS. Cells were pelleted and washed again with DMEM+10% CS. Finally cells were seeded in a 25-cm flask and cultured in DMEM+10% CS + 0.1 mM β-mercaptoethanol. Cells were immortalized by serial passaging (plated at 1:3 dilution and passaged at confluency) and began recovering from proliferation crisis after 13 (line 1) and 20 (line 2) passages.

Acly deletion and reconstitution in MEFs

For acute analysis, *Acly*$^{f/f}$ MEFs (line 2) were infected with adenoviral Cre recombinase (University of Pennsylvania Vector Core). For generation of stable lines PC7, PC8, and PC9, retroviral transduction of *Acly*$^{f/f}$ MEFs (line 2) with Cre recombinase was conducted as follows: A retroviral vector containing Cre recombinase (pBabe-puro-Cre, gift of L. Busino, University of Pennsylvania) was used to produce retrovirus in Phoenix E cells. MEFs were transduced with retrovirus and selected with 3 µg/mL of puromycin for 48 hours

until mock infected MEFs displayed no viable cells. Following selection, single cell clonal populations were generated by plating cells in a limiting dilution. Deletion of *Acly* was confirmed by Western blot.

For reconstitution experiments, wild-type ACLY or catalytically inactive (H760A) ACLY were cloned into pBabe-hygro retroviral vector. Retrovirus was produced in Phoenix E cells. PC7 and PC9 cells were transduced with retrovirus and selected with hygromycin (400 µg/mL) for 48 hours until mock infected MEFs displayed no viable cells. Reconstitution was confirmed by immunoblotting for ACLY expression.

CRISPR-Cas9 genetic editing

Guide RNA sequences were generated using a CRISPR design tool (www.crispr.mit.edu). The guide sequences used are as follows: mAcss2

(GCTGCACCGGCGTTCTGTGG), hACLY (GACCAGCTGATCAAACGTCG). Guides were cloned into the LentiCRISPRv2 plasmid[293] followed by lentiviral production in HEK-293T cells. Cells were infected and selected with puromycin until a separate mock-infected plate displayed complete cell death. Single-cell clonal expansion of the selected population was done to ensure complete loss of the target gene. Loss of target gene was determined by immunoblotting for the target protein.

Analysis of *Acly*$^{FAT-/-}$ mice

From 4 weeks to 16 weeks of age, mixed background *Acly*$^{f/f}$ and *Acly*$^{FAT-/-}$ were fed normal chow and weighed weekly. At 16 weeks of age mice were sacrificed and white fat [visceral (epididymal) and subcutaneous (inguinal)] depots were harvested. Depots were dissected into thirds with a third of each being fixed in formalin for histological evaluation, a third being digested in Trizol for RNA expression analysis and the final third digested in protein lysis buffer for protein analysis. For analysis of histone acetylation and acetyl-CoA levels, a separate cohort of *Acly*$^{FAT-/-}$ (n=6) and WT (*Acly*$^{f/f}$; n=7) mice, females aged 10 to 11 weeks, backcrossed onto a C57Bl/6 background, were used. Mice were fasted for 6 hours, sacrificed, and liver, VWAT and SWAT were removed. Organs were split in half; half snap frozen for acyl CoA analysis and the other processed fresh for histone extraction, as described below. The University of Pennsylvania's Institutional Animal Care and Use Committee (IACUC) approved all animal experiments.

Immunoblotting

Protein was extracted from cells using NP-40 lysis buffer (150 mM NaCl, 1.0% NP-40, 50 mM Tris-HCl pH 8.0) with protease inhibitors (Roche). Mouse tissue was lysed in RIPA lysis buffer (1%NP-40, 0.5% Deoxycholate, 0.1% SDS, 150nM NaCl,

50mM Tris plus protease and phosphatase inhibitors). Fat was chopped with scissors on ice to fine pieces, followed by homogenization with TissueLyser (30 Hz for 20s x 2). Samples were chilled on ice for 30 min, spun down, and infranatant saved and then sonicated. Protein concentration was determined using the BCA protein assay (ThermoScientific). Proteins were separated by SDS-PAGE and transferred to a nitrocellulose membrane (GE Health Sciences). Membranes were probed with the specified antibodies (see Antibodies and Reagents), and developed on a LI-COR Odyssey CLx scanner.

Antibodies and reagents

Antibodies used for Western blotting: ACLY (previously described[6] (Wellen et al., 2009)), ACSS2 (Cell Signaling Technologies #3658S), Tubulin (Sigma T6199), FASN (Cell Signaling Technologies #3189S), Lamin A/C (Cell Signaling Technologies #2032S), Parp (Cell Signaling Technologies #9542S), Cleaved Parp (Cell Signaling Technologies #9544T), Cleaved Caspase 3 (Cell Signaling Technologies #9661S), Acetyl-H3 (Upstate 06-599), Acetyl-H4 (Millipore 06-866), H4K5Ac (Millipore 07-327), H3K14Ac (Cell Signaling #7627S), H3K18Ac (Cell Signaling 9675P), H3K23Ac (Cell Signaling 9674S), H3K27Ac (Abcam ab4729). Secondary antibodies were IRDye680RD Goat Anti-Mouse (LI-COR 926-68070) and IRDye800CW Goat Anti-Rabbit (LI-COR 926-32211).

Reagents: ACLY inhibitor BMS-303141 (Tocris Bioscience)

Nuclear-cytoplasmic subcellular fractionation:

Fractionation was performed essentially as described[6]. Cells were harvested in cold Buffer A (10 mM HEPES pH 7.4, 10 mM KCl, 1.5 mM $MgCl_2$, 0.5 mM EDTA, 0.5 mM EGTA; Complete Mini (Roche) protease inhibitor (PIC) tablet and 0.1% NP-40

added fresh). Cells were lysed on ice for 15 minutes until the plasma membrane was broken (assessed by trypan blue staining). Cells were centrifuged at 1000 RCF for 5 min at 4ºC. Supernatant (cytosol) was transferred to a new microfuge tube and spun down again at high speed to clear debris. Pellet (nuclei) from initial spin was washed once with Buffer A without NP-40, then resuspended in equal volumes of cold Buffer B (10 mM HEPES pH 7.4, 0.42 M NaCl, 2.5% glycerol, 1.5 mM $MgCl_2$, 0.5 mM EDTA, 0.5 mM EGTA, 1 mM DTT; PIC added fresh). Samples were incubated on ice for 30 minutes with occasional vortexing, centrifuged 10 minutes at 15,000 RCF to clear debris, and the supernatant transferred to new tube (nuclei). Lamin A/C and FASN were used as nuclear and cytoplasmic markers, respectively.

Histone Acid Extraction for Immunoblotting

Acid extraction on isolated nuclei was performed as previously described (Lee et al., 2014). Histones for immunoblotting were extracted from nuclei by lysing cells with NIB-250 buffer (15 mM Tris-HCl (pH 7.5), 60 mM KCl, 15 mM NaCl, 5 mM $MgCl_2$, 1 mM $CaCl_2$, 250 mM sucrose, 1 mM DTT, 10 mM sodium butyrate, 0.1% NP-40, protease inhibitors) for 5 minutes on ice. Nuclei were pelleted by spinning lysate at 600 RCF for 5 minutes at 4ºC. Nuclei were washed with NIB-250 buffer without NP-40 twice. Histones were extracted from nuclei by resuspending the pellet in 0.4N H_2SO_4 and rotating overnight at 4ºC, insoluble nuclear debris was cleared by spinning at 11,000 RCF for 10 minutes at 4ºC. Histones were precipitated by adding 100% trichloroacetic acid (TCA) until final solution reached 20% TCA and allowed to precipitate overnight at 4ºC. Precipitated histones were spun down at 11,000 RCF for 10 minutes at 4ºC and washed with 1 mL acetone + 0.1% 12 N HCl followed by a

wash of 1 mL acetone. Histone pellet was air dried at room temperature for at least 30 minutes and resuspended in glass distilled H_2O.

YSI metabolite analysis:

Culture medium (glucose-free DMEM (Gibco) supplemented with 10% dFBS (Gibson), 10 mM glucose, and 100 µM acetate) was collected from cells after culturing for 48 hours. Glucose, lactate, glutamine, and glutamate levels in culture medium were measured using a YSI 2950 Bioanalyzer. Because of differences in proliferation rate and cell volume between clones, measurements were normalized to cell volume (cell number X mean cell volume) area under the curve. Metabolite consumption was defined as $v = V(x_{medium\ control} - x_{final})/A$, where v is metabolite consumption/ production, V is medium volume, x is metabolite concentration, and A is total cell volume area under the curve. A was calculated as $N(T)d/\ln 2(1-2^{-T/d})$, where N(T) is the final cell count, d is doubling time, and T is time of experiment. Cell counts and volume measurements were taken on a Coulter Counter (Beckman Coulter), and final cell count N(T) was multiplied by mean cellular volume to obtain total cellular volume per sample. Doubling time was calculated as d = (T)[log(2)/log(Q2/Q1)], where Q1 is starting cell number and Q2 is final cell number.

Quantitative RT-PCR

Cells were lysed using Trizol reagent (Ambion), and RNA was isolated as per Trizol extraction protocol. Adipose tissue were excised from animals and immediately frozen in liquid nitrogen, placed in Trizol, and lysed using a tissue homogenizer before RNA isolation as per Trizol extraction protocol. RNA was resuspended in DEPC H_2O and quantified on a Biotek Synergy HT Plate Reader. cDNA was generated from isolated RNA using High Capacity RNA-to-cDNA Kit (Applied

Biosystems), and diluted 1:20 in nuclease free water for quantitative RT-PCR reactions (qRT-PCR). qRT-PCR was run using *Power* SYBR Green PCR Master Mix (Applied Biosystems) for 40 cycles at standard reaction speed on a ViiA 7 Real-Time PCR System (Applied Biosystems). Primer sequences listed in the table below.

qRT-PCR primer sequences

Gene	Primer Sequence
Acly (mouse) Forward	TTCGTCAAACAGCACTTCC
Acly (mouse) Reverse	ATTTGGCTTCTTGGAGGTG
Acss2 (mouse) Forward	GCTTCTTTCCCATTCTTCGGT
Acss2 (mouse) Reverse	CCCGGACTCATTCAGGATTG
Glut4 (mouse) Forward	GCCCGAAAGAGTCTAAAGC
Glut4 (mouse) Reverse	CTTCCGTTTCTCATCCTTCAG
FASN (mouse) Forward	ATTGGTGGTGTGGACATGGTC
FASN (mouse) Reverse	CCCAGCCTTCCATCTCCTG
FABP4 (mouse) Forward	ACAAAATGTGTGATGCCTTTGTGGGAAC
FABP4 (mouse) Reverse	TCCGACTGACTATTGTAGTGTTTGATGCAA
PPARg1 (mouse) Forward	TGAAAGAAGCGGTGAACCACTG
PPARg1 (mouse) Reverse	TGGCATCTCGTGTCAACCATG
PPARg2 (mouse) Forward	TGGCATCTCTGTGTCAACCATG
PPARg2 (mouse) Reverse	GCATGGTGCCTTCGCTGA
AdipoQ (mouse) Forward	GCACTGGCAAGTTCTACTGCAA
AdipoQ (mouse) Reverse	GTAGGTGAAGAGAACGGCCTTGT
18S (mouse) Forward	AAATCAGTTATGGTTCCTTTGGTC
18S (mouse) Reverse	GCTCTAGAATTACCACAGTTATCCAA
E2F2 (human) Forward	TTTACCTCCTGAGCGAGTCA
E2F2 (human) Reverse	AGCACGTTGGTGATGTCATAG
MCM10 (human) Forward	CGGAACAAACCTAGTGGGATAA
MCM10 (human) Reverse	AGAAGGCTTCCACACAGATG
SKP2 (human) Forward	GTGTACAGCACATGGACCTAT
SKP2 (human) Reverse	CCAGGCTTAGATTCTGCAACT

Gas Chromatography/Mass Spectrometry of Fatty Acid Methyl Esters (GC/MS-FAME)

To measure glucose incorporation into lipids, $2x10^5$ cells were plated and allowed to adhere overnight. Culture medium was changed the following day to DMEM without glucose (Gibco) supplemented with 10% dialyzed fetal bovine serum (dFBS) (Gibco 26400044, Lot. 1616514), 10 mM [U-^{13}C]glucose (Cambridge Isotope Laboratories),

and 100 µM sodium acetate, and incubated for 48 hours. To measure acetate incorporation into lipids, DMEM without glucose was supplemented with 10% dFBS, 10 mM glucose, and 100 µM or 1 mM [1,2-^{13}C]acetate (Cambridge Isotope Laboratories). On day of harvest, cells were washed with 1x PBS, followed by 1x PBS + fatty acid free BSA before detachment with trypsin. Cells were spun down, and frozen at -80°C until day of extraction.

Fatty acids were extracted from cells by resuspending and sonicating cells in a mixture of methanol, distilled H_2O, and chloroform (2:1:2). Mixture was spun at 10,000 RCF for 10 minutes at 4°C to separate organic and aqueous phases. The organic phase was evaporated under nitrogen to obtain a dry lipid fraction for derivatization. Fatty acids were derivatized by adding 2 mL of IS solution (40 mL MeOH, 10 mL toluene, 5 mg butylated hydroxytoluene) and 2 µL of acetylchloride (Sigma) to the dried lipid fraction and heating at 95°C for 1 hour. Derivatized fatty acid methyl esters were then extracted by adding 5 mL of 6% potassium carbonate solution to separate hydrophobic and hydrophilic phases. The hydrophobic phase containing fatty acid methyl esters was analyzed by GC/MS on an Agilent GC/MS 7890A/5975A with a DB-5 column. Enrichment of ^{13}C into palmitate was determined using IsoCor[294].

Gas Chromatography/Mass Spectrometry of TCA cycle metabolites

Measurements of citrate and malate were conducted essentially as described[278]. Briefly, 6x10^5 cells (for 6 hour labeling) or 4x10^5 cells (for 24 hour labeling) were plated and allowed to adhere overnight. Culture medium was changed the following day to DMEM without glucose (Gibco), supplemented with 10% dialyzed fetal bovine serum (dFBS) (Gibco 26400044, Lot. 1616514), 10 mM [U-^{13}C]glucose (Cambridge

Isotope Laboratories), and 100 µM sodium acetate, and incubated for 6 or 24 hours. To measure acetate incorporation into TCA cycle metabolites, DMEM without glucose was supplemented with 10% dFBS, 10 mM glucose, and 100 µM [1,2-^{13}C]acetate (Cambridge Isotope Laboratories). At time of harvesting, media was removed from cells and cells were quickly scraped into 1 mL of cold methanol and collected into conical tubes. 0.3 mL of water was added to each sample, and samples were then sonicated for 60 seconds. Samples were then centrifuged for 15 minutes at 8,500 RPM at 4^{o}C. Following centrifugation, supernatant was transferred to a 4 ml vial, and samples were heated under nitrogen to evaporate methanol. For derivatization, pyridine and BSTFA-TCMS were added sequentially in a 1:1 ratio, and allowed to react at 54^{o}C for 30 minutes. Finally, samples were spun down for 10 minutes at 13,000 RPM at room temperature. Supernatants were transferred GC-MS vials with pulled glass inserts and were analyzed by GC/MS on an Agilent GC/MS 7890A/5975A with a DB-5 column. Enrichment of ^{13}C into TCA cycle intermediates was determined using IsoCor[295].

Mass Spectrometry Analysis of Histone Acetylation

To measure glucose incorporation into histone acetyl-groups, 10^5 cells were plated and allowed to adhere overnight. Culture medium was changed the following day to glucose-free DMEM (Gibco) supplemented with 10% dFBS (Gibson), 10 mM [U-^{13}C]glucose, and 100 µM acetate, and incubated for 24 hours. Measurement of acetate incorporation into histone acetyl-groups was done in identical conditions, but with 100 µM or 1mM [1,2-^{13}C]acetate and 10 mM glucose. Histones were acid extracted from cells using 0.4 N HCl. These samples were TCA precipitated, acetone washed, and prepared for mass spectrometry analysis as previously

described[296]. A Waters (Milford, MA) Acquity H-class UPLC system coupled to a Thermo (Waltham, MA) TSQ Quantum Access triple-quadrupole (QqQ) mass spectrometer was used to quantify modified histones. Selected reaction monitoring was used to monitor the elution of the acetylated and propionylated tryptic peptides. Transitions were created to distinguish between normal and heavy (^{13}C) acetylation marks on the histone H3 tail: histone H3 lysine 9 (H3K9), H3K14, H3K18, and H3K23.

QqQ MS Data Analysis:

Each acetylated and/or propionylated peak was identified by retention time and specific transitions. The resulting peak integration was conducted using Xcalibur software (version 2.1, Thermo). The fraction of a specific peptide (F_p) is calculated as $F_p = I_s / (\sum I_p)$, where I_S is the intensity of a specific peptide state and I_p is the intensity of any state of that peptide.

Detection parameters of tryptic peptides from histone H3

	Precursor ion (m/z)	Product ions (m/z)	Collision energy (eV)	Retention time (min)
KhSTGGKhAPR	495.282	817.444	18	0.4
		730.412	18	
		572.343	18	
KhSTGGKaAPR	494.276	815.437	18	0.4
		728.405	18	
		570.336	18	
KhSTGGKpAPR	501.286	829.453	18	0.7
		742.421	18	
		584.351	18	
KaSTGGKhAPR	494.278	817.444	18	0.4
		730.412	18	
		572.343	18	
KaSTGGKaAPR	493.275	815.437	18	0.4
		728.405	18	
		570.336	18	
KaSTGGKpAPR	500.282	829.453	18	0.7
		742.421	18	
		584.351	18	
KpSTGGKhAPR	501.288	817.444	18	0.7
		730.412	18	
		572.343	18	
KpSTGGKaAPR	500.284	815.437	18	0.7
		728.405	18	
		570.336	18	
KpSTGGKpAPR	507.291	829.453	18	1.1
		742.421	18	
		584.351	18	
KhQLATKhAAR	537.826	774.474	19	2.7
		661.390	19	
		590.353	19	
KhQLATKaAAR	536.822	772.468	19	2.7
		659.384	19	
		588.346	19	
KhQLATKpAAR	543.830	786.483	19	3.5
		673.399	19	
		602.362	19	
KaQLATKhAAR	536.824	774.474	19	2.7
		661.390	19	
		590.353	19	
KaQLATKaAAR	535.819	772.468	19	2.7
		659.384	19	
		588.346	19	
KaQLATKpAAR	542.827	786.483	19	3.5
		673.399	19	
		602.362	19	
KpQLATKhAAR	543.832	774.474	19	3.6
		661.390	19	
		590.353	19	
KpQLATKaAAR	542.829	772.468	19	3.6
		659.384	19	
		588.346	19	
KpQLATKpAAR	549.835	786.483	19	4.4
		673.399	19	
		602.362	19	

*p= propionylated, a= acetylated, h= 13C acetylated

Determination of acetyl-CoA and ^{13}C incorporation into acyl-CoAs:

Internal standard generation:

[$^{13}C_3{}^{15}N_1$]-labeled acyl-CoA internal standard was generated by culturing *pan*6-deficient *Saccharomyces cerevisiae* with [$^{13}C_3{}^{15}N_1$]- pantothenate (Isosciences, King of Prussia, PA), as described previously[291]. A 500 ml culture at stationary phase was resuspended in 100 ml of 10% (w/v) trichloroacetic acid (Sigma-Aldrich, St. Louis, MO cat. #T6399). The cells were dismembranated in 10 ml aliquots by sonication (60 0.5 s pulses) with a probe tip sonicator (Thermo Scientific) and centrifuged at 3000 g for 10 mins at 4°C. The cleared supernatant was stored at -80°C.

Cell treatment and harvest:

[U-^{13}C]glucose and [U-^{13}C]acetate incorporation into acyl-CoA thioesters were analysed in cells incubated in the presence of 10 mM [U-^{13}C]glucose (Cambridge Isotope Laboratories CLM-1396-1) or 100 µM [U-^{13}C]acetate (Cambridge Isotope Laboratories CLM- 440-1) for 6 hours. For relative acetyl-CoA determination cells were incubated in the same conditions in the absence of labeled substrate. Cells were removed from culture dish by scraping on ice and resuspended directly in the cell culture medium. Cell volume and concentration were determined by Coulter counter (Beckman-Coulter). An appropriate volume of each cell sample was pelleted by centrifugation (500 x g for 10 min at 4 °C) such that total cell volume in each cell pellet was equal.

Short chain acyl-CoA extraction:

Frozen tissue samples were cut to ~ 50 mg on a super chilled ceramic tile on dry ice. The weighed samples were added to 1 mL of thawed [$^{13}C_3{}^{15}N_1$]-labeled acyl-CoA internal standard in 1.5 mL Eppendorf tubes on ice. Cell pellets were

resuspended in 1 ml 10% (w/v) trichloroacetic acid. For relative acyl-CoA quantitation, 100 µl of [$^{13}C_3{}^{15}N_1$]-labeled acyl-CoA internal standard was added to each sample. Internal standard was omitted for ^{13}C labeling experiments. Samples were homogenized and dismembranated by 60 (for tissues) or 20 (for cell pellets) 0.5 s pulses with a probe tip sonicator (Thermo Scientific). The homogenised samples were centrifuged at 13,000 × *g* for 10 min at 4 °C. Supernatants were purified by solid-phase extraction using Oasis HLB 1cc (30 mg) SPE columns (Waters). Columns were washed with 1 mL methanol, equilibrated with 1 mL water, loaded with supernatant, desalted with 1 mL water, and eluted with 1 mL methanol containing 25mM ammonium acetate. The purified extracts were evaporated to dryness under nitrogen then resuspended in 55 µl 5% (w/v) 5-sulfosalicylic acid in water.

Liquid chromatography:

Analytes were separated before introduction to the mass spectrometer using a reversed-phase Phenomenex HPLC Luna C18 column with 5 mM ammonium acetate in water as solvent A, 5 mM ammonium acetate in acetonitrile/water (95:5, v/v) as solvent B, and acetonitrile/water/formic acid (80:20:0.1, v/v/v) as solvent C. Gradient conditions were as follows: 2% B for 1.5 min, increased to 25% over 3.5 min, increased to 100% B in 0.5 min and held for 8.5 min, washed with 100% C for 5 min, before equilibration for 5 min. The flow rate was 200 µl/min. For determination of [^{13}C]acetate incorporation into acetyl-CoA in primary mature adipocytes an alternative LC method was used, as described[297].

Mass-spectrometry:

For relative quantitation of acetyl-CoA levels in cells, samples were analyzed using an API 4000 triple-quadrupole mass spectrometer (Applied Biosystems, Foster City, CA, USA) in the positive ESI mode as described previously[291]. Acetyl-CoA was quantified by single reaction monitoring (SRM) of *m/z* 810.1/303.1 and the [$^{13}C_3{}^{15}N_1$]-labeled internal standard at *m/z* 814.1/307.1.

Samples (10 µl) were injected using a Leap CTC autosampler (CTC Analytics, Switzerland) and data were analyzed with Analyst 1.4.1 software (Applied Biosystems).

For [U-^{13}C]glucose and [U-^{13}C]acetate labeling and mouse tissue experiments, samples were injected by an Ultimate 3000 autosampler and analytes were detected using a Thermo Q Exactive instrument in positive ESI mode as described elsewhere[292]. Briefly, scan parameters were alternating full scan from 760 to 1800 *m/z* at 140,000 resolution and data-independent acquisition (DIA) looped three times with all fragment ions multiplexed at a normalized collision energy (NCE) of 20 at a resolution of 280,000. An isolation width of 7 *m/z* with an offset of 3 *m/z* was used to capture all relevant isotopologues for targeted acyl-CoA thioesters. Parent ion and product ion *m/z* transitions detected are indicated in the table below.

Species	**Isotopologue**	**Parent *m/z***	**Product *m/z***
Acetyl-CoA	M0	810.1331	303.1373
Acetyl-CoA	M1	811.1364	304.14066
Acetyl-CoA	M2	812.13976	305.14401
Acetyl-CoA	M3	814.14311	306.14737
Acetyl-CoA	M4	814.14647	307.15072
Acetyl-CoA	M5	815.14982	308.15408
Acetyl-CoA	[$^{13}C_3{}^{15}N_1$]-internal standard	814.1402	307.1444

Succinyl-CoA	M0	868.13853	361.14278
Succinyl-CoA	M1	869.14188	362.14614
Succinyl-CoA	M2	870.14524	363.14949
Succinyl-CoA	M3	871.14859	364.15285
Succinyl-CoA	M4	872.15195	365.1562
Succinyl-CoA	M5	873.1553	366.15956
Malonyl-CoA	M0	854.12288	347.12713
Malonyl-CoA	M1	855.12623	348.13049
Malonyl-CoA	M2	856.12959	349.13384
Malonyl-CoA	M3	857.13294	350.1372
Malonyl-CoA	M4	858.1363	351.14055
HMG-CoA	M0	912.16474	405.169
HMG-CoA	M1	913.1681	406.17235
HMG-CoA	M2	914.17145	407.17571
HMG-CoA	M3	915.17481	408.17906
HMG-CoA	M4	916.17816	409.18242
HMG-CoA	M5	917.18152	410.18577
HMG-CoA	M6	918.18487	411.18913
HMG-CoA	M7	919.18823	412.192482

For [^{13}C]acetate incorporation into acetyl-CoA in primary mature adipocytes, samples were injected by an Ultimate 3000 autosampler and analytes were detected using a Thermo Q Exactive HF instrument with HESI in negative mode. Instrument parameters were as follows, spray voltage 3000 V, capillary temperature 325 °C sheath gas 40 arbitrary units, auxillary gas 10 arbitrary units, spare gas 2 arbitrary units, S-lens RF level 55. Scan parameters were alternating full scan from 70 to 950 *m/z* at 120,000 resolution. Acetyl-CoA isotopologue ions were detected as listed in the table below.

Species	**Isotopologue**	***m/z***
Acetyl-CoA	M0	808.1185
Acetyl-CoA	M1	809.12185

Acetyl-CoA	M2	810.12521
Acetyl-CoA	M3	811.12856
Acetyl-CoA	M4	812.13192

Data were processed in Xcalibur, TraceFinder (Thermo), and isotopic enrichment was calculated to compensate for the non-linearity of isotopic enrichment as outlined and applied previously[298,299]. For acetyl-CoA determination in mouse tissues, the parent ion peak for acetyl-CoA M0 and the [$^{13}C_3{}^{15}N_1$]-acetyl-CoA internal standard were integrated to determine relative abundance between samples.

In vivo de novo lipogenesis analysis

Plasma D_2O enrichment:

The ^2H labeling of water from samples or standards was determined via deuterium acetone exchange[300,301]. 5 μls of sample or standard was reacted with 4 μls of 10N NaOH and 4 μls of a 5% (v/v) solution of acetone in acetonitrile for 24 hours. Acetone was extracted by the addition of 600 μl chloroform and 0.5 g Na2SO4 followed by vigorous mixing. 100 μls of the chloroform was then transferred to a GCMS vial. Acetone was measured using an Agilent DB-35MS column (30 m 3 0.25mm i.d. 3 0.25 mm, Agilent J&W Scientific) installed in an Agilent 7890A gas chromatograph (GC) interfaced with an Agilent 5975C mass spectrometer (MS) with the following temperature program: 60 °C initial, increase by 20 °C/min to 100 °C, increase by 50 °C/min to 220 °C, and hold for 1 min. The split ratio was 40:1 with a helium flow of 1 ml/min. Acetone eluted at approximately 1.5min. The mass spectrometer was operated in the electron impact mode (70 eV). The mass ions 58 and 59 were integrated and the % M1 (m/z 59) calculated. Known standards were

used to generate a standard curve and plasma % enrichment was determined from this. All samples were analyzed in triplicate.

Total fatty acids were extracted from tissues and plasma using a Bligh and Dyer based methanol/chloroform/water extraction with C16 D31 as an internal standard. Briefly, 500 μls MeOH, 500 μls $CHCL_3$, 200 μls H_2O and 10 μls 10 mM C16 D31/ 10 mgs tissue were added to weighed pre-ground tissue. This was vortexed for 10 minutes followed by centrifugation at 10,000 g for 5 minutes. The lower chloroform phase was dried and then derivitised to form fatty acid methyl esters via addition of 500 μls 2% H2SO4 and incubation at 50°C for 2 hours. FAMES were extracted via addition of 100 μls saturated salt solution and 500 μls hexane and these were analyzed using a Select FAME column (100m x 0.25mm i.d.) installed in an Aglient 7890A GC interfaced with an Agilent 5975C MS using the following temperature program: : 80 °C initial, increase by 20 °C/min to 170 °C, increase by 1 °C/min to 204 °C, then 20 °C/min to 250 °C and hold for 10 min.

Calculations:

The % mass isotopomer distributions of each fatty acid was determined and corrected for natural abundance using in-house algorithms adapted from Fernandez et al.[302]. Calculation of the fraction of newly synthesized fatty acids (FNS) was based on the method described by Lee et al.[303], where FNS is described by the following equation:

$$FNS=ME/(n \times p)$$

Where ME is the average number of deuterium atoms incorporated per molecule($ME = 1 \times m_1 + 2 \times m_2 + 3 \times m_3 \ldots$), p is the deuterium enrichment in water

and n is the maximum number of hydrogen atoms from water incorporated per molecule. N was determined using the equation:

$m2/m1 = (N-1)/2 \times p/q$

As described by Lee et al.[304] where q is the fraction of hydrogen atoms and p + q = 1. The molar amount of newly synthesized fatty acids was determined by:

MNS = FNS x total fatty acid amount (nmoles/mg tissue).

Acetate measurements:

Protein filtration from the samples:

200 ml of sample was filtered through 3 kDa cutoff nanosep centrifugation device (Pall Inc. Port Washington, NY), and recovered volume of the filtrate noted.

Sample preparation for NMR spectroscopy:

180 µl of filtrate was added to 20 µl of DSS (4,4-Dimethyl-4-silapentane-1-sulfonic acid, Cambridge Isotope Limited, Andover, MA) in D_2O to a final concentration of 0.16 mM.

Nuclear Magnetic Resonance (NMR) Spectroscopy:

All NMR spectra were acquired in Bruker Avance III HD NMR spectrometer equipped with a triple resonance inverse (TXI) 3 mm probe (Bruker Biospin, Billerica, MA) and a Bruker Samplejet for sample handling. One-dimensional NMR spectra were acquired using the first transient of a 2 dimensional NOESY and generally of the form RD-90-t-90-t_m-90-ACQ[305]. Where RD = relaxation delay, t = small time delay between pulses, t_m = mixing time and ACQ = acquisition. The water signal was saturated using continuous irradiation during RD and t_m. The spectra

were acquired using 76K data points and a 14 ppm spectral width over 384 scans with a 1 second interscan (relaxation) delay and 0.1 second mixing time. The FIDs were zero filled to 128K; 0.1 Hz of linear broadening was applied followed by Fourier transformation, baseline and phase correction using an automated program provided by Bruker Biospin.

Profiling of acetate signal from the NMR spectra:

The acetate signal was quantitatively profiled from the spectra using Chenomx v 8.0 (Edmonton, Canada)[306] by quantifying the acetate peak at 1.90 ppm (Supplementary Fig. 2A) relative to the DSS peak area. Proper care was taken to omit the effects of the overlapping signals (for example, lysine and arginine overlapping with the 1.90 ppm acetate peak) using the Chenomx targeted spectral fitting algorithm[307].

Histology

For histology, subcutaneous and visceral white fat tissue was fixed in formalin overnight, deyhydrated and submitted to the AFCRI Histology Core for paraffin embedding, sectioning and hematoxylin and eosin staining.

Primary adipocyte ^{13}C-acetate uptake

Primary adipocyte isolation was conducted as previously described[308], with minor modifications. Briefly, visceral white adipose tissues (VWAT) were removed from mice ages 12-16 weeks and weighed. Isolation buffer (1X Krebs-Ringer- Phosphate Buffer, 2% Hepes, 25 mg/mL BSA, 0.2 mM adenosine, 10 mM glucose, 100 µM [1,2-^{13}C]acetate, pH 7.5) and 1 mg/mL collagenase was prepared ahead of time and added to VWAT at 2 mL per gram of tissue while on ice. VWAT fat pads were chopped with scissors in the buffer for 5 minutes until no large chunks of tissue remained, and then incubated at 37^{o}C for 45 minutes while shaking to allow

collagenase digestion to occur. Following collagenase digestion, tissue suspension was passed through a 100 µm mesh filter and allowed to sit at room temperature until primary adipocytes separated from infranatant. Infranatant was subsequently removed and remaining adipocytes were washed 3x in isolation buffer without collagenase. Following washes, primary adipocytes were re-suspended in 3x cell volume of isolation buffer containing 100 µM [1,2-^{13}C]acetate and incubated at 37^{o}C for 4 hours while shaking. Following incubation, suspension was allowed to sit at room temperature until primary adipocytes separated from infranatant. Infranatant was subsequently removed and the remaining primary adipocytes were re-suspended in ice cold 10% tricholoroacetic acid, and frozen at -80^{o}C until samples could be analyzed for acyl-CoA species by mass spectrometry as described above.

FIGURES

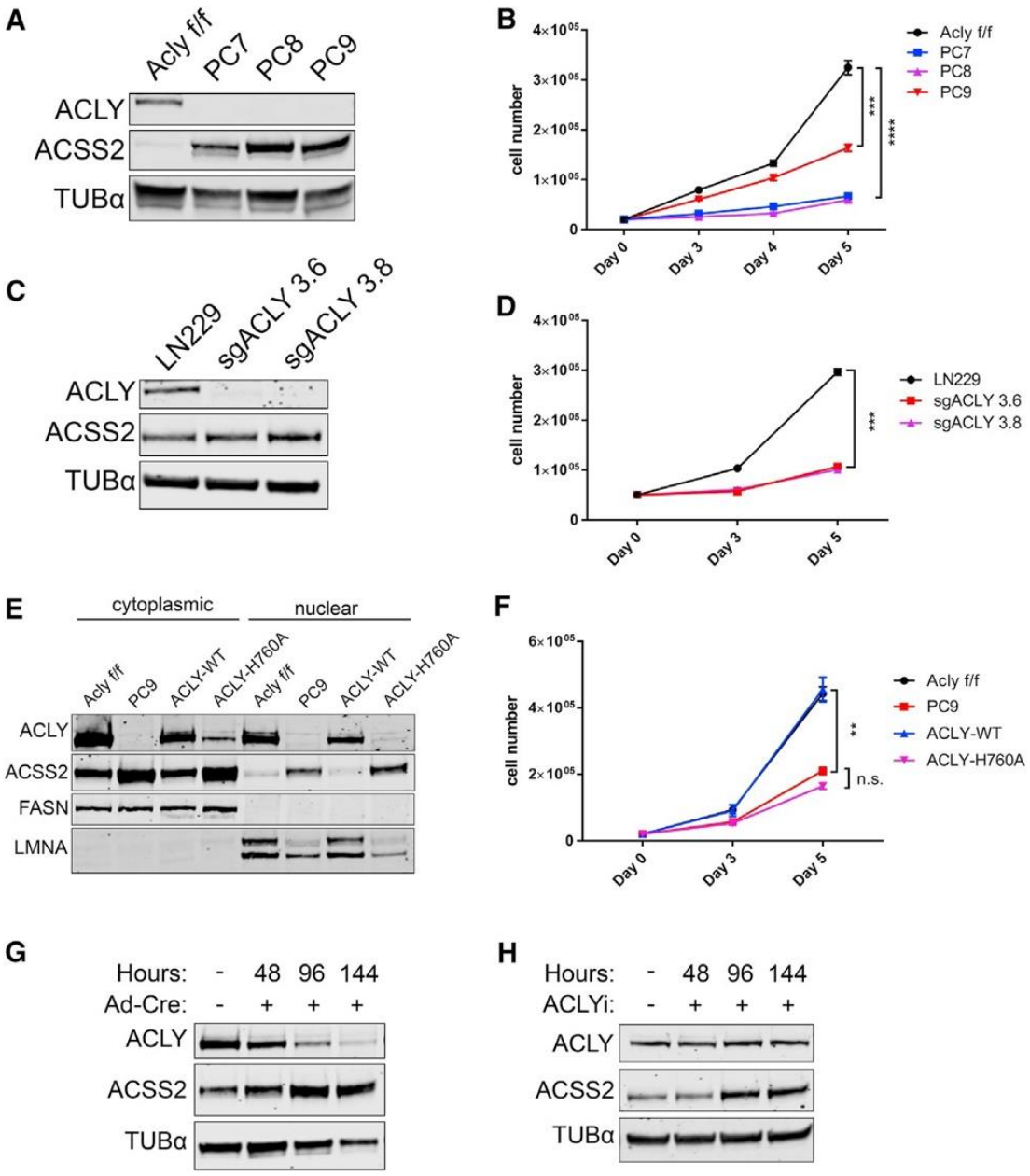

Figure 2.1 | Genetic Deletion of *Acly* Is Consistent with Cell Viability but Impairs Proliferation

(A) Western blot of three clonal ACLY-deficient (KO) cell lines (PC7, PC8, and PC9) generated from *Acly*$^{f/f}$ MEFs.

(B) Proliferation curve of *Acly*$^{f/f}$ and ACLY-KO MEFs over 5 days; mean ± SEM of triplicate wells, statistical significance compared to *Acly*$^{f/f}$.

(C) Western blot verification of ACLY knockout by CRISPR-Cas9 in LN229 glioblastoma cells.

(D) Proliferation curve of LN229 and two ACLY-knockout clonal cell lines over 5 days; error bars indicate mean ± SEM of triplicate wells, statistical significance compared to LN229.

(E) Western blot of nuclear and cytoplasmic fractions of *Acly*$^{f/f}$, PC9, and reconstituted ACLY-WT and ACLY-H760A PC9 cells. FASN and LMNA (lamin A/C) are cytoplasmic and nuclear markers, respectively.
(F) Proliferation curve of *Acly*$^{f/f}$ MEF and PC9 lines compared to PC9 reconstituted with ACLY-WT or ACLY-H760A over 5 days; error bars indicate mean ± SEM of triplicate wells, statistical significance compared to PC9.
(G) Western blot of ACLY and ACSS2 protein levels in *Acly*$^{f/f}$ MEFs over 144 hr following administration of Cre recombinase.
(H) Western blot of ACLY and ACSS2 protein levels in *Acly*$^{f/f}$ MEFs over 144 hr with pharmacological inhibition of ACLY (50 μM BMS-303141).
For all panels: **p < 0.01; ***p < 0.001; ****p < 0.0001; n.s., not significant. See also Figure S2.1.

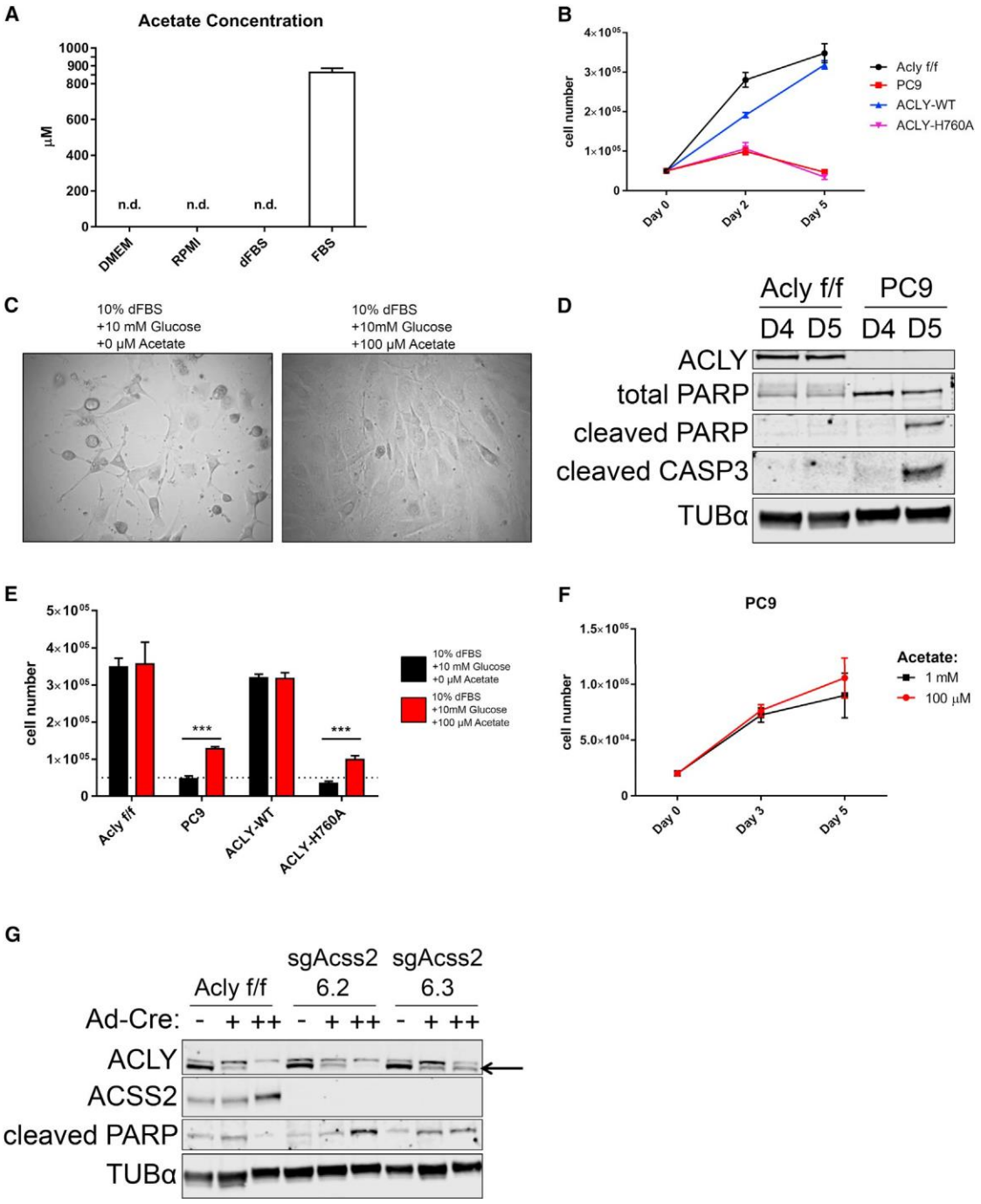

Figure 2.2 | ACLY-Deficient MEFs Require Exogenous Acetate for Viability

(A) Acetate concentrations in DMEM, RPMI, 100% dialyzed fetal bovine serum (dFBS), and 100% calf serum (CS); error bars indicate mean ± SEM of triplicate aliquots. See Figure S2.2A for spectrum. n.d., not detected.

(B) Proliferation curve over 5 days of *Acly*$^{f/f}$, PC9, PC9-ACLY-WT, and PC9-ACLY-H760A cells in acetate-free conditions (DMEM + 10% dFBS + 10 mM glucose); error bars indicate mean ± SEM of triplicate wells.
(C) Image of ACLY-deficient PC9 cells cultured for 5 days in DMEM + 10% dFBS + 10 mM glucose, without (left) or with (right) 100 μM sodium acetate.
(D) Western blot of apoptotic markers cleaved poly(ADP-ribose) polymerase (PARP) and cleaved caspase-3 (CASP3) in *Acly*$^{f/f}$ and PC9 cells cultured in acetate- free conditions (DMEM + 10% dFBS + 10 mM glucose) for 4 (D4) or 5 (D5) days.
(E) Cell numbers following 5 days in culture in DMEM + 10% dFBS + 10 mM glucose alone (black) or supplemented with 100 μM sodium acetate (red) in *Acly*$^{f/f}$, PC9, PC9-ACLY-WT, and PC9-ACLY-H760A cells; error bars indicate mean ± SEM of triplicates. ***$p < 0.001$. Dotted line represents cell number at plating.
(F) Proliferation of PC9 cells over 5 days cultured in DMEM + 10% dFBS + 10 mM glucose, with 100 μM or 1 mM sodium acetate; error bars indicate mean ± SEM of triplicate wells.
(G) Parental *Acly*$^{f/f}$ MEFs and two clones of ACSS2-deficient *Acly*$^{f/f}$ MEFs were administered Cre recombinase once (+) or twice (++) and proteins collected for western blot after 2 days (+) and 2 weeks (++). See Figure S2.2D for corresponding images.

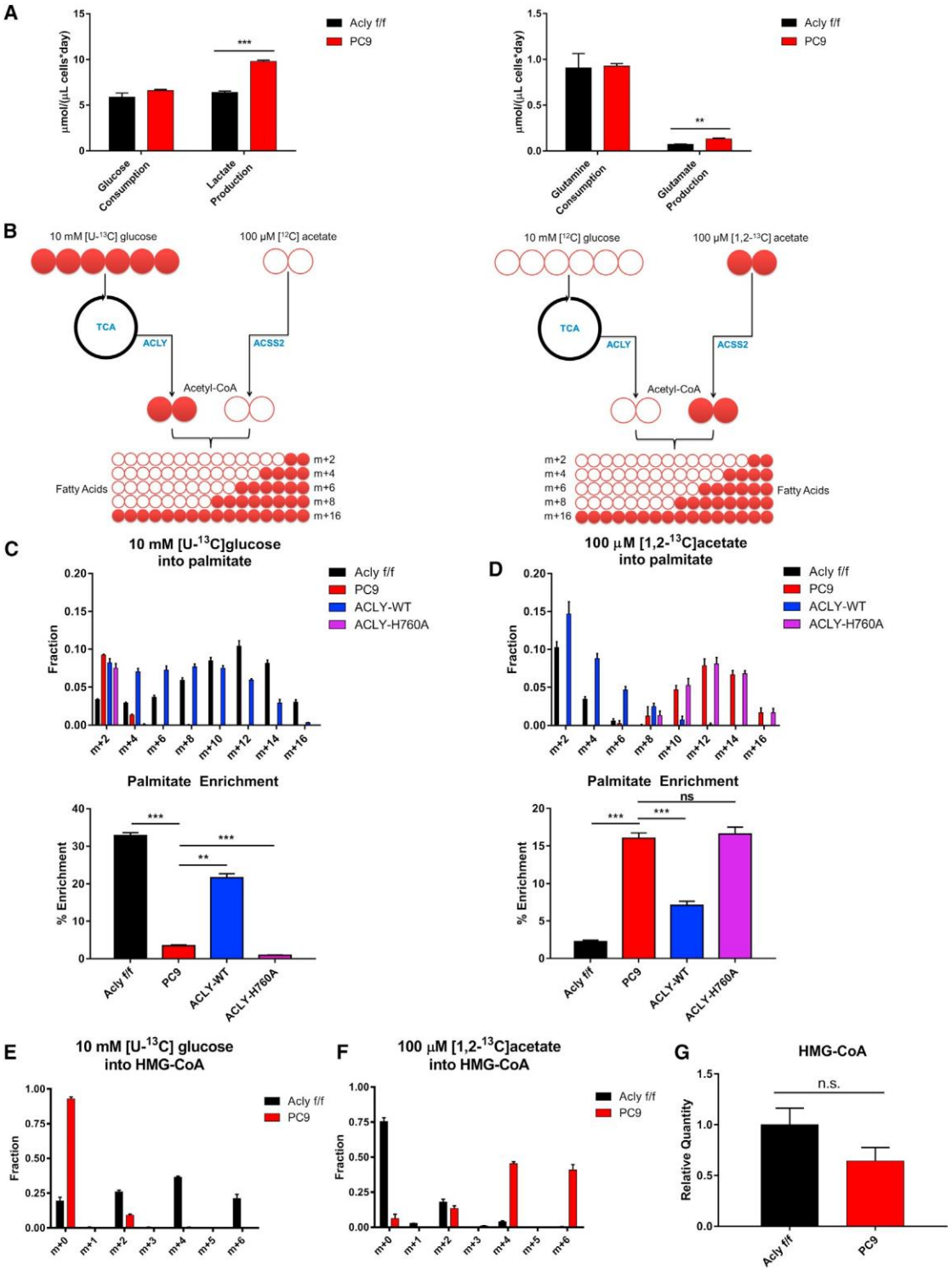
A
µmol/(µL cells*day)
Acly f/f
PC9
***
Glucose Consumption
Lactate Production
**
Glutamine Consumption
Glutamate Production
B
10 mM [U-13C] glucose
100 µM [12C] acetate
TCA
ACLY
ACSS2
Acetyl-CoA
Fatty Acids
m+2
m+4
m+6
m+8
m+16
10 mM [12C] glucose
100 µM [1,2-13C] acetate
C
10 mM [U-13C]glucose into palmitate
ACLY-WT
ACLY-H760A
Fraction
Palmitate Enrichment
% Enrichment
D
100 µM [1,2-13C]acetate into palmitate
ns
E
10 mM [U-13C] glucose into HMG-CoA
F
100 µM [1,2-13C]acetate into HMG-CoA
G
HMG-CoA
n.s.
Relative Quantity

Figure 2.3 | Acetate Supports Lipid Synthesis in the Absence of ACLY

(A) Measurements of glucose consumption and lactate production (left) and glutamine consumption and glutamate production (right), normalized to cell volume (cell number 3 mean cell volume); error bars indicate mean ± SEM of triplicate wells; **p < 0.01; ***p < 0.001. Experiment was performed in glucose-free DMEM + 10% dFBS + 10 mM glucose + 100 μM sodium acetate.

(B) Experimental design for heavy isotope labeling of fatty acids using [U-^{13}C]glucose, with unlabeled acetate present (left) and [1,2-^{13}C]acetate, with unlabeled glucose present (right).

(C) Isotopologue distribution of palmitate after 48-hr labeling in 10 mM [U-^{13}C]glucose in *Acly*$^{f/f}$, PC9, PC9-ACLY-WT, and PC9-ACLY-H760A MEFs (top). Expressed as percent enrichment of palmitate (bottom); error bars indicate mean ± SD of triplicates. **p < 0.01; ***p < 0.001.

(D) Isotopologues of palmitate after 48-hr labeling in 100 μM [1,2-^{13}C]acetate in *Acly*$^{f/f}$, PC9, PC9-ACLY-WT, PC9-Acly H760A MEFs (top). Expressed as percent enrichment of palmitate (bottom); error bars indicate mean ± SD of triplicates. ***p < 0.001; ns, not significant.

(E) Isotopologues of HMG-CoA upon 6-hr labeling in 10 mM [U-^{13}C]glucose (100 μM unlabeled acetate present) in *Acly*$^{f/f}$ and PC9 MEFs; error bars indicate mean ± SD of triplicates.

(F) Isotopologues of HMG-CoA upon 6-hr labeling in 100 μM [1,2-^{13}C]acetate (10 mM unlabeled glucose present) in *Acly*$^{f/f}$ and PC9 MEFs; error bars indicate mean ± SD of triplicates.

(G) Total HMG-CoA quantitation in cells cultured in DMEM + 10% dFBS + 10 mM glucose + 100 μM sodium acetate (unlabeled); error bars indicate mean ± SEM of triplicates. n.s., not significant.

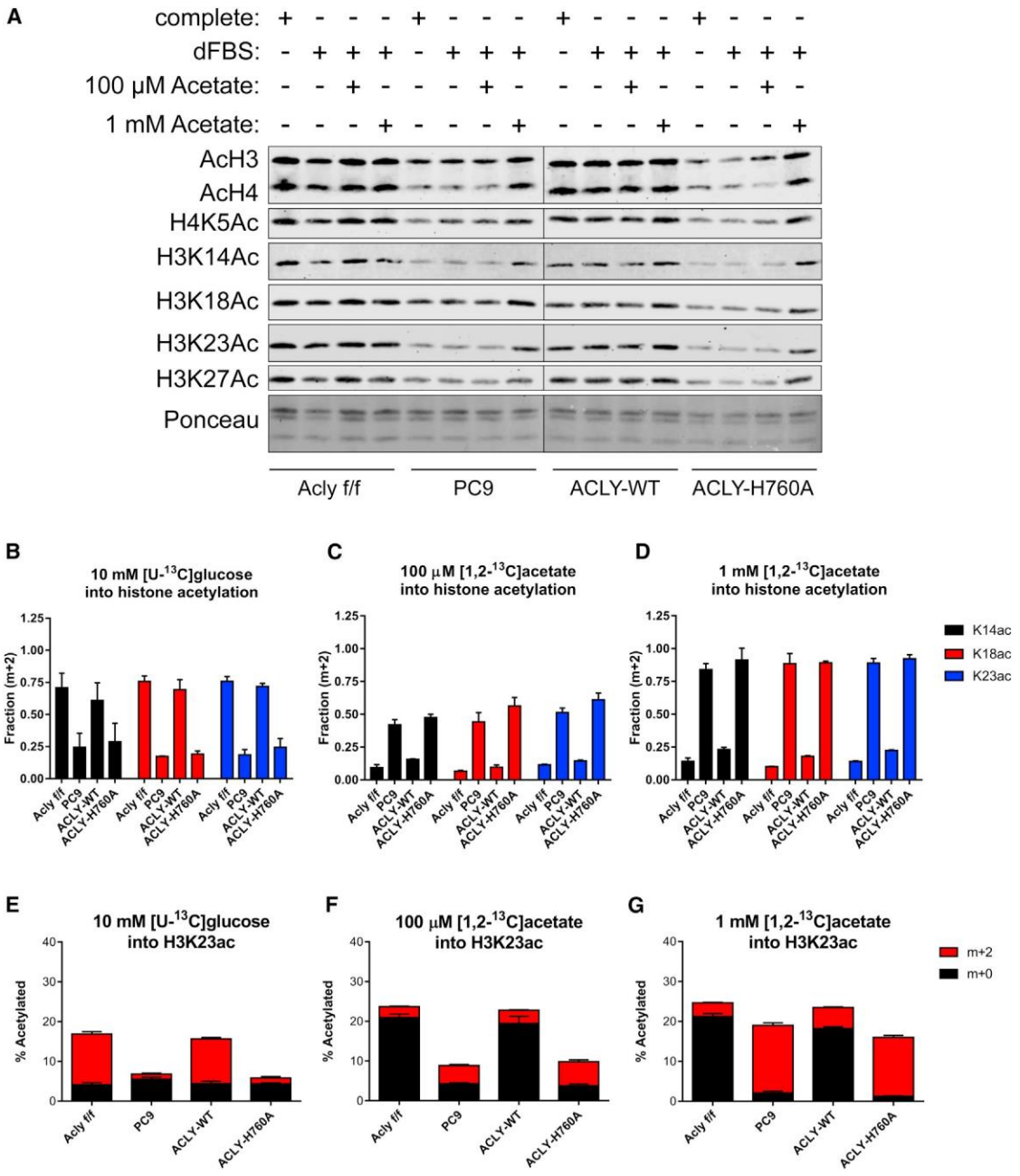

Figure 2.4 | ACLY Is Required for Sustaining Histone Acetylation Levels, despite ACSS2 Compensation

(A) Western blot of acetylated histones extracted from *Acly*$^{f/f}$, PC9, PC9-ACLY-WT, and PC9-ACLY-H760A MEFs cultured in complete medium (DMEM + 10% CS), dFBS medium (DMEM + 10% dFBS), +100 μM acetate medium (DMEM + 10% dFBS + 100 μM sodium acetate), and +1 mM acetate medium (DMEM + 10% dFBS + 1 mM sodium acetate) for 48 hr.

(B–D) Fractions of histone H3-K14, -K18, and -K23 acetylation (m+2) derived from 10 mM [U-^{13}C]glucose, with unlabeled 100 μM acetate present (B); 100 μM [1,2-^{13}C]acetate, with 10 mM

unlabeled glucose present (C); or 1 mM [1,2-^{13}C]acetate, with 10 mM unlabeled glucose present (D); error bars indicate mean ± SEM of triplicate samples. Labeling was for 24 hr (see also Figure S2.3B for experimental design).
(E–G) Overall percentage of H3K23 acetylated in each cell line (y axis), as well as the relative fraction of this acetylation incorporated from a labeled source (red): 10 mM [U-^{13}C]glucose (E), 100 μM [1,2-^{13}C]acetate (F), and 1 mM [1,2-^{13}C]acetate (G) or unlabeled sources (black); error bars indicate mean ± SEM of triplicate samples. The same dataset is represented in parts (B–D) and (E–G).

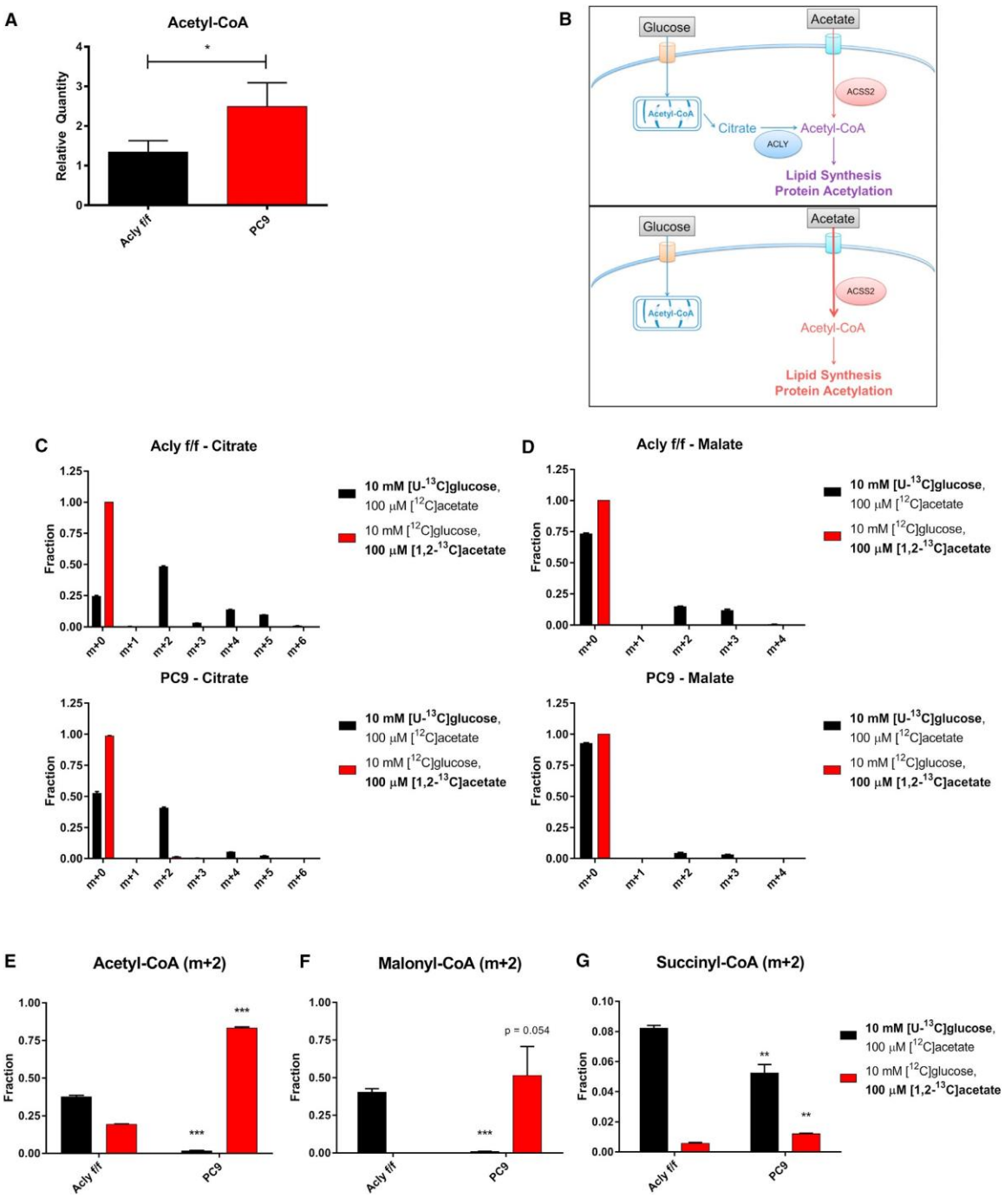

Figure 2.5 | Acetyl-CoA Pools Are Sustained by Acetate in the Absence of ACLY

(A) Relative whole-cell acetyl-CoA levels in *Acly*$^{f/f}$ and PC9 MEFs cultured in glucose-free DMEM + 10% dFBS + 10 mM glucose + 100 μM sodium acetate for 6 hr, normalized to cellular volume; error bars indicate mean ± SD of triplicates.

(B) Schematic of acetyl-CoA production from glucose and acetate with (top) or without (bottom) ACLY.
(C) Isotopologue distribution of citrate after 6-hr incubation with 10 mM [U-^{13}C]glucose, with 100 μM unlabeled acetate present (black) or 100 μM [1,2-^{13}C]acetate with 10 mM unlabeled glucose present (red), in *Acly*$^{f/f}$ (top) or PC9 (bottom) MEFs; error bars indicate mean ± SEM of triplicates.
(D) Isotopologue distribution of malate in the same conditions as (C).
(E–G) m+2 acetyl-CoA (E), malonyl-CoA (F), or succinyl-CoA (G) following 6-hr labeling in 10 mM [U-^{13}C]glucose (with 100 μM unlabeled acetate present) or 100 μM [1,2-^{13}C]acetate (with 10 mM unlabeled glucose present); error bars indicate mean ± SEM of triplicates. For (E–G), all statistical comparisons are to *Acly*$^{f/f}$ using Holm-Sidak test. For all panels: *$p < 0.05$; **$p < 0.01$; ***$p < 0.001$.

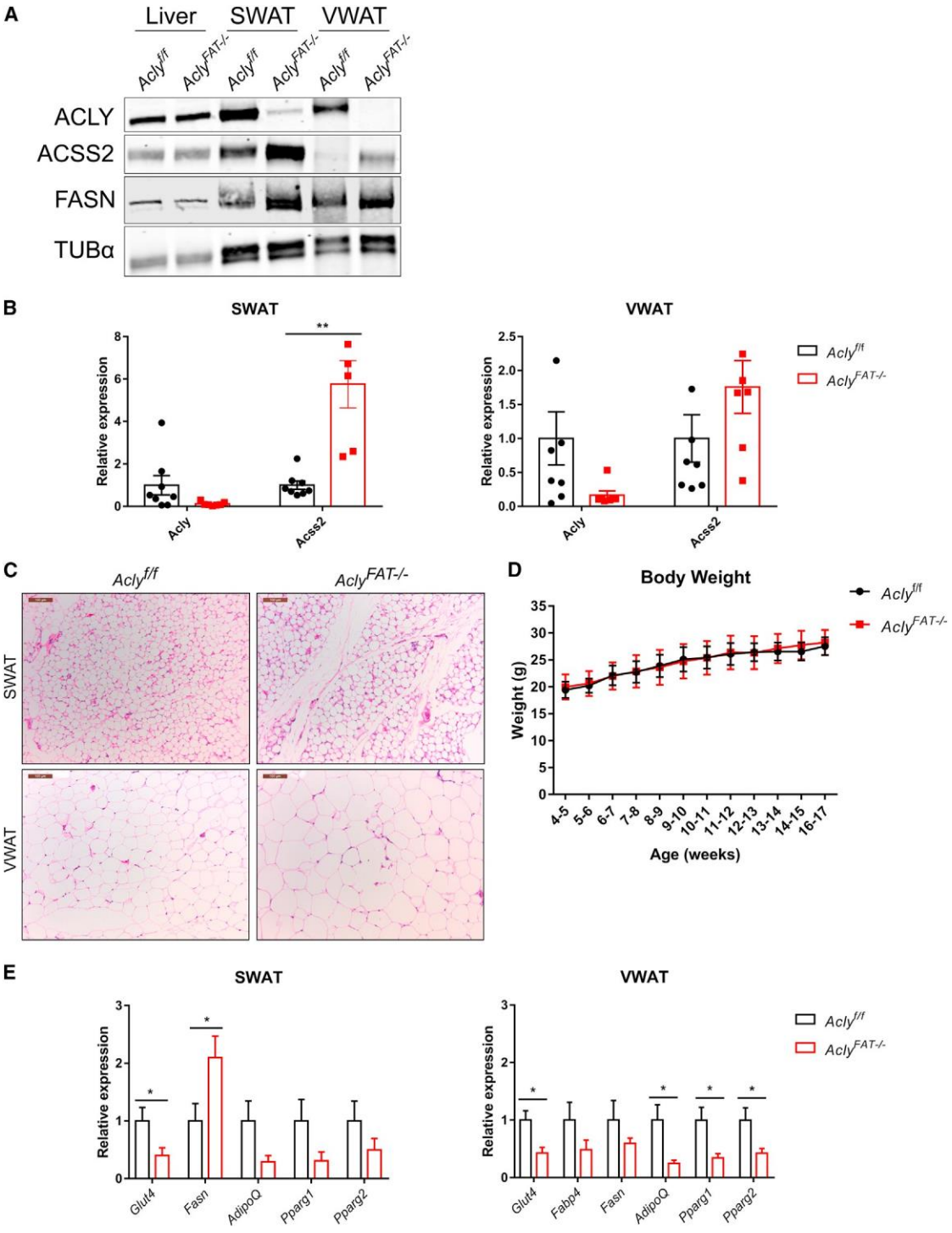

Figure 2.6 | ACSS2 Is Upregulated In Vivo upon Deletion of *Acly* from Adipocytes

(A) Western blot of liver, SWAT, and VWAT from *Acly*$^{f/f}$ and *Acly*$^{FAT-/-}$ mice.

(B) mRNA expression of *Acly* and *Acss2* in SWAT (left) and VWAT (right) from $Acly^{f/f}$ and $Acly^{FAT-/-}$ mice; error bars indicate mean ± SEM.
(C) Representative SWAT and VWAT histology from male 16-week-old $Acly^{f/f}$ and $Acly^{FAT-/-}$ mice. Scale bars, 100 μm.
(D) Body weight of male $Acly^{f/f}$ (n = 9) and $Acly^{FAT-/-}$ (n = 8) mice; error bars indicate mean ± SD.
(E) Expression of adipocyte genes in SWAT (left) and VWAT (right) from $Acly^{f/f}$ (n = 8) and $Acly^{FAT-/-}$ (n = 7) mice; error bars indicate mean ± SEM. For all panels: *p < 0.05; **p < 0.01.

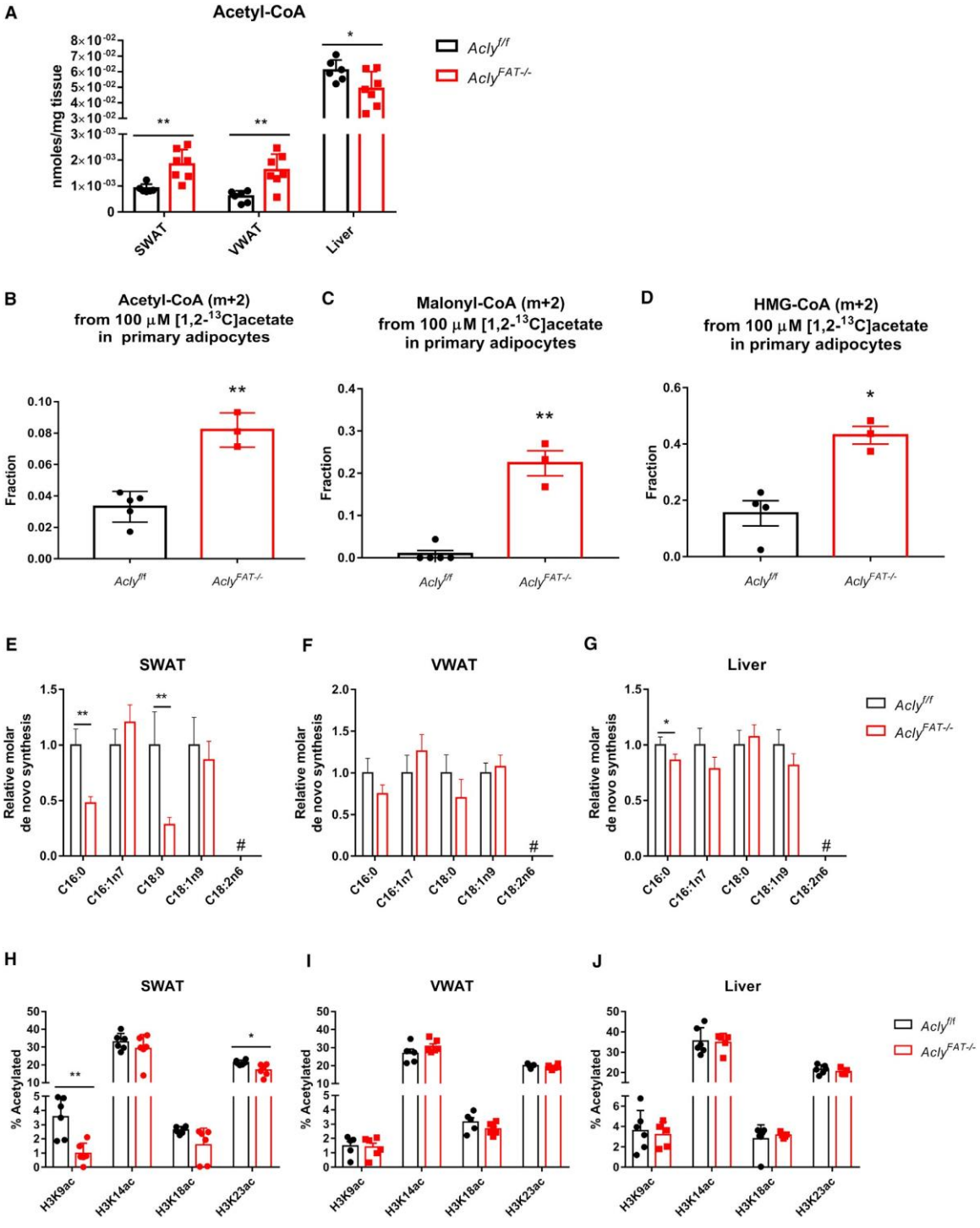

Figure 2.7 | ACLY-Deficient Adipose Tissue Exhibits Depot-Specific Alterations in DNL and Histone Acetylation

(A) Acetyl-CoA abundance in SWAT, VWAT, and liver in 11-week-old *Acly*$^{f/f}$ (n = 6) and *Acly*$^{FAT-/-}$ (n = 7) mice.

(B–D) Primary mature adipocytes were isolated from 12- to 16-week-old *Acly*$^{f/f}$ (n = 5) and *Acly*$^{FAT-/-}$ (n = 3) mice and labeled with 100 μM [1,2-^{13}C]acetate (with 5 mM unlabeled glucose present). Acetyl-CoA (B), malonyl-CoA (C), and HMG-CoA (D) enrichment from acetate was analyzed; error bars indicate mean ± SEM.
(E–G) Relative quantities of fatty acids synthesized de novo in SWAT (E), VWAT (F), and liver (G) of *Acly*$^{f/f}$ (n = 6) and *Acly*$^{FAT-/-}$ (n = 8) mice; error bars indicate mean ± SEM. The # sign indicates not synthesized de novo.
(H–J) Overall histone H3 acetylation levels in 11-week-old SWAT (H), VWAT (I), and liver (J) of *Acly*$^{f/f}$ (n = 6) and *Acly*$^{FAT-/-}$ (n = 7) mice; error bars indicate mean ± SEM.
For all panels: *p < 0.05; **p < 0.01.

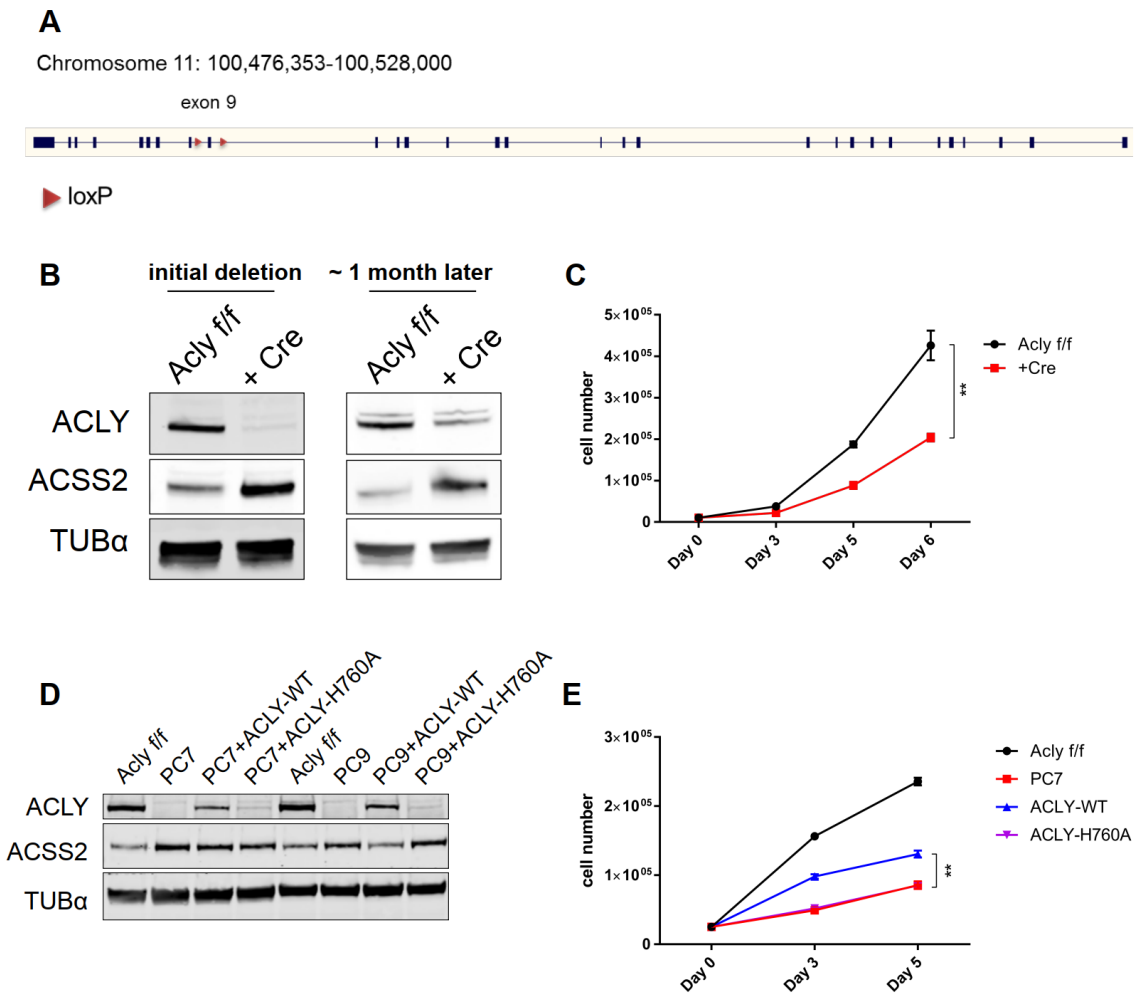

Figure S2.1 | Deletion of Acly from mouse embryonic fibroblasts, related to Fig. 2.1.

(A) Diagram of *Acly* locus in *Acly*$^{f/f}$ mice, loxP sites flanking exon 9 are depicted.

(B) Western blot of ACLY and ACSS2 expression in *Acly*$^{f/f}$ MEFs, +/- Cre treatment at the time of initial deletion and one month later.

(C) Proliferation curve of *Acly*$^{f/f}$ MEFs with or without Cre treatment over 6 days, mean +/- SEM of triplicate wells.

(D) Western blot of ACLY and ACSS2 expression in *Acly*$^{f/f}$ MEFs and PC7 and PC9 knockout lines that have been reconstituted with wild type ACLY (+ACLY-WT) or catalytically dead ACLY (+ACLY-H760A).

(E) Proliferation curve of *Acly*$^{f/f}$ MEF and PC7 lines compared to PC7 with reconstituted ACLY-WT or ACLY-H760A over 5 days, mean +/- SEM of triplicate wells, statistical significance compared to PC7.

For all panels: **, $p<0.01$.

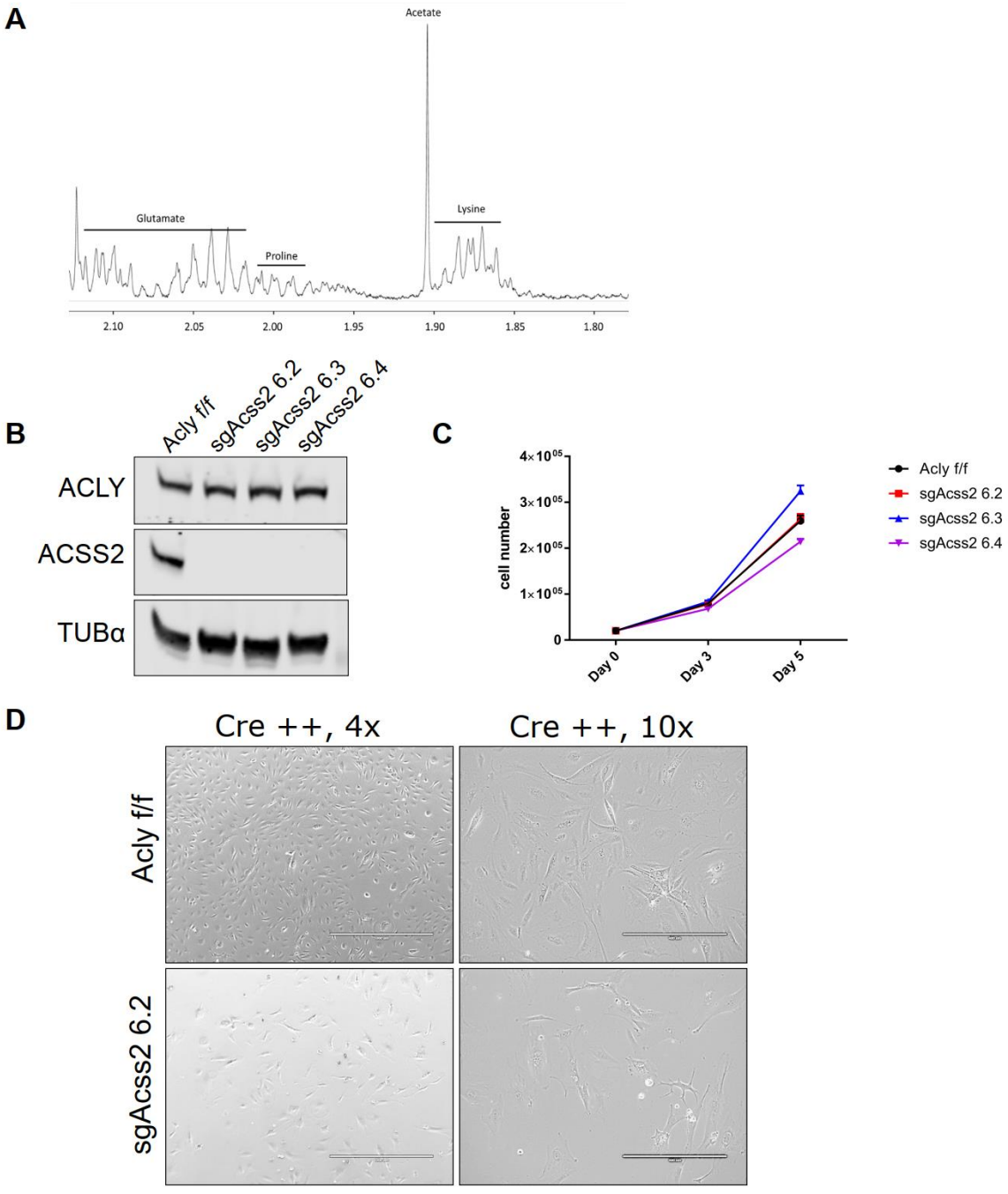

Figure S2.2 | Acetate sustains viability in the absence of ACLY, related to Fig. 2.2.

(A) NMR spectrum of undiluted calf serum.

(B) Western blot verification of Acss2 knockout using CRISPR-Cas9 gene editing in *Acly*$^{f/f}$ MEFs.
(C) Proliferation curve over 5 days of three ACSS2-deficient clonal cell lines as compared to *Acly*$^{f/f}$ MEFs, mean +/- SEM of triplicate wells.
(D) Representative images of *Acly*$^{f/f}$ MEFs and sgAcss2 6.2 *Acly*$^{f/f}$ MEFs, treated twice with adenoviral Cre-recombinase at 4x zoom (left panels, bar represents 1000 µm) and 10x zoom (right panels, bar represents 400 µm).

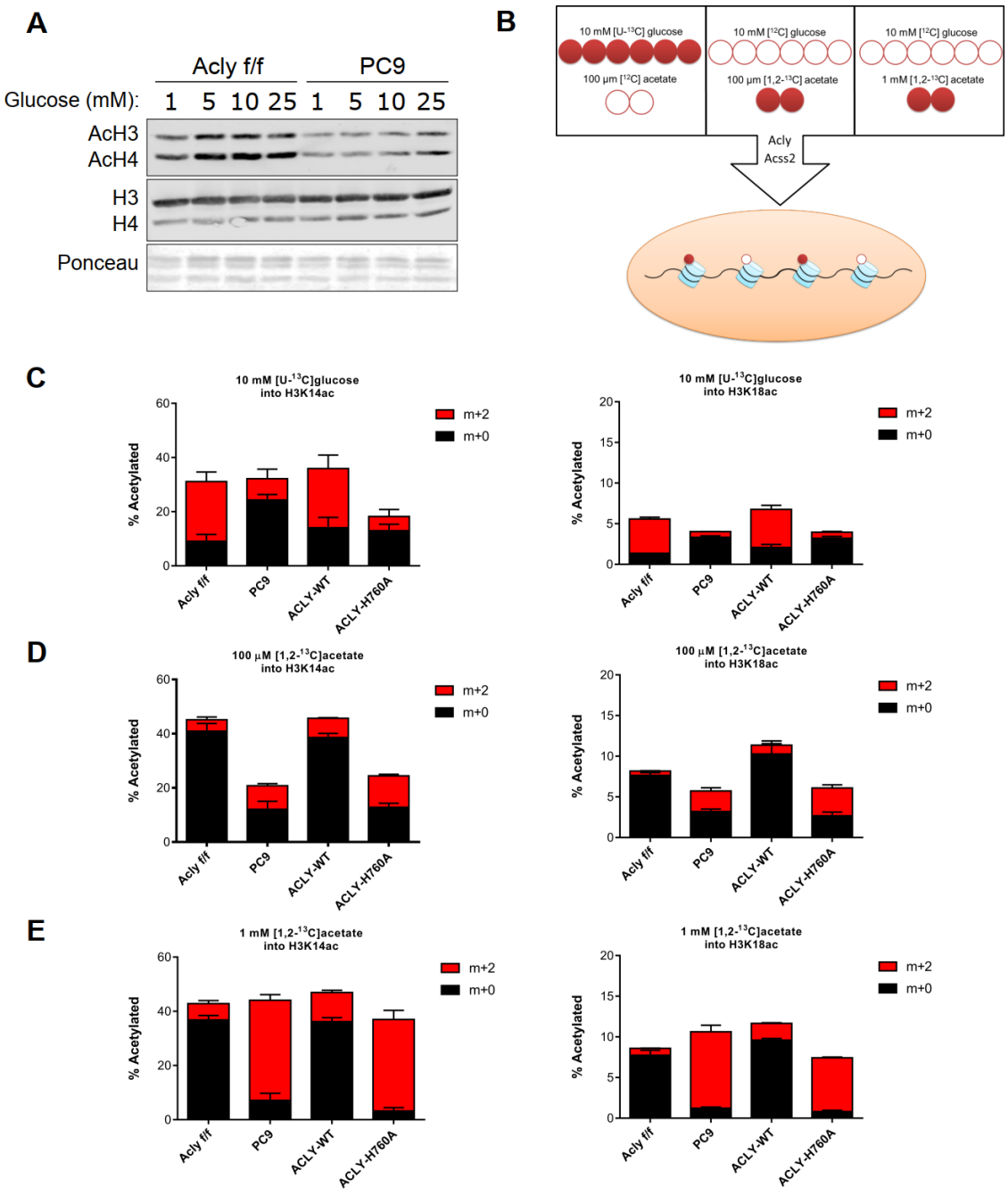

Figure S2.3 | ACLY is required for sustaining histone acetylation levels, related to Fig. 2.4.

(A) Histone acetylation in acid-extracted histones from *Acly*$^{f/f}$ and PC9 MEFs cultured for 24 hours in glucose-free DMEM supplemented with 10% dFBS and the indicated glucose concentrations. (B) Experimental design of heavy isotope labeling of histone acetylation using 10 mM [U-^{13}C]glucose with 100 µM unlabeled acetate present (left), 100 µM [1,2-^{13}C]acetate with 10 mM

unlabeled glucose present (center), and 1 mM [1,2-^{13}C]acetate with 10 mM unlabeled glucose present (right).
(C-E) Percent of total acetylation of H3K14 (left) and H3K18 (right) from labeled (red) and unlabeled (black) sources after labeling with 10 mM [U-^{13}C]glucose (C), 100 µM [1,2-^{13}C]acetate (D), or 1 mM [1,2-^{13}C]acetate (E), mean +/- SEM of triplicate samples.

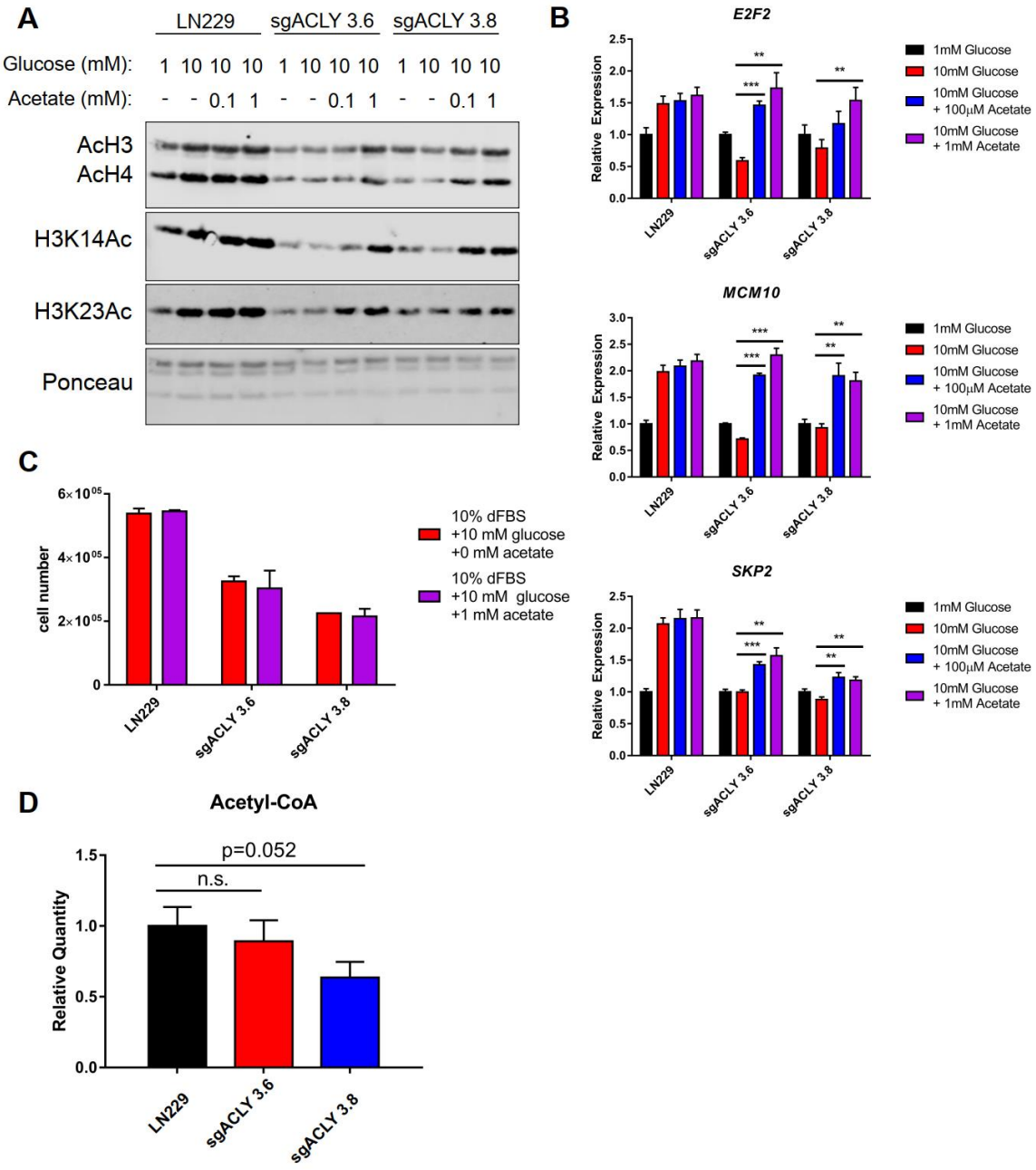

Figure S2.4 | Acetate regulates histone acetylation and gene expression in ACLY-deficient glioblastoma cells, related to Fig. 2.4.

(A) Histone acetylation in acid-extracted histones from LN229 parental and ACLY KO clones cultured for 24 hours in glucose-free RPMI + 10% dFBS + 1 or 10 mM glucose + 2 mM glutamine + 0, 0.1, or 1 mM acetate.

(B) Relative expression of *E2F2*, *MCM10*, and *SKP2* in LN229 parental and ACLY KO clones after 24 hours cultured in the same conditions as in panel A.

(C) Cell number after 48 hours of culture in indicated conditions.
(D) Relative whole cell acetyl-CoA levels in LN229 parental and ACLY KO clones cultured in glucose-free RPMI + 10% dFBS + 10 mM glucose + 100 µM acetate + 2 mM glutamine for 6 hours, normalized to cellular volume, mean +/- SEM of triplicate samples.

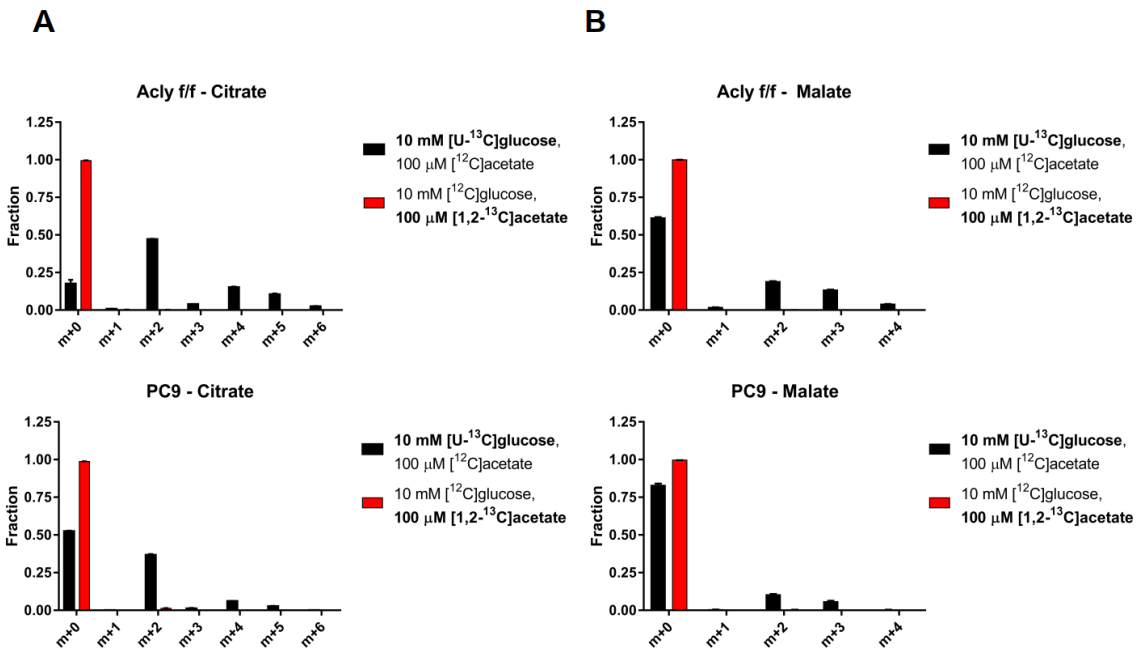

Figure S2.5 | Acetate contributes minimally to mitochondrial metabolism in the absence of ACLY, related to Figure 2.5.

(A,B) Isotopologue distribution of citrate (A) and malate (B) upon 24 hours labeling in 10 mM [U-^{13}C]glucose or 100 μM [1,2-^{13}C]acetate in *Acly$^{f/f}$* (top) and PC9 (bottom) MEFs, mean +/- SEM of triplicate samples.

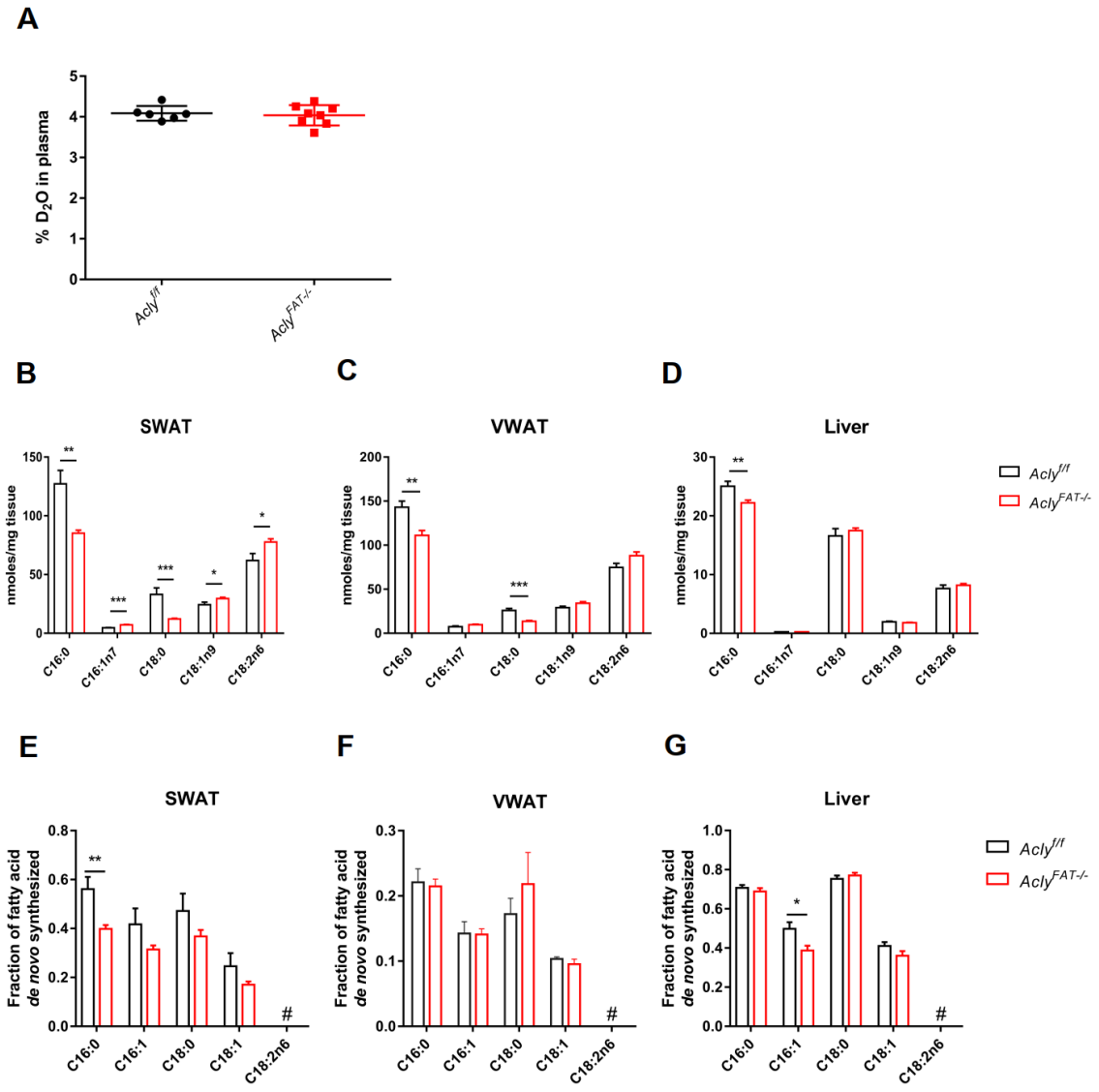

Figure S2.6 | Tissue fatty acid levels and enrichment after D_2O labeling of *Acly*$^{f/f}$ and *Acly*$^{FAT-/-}$ mice, related to Fig. 2.7.

(A) Plasma D_2O enrichment.

(B-D) Abundance of fatty acids in SWAT (B), VWAT (C), and liver (D).

(E-G) Fractions of fatty acids synthesized de novo present in SWAT (E), VWAT (F), and liver (G).

CHAPTER 3: Dietary fructose feeds hepatic lipogenesis via microbiome-derived acetate independent of citrate shuttling.

Abstract

Fructose consumption has risen dramatically in recent decades due to the use of sucrose and high fructose corn syrup in beverages and processed foods[238], contributing to rising rates of obesity and non-alcoholic fatty liver disease (NAFLD)[309–311]. Fructose intake triggers hepatic *de novo* lipogenesis (DNL)[229,311,312], a multistep process that utilizes acetyl-CoA as a substrate. ATP-citrate lyase (ACLY), the enzyme that cleaves cytosolic citrate to generate acetyl-CoA, is potently upregulated upon carbohydrate consumption[250]. Ongoing clinical trials are pursuing ACLY inhibition for treatment of metabolic diseases[313]. The route from dietary fructose to hepatic acetyl-CoA and lipids, however, remains unproven. Here we show that liver-specific *Acly* knockout (LAKO) mice are, unexpectedly, not protected from fructose-induced DNL or fatty liver. *In vivo* isotope tracer studies using ^{13}C-fructose gavage show that fructose-derived carbons are used for DNL even in the absence of ACLY. Dietary fructose is converted by the gut microbiome into acetate[314], which supplies lipogenic acetyl-CoA independently of ACLY[264]. Depletion of the microbiome or silencing of hepatic ACSS2, which generates acetyl-CoA from acetate, potently suppresses fructose conversion into hepatic acetyl-CoA and fatty acids. Thus, bolus fructose feeds hepatic acetyl-CoA pools indirectly via acetate, bypassing ACLY. When fructose is consumed more gradually via drinking water to facilitate its absorption in the small intestine, both ACLY and microbial acetate production contribute to lipogenesis. The DNL transcriptional program, on the other hand, is induced in response to fructose consumption in a manner that is both ACLY- and microbiome-independent, consistent with a direct role for hepatic fructolysis in activating the carbohydrate-response element-

binding protein (ChREBP). These data reveal a two-pronged mechanism regulating hepatic DNL, in which fructolysis within hepatocytes provides a signal to promote DNL, while fructose metabolism by the gut microbiota provides the substrate to feed DNL.

Main Text

Since ACLY links carbohydrate and lipid metabolism (Fig. 3.1a), we hypothesized that genetic deletion of *Acly* in hepatocytes would protect mice against fructose-induced lipid accumulation. While whole body *Acly* knockout is embryonic lethal[5], liver-specific *Acly* knockout (LAKO) mice were grossly indistinguishable from wild-type (WT) littermate controls, with similar body weights and organ sizes between genotypes when fed either standard chow or a high-fructose (60%) diet (HFrD) (Extended Data Fig. 3.1a-b). Fructose consumption triggered mild hepatic lipid accumulation in both WT and LAKO mice (Fig. 3.1b, Extended Data Fig. 3.1d). Neither fibrosis nor excess glycogen accumulation were observed (Extended Data Fig. 3.1c), consistent with prior observations[315]. ACLY protein was not detected within hepatocytes in LAKO livers (Extended Data Fig. 3.1e). Metabolomic and lipidomic analyses revealed striking diet-dependent changes, and relatively modest genotype-dependent differences (Extended Data Fig. 3.2a-b, 3.3a-c). Consistent with loss of ACLY activity, LAKO-specific accumulation of citrate and its downstream metabolite aconitate was observed (Extended Data Fig. 3.2c). Together, these data demonstrate that ACLY deficiency neither dramatically impacts global hepatic metabolite levels nor prevents fructose-induced accumulation of triglyceride.

To more specifically investigate the role of hepatic ACLY in fructose-induced steatosis without altering the overall diet, we fed mice standard chow diets with either normal drinking water (H_2O) or drinking water containing a 1:1 mixture of fructose and glucose

(15% each, Fruc:Gluc) (Extended Data Fig. 3.4a-c). Similar to HFrD, mice drinking Fruc:Gluc for 4 weeks developed mild hepatic steatosis regardless of ACLY expression (Extended Data Fig. 3.4d). Moreover, deuterated water (D_2O) tracing revealed that Fruc:Gluc consumption increases hepatic DNL to a similar extent in WT and LAKO mice (Fig. 3.1c). Thus, deletion of *Acly* from liver does not prevent induction of DNL in response to fructose consumption.

Given the unexpected result that hepatic ACLY is dispensable for fructose-induced DNL (Fig. 3.1c), we directly tested the impact of ACLY deficiency on fructose conversion into nascent fatty acids. WT and LAKO mice were gavaged with 1:1 fructose:glucose, with either glucose or fructose ^{13}C-labeled (Fig. 3.1d). Strikingly, fructose carbons were incorporated into fatty acids in LAKO and WT mice to a similar extent, while glucose carbons were barely used (Fig. 3.1e, Extended Data Fig. 3.5a). These data indicate that, in contrast with existing models of fructose metabolism, the use of fructose carbons for hepatic DNL does not require ACLY.

We next investigated the mechanisms of how fructose carbons are used for fatty acid synthesis in an ACLY-independent manner. It has been previously shown that the hepatic DNL program is activated in response to carbohydrate consumption by ChREBP[316,317]. Upon chronic high fructose consumption, livers of both WT and LAKO mice upregulated the highly active ChREBP-β isoform[285], along with lipogenic genes (*Acaca* and *Fasn*) and other ChREBP target genes, aldolase B (*AldoB)*, and ketohexokinase (*Khk)*[318] (Fig. 3.1f, Extended Data Fig. 3.6a). WT mice also exhibited upregulation of *Acly* on HFrD (Fig. 3.1f). The induction of the DNL program was also robust at the protein level (Fig. 3.1g, Extended Data Fig. 3.6b). Acyl-CoA synthetase short chain family member 2 (ACSS2), which

converts acetate into acetyl-CoA, was notably upregulated in fructose-consuming LAKO mice (Fig. 3.1g, Extended Data Fig. 3.6a-b). Moreover, the *Acss2* genomic locus showed increased histone H3K27 acetylation, as well as ChREBP binding, after Fruc:Gluc drinking, concurrent with induction of DNL transcriptional program (Extended Data Fig. 3.6c-e). We also confirmed ChREBP binding to the *Acss2* locus in a published ChREBP ChIP-Seq study dataset[319] (Extended Data Fig. 3.6f). Acss2 is also a known target of SREBP transcription factors, which are also activated in response to fructose consumption[9,320,321]. These data suggest that *Acss2* is component of the hepatic response to fructose consumption.

Since acetate conversion to acetyl-CoA by ACSS2 can support *de novo* lipogenesis in the absence of ACLY[264], we hypothesized that acetate might be an important source of acetyl-CoA for hepatic DNL in the context of fructose feeding (Fig. 3.2a). Acetate can be generated within mammalian cells through several mechanisms, including acetyl-CoA hydrolysis, histone deacetylation, and pyruvate to acetate conversion[322–324], prompting us to investigate whether fructose is converted to acetate in a cell autonomous manner in hepatocytes. In primary hepatocytes, high concentrations of glucose induce the DNL gene program[325]. Incubation of wild-type murine hepatocytes with 25 mM ^{13}C-fructose resulted in considerable labeling of fructolytic intermediates (Fig. 3.2b). Surprisingly, however, ^{13}C-fructose minimally labeled acetyl-CoA and malonyl-CoA, the core DNL substrates, in WT hepatocytes (Fig. 3.2c). In contrast, ^{13}C-acetate, even at a much lower concentration, labeled acetyl-CoA and malonyl-CoA, as well as HMG-CoA, an intermediate in the mevalonate pathway downstream of acetyl-CoA (Fig. 3.2c). Therefore, even when ACLY is intact, fructose catabolism may be uncoupled from DNL in primary hepatocytes, while exogenous acetate can directly feed into lipogenic acetyl-CoA pools.

These findings suggested the possibility that fructose may be converted to acetate by a different cell type prior to reaching the liver, in order to feed hepatic DNL. To test this possibility *in vivo*, we performed a ^{13}C-fructose tracing time course in mice. Orally administered ^{13}C-fructose quickly labeled fructose-1-phosphate (F1P) and pyruvate in the liver with peaks between 15-30 min, indicative of rapid hepatic fructolysis (Fig. 3.2d). Hepatic acetyl-CoA labeling was, however, much slower (peaking at 60-90 min) (Fig. 3.2d). The slower kinetic of acetyl-CoA labeling was closely aligned with the appearance of labeled acetate in the portal circulation (Fig. 3.2d). Labeling of hepatic fatty acids follows that of acetyl-CoA (peaking at 120-180 min) (Fig. 3.2d). These data suggest that fructose may primarily feed hepatic acetyl-CoA and fatty acid production indirectly via acetate generated from fructose.

We next sought to determine the source of fructose-derived acetate. While fructose is mainly taken up by the small intestine, unabsorbed fructose reaches the colon where the microbiome converts fructose into short chain fatty acids (SCFAs), including acetate[314]. To test if the microbiome is important for hepatic DNL, we depleted it with an antibiotic cocktail (Extended Data Fig. 3.7a-c, 3.8b). Antibiotic treatment did not suppress the levels of labeled fructose and glucose in the portal vein following an oral administration of ^{13}C-fructose (Extended Data Fig. 3.7d-e), indicative of intact small intestine fructose absorption and metabolism. The induction of hepatic DNL genes following fructose consumption is thought to be dependent on fructolytic and/or glycolytic intermediates[316,326], and silencing of hepatic *Khk* suppresses fructose-induced upregulation of DNL gene expression[321]. Consistent with normal passage of fructose from the intestine to the liver, DNL gene expression upon fructose consumption remained intact after antibiotic treatment (Extended Data Fig. 3.7f), as did labeling of F1P, pyruvate and

citrate in the liver (Fig. 3.3a). In contrast, microbiome depletion dramatically reduced the labeling of hepatic acetyl-CoA and palmitate, as well as fatty acids within circulating lipids, from ^{13}C-fructose (Fig. 3.3a,b, Extended Data Fig. 3.8a). This reduction was well matched with depleted portal and cecal labeling of acetate, as well as other short-chain fatty acids (Fig. 3.3a, Extended Data Fig. 3.7g-h). Antibiotic treatment also reduced total hepatic triglycerides (Fig. 3.3c), which is consistent with prior observations[240,327]. Thus, depletion of the microbiome suppresses hepatic DNL from ^{13}C-fructose, without impairing small intestine or hepatic fructose metabolism or induction of DNL gene expression.

We next aimed to determine if acetate is a key microbial product supporting DNL. To assess whether fructose intake led to an appreciable increase in portal acetate concentrations, we measured acetate in portal and systemic blood after gavage. Portal vein acetate concentrations increased approximately twofold over baseline (to > 1 mM) at 60-90 minutes after fructose gavage (Fig. 3.3d), corresponding with acetate labeling from fructose (Fig. 3.2d). Strikingly, the rise in portal acetate was absent in antibiotic treated animals (Fig. 3.3d). Acetate concentrations in systemic circulation were lower than that in the portal vein and did not markedly fluctuate after fructose consumption, suggesting that fructose-derived acetate is primarily cleared by the liver (Fig. 3.3d). Next, to assess whether acetate supports DNL downstream of microbial metabolism, mice were gavaged with ^{13}C-acetate, along with 1:1 fructose:glucose. This showed that DNL from ^{13}C-acetate, in contrast to that from ^{13}C-fructose, is not impacted by antibiotic treatment (Fig. 3.3e). Finally, to test if hepatic ACSS2 is required for fructose to feed DNL, ACSS2 in the liver was silenced using an adeno-associated viral hairpin targeting *Acss2*[328] (Extended Data Fig. 3.8c-e). Depletion of hepatic ACSS2 strongly suppressed the labeling of circulating lipids from ^{13}C-fructose (Fig. 3.3f). Altogether, these data point to a two-pronged

mechanism of fructose-dependent DNL, with cell autonomous effects of fructose and/or glucose in stimulating the hepatic DNL transcriptional program, but microbiome-dependent acetate production serving as the major source of fructose-derived acetyl-CoA for lipogenesis, via hepatic ACSS2, after consumption of a fructose bolus (Extended Data Fig. 3.10a).

Microbiome-dependent acetate production from fructose occurs when rate of ingestion exceeds small intestinal uptake capacity[314]. Thus, if fructose is consumed gradually, its contribution to DNL might occur to a greater extent via ACLY, and to a lesser extent via microbial acetate production. Still, upon providing Fruc:Gluc in the drinking water, DNL was comparably stimulated in the presence or absence of ACLY (Fig. 3.1c). To explore this further, mice were given ^{13}C-labeled fructose or glucose in drinking water for 24 hours (Fig. 3.4a). Fructose-derived carbons provided a substantial contribution to hepatic lipid pools, with greater than 20% of total liver fatty acid carbons being labeled from ^{13}C-fructose after 24 hours of Fruc:Gluc drinking, while ^{13}C-glucose contributed less (Fig. 3.4b). In this context of more gradual fructose intake, ACLY deficiency suppressed ^{13}C-fructose and -glucose contribution to hepatic fatty acids (Fig. 3.4b). Nevertheless, total DNL as measured by D_2O labeling was not different between WT and LAKO mice (Fig. 3.4c), indicating sufficient availability of other two-carbon unit donors. One possibility is assimilation of acetate from other sources (e.g. fiber fermentation). To test utilization acetate for lipogenesis, we supplemented Fruc:Gluc drinking water with ^{13}C-acetate upon initial exposure (naïve) as well as after 2 weeks of Fruc:Gluc water (conditioned) (Extended Data Fig. 3.9a). Fatty acid labeling from ^{13}C-acetate was higher in LAKO mice at baseline (Fig. 3.4d). After fructose conditioning, acetate contribution to DNL increased in WT animals, and this was further enhanced in LAKO mice (Fig. 3.4d), consistent with

increased hepatic ACSS2 expression in LAKO mice following fructose feeding, which preceded the onset of steatosis (Extended Data Fig. 3.9b-c). We next assessed the contribution of microbiome-derived acetate from all dietary sources in the context of sweetened water consumption. Antibiotic treatment suppressed total hepatic DNL in LAKO mice (Fig. 3.4e, Extended Data Fig. 3.9d). ChREBPβ and DNL gene expression were confirmed to be upregulated by Fruc:Gluc drinking in all groups (Fig. 3.4f). Finally, we examined DNL in Fruc:Gluc-drinking mice following silencing of hepatic ACSS2, finding that in the context of gradual fructose consumption via drinking water, loss of both ACLY and ACSS2 is necessary to suppress DNL (Fig. 3.4g). These data indicate that when fructose is consumed gradually to reduce its passage into the colon, the rate of DNL is established by signaling mechanisms (i.e., sugar-driven ChREBP activation), and DNL is suppressed only when acetyl-CoA production by both ACLY and ACSS2 is inhibited (Extended Data Fig. 3.10b).

In this study, we demonstrate that bolus fructose consumption triggers hepatic DNL independent of ACLY but dependent on fructose metabolism by gut microbiota. We found that fructose feeds hepatic fatty acid synthesis through its microbial metabolism to acetate, which reaches the liver via the portal vein. The induction of the DNL transcriptional program in the liver, on the other hand, appears to be independent of both ACLY and the microbiome, consistent with the notion that proximal fructolytic and/or glycolytic metabolites are important for ChREBP activation. When consumed more gradually, fructose can feed DNL in an ACLY-dependent manner. However, acetate from other sources is also readily available to the liver, rendering ACLY dispensable for DNL even when fructose is gradually consumed. The data also suggest that diet and microbiome could potentially impact the efficacy of ACLY inhibitors, currently in clinical trials for

hypercholesterolemia[329]. Prior studies using RNAi to silence hepatic ACLY have reported that ACLY deficiency decreases hepatic lipid in *db/db* mice, but increases hepatic lipid in mice fed a high fat diet[251,330]. In our own data, principal component analysis of hepatic triglycerides separated LAKO mice from WT mice on HFrD but not on chow (Extended Data Fig. 3.3c), supportive of the notion that ACLY may play distinct roles depending on diet. Thus, further study of the impact of ACLY deficiency in different nutritional contexts will be important to understand its physiological roles and to optimally leverage ACLY inhibitors for the treatment of metabolic diseases.

Although hepatic fructose metabolism does not appear to directly supply substantial amounts of lipogenic acetyl-CoA, fructolysis and/or glycolysis in hepatocytes remain important for DNL induction at least in part to activate the DNL transcriptional program (Extended Data Fig. 7f). This likely explains why KHK knockout mice are protected from fructose-induced fatty liver[331,332]. Thus, we propose a revised model of fructose-dependent DNL induction, in which hepatic fructose metabolism provides a signal to transcriptionally promote DNL while microbial fructose metabolism provides acetate to feed DNL (Extended Data Fig. 10a). These dual mechanisms may also explain higher lipogenic potential of fructose as compared to glucose[333], at least in the context of high dose sugar consumption, in that the small intestine rapidly absorbs even large loads of glucose, whereas fructose spills over to the gut microbiome to generate acetate[314]. The data also indicate that fructose-dependent activation of the DNL transcriptional program can trigger enhanced DNL from other acetate sources (Extended Data Fig. 10b). Thus, it will be important in the future to define how fructose interacts with other dietary sources of acetate, such as ethanol and fermentable fibers. NAFLD currently afflicts ~30% of the United States population and can be a precursor to non-alcoholic steatohepatitis and

hepatocellular carcinoma[334]. Understanding the fundamental pathways involved in hepatic DNL is important for the development of new therapeutic interventions for metabolic diseases. The current data elucidate a previously unappreciated interplay between diet, the gut microbiome, and host organ metabolism that contributes to fructose-induced NAFLD.

Methods

Generation of Liver-specific ACLY Knockout (LAKO) mice:

Generation of *Acly*$^{f/f}$ mice on a C57Bl6/J background was previously described[264]. To generate hepatocyte-specific *Acly* knockouts, *Acly*$^{f/f}$ mice were crossed to albumin-Cre transgenic mice (B6.Cg-Tg(Alb-Cre)21Mgn/J, Jackson Laboratory)[335].

Genoptying:

Genotyping of the recombined Acly allele was confirmed as previously described[264]. Genotyping of the Albumin-Cre allele was confirmed with the following primer sequences: AlbCre-5'F (CCTGCCAGCATGGATATAA), AlbCre-3'R (GTTGTCCTTTGTGCTGCTGA), Alb-TSP3 (GAAGCAGAAGCTTAGGAAGATGG), and the following cycling conditions: 1 cycle - 94^{o} x 5 min. 35 cycles - 94^{o} x 45 sec., 58^{o} x 45 sec., 72^{o} x 1 min. 1 cycle - 72^{o} x 10 min, hold at 4^{o}C.

Animal studies:

All animal protocols in this study were approved by the University of Pennsylvania's Institutional Animal Care and Use Committee (IACUC) and Princeton University's

IACUC. For diet studies, 4-week-old male mice were placed on either a regular chow diet (Lab Diet 5010) or a high-fructose chow diet (Teklad TD.89247) for indicated lengths of time. Weights of mice kept on each diet were taken weekly. For drinking water studies, mice were provided with regular tap water (filtered through a 0.22 µm filter) or a 15% (w/v) fructose:15% (w/v) glucose (Sigma F3510, G8270) in tap water (filtered through a 0.22 µm filter). To deplete the gut microbiome, mice were given a daily 10 µL/g body weight oral gavage consisting of 1 mg/mL ampicillin, 1 mg/mL gentamicin, 0.5 mg/mL vancomycin, 1 mg/mL neomycin, 1 mg/ml metronidazole in a 0.9% NaCl solution for 7-10 days. Studies were controlled to mice given the same 0.9% NaCl solution without antibiotics. To knockdown *Acss2*, 6-8 week-old male mice were injected via tail vein with 2.0 x 10^{11} GC/mouse AAV8.U6.shAcss2.CMV.eGFP.SV40 (University of Pennsylvania Vector Core) or AAV8.CMV.PI.eGFP.WPRE.bGH (Addgene) as control; experiments were performed 1 week after injection.

Histology:

For H&E, Periodic Acid Shiff, Trichrome staining: tissues were fixed in formalin overnight, dehydrated by titrating in ethanol (50%, 75%, 95%), and submitted to the Molecular Pathology and Imaging Core at the University of Pennsylvania for paraffin embedding, sectioning, and staining. For Oil Red O staining: tissues were fixed in formalin overnight, dehydrated by titrating in sucrose (10%, 20%, 30%), and embedded in Richard-Allan Scientific NEG-50 frozen section medium (ThermoFisher Scientific 6502) by freezing in 2-methylbutane that was cooled using dry ice. Tissues frozen in NEG-50 were submitted to the Molecular Pathology and Imaging Core at the University of Pennsylvania for cryosectioning and staining. Images were acquired on a Keyence BZ-X710 microscope.

Bacterial quantification:

Cecal contents were collected, snap frozen, and weighed before storage in -80C until use. DNA was extracted from cecal contents using a Fecal DNA extraction kit (IBI scientific IB47821) according to manufacturer instructions. Samples were diluted 1:1000 prior to use for RT-PCR. To establish a bacterial DNA standard, genomic DNA was extracted from *Stbl3* E. coli cells. A standard curve was generated using a 1:4 serial dilution starting with 10 ng of E. coli DNA. RT-PCR was performed as described, using previously published universal 16s primers (Forward: TCCTACGGGAGGCAGCAGT, Reverse: GGACTACCAGGGTATCTAATCCTGTT)[336]. Relative bacterial load was calculated by normalizing DNA content to initial cecal content weight.

Immunoblotting:

Protein extraction from tissue was performed by re-suspending frozen tissue in 0.5 mL of RIPA buffer (1% NP-40, 0.5% Deoxycholate, 0.1% SDS, 150 mM NaCl, 50 mM Tris plus protease and phosphatase inhibitors), and lysed using a tissue lyser (Qiagen) twice for 30 seconds at 20 Hz. Following lysis, samples were incubated on ice for 10 minutes, then spun down at 15,000 RCF for 5 minutes in 4^{o}C. Supernatant was collected and stored in -80^{o}C until immunoblotting. Antibodies used in this study: ATP-Citrate Lyase (Proteintech 15421-1-AP), Acyl-CoA Synthetase Family Member 2 (Cell Signaling Technology 3658S), Acetyl-CoA Carboxylase (Cell Signaling Technology 3676S), Fatty Acid Synthase (Cell Signaling Technology 3189S), Catalase (Cell Signaling Technology 14097S), Ribosomal Protein S6 (Cell Signaling Technology 2217S), IRDye800CW Goat Anti-Rabbit (LI-COR 926-32211). Immunoblots were developed using a LI-COR Odyssey Clx.

Quantitative RT-PCR:

RNA extraction from tissue was performed by re-suspending frozen tissue in 1 mL Trizol (Life Technologies), and lysed using a tissue lyser (Qiagen) for 60 seconds at 30 Hz, followed by manufacturer protocol for Trizol RNA extraction. cDNA was synthesized using high-capacity RNA-to-cDNA master mix (Applied Biosystems 4368814), as per the kit instructions. cDNA was diluted 1:20 and amplified using PowerUp SYBR Green Master Mix (Applied Biosystems A25778) on the ViiA-7 Real-Time PCR system. Fold change in expression was calculated using ΔCt, with 18S reference gene as an endogenous control. Primer sequences for RT-qPCR are: Aldob (Forward: GAAACCGCCTGCAAAGGATAA, Reverse: GAGGGTCTCGTGGAAAAGGAT), Khk (Forward: ATGTGGTGGACAAATACCCAGA, Reverse: CAAGCAAGGAAAGGACAGTGC), Acly (Forward: TTCGTCAAACAGCACTTCC, Reverse: ATTTGGCTTCTTGGAGGTG), Acss2 (Forward: GCTTCTTTCCCATTCTTCGGT, Reverse: CCCGGACTCATTCAGGATTG), Chrebpα (Forward: CGACACTCACCCACCTCTTC, Reverse: TTGTTCAGCCGGATCTTGTC), Chrebpβ (Forward: TCTGCAGATCGCGTGGAG, Reverse: CTTGTCCCGGCATAGCAAC), Fasn (Forward: ATTGGTGGTGTGGACATGGTC, Reverse: CCCAGCCTTCCATCTCCTG), Acc1 (Forward: ACAGTGGAGCTAGAATTGGAC, Reverse: ACTTCCCGACCAAGGACTTTG).

Measurement of *de novo* lipogenesis using isotope tracers:

To assess total lipogenesis, mice were provided with 50% (v/v) deuterated water (Sigma 151882) mixed into 15% fructose:15% glucose drinking water for 24 hours. Systemic blood was collected by cardiac puncture, allowed to coagulate on ice for 10 minutes, and spun down at 15,000 x RCF for 10 minutes at 4^{o}C to collect serum. To account for differences in drinking water consumption, calculated deuterium enrichment labeling in

serum water was used to normalize labeling into fatty acids. To assess lipogenesis from dietary carbohydrates, on day of experiment, mice were weighed and fasted from 10 a.m. until 3 p.m., when they were given an oral gavage consisting of a 1:1 mixture of glucose and fructose in a 0.9% NaCl saline. Doses used in this study ranged from 1.0g/kg of each sugar to 2.0g/kg of each hexose. [U-^{13}C]-glucose (CLM-1396-1) or [U-^{13}C]-fructose (CLM-1553-1) were provided with the corresponding unlabeled hexose. Six hours following gavage, systemic blood was collected by tail bleeding the mice and incubating the blood on ice for 15 minutes before spinning down at 15,000 x RCF for 10 minutes at 4^{o}C to collect serum. Tissues were collected using a clamp pre-cooled with liquid nitrogen. The frozen liver samples were ground at liquid nitrogen temperature with a Cryomill (Retsch, Newtown, PA). Saponification of lipids and LC-MS analysis were performed as previously described[337]. Briefly, serum (20 µL) or tissue powder (10 mg) was incubated with 1 mL of 0.3 M KOH in 90% methanol at 80°C for 1 hour in a 2 mL glass vial. Formic acid (0.1 mL) was then added for neutralization. The saponified fatty acids were extracted by adding 0.5 mL of hexane, vortexing, and transferring the top hexane layer to a new glass vial. Samples were then dried under a stream of N2 and dissolved in 1 mL of isopropanol:methanol (1:1, v/v) solution for LC-MS analysis. Separation was performed by reversed-phase ion-pairing chromatography on a C8 column coupled to negative-ion mode, full-scan LC-MS at 1-Hz scan time and 100,000 resolving power (stand-alone orbitrap; Thermo Fischer Scientific). Data analysis with MAVEN software and natural isotope correction were performed as previously described[338].

Primary Hepatocyte Isolation:

Hepatocytes were isolated using a two-step collagenase/DNAse digestion protocol[339] and plated in M199 media containing 5 mM glucose, 10% FBS, 500 nM dexamethasone and 1 nM insulin. Following attachment, cells were changed to M199 media containing 5 mM glucose, 500 nM dexamethasone and incubated overnight. Cells were switched to M199 containing 5 mM glucose, 10% FBS, 500 nM dexamethasone, 100 nM insulin and respective fructose and acetate supplementation for 6 hours on day of experiment.

Acyl-CoA measurements in primary hepatocytes:

Acyl-CoA measurements in primary hepatocytes were performed by liquid chromatograpy-mass spectrometry/high-resolution mass spectrometry (LC-MS/HRMS) as previously described[292]. Briefly, primary hepatocytes were isolated and cultured as described above in 6-well plates. At harvest, culture media was completely aspirated before harvesting cells in 0.5 mL ice-cold 10% trichloroacetic acid/well of a 6-well dish using a cell lifter. Samples were then sonicated for 10 x 0.5 second pulses to completely disrupt cellular membranes, and incubated on ice to precipitate proteins. Protein was pelleted at 16,000 x RCF for 10 minutes at 4^{o}C. Supernatant was collected and purified by solid-phase extraction using Oasis HLB 1cc (30 mg) SPE columns (Waters). Eluate was evaporated to dryness under nitrogen gas and re-suspended in 50 µL of 5% 5-sulfosalicylic acid (w/v) for injection. Samples were analyzed by an Ultimate 3000 autosampler coupled to a Thermo Q-Exactive Plus instrument in positive electrospray ionization (ESI) mode. For isotopic tracer analysis, isotopic enrichment from [U-^{13}C]-fructose (Cambridge Isotope Laboratories, CLM-1553) or [U-^{13}C]-acetate (Cambridge Isotope Laboratories, CLM-440-1) was calculated to compensate for the non-linearity of isotopic enrichment using the FluxFix calculator[340].

Fructolyic measurements in primary hepatocytes:

For fructolytic intermediate measurements in primary hepatocytes, culture media was completely aspirated before harvesting cells in 0.5 mL of cold 80:20 methanol:water/well of a 6-well dish using a cell lifter. Samples were then sonicated for 10 x 0.5 second pulses to completel disrupt cellular membranes, and incubated on ice. Samples were then spun down at 16,000 x RCF for 10 minutes at 4^{o}C. Supernatant was collected and dried under nitrogen gas flow in preparation for water-soluble metabolomic analysis.

Chromatin Immunoprecipitation (ChIP) – PCR:

For H3K27ac-ChIP qPCR studies, male mice were provided with Fruc:Gluc drinking water for 24 hours, and orally gavaged with 2.0 g/kg fructose + 2.0 g/kg glucose 1 hour prior to sacrifice. For ChREBP-ChIP qPCR studies, female mice were provided with Fruc:Gluc drinking water for 24 hours, and orally gavaged with 3.0 g/kg fructose + 3.0 g/kg glucose 1 hour prior to sacrifice. ChIP was performed as previously described[341] with adjustments to start from liver tissue. Briefly, liver tissues were harvested from mice 90 minutes following gavage, and 100 mg of tissue was weighed out. Tissues were homogenized by mincing briefly with razor blades followed by resuspension in 5 mL of ice-cold 1X PBS and several passages through a 16 gauge syringe needle into 15 mL conical tubes. Samples were crosslinked with 2% formaldehyde for 10 minutes at room temperature. The reactions were quenched with 0.25 M glycine. The cells were then washed with 1X PBS and resuspended in cell lysis buffer (10 mM Tris-HCl pH 8.1, 10 mM NaCl, 1.5 mM $MgCl_2$, 0.5% NP-40), supplemented with protease inhibitors (Roche). The cell pellet was resuspended in 0.5 mL of nuclear lysis buffer (50 mM Tris-HCl pH 8.1, 5 mM EDTA, 1% SDS) supplemented with protease inhibitors. The chromatin was fragmented with a Diagenode Bioruptor Pico (12 cycles of 30 s on followed by 30 s off, at 4°C). Samples were incubated with protein G magnetic beads (Millipore-Sigma 16-

662) and H3K27ac (Abcam ab4729), ChREBP (Novus Biologicals NB400-135), or Normal Rabbit IgG (Cell Signalling Technology 2729S) antibody overnight at 4°C. The next day, samples were washed 5 times with decreasingly stringent buffers. ChIP DNA was eluted off the beads by incubating beads in 125 µL elution buffer for 10 minutes at 65°C. The combined supernatant was then incubated overnight at 65°C to reverse crosslinks and proteinase K treated for 1 hour the next morning. Samples were purified using Macherey-Nagel DNA purification kit, with NTB binding buffer. Samples were diluted 1:5 in nuclease-free water prior to RT-qPCR reactions, which were performed as described above with the following primers: Mlxipl p1 (Forward: CGCACCCGGTCTACAGTTT, Reverse: GTGCCTCCTTCTCTCCTTAGC), Mlxipl p2 (Forward: GCCATCCACGTGCTAAGGA, Reverse: GGCTTTTAGACTGGGGTGTGG), Mlxipl igc (Forward: CCCAACAATCACCCAGCTTC, Reverse: GCGCCATCAGTACAAGCTCT), Pklr p1 (Forward: GGGAAGGATGCCCACTACAG, Reverse: TGGAAGCCTTGTACACTGGG), Pklr p2 (Forward: CCCAGTGTACAAGGCTTCCAT, Reverse: CTCTGCCTTTGTCAGTGGGA), Acss2 p1 (Forward: ATTGGATGCCTAGAGCACGG, Reverse: CGCATCAAGTTCCGAACACC), Acss2 p2 (Forward: TCAGGACAGTTTAGGGTGCAA, Reverse: TTACAAAGACCTGCCTCTGCC). Acss2 p3 (Forward: GAGACTCTGGCCTACCACCA, Reverse: GGGCAGGATTTGTGGCTTGT), Acss2 igc (Forward: GGCGAAAGAAGTTTCTGTTTTGG, Reverse: TTGCCTTTTCAGTGAGGCTGTC).

Triglyceride Measurements:

Triglyceride measurements were performed using a Triglyceride Colorimetric Assay Kit (Cayman Chemical 10010303) as per manufacturer instructions.

Metabolomics:

Water-soluble metabolite extraction was performed as previously described[314]. For serum samples, 100 µL -20°C 40:40:20 methanol:acetonitrile:water (extraction solvent) was added to 5 µL of serum sample and incubated on ice for 10 min, followed by vortexing and centrifugation at 16,000 x g for 10 min at 4°C. The supernatant (first extract) was transferred to a new tube. Then, 50 µL extraction solution was added to resuspend the pellet, followed by vortexing and centrifugation at 16,000 x g for 10 min at 4°C. The supernatant (second extract) was combined with the first extract. Then, 3 µL of the 150 µL extract was loaded to LC-MS. For tissue samples, frozen tissue samples were ground at liquid nitrogen temperature with a Cryomill (Retsch, Newtown, PA). The resulting tissue powder was weighed (~20 mg). The extraction was then done by adding -20°C extraction solvent to the powder and incubating in -20°C overnight, followed by vortexing and centrifugation at 16,000 x g for 10 min at 4°C. The volume of the extraction solution (µL) was 40 x the weight of tissue (mg) to make an extract of 25 mg tissue per mL solvent. Serum and tissue extracts were analyzed by LC-MS, using two different LC-MS methods chosen for optimal separation of glucose and fructose (in serum) and of hexose phosphate species (from tissues). Serum extracts were analyzed (without drying) using a quadrupole-orbitrap mass spectrometer (Q Exactive, Thermo Fisher Scientific, San Jose, CA) operating in negative ion mode, coupled to hydrophilic interaction chromatography via electrospray ionization and used to scan from m/z 70 to 1000 at 1 Hz and 75,000 resolution. LC separation was on a XBridge BEH Amide column (2.1 mm x 150 mm, 2.5 µm particle size, 130 Å pore size) using a gradient of solvent A (20 mM ammonium acetate, 20 mM ammonium hydroxide in 95:5 water: acetonitrile, pH 9.45) and solvent B (acetonitrile). Flow rate was 150 µl/min. The LC gradient was: 0 min, 85% B; 2 min, 85% B; 3 min, 80% B; 5 min, 80% B; 6 min, 75% B;

7 min, 75% B; 8 min, 70% B; 9 min, 70% B; 10 min, 50% B; 12 min, 50% B; 13 min, 25% B; 16 min, 25% B; 18 min, 0% B; 23 min, 0% B; 24 min, 85% B; 30 min, 85% B. Autosampler temperature was 5°C, and injection volume was 3 µL. Tissue extracts were dried under nitrogen gas flow and re-dissolved in LC-MS grade water. Metabolites were analyzed via reverse-phase ion-pairing chromatography coupled to an Exactive Orbitrap mass spectrometer (Thermo Fisher Scientific, San Jose, CA). The mass spectrometer was operated in negative ion mode with resolving power of 100,000 at m/z 200 and scan range of m/z 75-1000. The LC method was modified from an earlier method (Lu et al., 2010), using an Atlantis T3 column (150 mm × 2.1 mm, 3 µm particle size, 100 Å pore size), with a gradient of solvent A (97:3 water:methanol with 10 mM tributylamine and 15 mM acetic acid) and solvent B (methanol). The LC gradient was 0 min, 0% B, 200 µl/min; 2 min, 0% B, 200 µl/min; 4 min, 20% B, 200 µl/min; 13 min, 80% B, 200 µl/min; 17 min, 100% B, 200 µl/min; 17.5 min, 100% B, 300 µl/min; 20 min, 100% B, 300 µl/min; 20.5 min, 0% B, 300 µl/min; 24 min, 0% B, 300 µl/min; 25 min, 0% B, 200 µl/min. Other LC parameters, common to both methods, were column temperature 25°C, autosampler temperature 5°C, and injection volume 10 µL. Data analysis with MAVEN software and natural isotope correction were performed as previously described[338]. Volcano plot and principle component analysis of metabolomics data were generated using Metaboanalyst[342].

Acetate measurement:

Acetate was derivatized and measured by LC-MS. The derivatizing reagent was 12 mM EDC, 15 mM 3-Nitrophenylhydrazine and pyridine (2% v/v) in methanol. Reaction was stopped with quenching reagent consisting of 0.5 mM beta-mercaptoethanol and 0.1% formic acid in water. Serum (5 µL) was mixed with derivatizing reagent (100 µL) and

incubated for 1 hour at 4°C. Then, the samples were centrifuged at 16,000 x g for 10 min at 4°C, and 20 µL of supernatant was mixed with 200 µL of the quenching reagent. After centrifugation at 16,000 x g for 10 min at 4°C, supernatants were collected for LC-MS analysis. A quadrupole-time of flight mass spectrometer (Q-TOF, Agilent, Santa Clara, CA) operating in negative ion mode was coupled to C18 chromatography via electrospray ionization and used to scan from m/z 100 to 300 at 1 Hz and 15,000 resolution. LC separation was on an Acquity UPLC BEH C18 column (2.1 mm x 100 mm, 1.7 5 µm particle size, 130 Å pore size; Waters, Milford, MA) using a gradient of solvent A (0.01% formic acid in water) and solvent B (0.01% formic acid in isopropanol). Flow rate was 400 µL/min, except that from 6 min to 8 min flow rate was increased to 700 µL/min. The LC gradient was: 0 min, 10% B; 2 min, 15% B; 5 min, 25% B; 6 min, 100% B; 8 min, 100% B; 8.6 min, 10% B; 10.5 min, 10% B. Autosampler temperature was 5°C, and injection volume was 10 µL. Ion masses for derivatized acetate was 194.

Lipidomics:

Lipidomics was performed as previously described[343], with some modifications on an extraction step. Briefly, serum samples (10 µL) was dissolved in 100 µL of isopropanol. After centrifugation at 14,000 g at 4°C for 10 min, supernatant was transferred to a glass MS vial and injected into a 1290 Infinity UHPLC system coupled to Agilent 6550 iFunnel Q-TOF mass spectrometer. To cover both the positive charged and negative charged species, each sample was analyzed twice using the same LC gradient but with different mass spectrometer ionization modes. The LC separation was performed on an Agilent Poroshell 120 EC-C18 column (150 x 2.1 mm, 2.7 µm particle size) with a flow rate of 150 µL/min. Solvent A was 1 mM ammonium acetate + 0.2% acetic acid in water/methanol (90:10). Solvent B was 1 mM ammonium acetate + 0.2% acetic acid in

methanol/2-propanol (2:98). The solvent gradient in volume ratios was as follows: 0-2 min, 25% B; 2-4 min, 25 to 65% B; 4-16 min, 65 to 100% B; 16-20 min, 100% B; 20-21 min, 100 to 25% B; 21-27 min, 25% B. Principle component analysis was generated using Metaboanalyst[342] (https://www.metaboanalyst.ca) and heatmap of lipidomics data was generated using Morpheus (https://software.broadinstitute.org/morpheus).

Figures

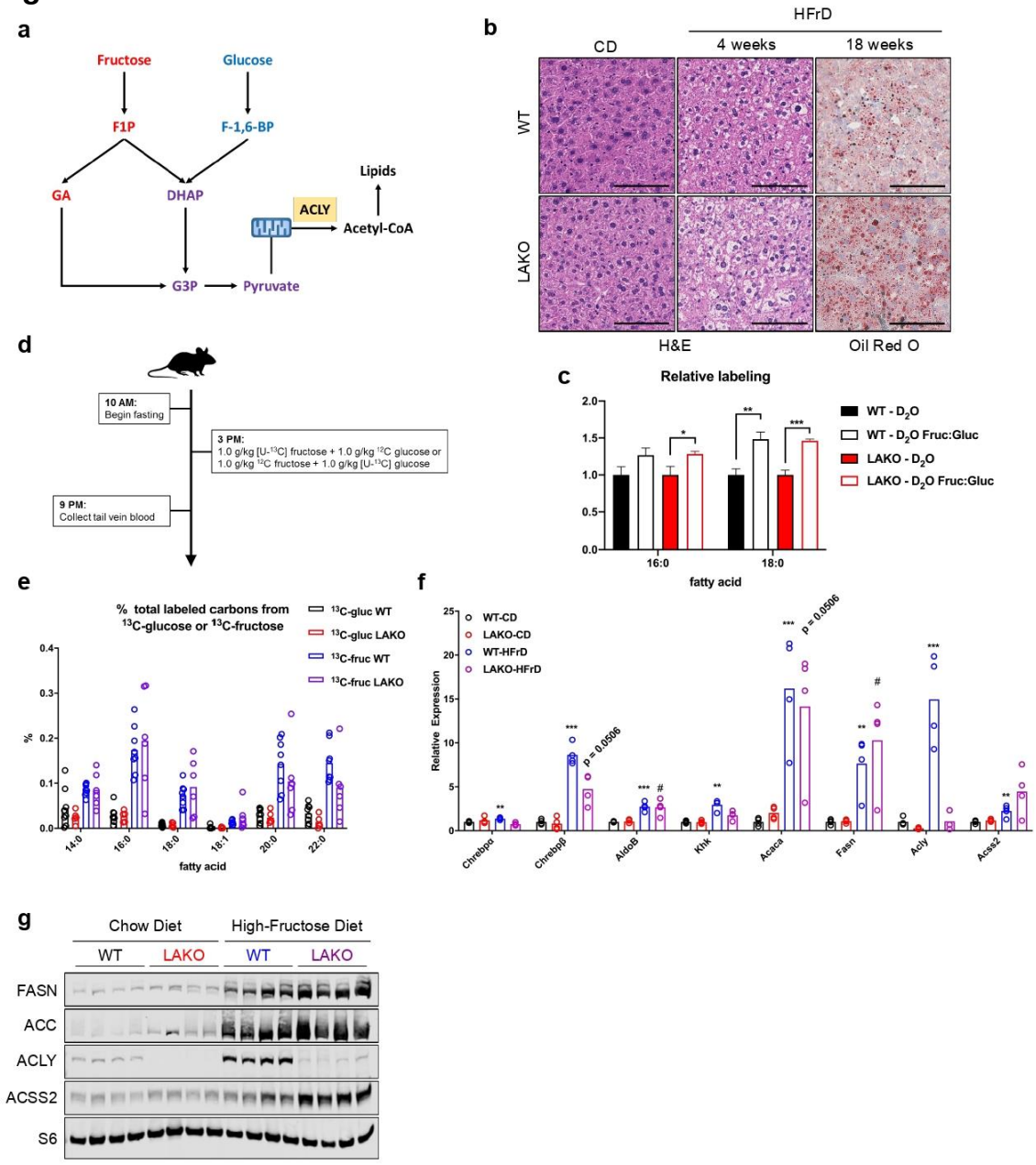

Figure 3.1 | Fructose-dependent fatty acid synthesis is ACLY-independent.
a, Schematic of fructolysis and glycolysis feeding into de novo lipogenesis. F1P = fructose-1-phosphate, F-1,6-BP = fructose-1,6-bisphosphate, GA = glyceraldehyde, DHAP = dihydroxyacetone phosphate, G3P = glyceraldehyde-3-phosphate.
b, H&E and Oil Red O histological stains of livers from WT or LAKO mice on chow (CD) or high fructose diet (HFrD) for 4 or 18 weeks. Scale bars = 100 µm.
c, Relative deuterium labeling in palmitic acid (16:0) and stearic acid (18:0) after 24-hour D_2O

labeling of mice, normalized to percent plasma D_2O labeling. D_2O (n = 4/group) set to 1 and compared to D_2O Fruc:Gluc (n = 6/group) within each genotype, data are mean ± SEM.
d, Experimental design for data shown in **e**.
e, % total labeled carbons in fatty acids from ^{13}C-glucose or ^{13}C-fructose.
f, mRNA expression of ChREBP and its target genes in livers of WT or LAKO mice fed on CD or HFrD (n = 4 mice/group), statistical comparisons WT-CD vs. WT-HFrD: ***P<0.001, LAKO-CD vs. LAKO-HFrD: #P<0.05 as determined by Holm-Sidak test.
g, Immunoblots of lipogenic enzymes in livers of WT or LAKO mice fed CD or HFrD for 4 weeks. For all panels, *P<0.05, **P<0.01, ***P<0.001.

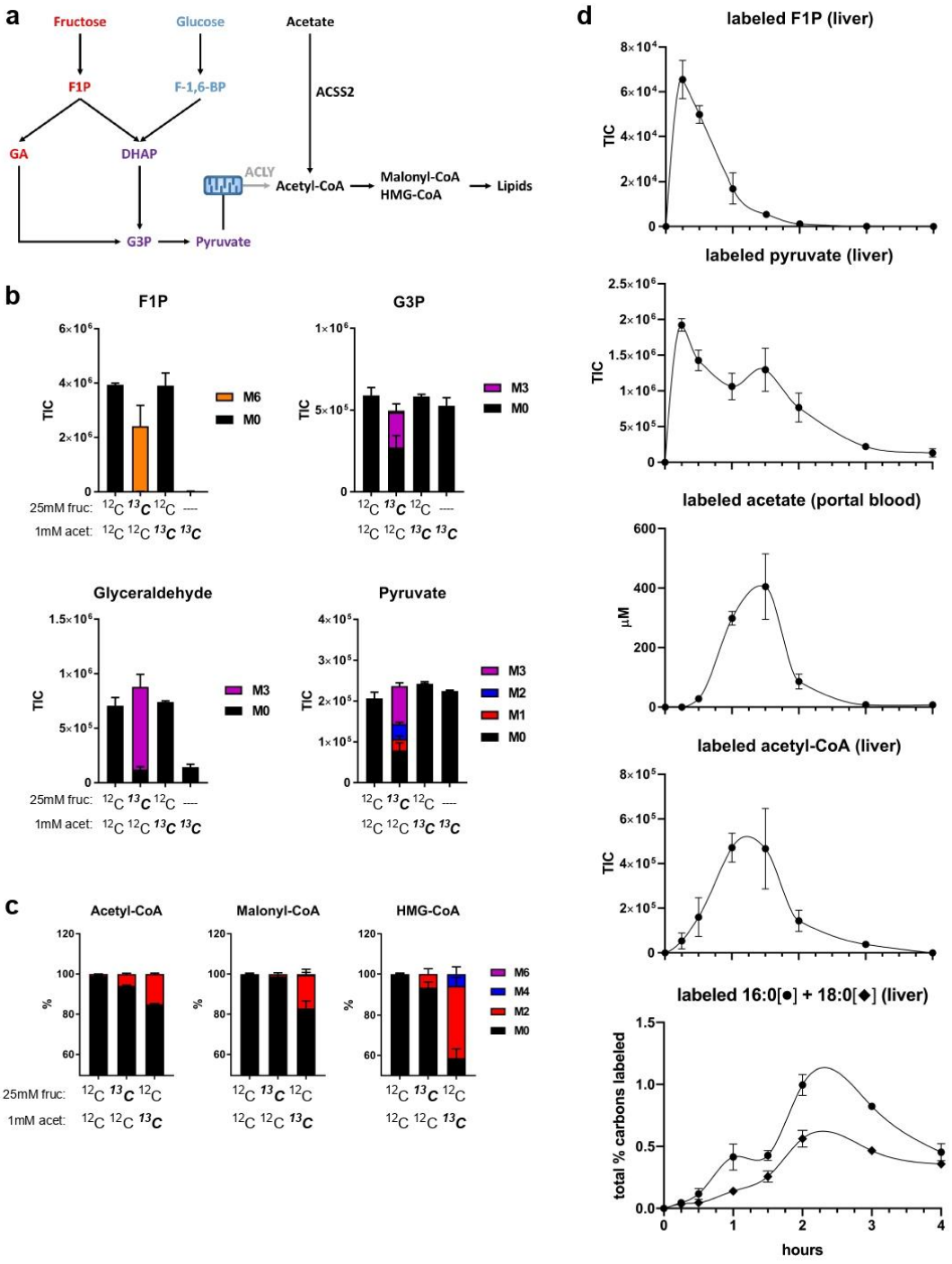

Figure 3.2 | Lipogenic acetyl-CoA is preferentially produced from acetate in hepatocytes.

a, Schematic of fructolysis, glycolysis, and acetate feeding into lipogenic acetyl-CoA and de novo lipogenesis.

b, Total ion counts (TIC) of fructolytic intermediates in primary hepatocytes following 6 hours of incubation with 5mM glucose + 25mM fructose + 1mM acetate, ^{13}C-labeled substrate indicated in bold, data are mean ± SD, n = 3.
c, % labeling of acetyl-CoA, malonyl-CoA, or HMG-CoA from [U-^{13}C]-fructose or [1,2-^{13}C]-acetate, data are mean ± SD, n = 3.
d, TIC of liver labeled F1P, pyruvate, and acetyl-CoA, concentrations (μM) of portal blood labeled acetate, and total % carbons labeled of liver 16:0 and 18:0 in WT mice gavaged with 2.0 g/kg [U-^{13}C]-fructose + 2.0 g/kg unlabeled glucose, data are mean ± SEM, n = 3/timepoint.

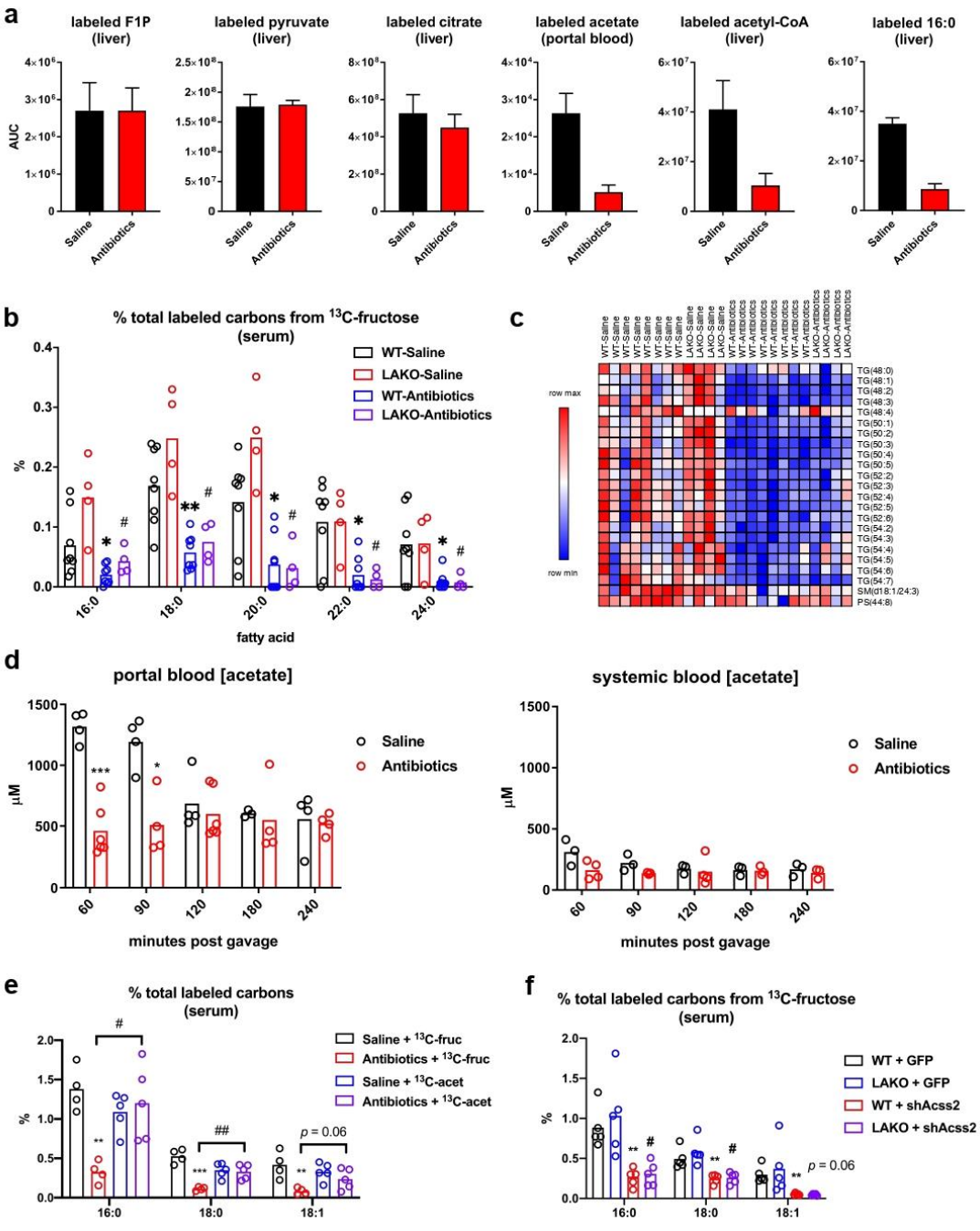

Figure 3.3 | Microbiome metabolism of fructose to acetate feeds hepatic de novo lipogenesis.

a, Area under curve (AUC 0-240 min) of labeled hepatic F1P, pyruvate, acetyl-CoA, palmitate and portal blood acetate in saline or antibiotic-treated WT mice following a gavage of 2.0 g/kg [U-^{13}C]-fructose + 2.0 g/kg glucose.

b, % total labeled carbons in saponified serum fatty acids in saline or antibiotic-treated WT and

LAKO mice following a gavage of 2.0 g/kg [U-^{13}C]-fructose + 2.0 g/kg glucose, *P<0.05, **P<0.01 WT-saline vs. WT-antibiotics, #P<0.05 LAKO-saline vs. LAKO-antibiotics.
c, Heat map of hepatic triglyceride abundance in livers of mice in **b**.
d, Concentrations of portal and systemic blood acetate following gavage, each data point represents an individual mouse sacrificed at indicated time. *P<0.05, ***P<0.001.
e, % total labeled carbons in saponified serum fatty acids from saline- or antibiotic-treated LAKO mice following a gavage of 2.0 g/kg fructose + 2.0 g/kg glucose + 0.5 g/kg acetate, ^{13}C-labeled substrate indicated. **P<0.01, ***P<0.001 saline vs. antibiotics, #P<0.05, ##P<0.01 ^{13}C-fruc vs. ^{13}C-acet.
f, % total labeled carbons in serum fatty acids from WT and LAKO mice 1 week after injection with AAV-GFP or AAV-shAcss2. **P<0.01 WT + GFP vs. WT + shAcss2, #P<0.05, ##P<0.01 LAKO + GFP vs. LAKO + shACSS2.

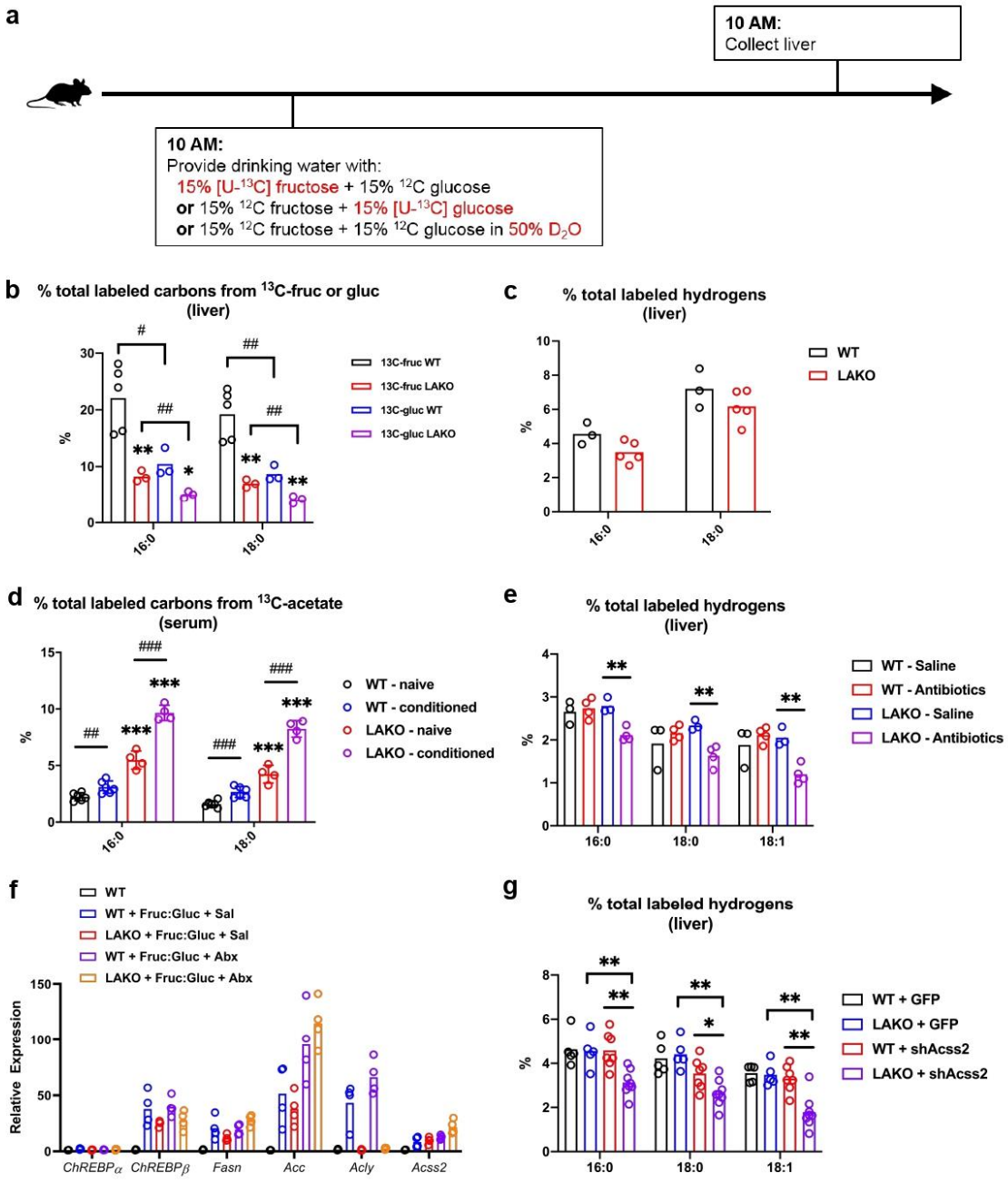

Figure 3.4 | Gradual fructose consumption promotes hepatic lipogenesis from ACLY- and ACSS2-derived acetyl-CoA.

a, Experimental design for gradual fructose consumption.

b, % total labeled carbons from [U-^{13}C]-fructose or glucose in hepatic 16:0 and 18:0, WT vs. LAKO: *, Fruc vs. Gluc: #.

c, % total labeled hydrogens from D_2O in hepatic 16:0 and 18:0.

d, % total labeled carbons from [1,2-^{13}C]-acetate supplemented Fruc:Gluc water in saponified

serum 16:0 and 18:0, see Extended Data Fig. 9a for experimental details, WT vs. LAKO: *, naïve vs. conditioned: #.

e, total % labeled hydrogens from Fruc:Gluc D_2O in hepatic 16:0 and 18:0 in WT and LAKO mice following 1 week of treatment with saline or antibiotics.

f, mRNA expression of ChREBP and downstream lipogenic genes in livers of mice in (e), Abx = antibiotics.

g, total % labeled hydrogens from Fruc:Gluc D_2O in hepatic fatty acids in WT and LAKO mice 1 week after injection with AAV-GFP or AAV-shAcss2. For all panels, */$^{\#}$P<0.05, **/$^{\#\#}$P<0.01, ***/$^{\#\#\#}$P<0.001.

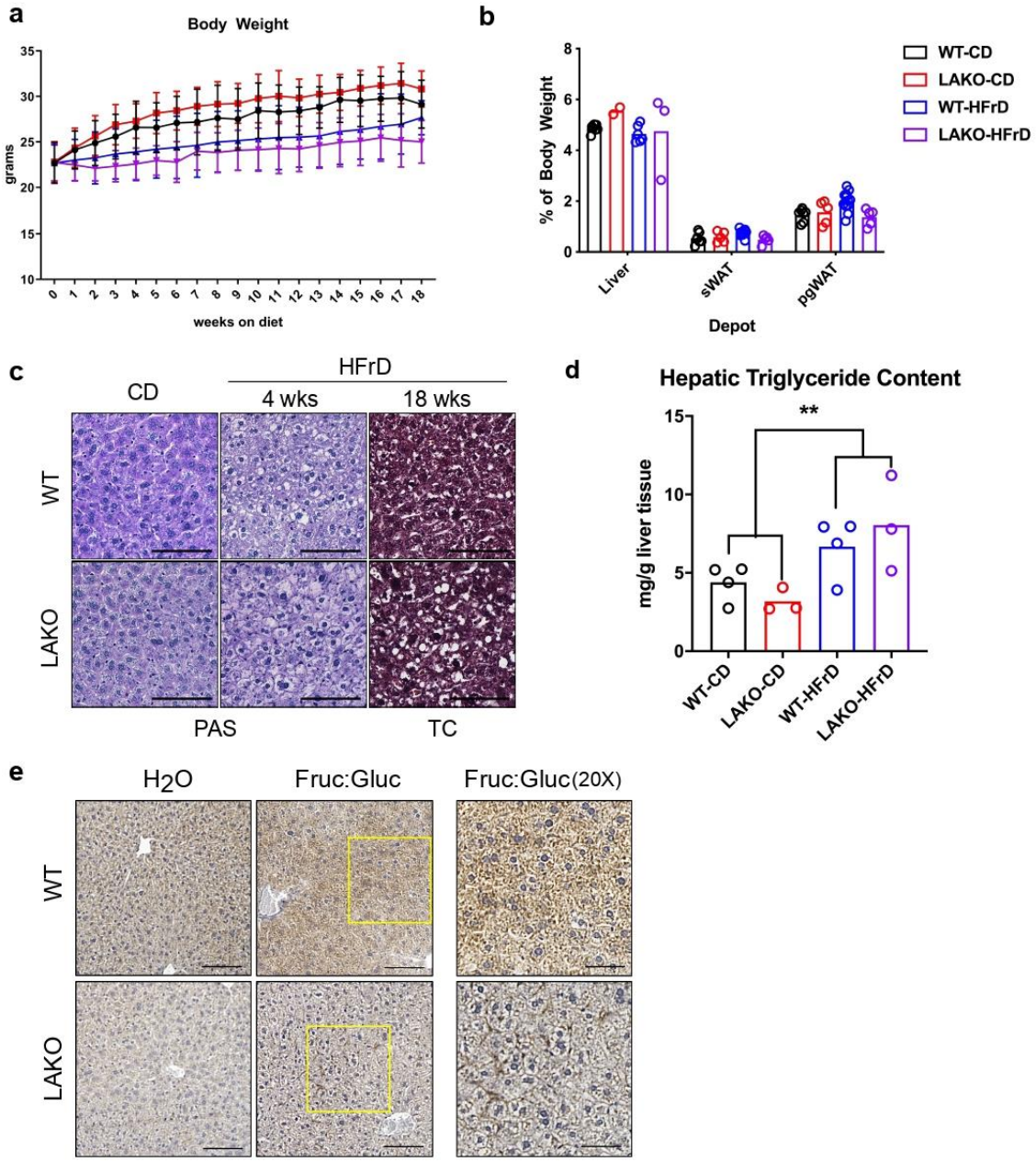

Extended Data Figure 3.1 | Hepatic ACLY deficiency minimally impacts the response to dietary fructose.

a, Body weights of WT and LAKO mice on CD or HFrD for 18 weeks (n = WT-CD:13, LAKO-CD:5, WT-HFrD:14, LAKO-HFrD:5).

b, Weights of liver, subcutaneous (sWAT) and perigonadal (pgWAT) adipose tissues in WT and LAKO mice on CD or HFrD for 18 weeks.

c, Representative images of Periodic Acid Schiff (PAS) stain for glycogen and Trichrome (TC) histological stain for fibrosis in livers from WT or LAKO mice on HFrD. Scale bars = 100 µm.

d, Triglyceride content in WT or LAKO mice on CD or HFrD for 18 weeks, n = (WT-CD: 4, LAKO-CD: 3, WT-HFrD: 4, LAKO-HFrD: 3), **P<0.01 as determined by Welch's T test.
e, Immunohistochemistry staining against ACLY in WT or LAKO mice on H_2O or Fruc:Gluc water for 4 weeks. Yellow boxes approximate location of 20X panels. Scale bars = 100 µm for 10X, 50 µm for 20X.
For all panels, data are mean ± SD.

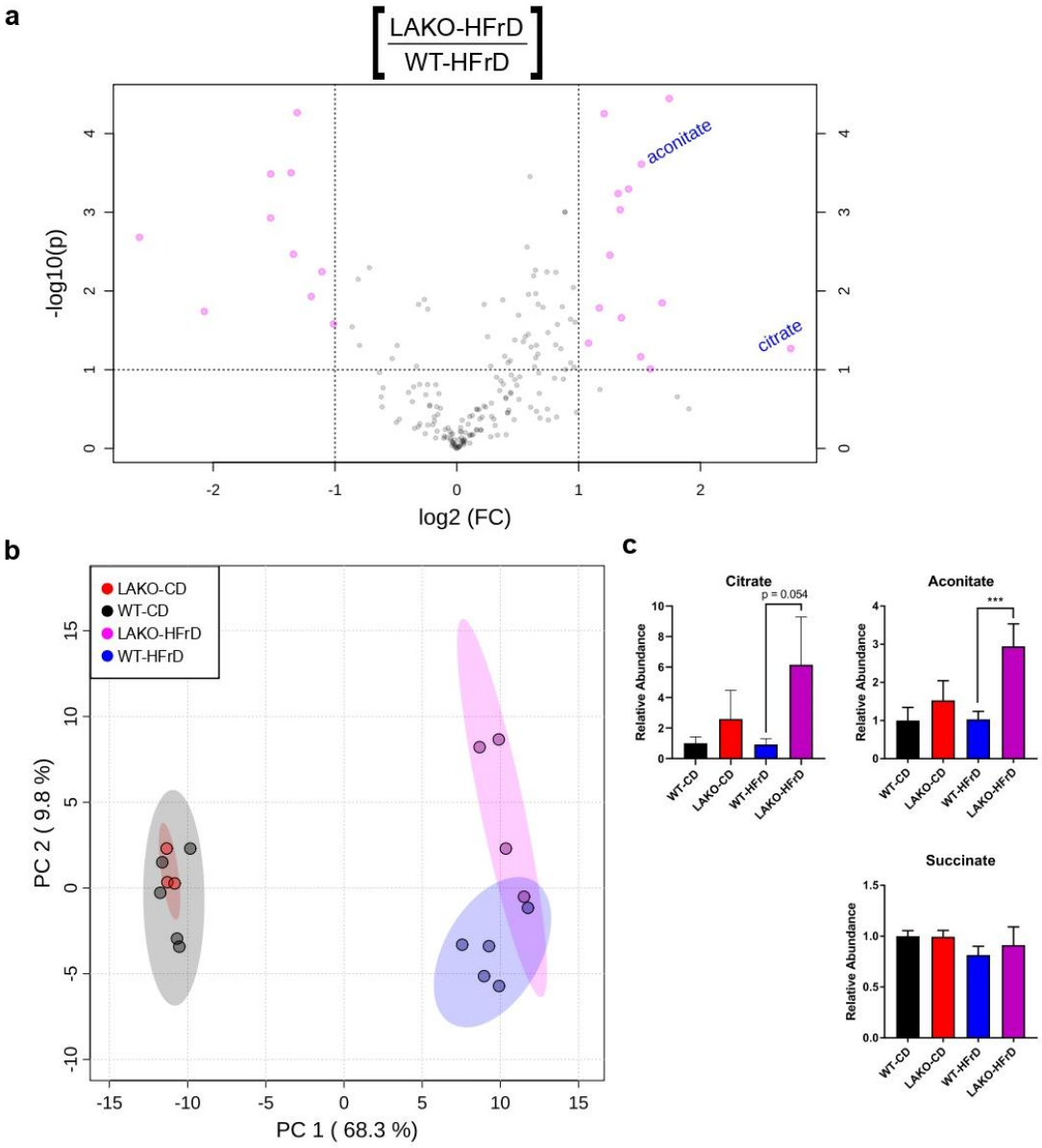

Extended Data Figure 3.2 | Hepatic ACLY deficiency results in only modest metabolic alterations on high fructose diet.

a, Volcano plot of intrahepatic metabolites in WT and LAKO mice on CD or HFrD for 4 weeks, pink dots indicate significant hits as determined by a fold-change threshold of 2 and P-value threshold of 0.1, assuming equal variance.

b, Principle component analysis of log-transformed data in Supplementary Table 1, each dot represents a unique sample, 95% CI shown in corresponding color.

c, Relative metabolite abundance, normalized to WT-CD group, ***P<0.001, n = (WT-CD:5, LAKO CD: 3, WT-HFrD: 5, LAKO-HFrD: 4).

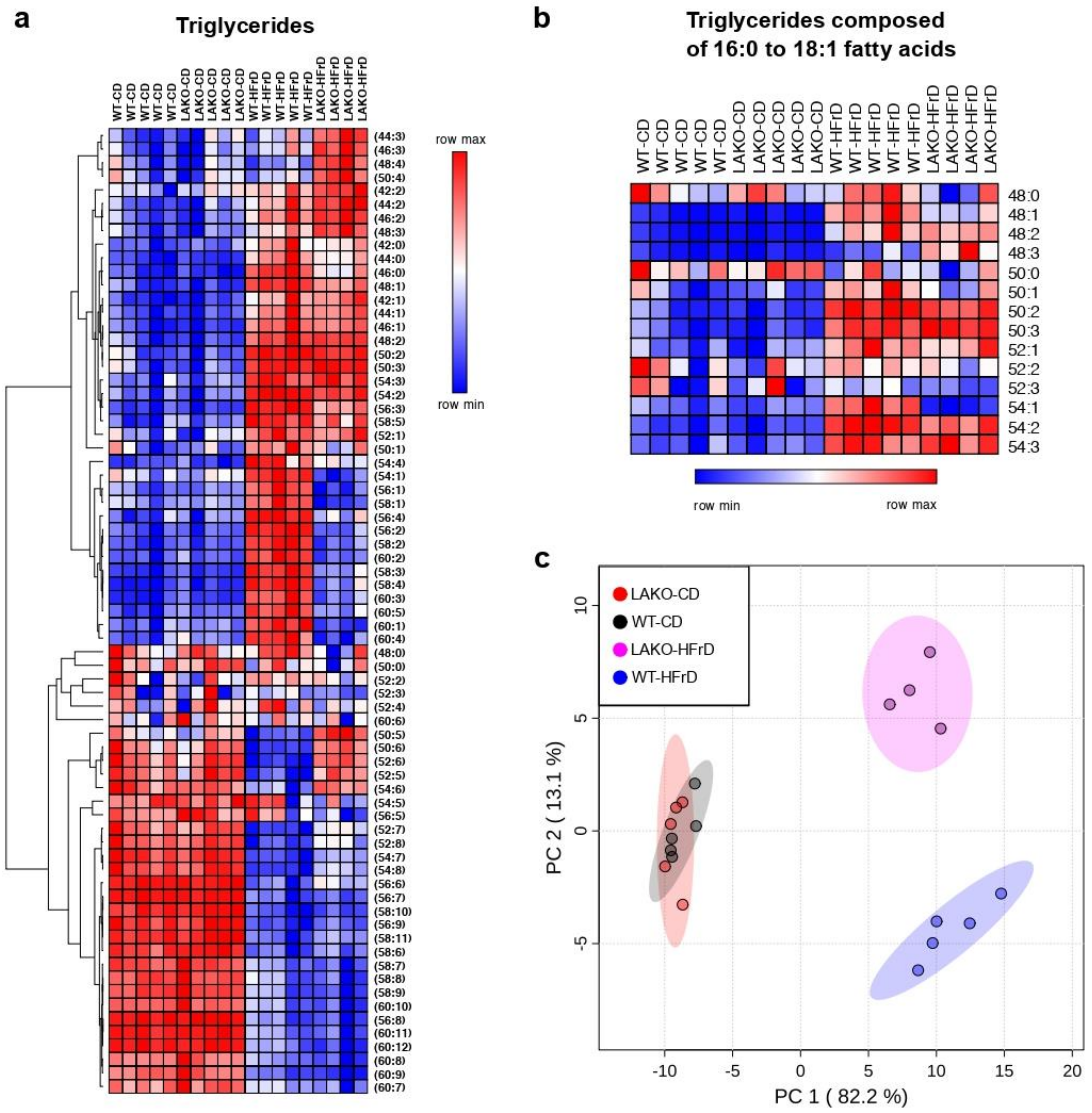

Extended Data Figure 3.3 | High fructose diet alters hepatic lipid metabolism.

a, Hierarchical clustering of relative hepatic triglyceride abundance in WT or LAKO mice on CD or HFrD for 4 weeks, clustering performed using one minus pearson correlation and average linkage.

b, Relative abundance of hepatic triglycerides composed of 16:0 to 18:1 fatty acids, subset of data in **a**.

c, Principle component analysis of log-transformed data in Supplementary Table 2, each dot represents a unique sample, 95% CI shown in corresponding color.

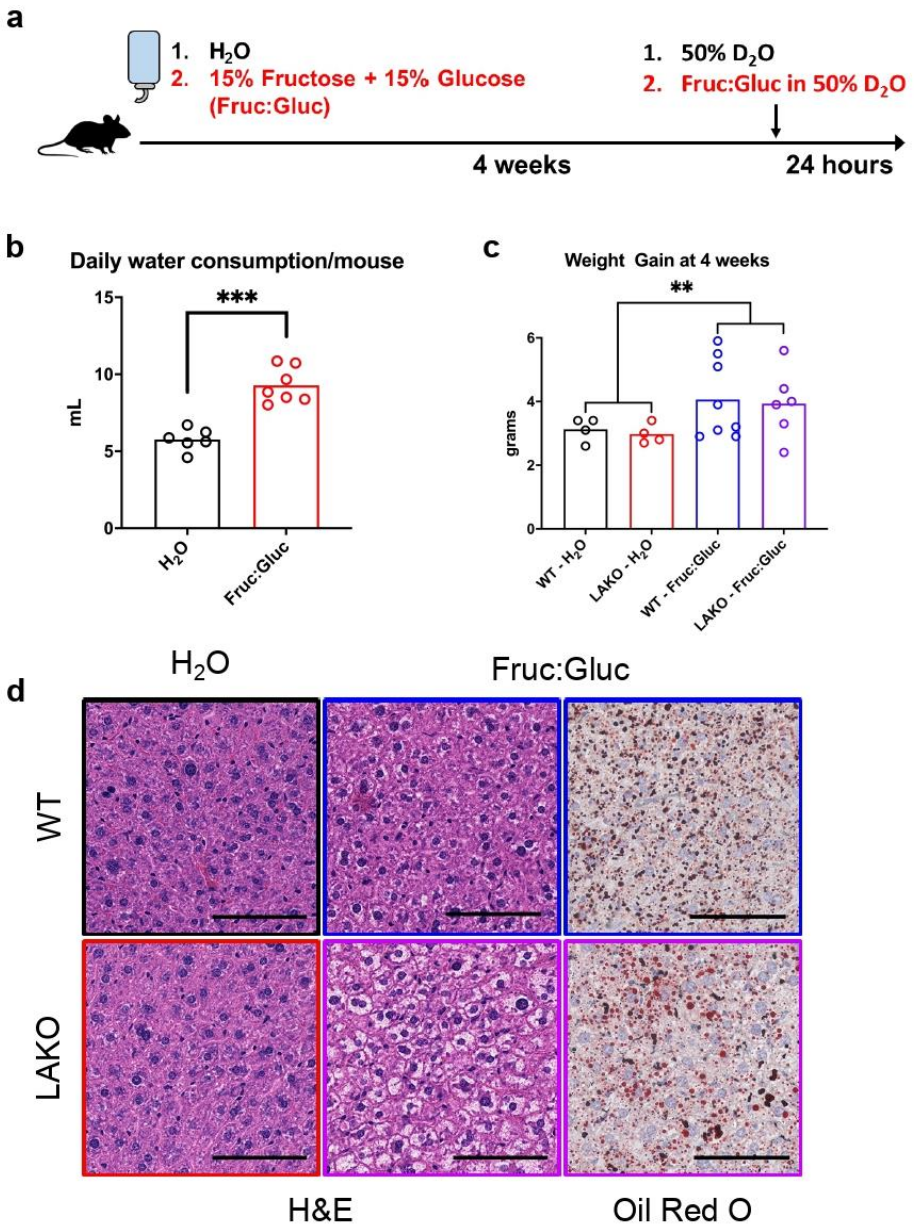

Extended Data Figure 3.4 | Sweetened drinking water consumption induces steatosis independently of ACLY.

a, Schematic of experimental set-up of drinking water study.

b, Daily consumption of unsweetened (H_2O) or 15% fructose + 15% glucose sweetened (Fruc:Gluc) water, ***P<0.001.

c, Weight gain of WT or LAKO mice given H_2O or Fruc:Gluc water for 4 weeks, **P<0.01 comparing all H2O vs. Fruc:Gluc mice.

d, H&E and Oil Red O histological stains of livers from WT or LAKO mice given H_2O or

fructose:glucose sweetened drinking water for 4 weeks. Scale bars = 100 µm.
For all panels, data are mean ± SD.

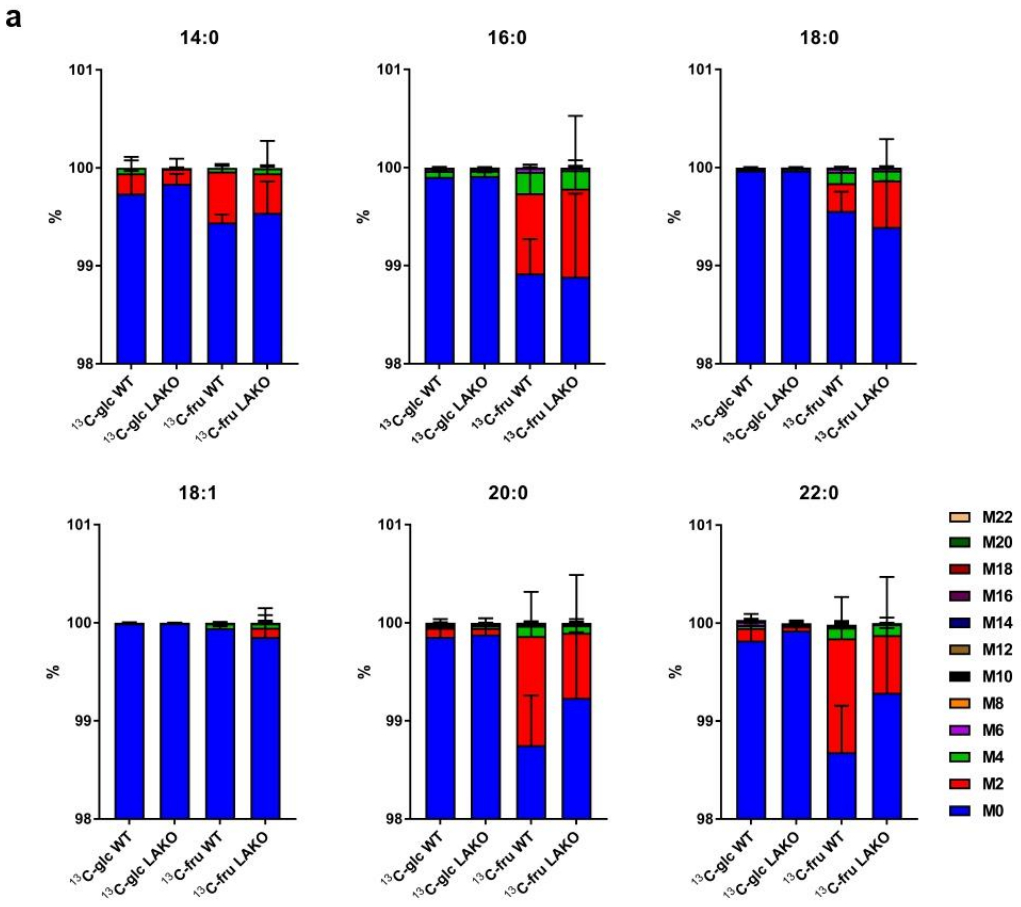

Extended Data Figure 3.5 | Fructose carbons contribute substantially to newly synthesized fatty acids in the liver independently of ACLY.
a, Isotopologue distribution of serum fatty acids from mice in Figure 1e, data are mean ± SD.

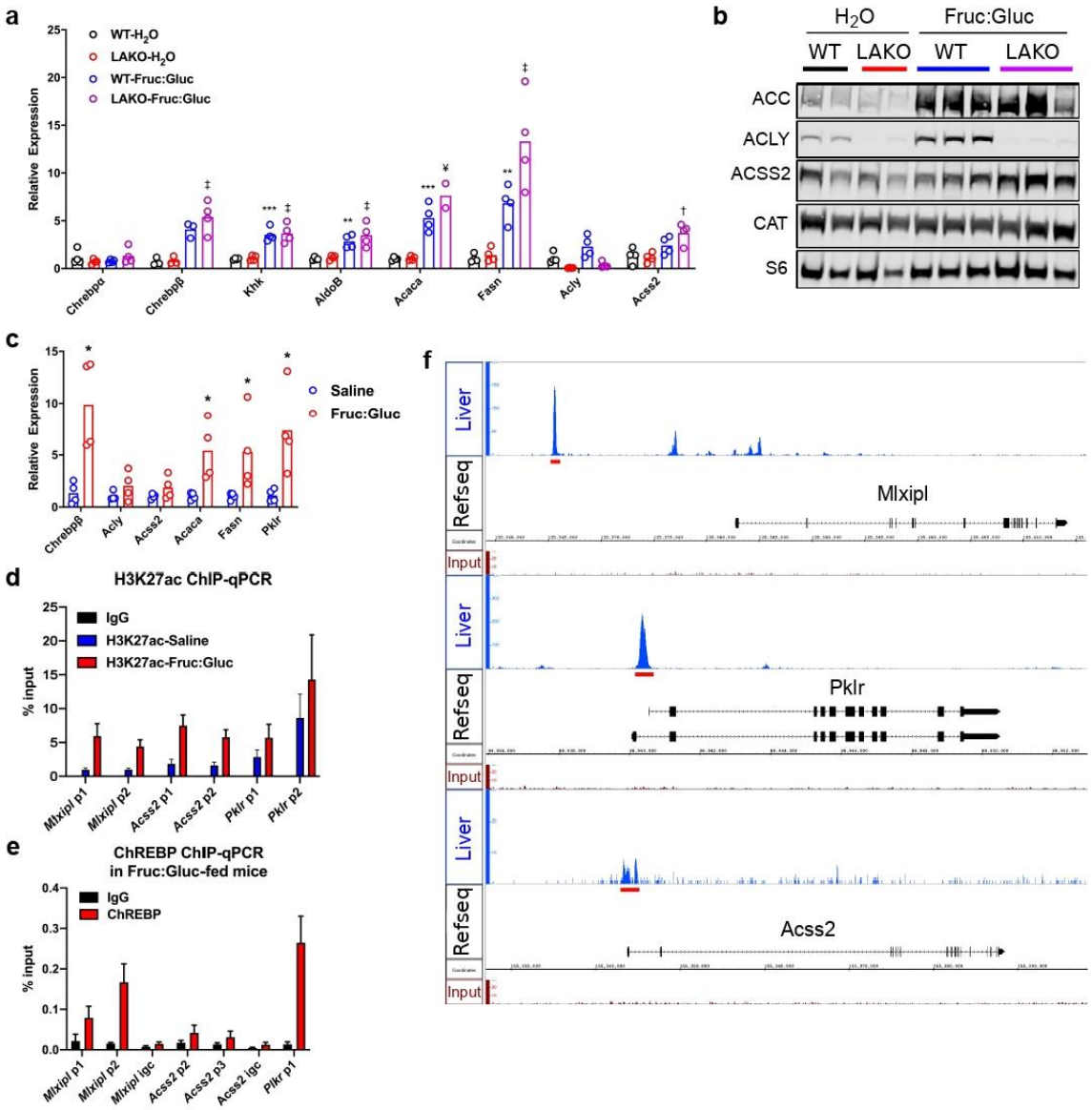

Extended Figure Data 3.6 | Fructose signals the use of acetate for de novo lipogenesis.

a, mRNA expression of lipogenic genes in livers of WT or LAKO mice given H_2O or Fruc:Gluc water for 4 weeks (n = 4/group), statistical comparisons WT-H_2O vs. WT-Fruc:Gluc: **P<0.01, ***P<0.001, LAKO-H_2O vs. LAKO-Fruc:Gluc:†P<0.05, ‡P<0.01, ¥P<0.001 as determined by Holm -Sidak test.

b, Immunoblots of lipogenic enzymes in livers of WT or LAKO mice given H_2O or Fruc:Gluc water for 4 weeks.

c, mRNA expression of ChREBP and its target genes in livers of WT mice provided either water for 24 hours followed by an oral gavage of saline, or Fruc:Gluc water for 24 hours, followed by an oral gavage of 2.0 g/kg glucose and 2.0 g/kg fructose (n = 4 mice/group), livers harvested 90

minutes after gavage, *P<0.05, as determined by Holm-Sidak test.
d, H3K27ac ChIP-qPCR under conditions used in panel **c**.
e, ChREBP ChIP-qPCR under conditions used in panel **c**, igc = intergenic control.
f, ChIP-seq tracks of Mlxipl, Pklr, Acss2 genomic loci[319], red bars indicate genomic regions used to design ChIP-qPCR primers.
For panels **d-e**, data are mean ± SEM.

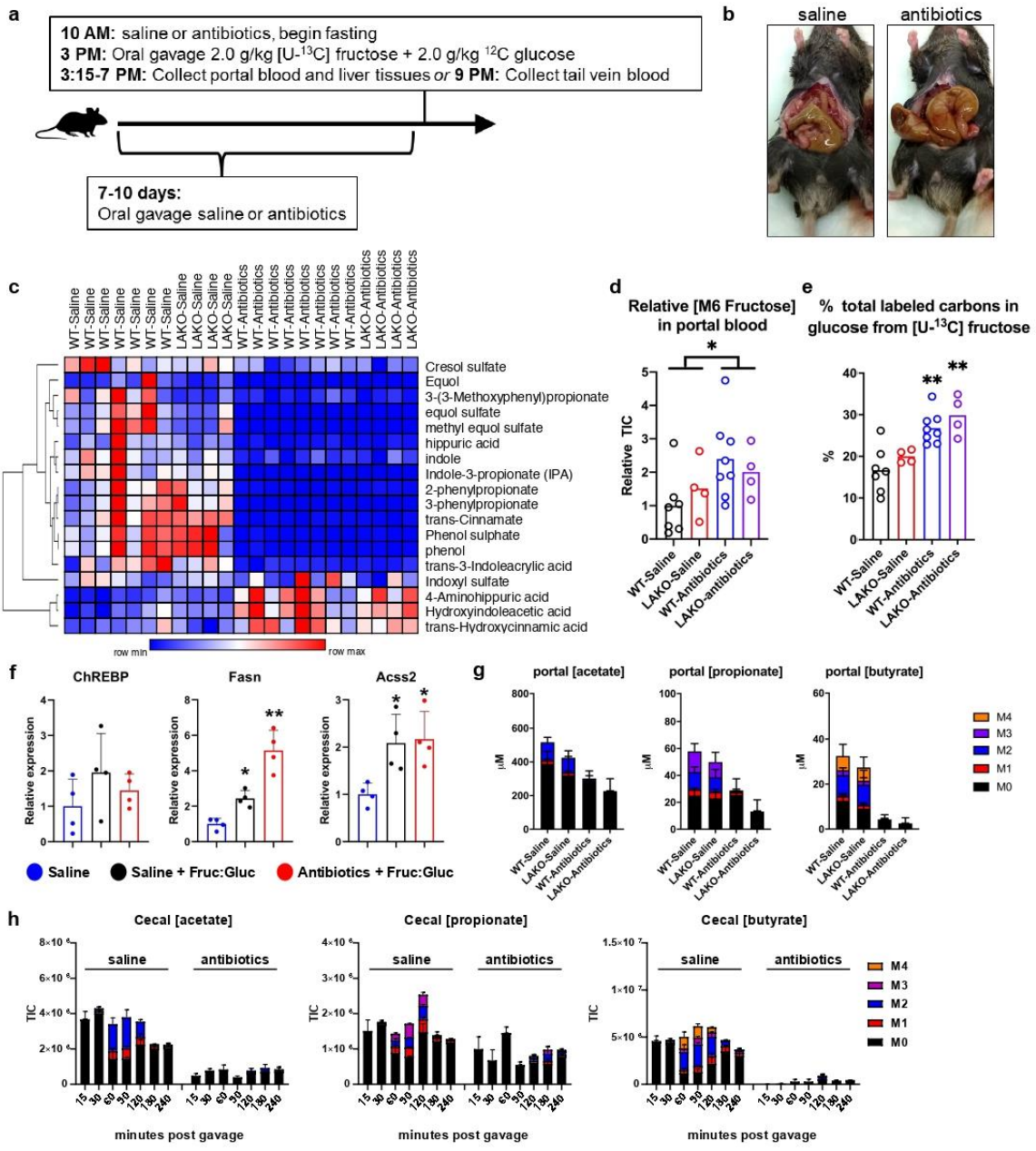

Extended Data Figure 3.7 | Antibiotic depletion of microbiome blocks substrate contribution, but not signaling, of de novo lipogenesis following fructose consumption.

a, Experimental set-up for antibiotic depletion of the microbiome followed by [U-^{13}C]-fructose tracing into DNL.

b, Representative images of cecums from a saline and antibiotic treated mouse.

c, Heat map of microbial metabolite abundance in the portal blood, collected 1 hour after gavage.

d-e, Abundance of portal blood [U-^{13}C]-fructose **(d)**, and % total labeled carbons in glucose **(e)**,

statistical comparisons vs. Saline.
f, mRNA expression of ChREBPβ, Acss2, and Fasn in liver, collected 1 hour after gavage, statistical comparisons vs. Saline
g, Concentrations (μM) of portal blood labeled acetate, propionate, and butyrate, n = (WT-Saline: 8, LAKO-Saline: 4, WT-Antibiotics: 8, LAKO-Antibiotics: 4). **h,** Abundance of cecal labeled acetate, propionate, and butyrate in WT mice, n = 3 mice/timepoint, except saline-180 n = 2 mice. For all panels, data are mean ± SD, *P<0.05, **P<0.01, as determined by Holm-Sidak test.

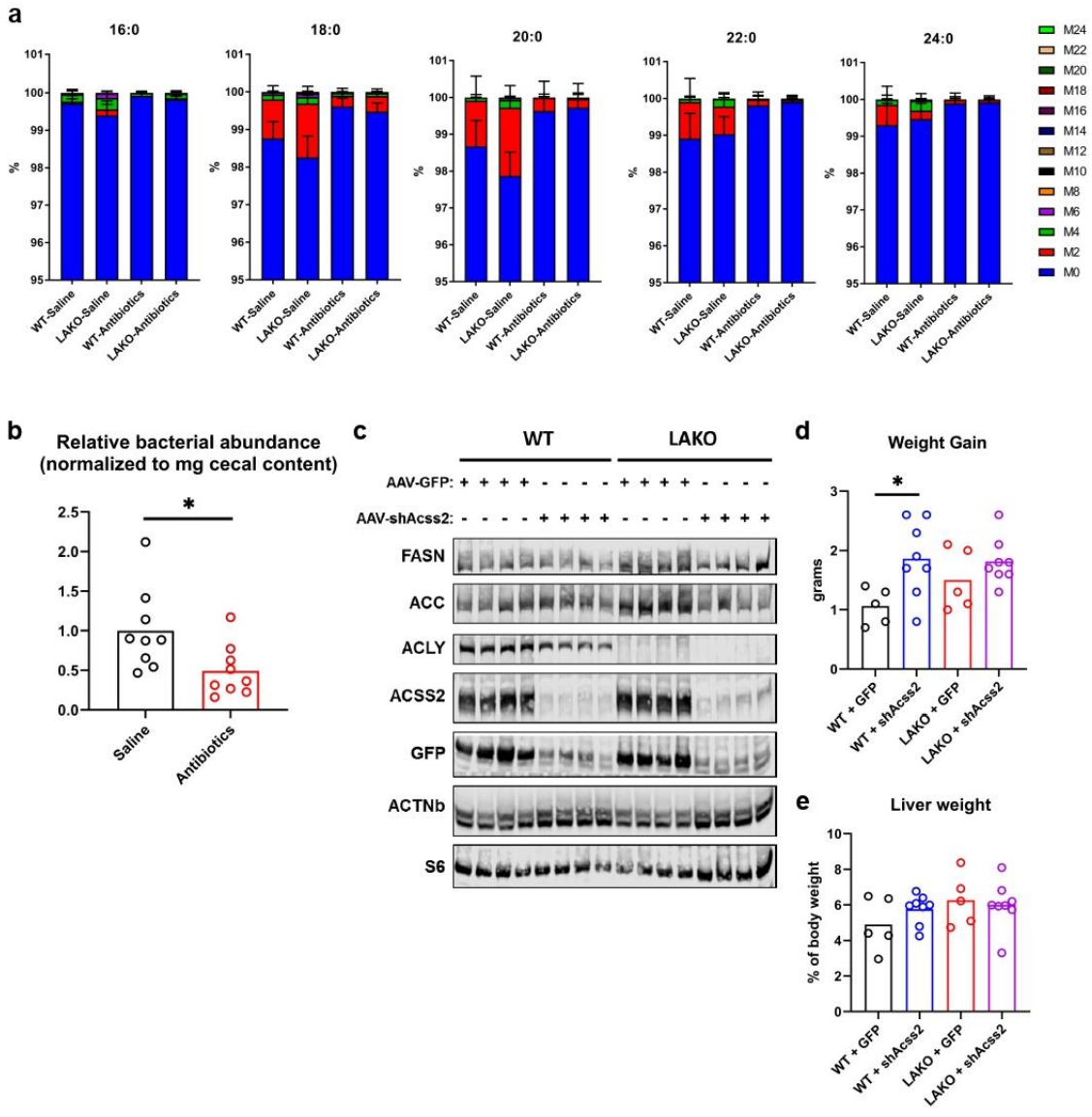

Extended Data Figure 3.8 | Bolus fructose-dependent DNL requires microbial acetate and hepatic ACSS2.

a, Isotopologue distribution of serum fatty acids, collected 6 hours after gavage, data are mean ± SD, n = (WT-Saline: 8, LAKO-Saline: 4, WT-Antibiotics: 8, LAKO-Antibiotics: 4).

b, Relative abundance of bacterial abundance in cecal contents from mice treated with saline or antibiotics as determined by 16s RT-qPCR to a reference standard of E. coli DNA. *P<0.05 as determined by Welch's t test.

c, Western blot of liver lysates from WT and LAKO mice 1 week following tail-vein injection with AAV8-GFP or AAV8-shAcss2.

d, Weight gain in WT and LAKO mice 1 week following tail-vein injection with AAV8-GFP or AAV8-shAcss2. *P<0.05 as determined by Holm-Sidak test.

e, Liver weight as % of body weight of WT and LAKO mice 1 week following tail-vein injection with AAV8-GFP or AAV8-shAcss2.

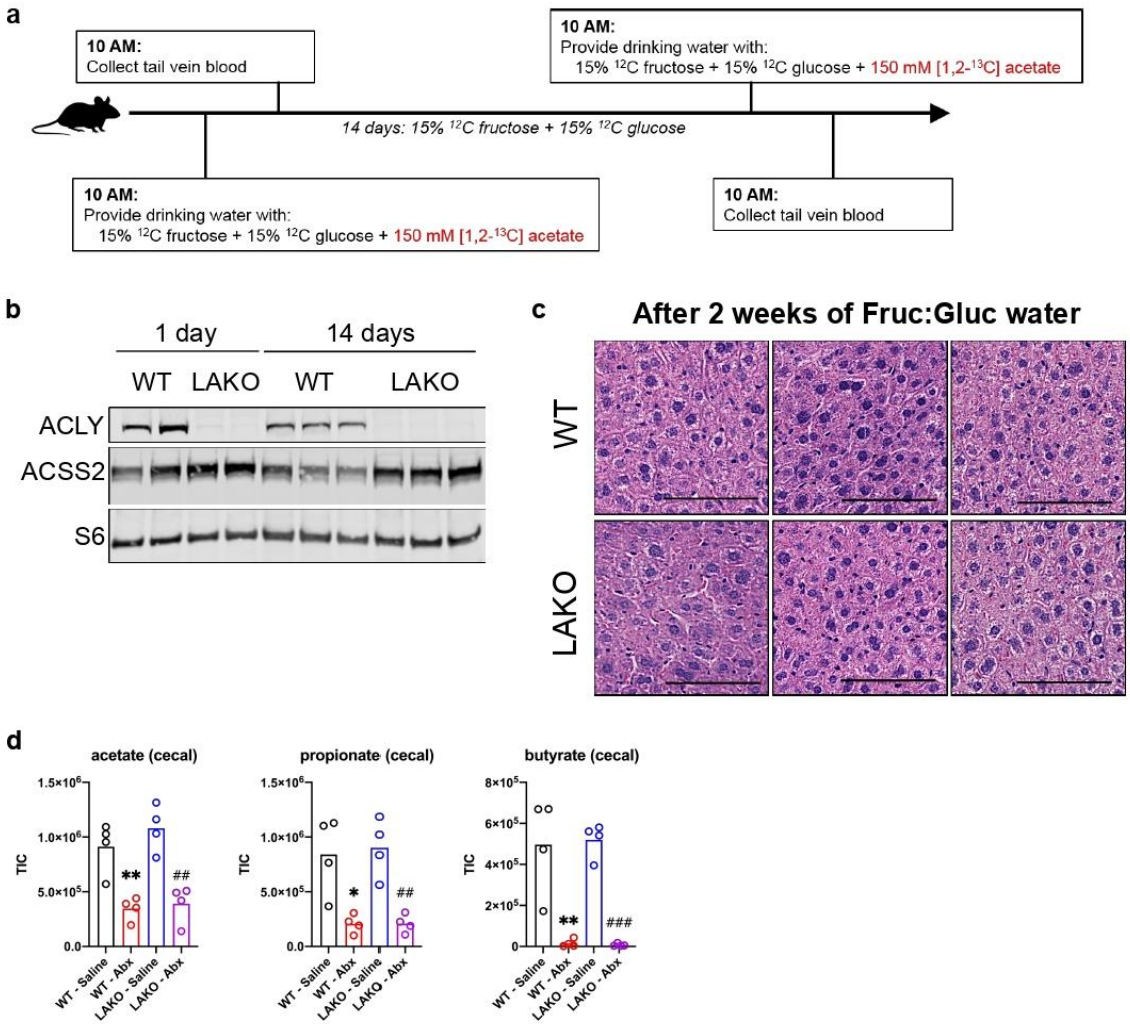

Extended Data Figure 3.9 | Gradual fructose consumption promotes greater acetate usage in LAKO mice.

a, Experimental set-up for [1,2-^{13}C]-acetate tracing into DNL prior to and after gradual fructose administration.

b, Western blot of ACLY, ACSS2, and S6 in liver lysates from WT and LAKO mice after 1 day or 14 days of Fruc:Gluc water.

c, Representative H&E stains of livers from WT and LAKO mice provided Fruc:Gluc water for 2 weeks. Scale bars = 100 µm

d, Relative abundance of acetate, propionate, and butyrate in the cecal contents of WT and LAKO mice treated with saline or antibiotics for 1 week. WT: *P<0.05, **P<0.01, LAKO: ##P<0.01, ###P<0.001.

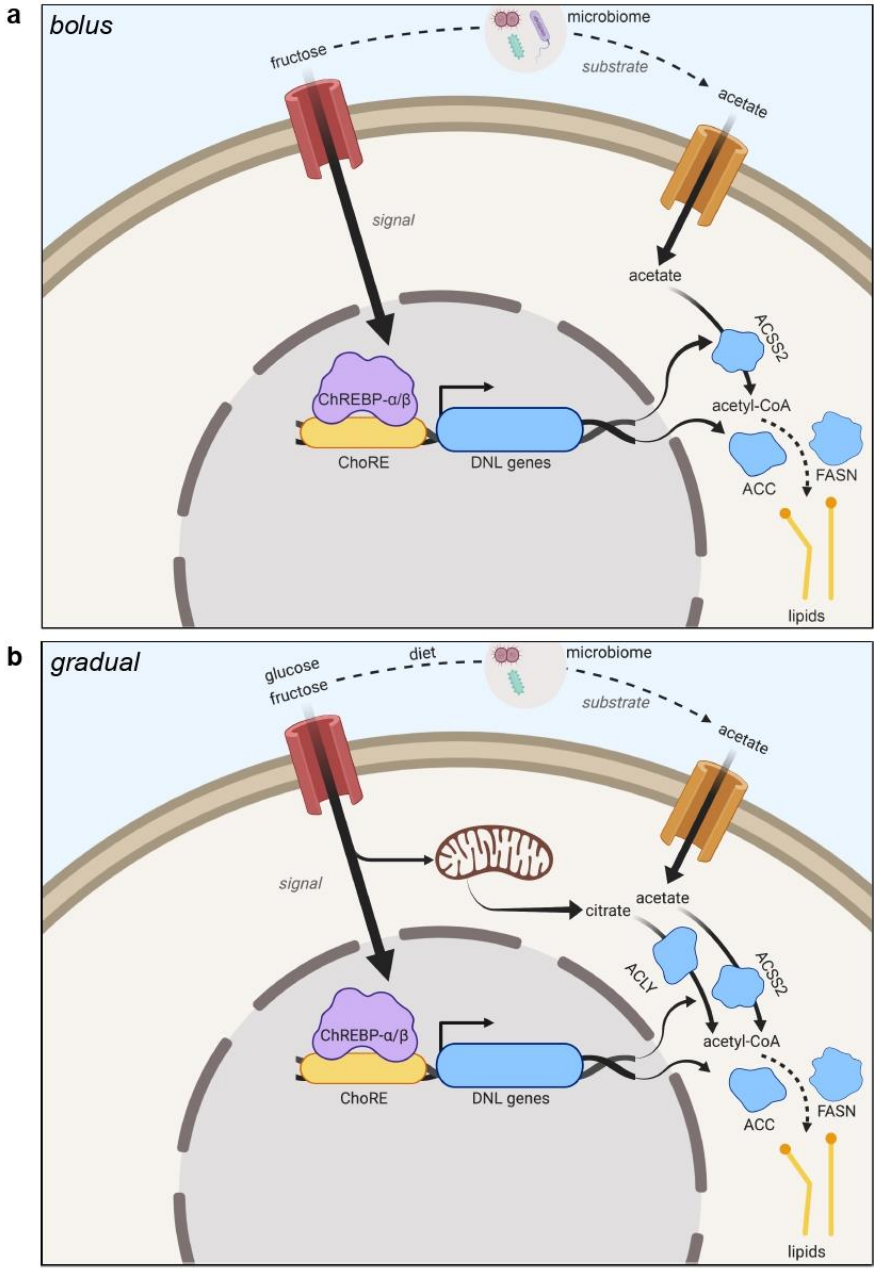

Extended Data Figure 3.10 | Fructose provides signal and substrate to promote hepatic de novo lipogenesis.

a, Proposed model of bolus fructose-induced hepatic DNL. Fructose catabolism in hepatocytes acts as a signal to induce DNL genes including ACSS2, while fructose metabolism by the gut microbiome provides acetate as a substrate to feed DNL, mediated by ACSS2.

b, Proposed model of gradual fructose-induced hepatic DNL. Like the bolus model, fructose catabolism in hepatocytes acts as a signal to induce DNL genes. Glucose and fructose catabolism provide citrate as a substrate to feed DNL, mediated by ACLY. Metabolism of fibers

and other dietary components by the gut microbiome provides also acetate as a substrate to feed DNL, mediated by ACSS2.

CHAPTER 4: Summary and Discussion

Summary of Findings:

Prior to this work, both ACLY and ACSS2 have been shown to contribute to nuclear-cytosolic acetyl-CoA pools in proliferating cells. While both enzymes have been proposed as therapeutic targets in the treatment of cancer and other diseases[70,313,344,345], their metabolic contributions to promoting disease have largely been investigated individually without taking the presence of the other into account. In this work, we studied how genetic deletion of ACLY affects ACSS2 and acetate contributions to acetyl-CoA metabolism in the same system. By doing so, we identified a metabolic switch between ACLY and ACSS2 upon loss of ACLY function, but not vice versa, to meet cellular demands for acetyl-CoA production. This metabolic flexibility enables cells to synthesize acetyl-CoA from acetate in the absence of ACLY, and maintain processes such as DNL. Not only do we demonstrate this in proliferating cells, but also in intact liver tissue in response to high sugar consumption, a context relevant to current public health.

Future Directions and Outstanding Questions:

This body of work establishes that mammalian cells can compensate for the loss of ACLY function by upregulating ACSS2 and acetate metabolism in order to meet acetyl-CoA demand. However, we also demonstrate that not all fates of acetyl-CoA, nor cellular functions, are sufficiently maintained in the absence of ACLY. These results raise further questions that warrant investigation.

First, ACLY loss in immortalized MEFs and cancer cell lines results in impaired proliferation, consistent with previous observations[173,276,279], but remain viable. This is

despite compensation for acetyl-CoA production from acetate via ACSS2, which is able to support lipid synthesis at physiological acetate concentrations. Although global histone acetylation is not maintained at comparable levels to WT cells in these conditions, supplementation of supraphysiological levels of acetate rescues global histone acetylation levels but not proliferation. One hypothesis for this is that ACLY has roles in other cellular functions that cannot be compensated for by ACSS2. Another hypothesis is that although global histone acetylation can be restored with acetate, ACLY and ACSS2 promote histone acetylation at unique sites of the genome. Indeed, evidence that ACLY promotes histone acetylation at double-stranded breaks in response to DNA damage to facilitate homologous recombination, and site-specific differences between glucose- and acetate-induced histone acetylation supports both of these theories[346,347]. However, the genome-wide locations of unique ACLY- and ACSS2-dependent histone acetylation sites, and the functional consequences of these differences, are still under-characterized.

Second, the molecular mechanism of ACSS2 upregulation following ACLY loss remains to be determined. Given our findings that both genetic and chemical depletion of ACLY activity promotes ACSS2 upregulation suggests that nuclear-cytosolic acetyl-CoA can be sensed by cells. However, whether acetyl-CoA itself, or another downstream product of acetyl-CoA is being sensed remains unknown. The transcription factor sterol regulatory element binding protein 2 (SREBP2) has been reported to regulate transcription of *ACSS2*[73]. The SREBP family of proteins are activated in response to decreases in intracellular cholesterol by its regulatory proteins INSIG and SCAP, which cleaves the SREBP precursor to generate mature SREBP. Thus, one hypothesis is that loss of ACLY activity depletes intracellular cholesterol abundance, thereby activating SREBP

and upregulating ACSS2 expression. However, in conditions that ACSS2 is upregulated, HMG-CoA, the metabolic intermediate between acetyl-CoA and cholesterol synthesis, is being synthesized from acetate (Figure 2.3). This suggests that cholesterol can be made in the context of ACLY-deficiency, but fails to suppress SREBP. Another possibility is that HMG-CoA is being synthesized from ACSS2-derived acetyl-CoA, but is not being utilized for cholesterol synthesis. In addition to cholesterol, HMG-CoA is utilized to synthesized isoprenoids for protein prenylation, ubiquinone synthesis, and dolichol synthesis. Whether one of these fates of HMG-CoA, or an entirely different product of acetyl-CoA is being sensed remains an open question.

Third, we identify that fructose-dependent lipogenesis depends, at least in part, on contributions from the gut microbiome. However, the exact specie(s) of bacteria involved is unclear. Moreover, how fructose consumption alters diversity of the gut microbiome is still an open question. One hypothesis is that continual fructose consumption causes a shift in microbial diversity to favor production of SCFAs and hepatic DNL. Fecal microbiome transplantation studies can be performed using germ-free mice to test if this is indeed the case. Furthermore, newborns acquire a significant proportion of their gut microbiomes from the mother[348]. In light of studies seeking to identify heritable risks for obesity[349], whether constant maternal fructose consumption promotes shifts to microbial diversity that could be passed onto offspring is an important open question. Further studies should be done to investigate 1) How fructose consumption alters the diversity of the gut microbiome, and 2) If modulating the gut microbiome can influence hepatic DNL to yield beneficial outcomes for treatment of diseases such as NAFLD.

Fourth, we show that DNL is largely maintained in liver, but not adipose tissue following ACLY deletion. This is despite elevated ACSS2 levels in ACLY-null adipose tissue,

suggesting that the extent or pattern of metabolic compensation may differ between tissues. How this occurs is currently unclear, but may involve nutrient availability *in vivo*. For instance, acetate availability to the liver from the portal vein is high relative to that available to adipose tissue in systemic circulation. Indeed, patterns of metabolite uptake and release between tissues is diverse[350], and warrants further investigation to understand tissue-specific responses to loss of ACLY activity.

Finally, loss of hepatic ACLY fails to suppress DNL in response to sugar consumption or protect against development of fatty liver disease due to compensation from acetate. Recent clinical evidence supports use of ETC-1002 to treat hypercholesterolemia in patients, but whether targeting ACLY will be effective in treating NAFLD or cancer remains unclear. A prediction of our findings is that targeting further downstream in the DNL pathway would be an effective therapeutic strategy. Indeed, inhibition of ACC prevents development of fatty liver, but promotes hypertriglyceridemia[351,352]. Thus, further investigation will be required to determine the utility of therapeutically targeting hepatic DNL for treatment of NAFLD. However, our findings that ACLY and ACSS2 can be simultaneously suppressed with minimal toxicity in liver, at least in the short term, provides preliminary evidence of a therapeutic window for targeting both enzymes in cancer. Coupled to our findings that ACLY inhibition can cause dependence on ACSS2 and exogenous acetate, a therapeutic strategy using ACLY inhibitors to sensitize cancer cells to ACSS2 inhibitors could be envisioned.

In conclusion, our data bridges current literature surrounding both ACLY and ACSS2, and provides a model in which substrate flexibility for acetyl-CoA may underlie disease phenotypes in the context of both cancer and metabolic diseases. This metabolic

flexibility should be acknowledged when considering therapeutic interventions targeting not only acetyl-CoA synthesis, but other metabolic pathways as well.

BIBLIOGRAPHY

1. Lee, J. V *et al.* Akt-dependent metabolic reprogramming regulates tumor cell Histone acetylation. *Cell Metab.* **20**, 306–319 (2014).

2. Mueckler, M. & Thorens, B. The SLC2 (GLUT) family of membrane transporters. *Mol. Aspects Med.* **34**, 121–38 (2013).

3. Morciano, P. *et al.* A conserved role for the mitochondrial citrate transporter Sea/SLC25A1 in the maintenance of chromosome integrity. *Hum. Mol. Genet.* **18**, 4180–4188 (2009).

4. Sutendra, G. *et al.* A Nuclear Pyruvate Dehydrogenase Complex Is Important for the Generation of Acetyl-CoA and Histone Acetylation. *Cell* **158**, 84–97 (2014).

5. Beigneux, A. P. *et al.* ATP-citrate lyase deficiency in the mouse. *J. Biol. Chem.* **279**, 9557–64 (2004).

6. Wellen, K. E. *et al.* ATP-citrate lyase links cellular metabolism to histone acetylation. *Science* **324**, 1076–80 (2009).

7. Schug, Z. T., Vande Voorde, J. & Gottlieb, E. The metabolic fate of acetate in cancer. *Nat. Rev. Cancer* **16**, 708–717 (2016).

8. Hui, S. *et al.* Glucose feeds the TCA cycle via circulating lactate. *Nature* **551**, 115–118 (2017).

9. Luong, A., Hannah, V. C., Brown, M. S. & Goldstein, J. L. Molecular characterization of human acetyl-CoA synthetase, an enzyme regulated by sterol regulatory element-binding proteins. *J. Biol. Chem.* **275**, 26458–26466 (2000).

10. Heiden, M. G. Vander, Cantley, L. C. & Thompson, C. B. Understanding the warburg effect: The metabolic requirements of cell proliferation. *Science (80-.).* **324**, 1029–1033 (2009).

11. Wise, D. R. & Thompson, C. B. Glutamine Addiction: A New Therapeutic Target in Cancer. **35**, 427–433 (2011).

12. Recouvreux, M. V. & Commisso, C. Macropinocytosis: A metabolic adaptation to nutrient stress in cancer. *Front. Endocrinol. (Lausanne).* **8**, 1–7 (2017).

13. Kinnaird, A., Zhao, S., Wellen, K. E. & Michelakis, E. D. Metabolic control of epigenetics in cancer. *Nat. Rev. Cancer* **16**, (2016).

14. Esteller, M. Epigenetics in cancer. *N. Engl. J. Med.* **358**, 1148–59 (2008).

15. Hanahan, D. & Weinberg, R. A. Hallmarks of cancer: the next generation. *Cell* **144**, 646–74 (2011).

16. Wellen, K. E. & Thompson, C. B. A two-way street: reciprocal regulation of

metabolism and signalling. *Nat. Rev. Mol. Cell Biol.* **13**, 270–276 (2012).

17. Kinnaird, A. & Michelakis, E. D. Metabolic modulation of cancer: a new frontier with great translational potential. *J. Mol. Med.* **93**, 127–142 (2015).

18. Chen, Y. *et al.* Quantitative acetylome analysis reveals the roles of SIRT1 in regulating diverse substrates and cellular pathways. *Mol. Cell. Proteomics* **11**, 1048–1062 (2012).

19. Choudhary, C. *et al.* Lysine acetylation targets protein complexes and co-regulates major cellular functions. *Science* **325**, 834–40 (2009).

20. Schölz, C. *et al.* Acetylation site specificities of lysine deacetylase inhibitors in human cells. *Nat. Biotechnol.* **33**, 415–425 (2015).

21. Pietrocola, F., Galluzzi, L., Bravo-San Pedro, J. M., Madeo, F. & Kroemer, G. Acetyl coenzyme A: a central metabolite and second messenger. *Cell Metab.* **21**, 805–21 (2015).

22. Huang, H., Sabari, B. R., Garcia, B. A., David Allis, C. & Zhao, Y. SnapShot: Histone modifications. *Cell* **159**, 458-458.e1 (2014).

23. Huang, H., Lin, S., Garcia, B. A. & Zhao, Y. Quantitative proteomic analysis of histone modifications. *Chem. Rev.* **115**, 2376–2418 (2015).

24. Polevoda, B. & Sherman, F. N(α)-terminal acetylation of eukaryotic proteins. *J. Biol. Chem.* **275**, 36479–36482 (2000).

25. Hollebeke, J., Van Damme, P. & Gevaert, K. N-terminal acetylation and other functions of Nα- acetyltransferases. *Biol. Chem.* **393**, 291–298 (2012).

26. Choudhary, C., Weinert, B. T., Nishida, Y., Verdin, E. & Mann, M. The growing landscape of lysine acetylation links metabolism and cell signalling. *Nat. Rev. Mol. Cell Biol.* **15**, 536–550 (2014).

27. Dhalluin, C. *et al.* Structure and ligand of a histone acetyltransferase bromodomain. *Nature* **399**, 491–496 (1999).

28. Zeng, L. & Zhou, M. M. Bromodomain: an acetyl-lysine binding domain. *FEBS Lett.* **513**, 124–8 (2002).

29. Wagner, G. R. & Hirschey, M. D. Nonenzymatic Protein Acylation as a Carbon Stress Regulated by Sirtuin Deacylases. *Mol. Cell* **54**, 5–16 (2014).

30. Olia, A. S. *et al.* Nonenzymatic Protein Acetylation Detected by NAPPA Protein Arrays. *ACS Chem. Biol.* **10**, 2034–2047 (2015).

31. Bonnet, S. *et al.* A Mitochondria-K+ Channel Axis Is Suppressed in Cancer and Its Normalization Promotes Apoptosis and Inhibits Cancer Growth. *Cancer Cell* **11**, 37–51 (2007).

32. Chen, L. B. Mitochondrial membrane potential in living cells. *Annu. Rev. Cell Biol.* **4**, 155–81 (1988).

33. Wagner, G. R. & Payne, R. M. Widespread and enzyme-independent Nε-acetylation and Nε-succinylation of proteins in the chemical conditions of the mitochondrial matrix. *J. Biol. Chem.* **288**, 29036–29045 (2013).

34. McBrian, M. a. *et al.* Histone Acetylation Regulates Intracellular pH. *Mol. Cell* **49**, 310–321 (2013).

35. Seligson, D. B. *et al.* Global levels of histone modifications predict prognosis in different cancers. *Am. J. Pathol.* **174**, 1619–1628 (2009).

36. Seligson, D. B. *et al.* Global histone modification patterns predict risk of prostate cancer recurrence. *Nature* **435**, 1262–1266 (2005).

37. Elsheikh, S. E. *et al.* Global histone modifications in breast cancer correlate with tumor phenotypes, prognostic factors, and patient outcome. *Cancer Res.* **69**, 3802–3809 (2009).

38. Mosashvilli, D. *et al.* Global histone acetylation levels: Prognostic relevance in patients with renal cell carcinoma. *Cancer Sci.* **101**, 2664–2669 (2010).

39. Tzao, C. *et al.* Prognostic significance of global histone modifications in resected squamous cell carcinoma of the esophagus. *Mod. Pathol.* **22**, 252–260 (2009).

40. Hoseok, I. *et al.* Association of global levels of histone modifications with recurrence-free survival in stage IIB and III esophageal squamous cell carcinomas. *Cancer Epidemiol. Biomarkers Prev.* **19**, 566–573 (2010).

41. Jencks, W. P. *Handbook of Biochemistry and Molecular Biology*. (CRC Press, 1976).

42. Nelson, D., Cox, M. M. *Lehninger Principles of Biochemistry*. (W. H. Freeman And Company, 2013).

43. Feinberg, A. P. & Vogelstein, B. Hypomethylation distinguishes genes of some human cancers from their normal counterparts. *Nature* **301**, 89–92 (1983).

44. Herman, J. G. *et al.* Silencing of the VHL tumor-suppressor gene by DNA methylation in renal carcinoma. *Proc. Natl. Acad. Sci. U. S. A.* **91**, 9700–4 (1994).

45. Greger, V., Passarge, E., Höpping, W., Messmer, E. & Horsthemke, B. Epigenetic changes may contribute to the formation and spontaneous regression of retinoblastoma. *Hum. Genet.* **83**, 155–8 (1989).

46. Esteller, M. Promoter Hypermethylation and BRCA1 Inactivation in Sporadic Breast and Ovarian Tumors. *J. Natl. Cancer Inst.* **92**, 564–569 (2000).

47. Bachman, K. E. *et al.* Histone modifications and silencing prior to DNA methylation of a tumor suppressor gene. *Cancer Cell* **3**, 89–95 (2003).

48. Albert, M. & Helin, K. Histone methyltransferases in cancer. *Semin. Cell Dev. Biol.* **21**, 209–20 (2010).

49. Shi, Y. *et al.* Histone demethylation mediated by the nuclear amine oxidase homolog LSD1. *Cell* **119**, 941–53 (2004).

50. Locasale, J. W. Serine, glycine and one-carbon units: cancer metabolism in full circle. *Nat. Rev. Cancer* **13**, 572–83 (2013).

51. Yang, M. & Vousden, K. H. Serine and one-carbon metabolism in cancer. *Nat. Rev. Cancer* **16**, 650–662 (2016).

52. Hardie, D. G., Ross, F. a. & Hawley, S. a. AMPK: a nutrient and energy sensor that maintains energy homeostasis. *Nat. Rev. Mol. Cell Biol.* **13**, 251–262 (2012).

53. Tsukada, Y. *et al.* Histone demethylation by a family of JmjC domain-containing proteins. *Nature* **439**, 811–816 (2006).

54. Xiao, M. *et al.* Inhibition of α-KG-dependent histone and DNA demethylases by fumarate and succinate that are accumulated in mutations of FH and SDH tumor suppressors. *Genes Dev.* **26**, 1326–1338 (2012).

55. Killian, J. K. *et al.* Succinate dehydrogenase mutation underlies global epigenomic divergence in gastrointestinal stromal tumor. *Cancer Discov.* **3**, 648–657 (2013).

56. Losman, J. A. & Kaelin, W. G. What a difference a hydroxyl makes: Mutant IDH, (R)-2-hydroxyglutarate, and cancer. *Genes Dev.* **27**, 836–852 (2013).

57. Albaugh, B. N., Arnold, K. M. & Denu, J. M. KAT(ching) Metabolism by the Tail: Insight into the Links between Lysine Acetyltransferases and Metabolism. *ChemBioChem* **12**, 290–298 (2011).

58. Meier, J. L. Metabolic mechanisms of epigenetic regulation. *ACS Chem. Biol.* **8**, 2607–2621 (2013).

59. Montgomery, D. C., Sorum, A. W., Guasch, L., Nicklaus, M. C. & Meier, J. L. Metabolic Regulation of Histone Acetyltransferases by Endogenous Acyl-CoA Cofactors. *Chem. Biol.* **22**, 1030–9 (2015).

60. Sabari, B. R. *et al.* Intracellular Crotonyl-CoA Stimulates Transcription through p300-Catalyzed Histone Crotonylation. *Mol. Cell* **58**, 203–215 (2015).

61. Houtkooper, R. H., Pirinen, E. & Auwerx, J. Sirtuins as regulators of metabolism and healthspan. *Nat. Rev. Mol. Cell Biol.* **13**, 225–238 (2012).

62. Latham, T. *et al.* Lactate, a product of glycolytic metabolism, inhibits histone deacetylase activity and promotes changes in gene expression. *Nucleic Acids Res.* **40**, 4794–4803 (2012).

63. Shimazu, T. *et al.* Suppression of oxidative stress by β-hydroxybutyrate, an endogenous histone deacetylase inhibitor. *Science* **339**, 211–4 (2013).

64. Cluntun, A. a. *et al.* The rate of glycolysis quantitatively mediates specific histone acetylation sites. *Cancer Metab.* **3**, 10 (2015).

65. Dromparis, P. & Michelakis, E. D. Mitochondria in vascular health and disease. *Annu. Rev. Physiol.* **75**, 95–126 (2013).

66. Wellen, K. E. *et al.* ATP-citrate lyase links cellular metabolism to histone acetylation. **324**, 1076–1080 (2009).

67. Wise, D. R. *et al.* Hypoxia promotes isocitrate dehydrogenase-dependent carboxylation of -ketoglutarate to citrate to support cell growth and viability. *Proc. Natl. Acad. Sci.* **108**, 19611–19616 (2011).

68. Metallo, C. M. *et al.* Reductive glutamine metabolism by IDH1 mediates lipogenesis under hypoxia. *Nature* **481**, 380–384 (2011).

69. Mullen, A. R. *et al.* Reductive carboxylation supports growth in tumour cells with defective mitochondria. *Nature* **481**, 385–388 (2011).

70. Comerford, S. A. *et al.* Acetate dependence of tumors. *Cell* **159**, 1591–602 (2014).

71. Mashimo, T. *et al.* Acetate is a bioenergetic substrate for human glioblastoma and brain metastases. *Cell* **159**, 1603–14 (2014).

72. Kamphorst, J. J., Chung, M. K., Fan, J. & Rabinowitz, J. D. Quantitative analysis of acetyl-CoA production in hypoxic cancer cells reveals substantial contribution from acetate. *Cancer Metab.* **2**, 23 (2014).

73. Schug, Z. T. *et al.* Acetyl-CoA synthetase 2 promotes acetate utilization and maintains cancer cell growth under metabolic stress. *Cancer Cell* **27**, 57–71 (2015).

74. Gao, X. *et al.* Acetate functions as an epigenetic metabolite to promote lipid synthesis under hypoxia. *Nat. Commun.* **7**, 11960 (2016).

75. Takahashi, H., McCaffery, J. M., Irizarry, R. a & Boeke, J. D. Nucleocytosolic acetyl-coenzyme a synthetase is required for histone acetylation and global transcription. *Mol. Cell* **23**, 207–17 (2006).

76. Chen, R. *et al.* The Acetate/ACSS2 Switch Regulates HIF-2 Stress Signaling in the Tumor Cell Microenvironment. *PLoS One* **10**, e0116515 (2015).

77. Xu, M. *et al.* An acetate switch regulates stress erythropoiesis. *Nat. Med.* **20**, 1–14 (2014).

78. Dang, C. V. MYC, metabolism, cell growth, and tumorigenesis. *Cold Spring Harb. Perspect. Biol.* **5**, 1–16 (2013).

79. Dang, C. V & Dang, C. V. c-Myc target genes involved in cell growth, apoptosis, and metabolism. *Mol. Cell. Biol.* **19**, 1–11 (1999).

80. Whiteman, E. L., Cho, H. & Birnbaum, M. J. Role of Akt/protein kinase B in metabolism. *Trends Endocrinol. Metab.* **13**, 444–451 (2002).

81. Morrish, F. *et al.* Myc-dependent mitochondrial generation of acetyl-CoA contributes to fatty acid biosynthesis and histone acetylation during cell cycle entry. *J. Biol. Chem.* **285**, 36267–36274 (2010).

82. Edmunds, L. R. *et al.* c-Myc and AMPK Control Cellular Energy Levels by Cooperatively Regulating Mitochondrial Structure and Function. *PLoS One* **10**, e0134049 (2015).

83. Morrish, F., Isern, N., Sadilek, M., Jeffrey, M. & Hockenbery, D. M. c-Myc activates multiple metabolic networks to generate substrates for cell-cycle entry. *Oncogene* **28**, 2485–2491 (2009).

84. Berwick, D. C., Hers, I., Heesom, K. J., Kelly Moule, S. & Tavaré, J. M. The identification of ATP-citrate lyase as a protein kinase B (Akt) substrate in primary adipocytes. *J. Biol. Chem.* **277**, 33895–33900 (2002).

85. Potapova, I. a., El-Maghrabi, M. R., Doronin, S. V. & Benjamin, W. B. Phosphorylation of recombinant human ATP:citrate lyase by cAMP-dependent protein kinase abolishes homotropic allosteric regulation of the enzyme by citrate and increases the enzyme activity. Allosteric activation of atp:citrate lyase by phosphorylated sug. *Biochemistry* **39**, 1169–1179 (2000).

86. Hitosugi, T. *et al.* Tyrosine Phosphorylation of Mitochondrial Pyruvate Dehydrogenase Kinase 1 Is Important for Cancer Metabolism. *Mol. Cell* **44**, 864–877 (2011).

87. Fan, J. *et al.* Tyr phosphorylation of PDP1 toggles recruitment between ACAT1 and SIRT3 to regulate the pyruvate dehydrogenase complex. *Mol. Cell* **53**, 534–48 (2014).

88. Fan, J. *et al.* Tyr-301 phosphorylation inhibits pyruvate dehydrogenase by blocking substrate binding and promotes the Warburg effect. *J. Biol. Chem.* **289**, 26533–41 (2014).

89. Dang, L. *et al.* Cancer-associated IDH1 mutations produce 2-hydroxyglutarate. *Nature* **462**, 739–744 (2009).

90. Yan, H. *et al.* IDH1 and IDH2 mutations in gliomas. *N. Engl. J. Med.* **360**, 765–73 (2009).

91. Ward, P. S. *et al.* The Common Feature of Leukemia-Associated IDH1 and IDH2 Mutations Is a Neomorphic Enzyme Activity Converting α-Ketoglutarate to 2-Hydroxyglutarate. *Cancer Cell* **17**, 225–234 (2010).

92. Parsons, D. W. *et al.* An integrated genomic analysis of human glioblastoma multiforme. *Science* **321**, 1807–1812 (2008).

93. Losman, J. *et al.* (R)-2-hydroxyglutarate is sufficient to promote leukemogenesis

and its effects are reversible. *Science* **339**, 1621–5 (2013).

94. Figueroa, M. E. *et al.* Leukemic IDH1 and IDH2 Mutations Result in a Hypermethylation Phenotype, Disrupt TET2 Function, and Impair Hematopoietic Differentiation. *Cancer Cell* **18**, 553–567 (2010).

95. Xu, W. *et al.* Oncometabolite 2-hydroxyglutarate is a competitive inhibitor of α-ketoglutarate-dependent dioxygenases. *Cancer Cell* **19**, 17–30 (2011).

96. Lu, C. *et al.* IDH mutation impairs histone demethylation and results in a block to cell differentiation. *Nature* **483**, 474–478 (2012).

97. Cairns, R. a. & Mak, T. W. Oncogenic isocitrate dehydrogenase mutations: Mechanisms, models, and clinical opportunities. *Cancer Discov.* **3**, 730–741 (2013).

98. Intlekofer, A. M. *et al.* Hypoxia Induces Production of L-2-Hydroxyglutarate. *Cell Metab.* **22**, 304–11 (2015).

99. Oldham, W. M., Clish, C. B., Yang, Y. & Loscalzo, J. Hypoxia-Mediated Increases in l-2-hydroxyglutarate Coordinate the Metabolic Response to Reductive Stress. *Cell Metab.* **22**, 291–303 (2015).

100. Letouzé, E. *et al.* SDH Mutations Establish a Hypermethylator Phenotype in Paraganglioma. *Cancer Cell* **23**, 739–752 (2013).

101. Carey, B. W., Finley, L. W. S., Cross, J. R., Allis, C. D. & Thompson, C. B. Intracellular α-ketoglutarate maintains the pluripotency of embryonic stem cells. *Nature* **518**, 413–416 (2014).

102. Mihaylova, M. M. & Shaw, R. J. The AMPK signalling pathway coordinates cell growth, autophagy and metabolism. *Nat. Cell Biol.* **13**, 1016–23 (2011).

103. Bungard, D. *et al.* Signaling kinase AMPK activates stress-promoted transcription via histone H2B phosphorylation. *Science* **329**, 1201–1205 (2010).

104. Mudd, S. H. & Poole, J. R. Labile methyl balances for normal humans on various dietary regimens. *Metabolism.* **24**, 721–35 (1975).

105. Poirier, L. A., Wise, C. K., Delongchamp, R. R. & Sinha, R. Blood determinations of S-adenosylmethionine, S-adenosylhomocysteine, and homocysteine: correlations with diet. *Cancer Epidemiol. Biomarkers Prev.* **10**, 649–55 (2001).

106. Lim, U. & Song, M.-A. Dietary and lifestyle factors of DNA methylation. *Methods Mol. Biol.* **863**, 359–76 (2012).

107. Pufulete, M. *et al.* Effect of folic acid supplementation on genomic DNA methylation in patients with colorectal adenoma. *Gut* **54**, 648–653 (2005).

108. Cravo, M. L. *et al.* Effect of folate supplementation on DNA methylation of rectal mucosa in patients with colonic adenomas: correlation with nutrient intake. *Clin.*

Nutr. **17**, 45–9 (1998).

109. Schernhammer, E. S. *et al.* Dietary folate, alcohol and B vitamins in relation to LINE-1 hypomethylation in colon cancer. *Gut* **59**, 794–9 (2010).

110. Kadaveru, K., Protiva, P., Greenspan, E. J., Kim, Y.-I. & Rosenberg, D. W. Dietary methyl donor depletion protects against intestinal tumorigenesis in Apc(Min/+) mice. *Cancer Prev. Res. (Phila).* **5**, 911–20 (2012).

111. Mentch, S. J. *et al.* Histone Methylation Dynamics and Gene Regulation Occur through the Sensing of One-Carbon Metabolism. *Cell Metab.* **22**, 861–73 (2015).

112. Cai, L., Sutter, B. M., Li, B. & Tu, B. P. Acetyl-CoA induces cell growth and proliferation by promoting the acetylation of histones at growth genes. *Mol. Cell* **42**, 426–37 (2011).

113. Donohoe, D. R. *et al.* The Warburg Effect Dictates the Mechanism of Butyrate-Mediated Histone Acetylation and Cell Proliferation. *Mol. Cell* **48**, 612–626 (2012).

114. Shi, L. & Tu, B. P. Acetyl-CoA induces transcription of the key G1 cyclin CLN3 to promote entry into the cell division cycle in Saccharomyces cerevisiae. *Proc. Natl. Acad. Sci. U. S. A.* **110**, 7318–23 (2013).

115. Henry, R. A., Kuo, Y., Bhattacharjee, V., Yen, T. J. & Andrews, A. J. Changing the selectivity of p300 by acetyl-CoA modulation of histone acetylation. *ACS Chem. Biol.* **10**, 146–56 (2015).

116. Denisov, I. G. & Sligar, S. G. A novel type of allosteric regulation: Functional cooperativity in monomeric proteins. *Arch. Biochem. Biophys.* **519**, 91–102 (2012).

117. Gao, L. *et al.* Simultaneous quantification of malonyl-CoA and several other short-chain acyl-CoAs in animal tissues by ion-pairing reversed-phase HPLC/MS. *J. Chromatogr. B Anal. Technol. Biomed. Life Sci.* **853**, 303–313 (2007).

118. Katoh, Y. *et al.* Methionine adenosyltransferase II serves as a transcriptional corepressor of Maf oncoprotein. *Mol. Cell* **41**, 554–66 (2011).

119. Kera, Y. *et al.* Methionine adenosyltransferase II-dependent histone H3K9 methylation at the COX-2 gene locus. *J. Biol. Chem.* **288**, 13592–601 (2013).

120. Matsuda, S. *et al.* Nuclear pyruvate kinase M2 complex serves as a transcriptional coactivator of arylhydrocarbon receptor. *Nucleic Acids Res.* **44**, 1–12 (2015).

121. Li, S. *et al.* Serine and SAM Responsive Complex SESAME Regulates Histone Modification Crosstalk by Sensing Cellular Metabolism. *Mol. Cell* 1–14 (2015). doi:10.1016/j.molcel.2015.09.024

122. Jiang, Y. *et al.* Local generation of fumarate promotes DNA repair through inhibition of histone H3 demethylation. *Nat. Cell Biol.* **17**, 1158–1168 (2015).

123. Moussaieff, A. *et al.* Glycolysis-Mediated Changes in Acetyl-CoA and Histone Acetylation Control the Early Differentiation of Embryonic Stem Cells. *Cell Metab.* **21**, 392–402 (2015).

124. Wang, J. *et al.* Dependence of mouse embryonic stem cells on threonine catabolism. *Science* **325**, 435–9 (2009).

125. Eisenberg, T. *et al.* Nucleocytosolic depletion of the energy metabolite acetyl-coenzyme a stimulates autophagy and prolongs lifespan. *Cell Metab.* **19**, 431–44 (2014).

126. Mariño, G. *et al.* Regulation of Autophagy by Cytosolic Acetyl-Coenzyme A. *Mol. Cell* **53**, 710–725 (2014).

127. Peng, Y. *et al.* Deficient import of acetyl-CoA into the ER lumen causes neurodegeneration and propensity to infections, inflammation, and cancer. *J. Neurosci.* **34**, 6772–89 (2014).

128. Yi, C. H. *et al.* Metabolic Regulation of Protein N-Alpha-Acetylation by Bcl-xL Promotes Cell Survival. *Cell* **146**, 607–620 (2011).

129. Peleg, S. *et al.* Life span extension by targeting a link between metabolism and histone acetylation in Drosophila. *EMBO Rep.* **17**, 455–69 (2016).

130. Shyh-Chang, N. *et al.* Influence of Threonine Metabolism on S-Adenosylmethionine and Histone Methylation. *Science* **339**, 222–226 (2012).

131. Shiraki, N. *et al.* Methionine metabolism regulates maintenance and differentiation of human pluripotent stem cells. *Cell Metab.* **19**, 780–794 (2014).

132. Sperber, H. *et al.* The metabolome regulates the epigenetic landscape during naive-to-primed human embryonic stem cell transition. *Nat. Cell Biol.* **17**, 1523–35 (2015).

133. Saha, S. K. *et al.* Mutant IDH inhibits HNF-4α to block hepatocyte differentiation and promote biliary cancer. *Nature* **513**, 110–4 (2014).

134. Lu, C. *et al.* Induction of sarcomas by mutant IDH2. *Genes Dev.* **27**, 1986–98 (2013).

135. Wang, F. *et al.* Targeted inhibition of mutant IDH2 in leukemia cells induces cellular differentiation. *Science* **340**, 622–6 (2013).

136. Rohle, D. *et al.* An inhibitor of mutant IDH1 delays growth and promotes differentiation of glioma cells. *Science* **340**, 626–30 (2013).

137. Turcan, S. *et al.* Efficient induction of differentiation and growth inhibition in IDH1 mutant glioma cells by the DNMT Inhibitor Decitabine. *Oncotarget* **4**, 1729–36 (2013).

138. Borodovsky, A. *et al.* 5-azacytidine reduces methylation, promotes differentiation

and induces tumor regression in a patient-derived IDH1 mutant glioma xenograft. *Oncotarget* **4**, 1737–47 (2013).

139. Flavahan, W. A. *et al.* Insulator dysfunction and oncogene activation in IDH mutant gliomas. *Nature* **529**, 110–114 (2015).

140. Katainen, R. *et al.* CTCF/cohesin-binding sites are frequently mutated in cancer. *Nat. Genet.* **47**, 818–21 (2015).

141. Ji, X. *et al.* 3D Chromosome Regulatory Landscape of Human Pluripotent Cells. *Cell Stem Cell* **18**, 262–75 (2016).

142. Hnisz, D. *et al.* Activation of proto-oncogenes by disruption of chromosome neighborhoods. *Science* **351**, 1454–1458 (2016).

143. Kim, H.-S. *et al.* SIRT3 is a mitochondria-localized tumor suppressor required for maintenance of mitochondrial integrity and metabolism during stress. *Cancer Cell* **17**, 41–52 (2010).

144. Paulin, R. *et al.* Sirtuin 3 deficiency is associated with inhibited mitochondrial function and pulmonary arterial hypertension in rodents and humans. *Cell Metab.* **20**, 827–839 (2014).

145. Finley, L. W. S. *et al.* SIRT3 opposes reprogramming of cancer cell metabolism through HIF1α destabilization. *Cancer Cell* **19**, 416–28 (2011).

146. Hirschey, M. D. *et al.* SIRT3 regulates mitochondrial fatty-acid oxidation by reversible enzyme deacetylation. *Nature* **464**, 121–5 (2010).

147. Bharathi, S. S. *et al.* Sirtuin 3 (SIRT3) protein regulates long-chain acyl-CoA dehydrogenase by deacetylating conserved lysines near the active site. *J. Biol. Chem.* **288**, 33837–47 (2013).

148. Yu, W., Dittenhafer-Reed, K. E. & Denu, J. M. SIRT3 protein deacetylates isocitrate dehydrogenase 2 (IDH2) and regulates mitochondrial redox status. *J. Biol. Chem.* **287**, 14078–86 (2012).

149. Finley, L. W. S. *et al.* Succinate dehydrogenase is a direct target of sirtuin 3 deacetylase activity. *PLoS One* **6**, e23295 (2011).

150. Cimen, H. *et al.* Regulation of succinate dehydrogenase activity by SIRT3 in mammalian mitochondria. *Biochemistry* **49**, 304–11 (2010).

151. Ahn, B.-H. *et al.* A role for the mitochondrial deacetylase Sirt3 in regulating energy homeostasis. *Proc. Natl. Acad. Sci. U. S. A.* **105**, 14447–52 (2008).

152. Tao, R. *et al.* Sirt3-mediated deacetylation of evolutionarily conserved lysine 122 regulates MnSOD activity in response to stress. *Mol. Cell* **40**, 893–904 (2010).

153. Lim, J.-H. *et al.* Sirtuin 1 modulates cellular responses to hypoxia by deacetylating hypoxia-inducible factor 1alpha. *Mol. Cell* **38**, 864–78 (2010).

154. Kim, J., Tchernyshyov, I., Semenza, G. L. & Dang, C. V. HIF-1-mediated expression of pyruvate dehydrogenase kinase: a metabolic switch required for cellular adaptation to hypoxia. *Cell Metab.* **3**, 177–85 (2006).

155. Izumi, H. *et al.* p300/CBP-associated factor (P/CAF) interacts with nuclear respiratory factor-1 to regulate the UDP-N-acetyl-alpha-d-galactosamine: polypeptide N-acetylgalactosaminyltransferase-3 gene. *Biochem. J.* **373**, 713–22 (2003).

156. Lerin, C. *et al.* GCN5 acetyltransferase complex controls glucose metabolism through transcriptional repression of PGC-1alpha. *Cell Metab.* **3**, 429–38 (2006).

157. Keith, B., Johnson, R. S. & Simon, M. C. HIF1α and HIF2α: sibling rivalry in hypoxic tumour growth and progression. *Nat. Rev. Cancer* **12**, 9–22 (2011).

158. Li, T. *et al.* Glyceraldehyde-3-phosphate dehydrogenase is activated by lysine 254 acetylation in response to glucose signal. *J. Biol. Chem.* **289**, 3775–85 (2014).

159. Ventura, M. *et al.* Nuclear translocation of glyceraldehyde-3-phosphate dehydrogenase is regulated by acetylation. *Int. J. Biochem. Cell Biol.* **42**, 1672–80 (2010).

160. Lv, L. *et al.* Mitogenic and oncogenic stimulation of K433 acetylation promotes PKM2 protein kinase activity and nuclear localization. *Mol. Cell* **52**, 340–52 (2013).

161. Vervoorts, J. *et al.* Stimulation of c-MYC transcriptional activity and acetylation by recruitment of the cofactor CBP. *EMBO Rep.* **4**, 484–90 (2003).

162. Faiola, F. *et al.* Dual regulation of c-Myc by p300 via acetylation-dependent control of Myc protein turnover and coactivation of Myc-induced transcription. *Mol. Cell. Biol.* **25**, 10220–34 (2005).

163. Patel, J. H. *et al.* The c-MYC oncoprotein is a substrate of the acetyltransferases hGCN5/PCAF and TIP60. *Mol. Cell. Biol.* **24**, 10826–10834 (2004).

164. Yuan, Z.-L., Guan, Y.-J., Chatterjee, D. & Chin, Y. E. Stat3 dimerization regulated by reversible acetylation of a single lysine residue. *Science* **307**, 269–73 (2005).

165. Masui, K. *et al.* Glucose-dependent acetylation of Rictor promotes targeted cancer therapy resistance. *Proc. Natl. Acad. Sci. U. S. A.* **112**, 9406–11 (2015).

166. Shan, C. *et al.* Lysine Acetylation Activates 6-Phosphogluconate Dehydrogenase to Promote Tumor Growth. *Mol. Cell* 1–14 (2014). doi:10.1016/j.molcel.2014.06.020

167. Patra, K. C. & Hay, N. The pentose phosphate pathway and cancer. *Trends Biochem. Sci.* **39**, 347–54 (2014).

168. Lin, R. *et al.* Acetylation stabilizes ATP-citrate lyase to promote lipid biosynthesis and tumor growth. *Mol. Cell* **51**, 506–18 (2013).

169. Hallows, W. C., Lee, S. & Denu, J. M. Sirtuins deacetylate and activate mammalian acetyl-CoA synthetases. *Proc. Natl. Acad. Sci. U. S. A.* **103**, 10230–5 (2006).

170. Kryukov, G. V *et al.* MTAP deletion confers enhanced dependency on the PRMT5 arginine methyltransferase in cancer cells. *Science* **351**, 1214–8 (2016).

171. Mavrakis, K. J. *et al.* Disordered methionine metabolism in MTAP/CDKN2A-deleted cancers leads to dependence on PRMT5. *Science* **351**, 1208–13 (2016).

172. Marjon, K. *et al.* MTAP Deletions in Cancer Create Vulnerability to Targeting of the MAT2A/PRMT5/RIOK1 Axis. *Cell Rep.* **15**, 574–587 (2016).

173. Hatzivassiliou, G. *et al.* ATP citrate lyase inhibition can suppress tumor cell growth. *Cancer Cell* **8**, 311–21 (2005).

174. Pearce, N. J. *et al.* The role of ATP citrate-lyase in the metabolic regulation of plasma lipids. Hypolipidaemic effects of SB-204990, a lactone prodrug of the potent ATP citrate-lyase inhibitor SB-201076. *Biochem. J.* **334 (Pt 1**, 113–119 (1998).

175. Li, J. J. *et al.* 2-Hydroxy-N-arylbenzenesulfonamides as ATP-citrate lyase inhibitors. *Bioorganic Med. Chem. Lett.* **17**, 3208–3211 (2007).

176. Gutierrez, M. J. *et al.* Efficacy and safety of ETC-1002, a novel investigational low-density lipoprotein-cholesterol-lowering therapy for the treatment of patients with hypercholesterolemia and type 2 diabetes mellitus. *Arterioscler. Thromb. Vasc. Biol.* **34**, 676–683 (2014).

177. Filippov, S., Pinkosky, S. L. & Newton, R. S. LDL-cholesterol reduction in patients with hypercholesterolemia by modulation of adenosine triphosphate-citrate lyase and adenosine monophosphate-activated protein kinase. *Curr. Opin. Lipidol.* **25**, 309–15 (2014).

178. Ballantyne, C. M. *et al.* Efficacy and Safety of a Novel Dual Modulator of Adenosine Triphosphate - Citrate Lyase and Adenosine Monophosphate - Activated Protein Kinase in Subjects with Hypercholesterolemia: The Results of a Double-Blind, Parallel Group, Multicenter, Placebo Contr. *J. Am. Coll. Cardiol.* **62**, (2013).

179. Madeo, F., Pietrocola, F., Eisenberg, T. & Kroemer, G. Caloric restriction mimetics: towards a molecular definition. *Nat. Rev. Drug Discov.* **13**, 727–40 (2014).

180. Onakpoya, I., Hung, S. K., Perry, R., Wider, B. & Ernst, E. The Use of Garcinia Extract (Hydroxycitric Acid) as a Weight loss Supplement: A Systematic Review and Meta-Analysis of Randomised Clinical Trials. *J. Obes.* **2011**, 509038 (2011).

181. Michelakis, E. D. *et al.* Metabolic modulation of glioblastoma with dichloroacetate. *Sci. Transl. Med.* **2**, 31ra34 (2010).

182. Chu, Q. S.-C. *et al.* A phase I open-labeled, single-arm, dose-escalation, study of dichloroacetate (DCA) in patients with advanced solid tumors. *Invest. New Drugs* **33**, 603–10 (2015).

183. Dunbar, E. M. *et al.* Phase 1 trial of dichloroacetate (DCA) in adults with recurrent malignant brain tumors. *Invest. New Drugs* **32**, 452–64 (2014).

184. Shan, C. *et al.* Tyr-94 phosphorylation inhibits pyruvate dehydrogenase phosphatase 1 and promotes tumor growth. *J. Biol. Chem.* **289**, 21413–22 (2014).

185. Falkenberg, K. J. & Johnstone, R. W. Histone deacetylases and their inhibitors in cancer, neurological diseases and immune disorders. *Nat. Rev. Drug Discov.* **13**, 673–91 (2014).

186. Bantscheff, M. *et al.* Chemoproteomics profiling of HDAC inhibitors reveals selective targeting of HDAC complexes. *Nat. Biotechnol.* **29**, 255–65 (2011).

187. West, A. C. & Johnstone, R. W. New and emerging HDAC inhibitors for cancer treatment. *J Clin Invest.* **124**, 30–39 (2014).

188. Wakil, S. J., Stoops, J. K. & Joshi, V. C. Fatty acid synthesis and its regulation. *Annu. Rev. Biochem.* **52**, 537–79 (1983).

189. Van Meer, G., Voelker, D. R. & Feigenson, G. W. Membrane lipids: Where they are and how they behave. *Nat. Rev. Mol. Cell Biol.* **9**, 112–124 (2008).

190. Thiam, A. R., Farese, R. V & Walther, T. C. The biophysics and cell biology of lipid droplets. *Nat. Rev. Mol. Cell Biol.* **14**, 775–86 (2013).

191. Foretz, M. *et al.* ADD1/SREBP-1c Is Required in the Activation of Hepatic Lipogenic Gene Expression by Glucose. *Mol. Cell. Biol.* **19**, 3760–3768 (1999).

192. Shimano, H. Sterol regulatory element-binding proteins (SREBPs): Transcriptional regulators of lipid synthetic genes. *Prog. Lipid Res.* **40**, 439–452 (2001).

193. Carrer, A. *et al.* Acetyl-CoA metabolism supports multistep pancreatic tumorigenesis. *Cancer Discov.* **9**, 416–435 (2019).

194. White, P. J. *et al.* The BCKDH Kinase and Phosphatase Integrate BCAA and Lipid Metabolism via Regulation of ATP-Citrate Lyase. *Cell Metab.* **27**, 1281-1293.e7 (2018).

195. Witters, L. A. & Kemp, B. E. Insulin activation of acetyl-CoA carboxylase accompanied by inhibition of the 5'-AMP-activated protein kinase. *J. Biol. Chem.* **267**, 2864–2867 (1992).

196. Brownsey, R. W., Boone, a N., Elliott, J. E., Kulpa, J. E. & Lee, W. M. Regulation of acetyl-CoA carboxylase. *Biochem. Soc. Trans.* **34**, 223–227 (2006).

197. McGarry, J. D., Mannaerts, G. P. & Foster, D. W. A possible role for malonyl-CoA in the regulation of hepatic fatty acid oxidation and ketogenesis. *J. Clin. Invest.* **60**,

265–70 (1977).

198. Schaffer, J. E. Lipotoxicity: when tissues overeat. *Curr. Opin. Lipidol.* **14**, 281–7 (2003).

199. Menendez, J. A. & Lupu, R. Fatty acid synthase and the lipogenic phenotype in cancer pathogenesis. *Nat. Rev. Cancer* **7**, 763–777 (2007).

200. Swinnen, J. V., Brusselmans, K. & Verhoeven, G. Increased lipogenesis in cancer cells: New players, novel targets. *Curr. Opin. Clin. Nutr. Metab. Care* **9**, 358–365 (2006).

201. Harriman, G. *et al.* Acetyl-CoA carboxylase inhibition by ND-630 reduces hepatic steatosis, improves insulin sensitivity, and modulates dyslipidemia in rats. *Proc. Natl. Acad. Sci. U. S. A.* **113**, E1796-805 (2016).

202. Lawitz, E. J. *et al.* Acetyl-CoA Carboxylase Inhibitor GS-0976 for 12 Weeks Reduces Hepatic De Novo Lipogenesis and Steatosis in Patients With Nonalcoholic Steatohepatitis. *Clin. Gastroenterol. Hepatol.* (2018). doi:10.1016/j.cgh.2018.04.042

203. Svensson, R. U. *et al.* Inhibition of acetyl-CoA carboxylase suppresses fatty acid synthesis and tumor growth of non-small-cell lung cancer in preclinical models. *Nat. Med.* **22**, 1108–1119 (2016).

204. Jones, S. F. & Infante, J. R. Molecular Pathways: Fatty Acid Synthase. *Clin. Cancer Res.* **21**, 5434–8 (2015).

205. Mullen, P. J., Yu, R., Longo, J., Archer, M. C. & Penn, L. Z. The interplay between cell signalling and the mevalonate pathway in cancer. *Nat. Rev. Cancer* **16**, 718–731 (2016).

206. Sakai, J. *et al.* Sterol-regulated release of SREBP-2 from cell membranes requires two sequential cleavages, one within a transmembrane segment. *Cell* **85**, 1037–1046 (1996).

207. Leung, T. T. & Bauman, D. E. In vivo studies of the site of fatty acid synthesis in the rabbit. *Int. J. Biochem.* **6**, 801–805 (1975).

208. El-Serag, H. B. Hepatocellular carcinoma. *N. Engl. J. Med.* **365**, 1118–27 (2011).

209. El-Serag, H. B. & Rudolph, K. L. Hepatocellular Carcinoma: Epidemiology and Molecular Carcinogenesis. *Gastroenterology* **132**, 2557–2576 (2007).

210. Njei, B., Rotman, Y., Ditah, I. & Lim, J. K. Emerging trends in hepatocellular carcinoma incidence and mortality. *Hepatology* **61**, 191–199 (2015).

211. Siegel, R. L., Miller, K. D. & Jemal, A. Cancer statistics, 2016. *CA. Cancer J. Clin.* **66**, 7–30 (2016).

212. Llovet, J. M., Villanueva, A., Lachenmayer, A. & Finn, R. S. Advances in targeted

therapies for hepatocellular carcinoma in the genomic era. *Nat. Rev. Clin. Oncol.* **12**, 408–24 (2015).

213. Liu, G., Dong, C. & Liu, L. Integrated Multiple “-omics” Data Reveal Subtypes of Hepatocellular Carcinoma. *PLoS One* **11**, e0165457 (2016).

214. Hassan, M. M., Frome, A., Patt, Y. Z. & El-Serag, H. B. Rising prevalence of hepatitis C virus infection among patients recently diagnosed with hepatocellular carcinoma in the United States. *J. Clin. Gastroenterol.* **35**, 266–9 (2002).

215. Ertle, J. *et al.* Non-alcoholic fatty liver disease progresses to hepatocellular carcinoma in the absence of apparent cirrhosis. *Int. J. Cancer* **128**, 2436–2443 (2011).

216. Ogden, C. L. *et al.* Prevalence of overweight and obesity in the United States, 1999-2004. *JAMA* **295**, 1549–55 (2006).

217. Ogden, C. L. L., Carroll, M. D. D., Kit, B. K. K. & Flegal, K. M. M. Prevalence of childhood and adult obesity in the United States, 2011-2012. *Jama* **311**, 806–814 (2014).

218. Calle, E. E., Rodriguez, C., Walker-Thurmond, K. & Thun, M. J. Overweight, obesity, and mortality from cancer in a prospectively studied cohort of U.S. adults. *N. Engl. J. Med.* **348**, 1625–38 (2003).

219. Larsson, S. C. & Wolk, A. Overweight, obesity and risk of liver cancer: a meta-analysis of cohort studies. *Br. J. Cancer* **97**, 1005–8 (2007).

220. El-Serag, H. B., Hampel, H. & Javadi, F. The association between diabetes and hepatocellular carcinoma: A systematic review of epidemiologic evidence. *Clin. Gastroenterol. Hepatol.* **4**, 369–380 (2006).

221. Wang, P., Kang, D., Cao, W., Wang, Y. & Liu, Z. Diabetes mellitus and risk of hepatocellular carcinoma: a systematic review and meta-analysis. *Diabetes. Metab. Res. Rev.* **28**, 109–22 (2012).

222. Marrero, J. A. *et al.* NAFLD may be a common underlying liver disease in patients with hepatocellular carcinoma in the United States. *Hepatology* **36**, 1349–1354 (2002).

223. Bugianesi, E. *et al.* Expanding the natural history of nonalcoholic steatohepatitis: From cryptogenic cirrhosis to hepatocellular carcinoma. *Gastroenterology* **123**, 134–140 (2002).

224. Siegel, A. B. & Zhu, A. X. Metabolic syndrome and hepatocellular carcinoma: Two growing epidemics with a potential link. *Cancer* **115**, 5651–5661 (2009).

225. Park, E. J. *et al.* Dietary and Genetic Obesity Promote Liver Inflammation and Tumorigenesis by Enhancing IL-6 and TNF Expression. *Cell* **140**, 197–208 (2010).

226. Dowman, J. K. *et al.* Development of hepatocellular carcinoma in a murine model of nonalcoholic steatohepatitis induced by use of a high-fat/fructose diet and sedentary lifestyle. *Am. J. Pathol.* **184**, 1550–1561 (2014).

227. Kishida, N. *et al.* Development of a novel mouse model of hepatocellular carcinoma with nonalcoholic steatohepatitis using a high-fat, choline-deficient diet and intraperitoneal injection of diethylnitrosamine. *BMC Gastroenterol.* **16**, 61 (2016).

228. Nakagawa, H. *et al.* ER Stress Cooperates with Hypernutrition to Trigger TNF-Dependent Spontaneous HCC Development. *Cancer Cell* **26**, 331–343 (2014).

229. Lambert, J. E., Ramos-Roman, M. A., Browning, J. D. & Parks, E. J. Increased de novo lipogenesis is a distinct characteristic of individuals with nonalcoholic fatty liver disease. *Gastroenterology* **146**, 726–735 (2014).

230. Donnelly, K. L. *et al.* Sources of fatty acids stored in liver and secreted via lipoproteins in patients with nonalcoholic fatty liver disease. *J. Clin. Invest.* **115**, 1343–1351 (2005).

231. Min, H. K. *et al.* Increased hepatic synthesis and dysregulation of cholesterol metabolism is associated with the severity of nonalcoholic fatty liver disease. *Cell Metab.* **15**, 665–674 (2012).

232. Yahagi, N. *et al.* Co-ordinate activation of lipogenic enzymes in hepatocellular carcinoma. *Eur. J. Cancer* **41**, 1316–1322 (2005).

233. Stanhope, K. L. *et al.* Consuming fructose-sweetened, not glucose-sweetened, beverages increase visceral adiposity and lipids and decrease insulin sensitivity in overweight/obese men. *J. Clin. Invest.* **1334**, 1322–1334 (2009).

234. Koo, H. Y., Miyashita, M., Simon Cho, B. H. & Nakamura, M. T. Replacing dietary glucose with fructose increases ChREBP activity and SREBP-1 protein in rat liver nucleus. *Biochem. Biophys. Res. Commun.* **390**, 285–289 (2009).

235. Jiang, L. *et al.* Leptin contributes to the adaptive responses of mice to high-fat diet intake through suppressing the lipogenic pathway. *PLoS One* **4**, e6884 (2009).

236. Carrer, A. *et al.* Impact of High Fat Diet on Tissue Acyl-CoA and Histone Acetylation Levels. *J. Biol. Chem.* jbc.M116.750620 (2017). doi:10.1074/jbc.M116.750620

237. Sobrecases, H. *et al.* Effects of short-term overfeeding with fructose, fat and fructose plus fat on plasma and hepatic lipids in healthy men. *Diabetes Metab.* **36**, 244–6 (2010).

238. Bray, G. A., Nielsen, S. J. & Popkin, B. M. Consumption of high-fructose corn syrup in beverages may play a role in the epidemic of obesity. *Am. J. Clin. Nutr.* **79**, 537–43 (2004).

239. Marriott, B. P., Cole, N. & Lee, E. National estimates of dietary fructose intake

increased from 1977 to 2004 in the United States. *J. Nutr.* **139**, 1228S-1235S (2009).

240. Bergheim, I. *et al.* Antibiotics protect against fructose-induced hepatic lipid accumulation in mice: Role of endotoxin. *J. Hepatol.* **48**, 983–992 (2008).

241. Lê, K. A. *et al.* Fructose overconsumption causes dyslipidemia and ectopic lipid deposition in healthy subjects with and without a family history of type 2 diabetes. *Am. J. Clin. Nutr.* **89**, 1760–1765 (2009).

242. Kawasaki, T. *et al.* Rats fed fructose-enriched diets have characteristics of nonalcoholic hepatic steatosis. *J. Nutr.* **139**, 2067–71 (2009).

243. Abdelmalek, M. F. *et al.* Increased fructose consumption is associated with fibrosis severity in patients with nonalcoholic fatty liver disease. *Hepatology* **51**, 1961–1971 (2010).

244. Kanuri, G., Spruss, A., Wagnerberger, S., Bischoff, S. C. & Bergheim, I. Role of tumor necrosis factor alpha (TNFalpha) in the onset of fructose-induced nonalcoholic fatty liver disease in mice. *J Nutr Biochem* **22**, 527–534 (2011).

245. Vasiljević, A. *et al.* Hepatic inflammation induced by high-fructose diet is associated with altered 11βHSD1 expression in the liver of Wistar rats. *Eur. J. Nutr.* **53**, 1393–402 (2014).

246. Schultz, A., Barbosa-da-Silva, S., Aguila, M. B. & Mandarim-de-Lacerda, C. A. Differences and similarities in hepatic lipogenesis, gluconeogenesis and oxidative imbalance in mice fed diets rich in fructose or sucrose. *Food Funct.* **6**, 1684–91 (2015).

247. Kumamoto, R. *et al.* Dietary fructose enhances the incidence of precancerous hepatocytes induced by administration of diethylnitrosamine in rat. *Eur. J. Med. Res.* **18**, 54 (2013).

248. Ozawa, T., Maehara, N., Kai, T., Arai, S. & Miyazaki, T. Dietary fructose-induced hepatocellular carcinoma development manifested in mice lacking apoptosis inhibitor of macrophage (AIM). *Genes to Cells* 1320–1332 (2016). doi:10.1111/gtc.12446

249. MacDonald, M. J., Longacre, M. J., Warner, T. F. & Thonpho, A. High level of ATP citrate lyase expression in human and rat pancreatic islets. *Horm. Metab. Res.* **45**, 391–3 (2013).

250. Fukuda, H., Katsurada, A. & Iritani, N. Effects of nutrients and hormones on gene expression of ATP citrate-lyase in rat liver. *Eur. J. Biochem.* **209**, 217–22 (1992).

251. Wang, Q. *et al.* Abrogation of hepatic ATP-citrate lyase protects against fatty liver and ameliorates hyperglycemia in leptin receptor-deficient mice. *Hepatology* **49**, 1166–75 (2009).

252. Calvisi, D. F. *et al.* Increased lipogenesis, induced by AKT-mTORC1-RPS6

signaling, promotes development of human hepatocellular carcinoma. *Gastroenterology* **140**, 1071–1083 (2011).

253. Teng, C.-F., Wu, H.-C., Hsieh, W.-C., Tsai, H.-W. & Su, I.-J. Activation of ATP citrate lyase by mTOR signal induces disturbed lipid metabolism in hepatitis B virus pre-S2 mutant tumorigenesis. *J. Virol.* **89**, 605–14 (2015).

254. Sullivan, A. C., Triscari, J., Hamilton, J. G., Miller, O. N. & Wheatley, V. R. Effect of (-)-hydroxycitrate upon the accumulation of lipid in the rat. I. Lipogenesis. *Lipids* **9**, 121–8 (1974).

255. Sullivan, A. C., Triscari, J., Hamilton, J. G. & Miller, O. N. Effect of (-)-hydroxycitrate upon the accumulation of lipid in the rat. II. Appetite. *Lipids* **9**, 129–34 (1974).

256. Sullivan, A. C., Singh, M., Srere, P. A. & Glusker, J. P. Reactivity and inhibitor potential of hydroxycitrate isomers with citrate synthase, citrate lyase, and ATP citrate lyase. *J. Biol. Chem.* **252**, 7583–90 (1977).

257. Sullivan, C. & Triscari, J. Metabolic regulation as a control for lipid disorders. I. Influence of (-)-hydroxycitrate on experimentally induced obesity in the rodent. *Am. J. Clin. Nutr.* **30**, 767–76 (1977).

258. Sullivan, A. C., Triscari, J. & Spiegel, J. E. Metabolic regulation as a control for lipid disorders. II. Influence of (-)-hydroxycitrate on genetically and experimentally induced hypertriglyceridemia in the rat. *Am. J. Clin. Nutr.* **30**, 777–84 (1977).

259. Thompson, P. D. *et al.* Use of ETC-1002 to treat hypercholesterolemia in patients with statin intolerance. *J. Clin. Lipidol.* **9**, 295–304 (2015).

260. Pinkosky, S. L. *et al.* Liver-specific ATP-citrate lyase inhibition by bempedoic acid decreases LDL-C and attenuates atherosclerosis. *Nat. Commun.* **7**, 13457 (2016).

261. Ray, K. K. *et al.* Safety and efficacy of bempedoic acid to reduce LDL cholesterol. *N. Engl. J. Med.* **380**, 1022–1032 (2019).

262. Llovet, J. M. *et al.* Sorafenib in advanced hepatocellular carcinoma. *N. Engl. J. Med.* **359**, 378–90 (2008).

263. El-Serag, H. B. Hepatocellular carcinoma: Recent trends in the United States. *Gastroenterology* **127**, 27–34 (2004).

264. Zhao, S. *et al.* ATP-Citrate Lyase Controls a Glucose-to-Acetate Metabolic Switch. *Cell Rep.* **17**, 1037–1052 (2016).

265. Carrer, A. & Wellen, K. E. Metabolism and epigenetics: a link cancer cells exploit. *Curr. Opin. Biotechnol.* **34**, 23–29 (2014).

266. Covarrubias, A. J. *et al.* Akt-mTORC1 signaling regulates Acly to integrate metabolic input to control of macrophage activation. *Elife* **5**, 1–19 (2016).

267. Yoshii, Y. *et al.* Cytosolic acetyl-CoA synthetase affected tumor cell survival under hypoxia: The possible function in tumor acetyl-CoA/acetate metabolism. *Cancer Sci.* **100**, 821–827 (2009).

268. Balmer, M. L. *et al.* Memory CD8(+) T Cells Require Increased Concentrations of Acetate Induced by Stress for Optimal Function. *Immunity* **44**, 1312–24 (2016).

269. Herrmann, D. B., Herz, R. & Fröhlich, J. Role of gastrointestinal tract and liver in acetate metabolism in rat and man. *Eur. J. Clin. Invest.* **15**, 221–6 (1985).

270. LUNDQUIST, F., TYGSTRUP, N., WINKLER, K., MELLEMGAARD, K. & MUNCK-PETERSEN, S. Ethanol metabolism and production of free acetate in the human liver. *J. Clin. Invest.* **41**, 955–61 (1962).

271. Perry, R. J. *et al.* Acetate mediates a microbiome-brain-β-cell axis to promote metabolic syndrome. *Nature* **534**, 213–7 (2016).

272. Scheppach, W., Pomare, E. W., Elia, M. & Cummings, J. H. The contribution of the large intestine to blood acetate in man. *Clin. Sci.* **80**, 177–182 (1991).

273. Skutches, C. L., Holroyde, C. P., Myers, R. N., Paul, P. & Reichard, G. a. Plasma acetate turnover and oxidation. *J. Clin. Invest.* **64**, 708–713 (1979).

274. Tollinger, C. D., Vreman, H. J. & Weiner, M. W. Measurement of acetate in human blood by gas chromatography: Effects of sample preparation, feeding, and various diseases. *Clin. Chem.* **25**, 1787–1790 (1979).

275. Madiraju, P., Pande, S. V., Prentki, M. & Madiraju, S. R. M. Mitochondrial acetylcarnitine provides acetyl groups for nuclear histone acetylation. *Epigenetics* **4**, 399–403 (2009).

276. Bauer, D. E., Hatzivassiliou, G., Zhao, F., Andreadis, C. & Thompson, C. B. ATP citrate lyase is an important component of cell growth and transformation. *Oncogene* **24**, 6314–22 (2005).

277. Migita, T. *et al.* ATP citrate lyase: Activation and therapeutic implications in non-small cell lung cancer. *Cancer Res.* **68**, 8547–8554 (2008).

278. Shah, S. *et al.* Targeting ACLY sensitizes castration-resistant prostate cancer cells to AR antagonism by impinging on an ACLY-AMPK-AR feedback mechanism. *Oncotarget* **7**, 43713–30 (2016).

279. Zaidi, N., Royaux, I., Swinnen, J. V & Smans, K. ATP citrate lyase knockdown induces growth arrest and apoptosis through different cell- and environment-dependent mechanisms. *Mol. Cancer Ther.* **11**, 1925–35 (2012).

280. Hanai, J. *et al.* Inhibition of lung cancer growth: ATP citrate lyase knockdown and statin treatment leads to dual blockade of mitogen-activated protein kinase (MAPK) and phosphatidylinositol-3-kinase (PI3K)/AKT pathways. *J. Cell. Physiol.* **227**, 1709–20 (2012).

281. Lee, J.-H. *et al.* ATP-citrate lyase regulates cellular senescence via AMPK- and p53-dependent pathway. *FEBS J.* (2014). doi:10.1111/febs.13139

282. Hanai, J.-I., Doro, N., Seth, P. & Sukhatme, V. P. ATP citrate lyase knockdown impacts cancer stem cells in vitro. *Cell Death Dis.* **4**, e696 (2013).

283. Chen, W. W., Freinkman, E., Wang, T., Birsoy, K. & Sabatini, D. M. Absolute Quantification of Matrix Metabolites Reveals the Dynamics of Mitochondrial Metabolism. *Cell* **166**, 1324-1337.e11 (2016).

284. Herman, M. A. & Kahn, B. B. Glucose transport and sensing in the maintenance of glucose homeostasis and metabolic harmony. *J. Clin. Invest.* **116**, 1767–75 (2006).

285. Herman, M. A. *et al.* A novel ChREBP isoform in adipose tissue regulates systemic glucose metabolism. *Nature* **484**, 333–8 (2012).

286. Lee, K. Y. *et al.* Lessons on conditional gene targeting in mouse adipose tissue. *Diabetes* **62**, 864–74 (2013).

287. Yun, M. *et al.* The importance of acetyl coenzyme A synthetase for 11C-acetate uptake and cell survival in hepatocellular carcinoma. *J. Nucl. Med.* **50**, 1222–1228 (2009).

288. Cao, H. *et al.* Identification of a lipokine, a lipid hormone linking adipose tissue to systemic metabolism. *Cell* **134**, 933–44 (2008).

289. Martínez-Reyes, I. *et al.* TCA Cycle and Mitochondrial Membrane Potential Are Necessary for Diverse Biological Functions. *Mol. Cell* **61**, 199–209 (2016).

290. Skarnes, W. C. *et al.* A conditional knockout resource for the genome-wide study of mouse gene function. *Nature* **474**, 337–42 (2011).

291. Snyder, N. W. *et al.* Production of stable isotope-labeled acyl-coenzyme A thioesters by yeast stable isotope labeling by essential nutrients in cell culture. *Anal. Biochem.* **474**, 59–65 (2015).

292. Frey, A. J. *et al.* LC-quadrupole/Orbitrap high-resolution mass spectrometry enables stable isotope-resolved simultaneous quantification and 13C-isotopic labeling of acyl-coenzyme A thioesters. *Anal. Bioanal. Chem.* **408**, 3651–3658 (2016).

293. Sanjana, N. E., Shalem, O. & Zhang, F. Improved vectors and genome-wide libraries for CRISPR screening. *Nat. Methods* **11**, 783–784 (2014).

294. Millard, P., Letisse, F., Sokol, S. & Portais, J.-C. IsoCor: correcting MS data in isotope labeling experiments. *Bioinformatics* **28**, 1294–6 (2012).

295. Millard, P., Letisse, F., Sokol, S. & Portais, J.-C. IsoCor: correcting MS data in isotope labeling experiments. *Bioinformatics* **28**, 1294–6 (2012).

296. Kuo, Y.-M., Henry, R. A. & Andrews, A. J. A quantitative multiplexed mass spectrometry assay for studying the kinetic of residue-specific histone acetylation. *Methods* **70**, 127–33 (2014).

297. Guo, L. *et al.* Diisopropylethylamine/hexafluoroisopropanol-mediated ion-pairing ultra-high-performance liquid chromatography/mass spectrometry for phosphate and carboxylate metabolite analysis: utility for studying cellular metabolism. *Rapid Commun. Mass Spectrom.* **30**, 1835–45 (2016).

298. Fernandez, C. A., Rosiers, C. Des, Previs, S. F., David, F. & Brunengraber, H. Correction of13C Mass Isotopomer Distributions for Natural Stable Isotope Abundance. *J. Mass Spectrom.* **31**, 255–262 (1996).

299. Worth, A. J., Basu, S. S., Snyder, N. W., Mesaros, C. & Blair, I. A. Inhibition of neuronal cell mitochondrial complex i with rotenone increases lipid β-oxidation, supporting acetyl-coenzyme a levels. *J. Biol. Chem.* **289**, 26895–26903 (2014).

300. McCabe, B. J. *et al.* Reproducibility of gas chromatography–mass spectrometry measurements of 2H labeling of water: Application for measuring body composition in mice. *Anal. Biochem.* **350**, 171–176 (2006).

301. Yang, D. *et al.* Assay of low deuterium enrichment of water by isotopic exchange with [U-13C3]acetone and gas chromatography-mass spectrometry. *Anal. Biochem.* **258**, 315–21 (1998).

302. Fernandez, C. A., Rosiers, C. Des, Previs, S. F., David, F. & Brunengraber, H. Correction of13C Mass Isotopomer Distributions for Natural Stable Isotope Abundance. *J. Mass Spectrom.* **31**, 255–262 (1996).

303. Lee, W. N., Bassilian, S., Lim, S. & Boros, L. G. Loss of regulation of lipogenesis in the Zucker diabetic (ZDF) rat. *Am. J. Physiol. Endocrinol. Metab.* **279**, E425-32 (2000).

304. Lee, W. N. *et al.* In vivo measurement of fatty acids and cholesterol synthesis using D2O and mass isotopomer analysis. *Am. J. Physiol.* **266**, E699-708 (1994).

305. Beckonert, O. *et al.* Metabolic profiling, metabolomic and metabonomic procedures for NMR spectroscopy of urine, plasma, serum and tissue extracts. *Nat. Protoc.* **2**, 2692–703 (2007).

306. Weljie, A. M., Newton, J., Mercier, P., Carlson, E. & Slupsky, C. M. Targeted profiling: quantitative analysis of 1H NMR metabolomics data. *Anal. Chem.* **78**, 4430–42 (2006).

307. Weljie, A. M., Newton, J., Mercier, P., Carlson, E. & Slupsky, C. M. Targeted profiling: quantitative analysis of 1H NMR metabolomics data. *Anal. Chem.* **78**, 4430–42 (2006).

308. Wellen, K. E. *et al.* Coordinated regulation of nutrient and inflammatory responses by STAMP2 is essential for metabolic homeostasis. *Cell* **129**, 537–48 (2007).

309. Jensen, T. *et al.* Fructose and sugar: A major mediator of non-alcoholic fatty liver disease. *J. Hepatol.* **68**, 1063–1075 (2018).

310. Hannou, S. A., Haslam, D. E., McKeown, N. M. & Herman, M. A. Fructose metabolism and metabolic disease. *J. Clin. Invest.* **128**, 545–555 (2018).

311. Softic, S., Cohen, D. E. & Kahn, C. R. Role of Dietary Fructose and Hepatic De Novo Lipogenesis in Fatty Liver Disease. *Dig. Dis. Sci.* **61**, 1282–1293 (2016).

312. Donnelly, K. L. *et al.* Sources of fatty acids stored in liver and secreted via lipoproteins in patients with nonalcoholic fatty liver disease. *J. Clin. Invest.* **115**, 1343–51 (2005).

313. Pinkosky, S. L., Groot, P. H. E., Lalwani, N. D. & Steinberg, G. R. Targeting ATP-Citrate Lyase in Hyperlipidemia and Metabolic Disorders. *Trends Mol. Med.* **23**, 1047–1063 (2017).

314. Jang, C. *et al.* The Small Intestine Converts Dietary Fructose into Glucose and Organic Acids. *Cell Metab.* **27**, 351-361.e3 (2018).

315. Bertola, A. Rodent models of fatty liver diseases. *Liver Res.* **2**, 3–13 (2018).

316. Herman, M. A. & Samuel, V. T. The Sweet Path to Metabolic Demise: Fructose and Lipid Synthesis. *Trends Endocrinol. Metab.* **27**, 719–730 (2016).

317. Uyeda, K. & Repa, J. J. Carbohydrate response element binding protein, ChREBP, a transcription factor coupling hepatic glucose utilization and lipid synthesis. *Cell Metab.* **4**, 107–110 (2006).

318. Iizuka, K. The role of carbohydrate response element binding protein in intestinal and hepatic fructose metabolism. *Nutrients* **9**, 1–12 (2017).

319. Poungvarin, N. *et al.* Genome-Wide Analysis of ChREBP Binding Sites on Male Mouse Liver and White Adipose Chromatin. *Endocrinology* **156**, 1982–94 (2015).

320. Ikeda, Y. *et al.* Transcriptional Regulation of the Murine Acetyl-CoA Synthetase 1 Gene through Multiple Clustered Binding Sites for Sterol Regulatory Element-binding Proteins and a Single Neighboring Site for Sp1. *J. Biol. Chem.* **276**, 34259–34269 (2001).

321. Softic, S. *et al.* Divergent effects of glucose and fructose on hepatic lipogenesis and insulin signaling. *J. Clin. Invest.* **127**, 4059–4074 (2017).

322. Liu, X. *et al.* Acetate Production from Glucose and Coupling to Mitochondrial Metabolism in Mammals. *Cell* **175**, 502-513.e13 (2018).

323. Bulusu, V. *et al.* Acetate Recapturing by Nuclear Acetyl-CoA Synthetase 2 Prevents Loss of Histone Acetylation during Oxygen and Serum Limitation. *Cell Rep.* **18**, 647–658 (2017).

324. Lu, M. *et al.* ACOT12-Dependent Alteration of Acetyl-CoA Drives Hepatocellular

Carcinoma Metastasis by Epigenetic Induction of Epithelial-Mesenchymal Transition. *Cell Metab.* 1–15 (2019). doi:10.1016/j.cmet.2018.12.019

325. Iroz, A. *et al.* A Specific ChREBP and PPARα Cross-Talk Is Required for the Glucose-Mediated FGF21 Response. *Cell Rep.* **21**, 403–416 (2017).

326. Ter Horst, K. W. & Serlie, M. J. Fructose consumption, lipogenesis, and non-alcoholic fatty liver disease. *Nutrients* **9**, 1–20 (2017).

327. Kaden-Volynets, V. *et al.* Lack of liver steatosis in germ-free mice following hypercaloric diets. *Eur. J. Nutr.* **0**, 1–13 (2018).

328. Mews, P. *et al.* Acetyl-CoA synthetase regulates histone acetylation and hippocampal memory. *Nature* **546**, 381–386 (2017).

329. Zagelbaum, N. K., Yandrapalli, S., Nabors, C. & Frishman, W. H. Bempedoic Acid (ETC-1002): ATP Citrate Lyase Inhibitor: Review of a First-in-Class Medication with Potential Benefit in Statin-Refractory Cases. *Cardiol. Rev.* **27**, 49–56 (2018).

330. Wang, Q. *et al.* Deficiency in hepatic ATP-citrate lyase affects VLDL-triglyceride mobilization and liver fatty acid composition in mice. *J. Lipid Res.* **51**, 2516–26 (2010).

331. Lanaspa, M. A. *et al.* Ketohexokinase C blockade ameliorates fructose-induced metabolic dysfunction in fructose-sensitive mice. *J. Clin. Invest.* **128**, 2226–2238 (2018).

332. Ishimoto, T. *et al.* Opposing effects of fructokinase C and A isoforms on fructose-induced metabolic syndrome in mice. *Proc. Natl. Acad. Sci. U. S. A.* **109**, 4320–5 (2012).

333. Parks, E. J., Skokan, L. E., Timlin, M. T. & Dingfelder, C. S. Dietary Sugars Stimulate Fatty Acid Synthesis in Adults. *J. Nutr.* 1039–1046 (2008). doi:10.1016/j.bbi.2008.05.010

334. Perumpail, B. J. *et al.* Clinical epidemiology and disease burden of nonalcoholic fatty liver disease. *World J. Gastroenterol.* **23**, 8263–8276 (2017).

335. Postic, C. *et al.* Dual roles for glucokinase in glucose homeostasis as determined by liver and pancreatic b cell-specific gene knock-outs using Cre recombinase. *J. Biol. Chem.* **274**, 305–315 (1999).

336. Nadkarni, M. A., Martin, F. E., Jacques, N. A. & Hunter, N. Determination of bacterial load by real-time PCR using a broad-range (universal) probe and primers set. *Microbiology* **148**, 257–266 (2002).

337. Guan, D. *et al.* Diet-Induced Circadian Enhancer Remodeling Synchronizes Opposing Hepatic Lipid Metabolic Processes. *Cell* **174**, 831-842.e12 (2018).

338. Su, X., Lu, W. & Rabinowitz, J. D. Metabolite Spectral Accuracy on Orbitraps. *Anal. Chem.* **89**, 5940–5948 (2017).

339. Titchenell, P. M., Chu, Q., Monks, B. R. & Birnbaum, M. J. Hepatic insulin signalling is dispensable for suppression of glucose output by insulin in vivo. *Nat. Commun.* **6**, 1–9 (2015).

340. Trefely, S., Ashwell, P. & Snyder, N. W. FluxFix: automatic isotopologue normalization for metabolic tracer analysis. *BMC Bioinformatics* **17**, 485 (2016).

341. Lee, J. V. *et al.* Acetyl-CoA promotes glioblastoma cell adhesion and migration through Ca^{2+}-NFAT signaling. *Genes Dev.* **32**, (2018).

342. Chong, J. *et al.* MetaboAnalyst 4.0: towards more transparent and integrative metabolomics analysis. *Nucleic Acids Res.* **46**, W486–W494 (2018).

343. Neinast, M. D. *et al.* Quantitative Analysis of the Whole-Body Metabolic Fate of Branched-Chain Amino Acids. *Cell Metab.* 1–13 (2018). doi:10.1016/j.cmet.2018.10.013

344. Zaidi, N., Swinnen, J. V & Smans, K. ATP-citrate lyase: a key player in cancer metabolism. *Cancer Res.* **72**, 3709–14 (2012).

345. Bose, S., Ramesh, V. & Locasale, J. W. Acetate Metabolism in Physiology, Cancer, and Beyond. *Trends Cell Biol.* **29**, 695–703 (2019).

346. Sivanand, S. *et al.* Nuclear Acetyl-CoA Production by ACLY Promotes Homologous Recombination. *Mol. Cell* **67**, (2017).

347. Lee, J. V. *et al.* Acetyl-CoA promotes glioblastoma cell adhesion and migration through Ca2+-NFAT signaling. *Genes Dev.* **32**, (2018).

348. Mueller, N. T., Bakacs, E., Combellick, J., Grigoryan, Z. & Dominguez-Bello, M. G. The infant microbiome development: mom matters. *Trends Mol. Med.* **21**, 109–17 (2015).

349. Alonso, R., Farías, M., Alvarez, V. & Cuevas, A. The Genetics of Obesity. *Transl. Cardiometabolic Genomic Med.* 161–177 (2015). doi:10.1016/B978-0-12-799961-6.00007-X

350. Jang, C. *et al.* Metabolite Exchange between Mammalian Organs Quantified in Pigs. *Cell Metab.* **30**, 594-606.e3 (2019).

351. Kim, C. W. *et al.* Acetyl CoA Carboxylase Inhibition Reduces Hepatic Steatosis but Elevates Plasma Triglycerides in Mice and Humans: A Bedside to Bench Investigation. *Cell Metab.* **26**, 394-406.e6 (2017).

352. Goedeke, L. *et al.* Acetyl-CoA Carboxylase Inhibition Reverses NAFLD and Hepatic Insulin Resistance but Promotes Hypertriglyceridemia in Rodents. *Hepatology* **68**, 2197–2211 (2018).

353. Eckel-Mahan, K. & Sassone-Corsi, P. Metabolism and the circadian clock converge. *Physiol. Rev.* **93**, 107–35 (2013).

354. Sahar, S. *et al.* Circadian control of fatty acid elongation by SIRT1 protein-mediated deacetylation of acetyl-coenzyme a synthetase 1. *J. Biol. Chem.* **289**, 6091–6097 (2014).

355. Chow, J. D. Y. *et al.* Genetic inhibition of hepatic acetyl-CoA carboxylase activity increases liver fat and alters global protein acetylation. *Mol. Metab.* **3**, 419–431 (2014).

356. Cahill, G. F. Fuel metabolism in starvation. *Annu. Rev. Nutr.* **26**, 1–22 (2006).

357. Cederbaum, A. I. Alcohol metabolism. *Clin. Liver Dis.* **16**, 667–85 (2012).